

**ELITE ROWING:
TECHNIQUE AND PERFORMANCE**

by

ANDREW JAMES MURPHY

Thesis submitted to the University of London in conformity with the
requirements for the degree of Doctor of Philosophy and for
the Diploma of Imperial College London

Department of Bioengineering and Division of Surgery (SORA)
Imperial College London

June 2009

Abstract

In elite rowing competition the difference between Gold and Silver is often less than one second, and there is a high incidence of injury amongst the sport's athletes. Previous studies into rowing have described kinetic and kinematic profiles, commented on the effects of factors such as fatigue and training status, and identified some aspects of rowing technique that may be associated with improvements in performance, or with injury mechanisms. However, such work has often been subject to significant errors and limitations, such as: restricting kinematic analysis to two-dimensions, small sample sizes, and lack of clinical and performance relevance. Furthermore there has been no one body of work to date that has published a comprehensive analysis of elite rowers' technique and described its relevance to performance. This represents a gap in the performance literature.

The primary aim of this thesis was to describe and analyse the kinetic output and three-dimensional kinematics of elite rowers. It was hypothesised that a comprehensive and explicit description of athletes' technique could be compiled, and that aspects of this technique would be influenced by exercise intensity and longitudinal training. Furthermore, it was thought that discrete aspects of technique could be used to predict high levels of athletic performance, and individual's risk of spinal and knee injuries.

A custom experimental methodology was developed and several pilot studies optimised and validated the method. More than eleven hundred rowing trials were completed by members of the Great Britain elite rowing squad over a period of twenty six months. This provided kinetic and kinematic data that was treated and analysed using custom written software, and subjected to statistical modelling.

The thesis described the method and kinematic model that was utilised. A detailed description of elite athletes' rowing technique and kinematics was produced. Increasing exercise intensity influenced some of the measured parameters, and longitudinal feedback, and coaching interventions were effective in influencing the elite participants. Adopting a kyphotic posture in the lumbar region of the spine at any point in the rowing stroke was found to be detrimental to rowing performance, and may be linked to an increased risk of lumbar injury. Rapid extension of the lumbar spine was also thought to pose an injury risk, however it was found that athletes who extended the lumbar spine at the finish of the stroke exhibited better performance than those who did not. The kinematic characteristics of the lower limbs may positively influence rowers' performance, and provide protection against spinal injury.

Acknowledgments

I have accumulated many debts whilst developing this thesis. For being given the opportunity to carry out the project, for their guidance, and for their invaluable and insightful contributions to the work, I express sincere thanks to my supervisors Anthony Bull and Alison McGregor. I also acknowledge the work of Samson Chee who commissioned many of the tools that I used, without which I would not have made it to the end.

The support of Imperial College, British International Rowing, and UK Sport allowed me focus on my task, and has given me many opportunities for learning, and furthering my professional skills and experience. Thank you. In particular I am indebted to Paul Thompson, Robin Williams, Miles Forbes Thomas, John Keogh and Darren Whiter. All of whom gave so generously of their enthusiasm, time, and expertise. I also offer my thanks to David Tanner, Scott Drawer, Rosie Mayglothling and Nikolai Boehlke for the experiences I have enjoyed, and for their continuing support. In addition to this I wish to express my gratitude, admiration, and best wishes to all of the appallingly talented and dedicated athletes that I have worked with over the last few years.

Many other colleagues and co-workers have helped me too. Specific thanks must go to Dominic Southgate, Clarice Chung, Angelo Tardugno and Spyridon Masouros. These and many others in the Department of Bioengineering assisted me with challenging work problems, acted as sounding board to my frustrations, and generally provided an enjoyable, creative, and fruitful working environment.

I am forever beholden to my family and my friends for their part in this work. To Jack and Jen, to Katy, to my brother Richard and my sister Alison, and to my Aunt Anne, thank you all for your love, your belief in me, your encouragement, and certainly for your very welcome distractions. I can not thank my mum Joan and my dad Jim enough for their support of every conceivable kind. This has been without question, condition or limitation since I came into this world. Finally to Laureen, thank you for everything, but mostly for changing my life.

Contents

Abstract	2
Acknowledgments	3
Contents	4
List of Figures	9
List of Tables	12
Glossary and Nomenclature	14
Reference for Kinematics Directions	16

PART 1

DEVELOPMENT OF A METHOD TO MEASURE THE STROKE PROFILE AND 3D KINEMATICS OF ELITE ROWERS

Chapter 1 Introduction	18
1.1 Aims	20
1.2 Scope of the thesis	20
Chapter 2 Rowing Performance	22
2.1 An interdisciplinary approach.....	22
2.2 Technique, performance, and kinematics in land-based measurements.....	24
Chapter 3 Instrumentation and Configuration	29
3.1 Hardware	29
3.2 Electromagnetic motion tracking and ergometer rowing	30
3.2.1 <i>Generation of magnetic fields</i>	31
3.2.2 <i>Metals and interfering fields</i>	31
3.2.3 <i>Transmitter to sensor distance</i>	33
3.3 Optimisation of the tracking hardware	35
3.3.1 <i>Aims</i>	35
3.3.2 <i>Optimising the laboratory layout</i>	35
3.3.2.1 <i>Determination of the aims</i>	36
3.3.2.2 <i>Materials</i>	37
3.3.2.3 <i>Experimental methodology</i>	38
3.3.2.4 <i>Results</i>	40
3.3.2.5 <i>Discussion</i>	43
3.3.3 <i>Assessing the measurement accuracy of the tracking hardware</i>	44
3.3.3.1 <i>The experimental volume</i>	45
3.3.3.2 <i>Materials</i>	46
3.3.3.3 <i>Experimental methodology</i>	46
3.3.3.4 <i>Computations – orientation</i>	47
3.3.3.5 <i>Computations – position</i>	48
3.3.3.6 <i>Results – orientation</i>	48

3.3.3.7	Results – position	49
3.3.4	<i>Discussion and conclusions</i>	51
3.4	Seat instrumentation calibration	52
3.4.1	<i>Equipment and laboratory setup</i>	52
3.4.2	<i>Experimental methodology</i>	53
3.4.3	<i>Computations</i>	54
3.4.4	<i>Results</i>	57
3.4.5	<i>Discussion and conclusions</i>	58
3.5	Summary.....	59
Chapter 4	Methodology	60
4.1	Recording three-dimensional kinematics.....	60
4.1.1	<i>Digitisation of anatomical points</i>	61
4.1.2	<i>Digitising in the current study</i>	62
4.1.3	<i>Functional identification of joint centres</i>	63
4.1.4	<i>Identifying the location of the hip joint centre</i>	63
4.1.5	<i>Anthropometric based prediction of position</i>	64
4.1.6	<i>Identifying the location of the lumbosacral junction</i>	64
4.1.6.1	Obtaining data	64
4.1.6.2	Computations	66
4.1.6.3	Results	67
4.1.6.4	Discussion and conclusions.....	69
4.2	Athlete preparation	70
4.2.1	<i>The electromagnetic sensors</i>	70
4.2.2	<i>Non-performance trials</i>	72
4.3	Coordinate systems.....	73
4.4	The ergometer test	80
Chapter 5	Data Processing and Error Analysis	82
5.1	Acquisition of 3D kinematics	82
5.2	Data normalisation.....	83
5.2.1	<i>Additional considerations for data normalisation</i>	86
5.2.1.1	Validation of stroke identification.....	86
5.2.1.2	Effect of stroke identification inaccuracy.....	88
5.3	Data extraction.....	88
5.3.1	<i>Description of the variables</i>	90
5.3.1.1	Additional considerations for centre of pressure.....	93
5.3.1.2	Three dimensional kinematics and associated errors	95
5.4	Statistics.....	97
5.5	Summary and hypotheses	98

PART 2

RESULTS OF ANALYSIS OF THE STROKE PROFILE AND 3D KINEMATICS OF ELITE ROWERS

Chapter 6	Descriptive Results	101
6.1	Scale of athlete testing.....	101
6.2	Laboratory setup and directions of movement	104
6.3	How athletes row and move	105
6.3.1	<i>Athletes' stroke profile</i>	107
6.3.2	<i>Athletes' kinematics</i>	113
6.3.3	<i>Variability of kinematics</i>	137
6.3.4	<i>Summary of descriptive data</i>	138
6.3.4.1	Explanation of seemingly inconsistent results	139
6.3.4.2	Differences between athlete groups.....	140
6.3.4.3	Other results	141
Chapter 7	Effect of Exercise Intensity	143
7.1	Interpreting the test results.....	143
7.2	Results	144
7.2.1	<i>Significant results for more than one athlete group</i>	146
7.2.2	<i>Significant results for HWW-SCULL</i>	154
7.2.3	<i>Significant results for HWW-SWEEP</i>	157
7.2.4	<i>Significant results for LWM</i>	158
7.2.5	<i>All athletes: significant ANOVA RM, non-significant post hoc</i>	159
7.2.6	<i>Flagged variables</i>	161
7.3	Summary of results regarding exercise intensity.....	162
7.3.1	<i>HWW-SCULL only</i>	163
7.3.2	<i>HWW-SWEEP only</i>	163
7.3.3	<i>LWM only</i>	164
7.3.4	<i>Other results</i>	164
Chapter 8	Effect of Longitudinal Training	165
8.1	Significant results for all Steps	168
8.1.1	<i>Stroke profile</i>	169
8.1.2	<i>Kinematics at the catch of the stroke</i>	170
8.1.3	<i>Kinematics at peak handle force during the drive phase</i>	173
8.1.4	<i>Kinematics at the finish of the stroke</i>	175
8.1.5	<i>Kinematics at knees up in the recovery phase</i>	178
8.2	Significant results for Step 2.....	181
8.3	Significant results for Step 4.....	183
8.4	Significant results for Step 6.....	184
8.5	All Steps: significant ANOVA RM, non significant post hoc.....	185
8.6	Flagged variables	186
8.7	Summary of results regarding longitudinal training	186

9.1 Dependent variables 190

 9.1.1 Performance variables 191

 9.1.2 Injury variables 192

 9.1.2.1 Injury variables – Relevant to the lumbar spine 192

 9.1.2.2 Injury variable – Relevant to the knee 194

9.2 Introduction to statistical methods 195

 9.2.1 Assumptions underlying multiple regression 195

 9.2.2 Evaluating the appropriateness of regression models 195

 9.2.3 Designing a multiple regression model 196

9.3 Current method for data analysis 197

 9.3.1 Data reduction 197

 9.3.2 Curve estimation 197

 9.3.3 Multiple regression analysis 198

9.4 Results 199

 9.4.1 Concerning rowing performance 201

 9.4.1.1 Timing of the finish 201

 9.4.1.2 Rate of force production 206

 9.4.1.3 Stroke length 210

 9.4.1.4 Power output 214

 9.4.1.5 Seat force and COP 1 (Seat 1) 218

 9.4.1.6 Seat force and COP 2 (Seat 2) 222

 9.4.1.7 Minimum seat force and bodyweight (Seat BW) 226

 9.4.1.8 Summary regarding 3D kinematics and performance 230

 9.4.1.9 Relationships between dependent variables, and other stroke profile variables linked with improving performance 231

 9.4.2 Concerning injury 234

 9.4.2.1 Change in flexion/extension about LSJ during the drive phase 234

 9.4.2.2 Rate of change of LSJ alpha under loading – LSJ extension 238

 9.4.2.3 Rate of change of LSJ alpha under loading – LSJ flexion 242

 9.4.2.4 Level of HJC abduction/adduction when in 20° of KJC flexion 243

 9.4.2.5 Summary regarding kinematics and injury 243

9.5 Summary 244

PART 3

DISCUSSION AND CONCLUSIONS

Chapter 10	Discussion of PART 2	248
10.1	Rowing technique and performance	248
10.1.1	<i>Descriptive</i>	248
10.1.2	<i>Exercise intensity</i>	254
10.1.3	<i>Longitudinal training</i>	256
10.1.4	<i>Athletic performance</i>	257
10.2	Spinal injury and low back pain	260
Chapter 11	General Discussion, Summary and Future Work	267
References		273
Appendix 1		281
Appendix 2		282
Appendix 3		283
Appendix 4		286
Appendix 5		289

List of Figures

Figure 1.1: The drive phase of the rowing stroke	19
Figure 1.2: The aims and scope of the current research	21
Figure 3.1: The laboratory setup during athlete testing	30
Figure 3.2: Overhead view of the laboratory layout used in previous studies into rowing biomechanics. The axis frame is the FOB transmitter axis system	36
Figure 3.3: The board used during laboratory optimisation trials. The axis frame is the FOB transmitter axis system	38
Figure 3.4: Location of the FOB transmitter during optimisation trials	38
Figure 3.5: Three levels of board positioning during optimisation trials	39
Figure 3.6: Average, maximum and standard deviation of errors recorded during the laboratory optimisation study, with the ergometer in situ	42
Figure 3.7: Scale view of the experimental setup used during the FOB measurement accuracy assessment	45
Figure 3.8: Sensor mounting block and block holder used during the FOB accuracy assessment	46
Figure 3.9: FOB system accuracy for orientation. Maximum measurement errors	49
Figure 3.10: FOB system accuracy for orientation. Measurement error for all sensor rotations	49
Figure 3.11: FOB system accuracy for position	50
Figure 3.12: Ergometer seat bracket and force transducers	52
Figure 3.13: Vertical point loading apparatus for seat force calibration	53
Figure 3.14: Ergometer seat instrumentation schematic	55
Figure 3.15: Reduction in measurement error from the seat calibration experiment	57
Figure 3.16: Impact of the seat calibration study on COP measurement	58
Figure 4.1: Digitisation of an anatomical point schematic	62
Figure 4.2: Anatomy used for regression identification of LSJ	65
Figure 4.3: Pelvis local axis system used for regression identification of LSJ	66
Figure 4.4: Location of FOB sensor 1 (S1) and sensor 2 (S2) during athlete testing	71
Figure 4.5: FOB sensor 3 (S3), mounting block and stylus complex	71
Figure 4.6: Digitisation and functional assessment of anatomical locations	72
Figure 4.7: Global/laboratory axis system used during athlete testing	74
Figure 4.8: BACK, PELVIS and LSJ coordinate frames	75
Figure 4.9: PELVIS, FEMUR and HJC coordinate frames	76
Figure 4.10: FEMUR, TIBIA and KJC coordinate frames	77
Figure 4.11: TIBIA, POSFOOT and AJC coordinate frames	78
Figure 4.12: Calculation of the angle at FJC	79
Figure 5.1: Identification of individual rowing strokes within raw data	84
Figure 5.2: Pseudocode used for stroke identification	84
Figure 5.3: Pseudocode rejected for use in stroke identification – version 1	86
Figure 5.4: Strokes identified using different algorithms	87
Figure 5.5: Pseudocode rejected for use in stroke identification – version 2	87
Figure 5.6: Errors in stroke identification	89
Figure 5.7: Example of how centre of pressure data was used	92
Figure 5.8: Determination of COP filter magnitude	93
Figure 5.9: Filtered centre of pressure coordinates	94
Figure 5.10: All invalid, unfiltered centre of pressure coordinates	95

Figure 5.11: The data analysis process	98
Figure 6.1: Overhead view of the laboratory setup used during athlete testing sessions.....	104
Figure 6.2: Mean and standard deviation of the timing of stroke events for all athlete groups	107
Figure 6.3: Handle force for all athlete groups	108
Figure 6.4: Seat force for all athlete groups.....	109
Figure 6.5: Centre of pressure trajectory for all athlete groups.....	111
Figure 6.6: Stroke; Power Output, Work Done, and Length for all athlete groups.....	112
Figure 6.7: Trajectory of LSJ X for all athlete groups	113
Figure 6.8: Trajectory of HJC X for all athlete groups	114
Figure 6.9: Trajectory of KJC X for all athlete groups	115
Figure 6.10: Trajectory of AJC X for all athlete groups	116
Figure 6.11: Trajectory of LSJ Y for all athlete groups.....	117
Figure 6.12: Trajectory of HJC Y for all athlete groups	118
Figure 6.13: Trajectory of KJC Y for all athlete groups	119
Figure 6.14: Trajectory of AJC Y for all athlete groups	120
Figure 6.15: Trajectory of LSJ Z for all athlete groups	121
Figure 6.16: Trajectory of HJC Z for all athlete groups.....	122
Figure 6.17: Trajectory of KJC Z for all athlete groups.....	123
Figure 6.18: Trajectory of AJC Z for all athlete groups.....	124
Figure 6.19: LSJ alpha angle for all athlete groups.....	125
Figure 6.20: Lumbopelvic ratio for all athlete groups	126
Figure 6.21: HJC alpha angle for all athlete groups.....	127
Figure 6.22: KJC alpha angle for all athlete groups.....	128
Figure 6.23: AJC alpha angle for all athlete groups.....	129
Figure 6.24: FJC alpha angle for all athlete groups	130
Figure 6.25: LSJ beta angle for all athlete groups.....	131
Figure 6.26: HJC beta angle for all athlete groups.....	132
Figure 6.27: AJC beta angle for all athlete groups.....	133
Figure 6.28: LSJ gamma angle for all athlete groups	134
Figure 6.29: HJC gamma angle for all athlete groups.....	135
Figure 6.30: AJC gamma angle for all athlete groups.....	136
Figure 7.1: The mean and standard deviation of timing of peak handle force (a) and timing of the finish (b) for all athlete groups, for all Steps.....	147
Figure 7.2: Mean and standard deviation of normalised maximum handle force (a) and rate of force production (b) for all athlete groups, for all Steps	148
Figure 7.3: Mean and standard deviation of minimum seat force (a) and magnitude of suspension (b) for all athlete groups, for all Steps	149
Figure 7.4: Mean and standard deviation of power (a), work (b), stroke length (c) and stroke rate (d) for all athlete groups, for all Steps.....	150
Figure 7.5: Mean and standard deviation of maximum and catch position of the HJC in the Z direction (a) and Maximum value, and value at the catch for KJC α (b) for all athlete groups, for all Steps	152
Figure 7.6: Mean and standard deviation for KJC α at the finish (a) and during the recovery (b)	156
Figure 8.1: Mean and standard error for peak handle force (a) and stroke length (b).....	169
Figure 8.2: Mean and standard error for LSJ X at the catch (a) and LSJ Y at the catch (b)....	170
Figure 8.3: Mean and standard error of LSJ alpha at the catch.....	171
Figure 8.4: Mean and standard error of KJC X at the catch.....	171
Figure 8.5: Mean and standard error of AJC Y at the catch (a) and AJC Z at the catch (b)....	172

Figure 8.6: Mean and standard error of LSJ Y at peak handle force	173
Figure 8.7: Mean and standard error of LSJ alpha at peak handle force.....	173
Figure 8.8: Mean and standard error of KJC X at peak handle force.....	174
Figure 8.9: Mean and standard error of AJC Y at peak handle force.....	174
Figure 8.10: Mean and standard error of LSJ Y at the finish (a) and LSJ Z at the finish (b)...	175
Figure 8.11: Mean and standard error of LSJ alpha at the finish	176
Figure 8.12: Mean and standard error of KJC X at the finish.....	176
Figure 8.13: Mean and standard error of AJC Y at the finish.....	177
Figure 8.14: Mean and standard error of FJC alpha at the finish.....	177
Figure 8.15: Mean and standard error of LSJ Y when knees break (a) and LSJ Z when knees break (b)	178
Figure 8.16: Mean and standard error for LSJ alpha when the knees break	179
Figure 8.17: Mean and standard error of KJC X when knees break	180
Figure 8.18: Mean and standard error of AJC Y when knees break	180
Figure 8.19: Schematic showing the effect of decreasing posterior rotation of the pelvis on intersegmental flexion/extension angles at LSJ and HJC	182
Figure 9.1: Calculation of a performance indicating dependent variable	192
Figure 9.2: Calculation of variables linked to LSJ injury	194
Figure 9.3: Assessment of the assumptions of normality and constant variance with respect to Finish timing	202
Figure 9.4: Assessment of the assumption of linearity with respect to Finish timing.....	203
Figure 9.5: Assessment of the assumptions of normality and constant variance with respect to Slope of handle force	206
Figure 9.6: Assessment of the assumption of linearity with respect to Slope of handle force.	207
Figure 9.7: Assessment of the assumptions of normality and constant variance with respect to Stroke length	210
Figure 9.8: Assessment of the assumption of linearity with respect to Stroke length.....	211
Figure 9.9: Assessment of the assumptions of normality and constant variance with respect to Power output	214
Figure 9.10: Assessment of the assumption of linearity with respect to Power output.....	215
Figure 9.11: Assessment of the assumptions of normality and constant variance with respect to Seat 1	218
Figure 9.12: Assessment of the assumption of linearity with respect to Seat 1	219
Figure 9.13: Assessment of the assumptions of normality and constant variance with respect to Seat 2.....	222
Figure 9.14: Assessment of the assumption of linearity with respect to Seat 2	223
Figure 9.15: Assessment of the assumptions of normality and constant variance with respect to Seat BW	226
Figure 9.16: Assessment of the assumption of linearity with respect to Seat BW.....	227
Figure 9.17: Assessment of the assumptions of normality and constant variance with respect to LSJ delta.....	235
Figure 9.18: Assessment of the assumption of linearity with respect to LSJ delta.....	236
Figure 9.19: Assessment of the assumptions of normality and constant variance with respect to Max LSJ HF	239
Figure 9.20: Assessment of the assumption of linearity with respect to Max LSJ HF	240
Figure 10.1: Hypothetical model of lumbar injury risk to the spine	265

List of Tables

Table 2.1: Previous research into rowing: measurements, aims, and limitations.....	28
Table 3.1: Effect of the rowing machine on FOB measurement accuracy (independent samples t tests).....	41
Table 3.2: Errors associated with the laboratory optimisation study	41
Table 3.3: The effect of global sensor position of FOB performance.....	42
Table 3.4: Sensor coordinates during assessment of the repeatability of transmitter placement.....	43
Table 3.5: FOB system accuracy for orientation.....	48
Table 3.6: FOB system accuracy for position.....	50
Table 3.7: Experimental trial protocol during seat calibration.....	54
Table 3.8: Comparison of measurement errors relevant to the seat instrumentation	58
Table 4.1: Digitised anatomical points.....	63
Table 4.2: Anatomy and measurements used for regression identification of LSJ.....	66
Table 4.3: Offsets and associated errors for prediction of LSJ position (n = 16).....	68
Table 4.4: Leave one out analysis validation of the LSJ offset.....	69
Table 4.5: Anatomical points used in the kinematic model	73
Table 4.6: Structure of an ergometer Step test.....	81
Table 5.1: The content of raw and processed Step test files	85
Table 5.2: Dependent variables extracted from experimental data.....	90
Table 6.1: Number of athletes tested and Steps completed during each session	102
Table 6.2: All Steps recorded and number of individual rowing strokes therein.....	102
Table 6.3: Testing sessions attended, and Steps completed by each athlete	103
Table 6.4: Clinical rotations measured in the current study.....	105
Table 6.5: Zones of exercise intensity.....	106
Table 6.6: Variability of all kinematic data.....	138
Table 7.1: Results of ANOVA RM with changing exercise intensity	144
Table 7.2: Correlations between extremes of kinematic measurements and at the stroke catch and finish.....	145
Table 7.3: Significant dependent variables common to more than one athlete group	146
Table 7.4: Results of Bonferroni post hoc analysis for variables that changed significantly with exercise intensity.....	153
Table 7.5: Significant dependent variables for the HWW-SCULL group.....	154
Table 7.6: Significant dependent variables for the HWW-SWEEP group.....	157
Table 7.7: Significant dependent variables for the LWM group.....	158
Table 7.8: Exercise intensity: Significant variables from ANOVA RM with non-significant Bonferroni post hoc.....	160
Table 7.9: Category four variables for all athlete groups.....	161
Table 8.1: Dependent variables considered during longitudinal analysis.....	166
Table 8.2: Results of ANOVA RM regarding longitudinal training.....	167
Table 8.3: Dependent variables that showed significant change across several testing sessions during Step 2, Step 4 and Step 6	168
Table 8.4: Dependent variables that showed significant change across several testing sessions during Step 2	181
Table 8.5: Dependent variables that showed significant change across several testing sessions during Step 4.....	183
Table 8.6: Dependent variables that showed significant change across several testing sessions during Step 4.....	184

Table 8.7: Longitudinal training: Significant variables from ANOVA RM with non-significant Bonferroni post hoc.....	185
Table 9.1: Variables included in the current dataset	190
Table 9.2: The dependent variables considered during regression analyses.....	191
Table 9.3: Descriptive statistics of selected variables.....	199
Table 9.4: The MREG calculated equation for Finish timing.....	204
Table 9.5: The MREG calculated equation for Slope of handle force.....	208
Table 9.6: The MREG calculated equation for Stroke length.....	212
Table 9.7: The MREG calculated equation for Power output.....	216
Table 9.8: The MREG calculated equation for Seat 1	220
Table 9.9: The MREG calculated equation for Seat 2	224
Table 9.10: The MREG calculated equation for Seat BW	228
Table 9.11: Kinematic variables linked with multiple performance measures	230
Table 9.12: The MREG calculated equation for LSJ delta	237
Table 9.13: The MREG calculated equation for Max LSJ HF.....	241
Table 9.14: Summary of the quality of fit of MREG models, and the number of associated explanatory variables	245
Table 10.1: Average range of motion and standard deviation (SD) of joint centres' trajectory during elite ergometer rowing	250
Table 10.2: Average range of motion and standard deviation (SD) of joint centres' rotation during elite ergometer rowing	251
Table 10.3: Correlation coefficients for LSJ alpha at different points in the rowing stroke....	254

Glossary and Nomenclature

Athlete group / boat class	A category of athletes
Sweep rower	An athlete who works a single oar/blade during on water rowing
Sculler	An athlete who works two oars/blades during on water rowing
Catch	The beginning of the rowing stroke
Drive phase	The propulsive part of the rowing stroke
MHF	Maximum handle force - time point in the drive phase often used to observe other variables
Finish	The end of the propulsive part of the rowing stroke
Recovery phase	The stroke phase when the athlete returns from the finish to the catch position
Rockover	The start of the recovery - the athlete's trunk rocks up and over their hips in an anterior direction
Knee Up/Knees break	The point in the recovery when the knees begin to rise/flex often used to observe other variables
Stroke profile	Group of dependent variables - any dependent variable in the current study that is not a measure of three-dimensional kinematics
AJC	The ankle joint centre
alpha	Flexion extension intersegmental angle
ANOVA RM	Analysis of variance with repeated measures
ANTFOOT	Body segment - the anterior segment of the foot
BACK	Body segment - the lumbar spine
beta	Abduction adduction, side flexion intersegmental angle
BM	Body mass
BW	Bodyweight
COP	Centre of pressure on the rowing ergometer seat
COP drift – Finish (mm)	Measurement of COP deviation in the medial lateral direction
COP drift – MHF (mm)	Measurement of COP deviation in the medial lateral direction
COP drift, MHF-Fin (mm)	Measurement of COP deviation in the medial lateral direction
COP drift, Recovery (mm)	Measurement of COP deviation in the medial lateral direction
COP drift, Stroke (mm)	Measurement of COP deviation in the medial lateral direction
COP Z @ Catch (mm)	Location of the COP in the anterior posterior direction at the catch
COP Z @ Finish (mm)	Location of the COP in the anterior posterior direction at the finish
COP Z @ MHF (mm)	Location of the COP in the anterior posterior direction whilst peak handle force is being exerted
EM	Electromagnetic - refers to motion tracking system
FEMUR	Body segment - the thigh
Finish (%)	The timing of the finish of the rowing stroke
FJC	The foot joint centre - point of rotation of ANTFOOT and POSFOOT
FOB	The Flock of Birds motion tracking hardware
gamma	Internal external rotation, twist intersegmental angle
GG	Greenhouse-Geisser statistical adjustment
HF	Huynh-Feldt statistical adjustment
HJC	The hip joint centre
HJC Q	The magnitude of HJC abduction adduction when the knee is in 20° of flexion - related to injury
HWW-SCULL	Athlete group - heavyweight female scullers
HWW-SWEEP	Athlete group - heavyweight female sweep rowers
KJC	The knee joint centre
Knees up (%)	The timing of the knees breaking in the recovery of the rowing stroke
KS	Kolmogorov-Smirnov statistical assessment of the distribution of data
LASIS	Anatomical point - the left anterior superior iliac spine
LEPI	Anatomical point - the lateral femoral epicondyle
LMAL	Anatomical point - the lateral malleolus
LPSIS	Anatomical point - the left posterior superior iliac spine
LR	Long range version of an electromagnetic motion tracking system
LSJ	The junction of the fifth lumbar and first sacral vertebrae
LSJ delta	Change in LSJ flexion extension during the early part of the drive phase
LWM	Athlete group - lightweight men
LWW	Athlete group - lightweight women

Max H Force/BM (N/kg×100)	The peak handle force exerted during rowing, normalised by the athlete's body mass
Max handle force (%)	The timing of the peak handle force exerted during the rowing stroke
Max handle force (N)	The peak handle force exerted during rowing
Max LSJ HF	Maximum value of the product of the instantaneous rate of change of flexion extension about LSJ and tensile force exerted on the handle during the drive phase - related to spinal injury
Min LSJ HF	Minimum value of the product of the instantaneous rate of change of flexion extension about LSJ and tensile force exerted on the handle during the drive phase - related to spinal injury
Max seat force (N)	The maximum recorded seat force during rowing - this involves the athlete not supporting their bodyweight through the ergometer seat
MEPI	Anatomical point - the medial femoral epicondyle
METS	Anatomical point - the dorsal aspect of the fifth metatarsal head
Min seat force (N)	The minimum recorded seat force during rowing - this involves the athlete exerting significant force on the seat
MMAL	Anatomical point - the medial malleolus
MREG	Multiple regression modelling in statistics
MS	Mauchly's test of sphericity - for validation of statistical methods
PCA	Principal component analysis
PEL1	Anatomical point - location within the pelvis used in kinematic modelling
PEL2	Anatomical point - location within the pelvis used in kinematic modelling
PEL3	Anatomical point - location within the pelvis used in kinematic modelling
PEL4	Anatomical point - location within the pelvis used in kinematic modelling
PELVIS	Body segment - the pelvis
PLA	Vertical point loading apparatus used in calibration of hardware
POSFOOT	Body segment - posterior segment of the foot
Power output (W)	Power generated by an athlete during rowing
Quality COP X @ Catch	Deviation of COP in the medial lateral direction at the catch
Quality COP X @ Finish	Deviation of COP in the medial lateral direction at the finish
Quality COP X @ MHF	Deviation of COP in the medial lateral direction whilst peak handle force is being exerted
Quality LP ratio @ Catch	Measurement of the alignment of BACK and PELVIS at the catch
Quality LP ratio @ Finish	Measurement of the alignment of BACK and PELVIS at the finish
Quality LP ratio @ MHF	Measurement of the alignment of BACK and PELVIS whilst peak handle force is being exerted
RASIS	Anatomical point - right anterior superior iliac spine
RPSIS	Anatomical point - right posterior superior iliac spine
S1	Flock of Birds sensor number 1
S2	Flock of Birds sensor number 2
S3	Flock of Birds sensor number 3
S4	Flock of Birds sensor number 4
Seat 1	The sum of the product of instantaneous medial lateral motion on the ergometer seat, and the vertical component of seat force - between the catch and max handle force - performance measure
Seat 2	The sum of the product of instantaneous medial lateral motion on the ergometer seat, and the vertical component of seat force - between the catch and the finish - performance measure
Seat BW	The difference between the athlete's BW and the absolute value of peak downwards force on the seat - performance measure
Seat force @ MHF (N)	Magnitude of the force exerted on the seat whilst maximum handle force is being exerted
Slope of handle force	Rate of handle force production during rowing
SR	Short range version of an electromagnetic motion tracking system
Step	A piece of rowing completed by an athlete - athletes performed Step tests in the current study
Stroke length (mm)	The length of the rowing stroke as measured by handle displacement
Stroke rate (/min)	The number of strokes performed per minute during rowing
Suspension 1 (BW(s))	Measurement of the way in which an athlete suspended away from the ergometer seat during the first part of the drive phase
Suspension 2 (BW(s))	Measurement of the way in which an athlete suspended away from the ergometer seat during the entire drive phase
SW	Shapiro-Wilk statistical assessment of the distribution of data
TIBIA	Body segment - the shank
Work done (J)	The work done by an athlete during rowing
X	The laboratory medial lateral axis
Y	The laboratory vertical axis
Z	The laboratory anterior posterior axis
Z handle minus Z KJC	Measurement of the relative position of the ergometer handle and the KJC in the anterior posterior direction during the recovery in rowing

Reference for Kinematics Directions

Direction of drive phase

Bow-wards

Posterior



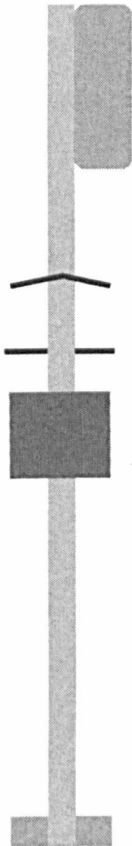
Direction of recovery phase

Sternwards

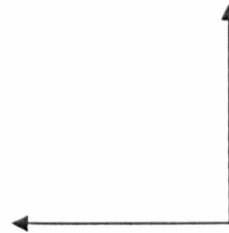
Anterior



The rowing ergometer



Z axis



X axis

The Y axis is vertical and positive superiorly

PART 1

Development of a method to measure the stroke profile and 3D kinematics of elite rowers

Chapter 1

Introduction

The sport of rowing is highly physically demanding. At the elite level there are few other sports that call for the same combination of flexibility, muscular power and aerobic endurance, all of which must be delivered with strict timing and teamwork. On the water there are two distinct groups of athletes within the sport, these are sweep rowers (where each member of a crew works a single oar/blade) and scullers (each athlete has two blades), and the number of athletes in a crew can be 1, 2, 4 or 8. Combined with this, athletes can be classified as either open weight/heavyweight or lightweight (men; individual < 72 kg, crew average < 70 kg, women; individual < 59 kg, crew average < 57 kg). Together these parameters determine what is known as the boat class. International crews commonly compete over 2000 m, during which an athlete will perform around 230 strokes, each requiring a delivery of force that will peak at approximately 400 N per arm; 400 N on each blade in sculling and 800 N per blade in sweep rowing (Kleshnev, 2005). The race will last between 5 min 40 s and 8 min depending on the boat class (Thompson, 2005). The training undertaken by elite athletes is extensive and varied. Most rowing programs train and test their athletes in the gymnasium, on the water, and on the rowing machine/rowing ergometer. Thompson (2005) states that due to its usefulness for acquiring objective data related to fitness levels, mental toughness and technical ability, the rowing ergometer should be the apparatus around which coaches base their testing.

The fundamental basis of rowing is the precise repetition of a basic action called the rowing stroke. The technique required to perform the stroke consists of a cyclical movement that elite athletes perform approximately 4000 times every day of their training lives and can be split into two distinct phases: the drive (Figure 1.1), and the recovery. The drive phase is the 'work' phase, and commences at the catch position; in this position the athlete's lower limbs are in full flexion combined with full extension of the upper limbs. From this point, and whilst holding a strong position through the trunk and arms, the athlete will begin working their muscles to push through their feet and extend the legs (leg press), following this, and with the legs still working, the trunk should begin to rotate (trunk swing) posteriorly about the hips whilst the arms remain extended with the shoulders relaxed and the handle travelling in a straight line. Towards the end of the drive phase the leg press and trunk swing are still working together as the arms commence their pull through to the trunk, thus completing the drive; the majority of the force and power an athlete develops during their stroke should be generated by the legs, not the back and arms. The position that the athlete is now in is known as the finish, here the lower limbs are in full extension whilst the upper limbs are in full flexion.

CATCH -----> FINISH

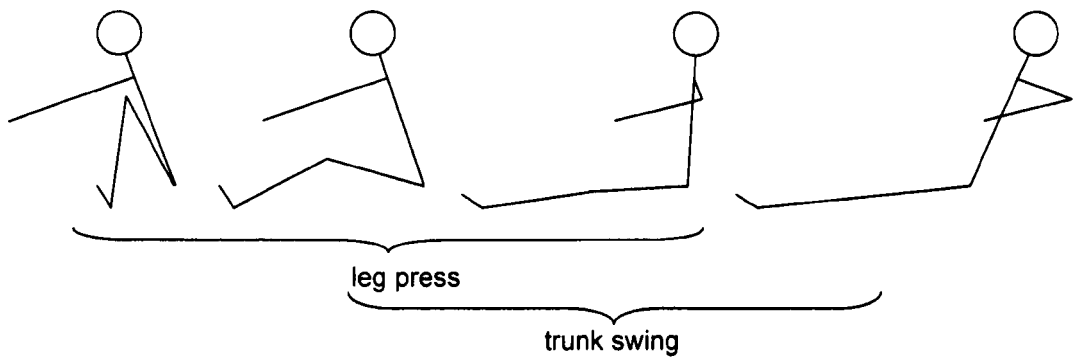


Figure 1.1: The drive phase of the rowing stroke

The recovery phase is the return of the rower from the finish position to the instant before the catch of the next stroke. During the recovery there are many discrete and continuous movements, the sequencing of which is very important. Depending on the number of strokes being performed each minute (stroke rate) and the particular technique of an individual, the drive duration to recovery duration ratio will normally be between 1:3 (low stroke rate) and 1:1 (high stroke rate).

Considering the repetitive nature of this movement, and the volume and intensity of training that is accepted by elite rowers there is undoubtedly the potential for injuries to occur; Great Britain's elite rowers complete 49 weeks of training a year, that is 900-1000 hours, around 8000 km of rowing, including 1000 km on ergometers, plus weight training, cycling, running and circuit training.¹ Hickey et al. (1997) noted the significant incidence of chest injuries, rib stress fractures and low back injuries in elite rowers. Hickey et al.'s (1997) study of ten years of medical records for 172 elite rowers found that in females the most common sites of injury were the chest (22.6%), lumbar spine (15.2%), and forearm/wrist (14.7%), whilst in males they were the lumbar spine (25%), forearm/wrist (15.5%), and knee (12.9%). They also found that chronic injuries were more common than acute injuries: 72.1% vs 27.9%, and 69.8% vs 30.2%, in females and males respectively. Training regimes and rowing technique are thought to be largely responsible for this significant lumbar injury rate (Bull and McGregor, 2000). Consequently an understanding of such injuries, and their prevention and management is paramount if athletes are to perform optimally. Furthermore, 24% of all gold medal races in the last six Olympic Games have been decided by less than 1 second (www.worldrowing.com),²

¹ Personal communication with the coaching staff of the Great Britain Rowing squad.

² Gold medal winning margins for six successive Olympic Games have been: Seoul (1988) – 2.62s, Barcelona (1992) – 1.97s, Atlanta (1996) – 1.98s, Sydney (2000) – 1.52s, Athens (2004) – 1.62s, Beijing (2008) – 1.28s. The times shown are the average margin for all fourteen classes contested at each Olympic Games (www.worldrowing.com – accessed 01/06/2009).

and this has led to a drive to understand the mechanisms by which excellent performance can be achieved, whilst maintaining the health of the athlete.

1.1 Aims

The primary aim of this work was to, describe and analyse performance parameters, the mechanics of movement and three-dimensional kinematics of elite rowers, as captured during ergometer-based exercise.

It was hypothesised that this biomechanical analysis would provide information on how rowing technique may be linked to the prevalence of injury and pain within the sport, and render insight into which discrete aspects of technique influence an athlete's performance. As such this analysis may be used as a valuable coaching tool to analyse this demanding and highly competitive sport, seeking to emphasise and add vigour to coaching philosophy, as well as challenging it and offering new ideas that may provide even the smallest edge at the top level of athletic endeavour.

1.2 Scope of the thesis

In order to objectively measure the data required to accomplish the objectives a number of discrete procedural and methodological issues had to be solved, these included; i) the instrumentation of a rowing ergometer, ii) the development of software that acquired data from this instrumentation and an electromagnetic motion tracking system, and displayed a real-time visual feedback package, iii) optimisation and calibration procedures which would ensure the most accurate data possible could be gathered during testing sessions, iv) designing a robust and repeatable experimental protocol that permitted acquisition of all of the information needed for subsequent analyses, and v) writing various software programs which treated the acquired datasets and provided usable outputs. The first two of these projects are not discussed within this thesis as they were carried out by other researchers (Chee et al., 2009). The chapter following this one highlights the different ways in which rowing performance can be improved, and includes some of the research that has previously been conducted in the field of the current study. The completion of the other tasks listed above is discussed in some detail in Chapter 3, Chapter 4 and Chapter 5. Once these projects have been presented the focus moves on to present and discuss the results obtained from the athlete testing conducted during the course of the current research (PART 2). Here various strands of performance including force profiles and kinematic measurements are considered, before some recommendations as to how an athlete might attempt to improve their rowing technique and avoid injury are offered. Figure 1.2 describes the goals and contents of the thesis.

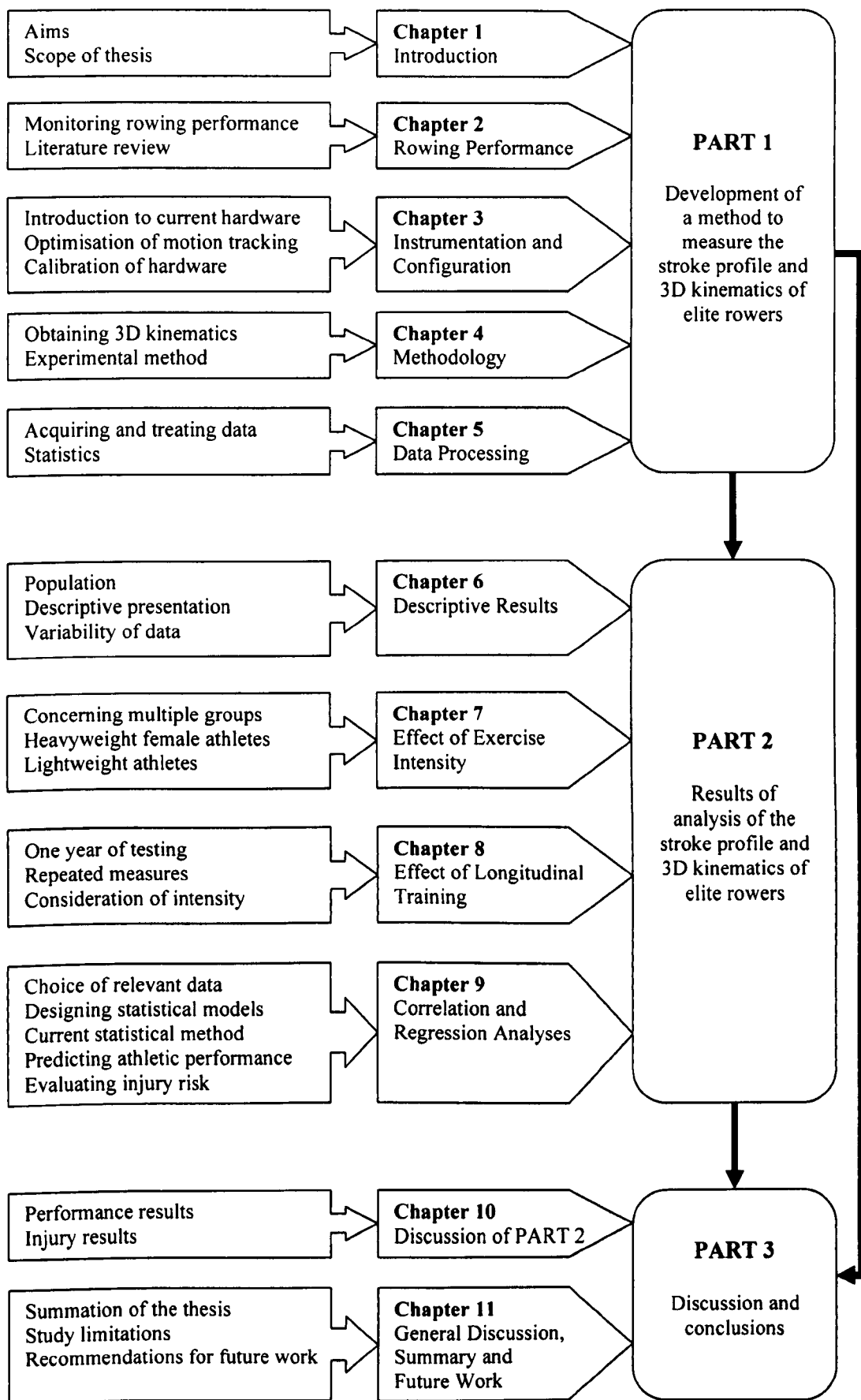


Figure 1.2: The aims and scope of the current research

Chapter 2

Rowing Performance

The aim of this chapter is to introduce the way in which elite rowers exploit many disciplines to achieve the best possible performance in their sport. After an overview of various techniques, more specific attention is paid to some of the biomechanical investigations that have previously considered performance and injury in rowing.

2.1 An interdisciplinary approach

An objective of every competitive rower is to improve their performance, and Nolte (2005) states that there are two ways to row faster:

1. Rowers can produce more energy
2. Rowers can use their energy more efficiently

If we are to follow these principles we might suggest that nutrition, physiology, psychology, sports medicine and sociology can allow the athlete to produce more energy, whilst biomechanics insight into technique modification through optimisation of force and levers, power generation and movement patterns, injury reduction, and equipment design can facilitate more efficient use of that energy.

Nutrition, often referred to as the base for human performance not only provides the fuel for biological work (at both the micro and macro level), but also the chemicals that contribute to energy release from these nutrients. Furthermore, adequate nutrition is vital for gaining elements involved in repairing and synthesizing tissue, and optimising the results of any considerable training regime (McArdle et al., 2001). More specifically for rowing, an elite athlete's nutritional strategy will include consideration of an appropriately balanced diet, ensuring good hydration at all times, possible dietary supplements, pre-race and training intake of fuels, post effort recovery, making weight (depending on restrictions), post weigh-in recovery, and the inclusion of "psychologically comfortable" foods.

Exercise physiology has seen an explosion in popularity over recent decades; in 1966 the number of hits offered by a computer search of Index Medicus (Medline) entire historical database, using the words "exercise" or "exertion" as a topic was 703, by 1996 this number had risen to 2,069, and by the year 2000 this same search yielded 43,625 search results (McArdle et al., 2001). Today the sports physiologist may consider or specialise in (amongst others) energy

transfer, delivery and utilisation, skeletal muscle structure and function, training for aerobic and anaerobic power, the effects of environmental stress (for example altitude and heat), body composition, and disease prevention. In rowing the usual 2000 m race course demands both aerobic ($\approx 80\%$) and anaerobic ($\approx 20\%$) power, and the exercise physiologist will often be involved in measuring aerobic power, cardiopulmonary function and dynamics, blood lactate, and muscle strength and fibre characteristics (Shephard, 1998). Thompson (2005) states that effective rowing requires flexibility, the capacity to produce power, balanced skeletal muscle groups and a strong aerobic capacity. And, in addition to all of the possible considerations of traditional exercise physiology, able bodied (that is, not physically disabled athletes) rowing is particularly complex as it requires coordination of almost every muscle group in the body, places the physiological system under considerable strain during training and racing, comprises both static (e.g. back and arms at the catch) and dynamic activity, and, unlike most forms of human locomotion both legs are used simultaneously (Secher, 1993).

The psychology of elite athletes is another discipline that is considered by many as having a great deal of potential in improving the performance of individuals and teams; according to Weinberg and Gould (1999) most people study sport and exercise psychology to understand how psychological wellbeing can influence a person's physical performance, and to understand how participation in sport affects an individual's psychological wellbeing and development. An applied sport psychologist might help athletes to acknowledge and address issues and techniques such as anxiety, motivation, self-efficacy, team dynamics, goal setting, stress management, confidence, mental imagery, self talk, coping strategies, and concentration (Morris and Summers, 1995). Thompson (2005) reports that in competitive rowing, mental skills and racing strategies should have the same emphasis as physiological adaptations and technical improvement.

In addition to the three disciplines discussed above there is sports medicine, which encompasses many services, though broadly may be described as the prevention, diagnosis and treatment of injury and disease. As elite athletes perform so often, frequently including foreign training camps and competition, and due to the pressures exerted by team selection and media responsibilities, sociology is another key component of an athlete's well being, which can in turn affect their performance.

The application of biomechanics to sport can be divided into three, interrelated, broad areas: technique modification for performance enhancement, injury reduction, and equipment design. An awareness of the mechanics of an athlete's movement equips support staff and athletes with data to help optimise rowing performance and manage rehabilitation and injury prevention

programs. The next section discusses much of the literature that has previously been published concerning biomechanical investigations into rowing activity.

2.2 Technique, performance, and kinematics in land-based measurements

Whilst opinion varies on what the ideal rowing stroke should look like, the rowing action may be considered to virtually be a closed skill,¹ hence it is ideally suited to have biomechanical investigations conducted upon it. Indeed reliability studies that considered short, high intensity endurance events (Macfarlane et al., 1997; Schabert et al., 1999) concluded that testing protocols performed on land based rowing machines provided an excellent mechanism for reliably testing and retesting the performance parameters of athletes.

When a rower adopts the goal of perfecting a particular technique, it is the aim of that athlete to refine the skill to the best of their ability and reproduce their movement and muscle activity patterns stroke after stroke. It is then the role of the coach and sports scientist to observe the technique from their own specialised point of view, identify areas where the technique is not being performed as well as it should be, and search for new refinements of the skill which will improve the performance of the athlete or aid them in avoiding injury.

From a biomechanical point of view this type of observation is performed through the use of specialised measurement systems. These systems vary in level of complexity. Hartmann et al. (1993) used just a single strain gauge and an ultrasound echo system (for pulling force and ergometer handle velocity measurements) to provide data that was then used to describe the performance of world class male and female rowers. Bernstein et al. (2002), Caplan and Gardner (2005) and Colloud et al. (2006b), again using only measures of force and handle displacement, demonstrated ways in which not only performance variables can be analysed, but also technical issues relating to differing ergometer setups, injury and fatigue. Furthermore, in a study of the biomechanical differences seen between different classes of rowers; Smith and Spinks (1995) found that by quantifying only four variables they were able to design a model that was 88.9% effective at identifying novice volunteers, 73.9% effective in correctly grouping “good” rowers, and 100% effective at categorizing elite individuals. Shiang and Tsai (1998) conclude that even a limited biomechanical analysis can be a useful coaching tool.

While the studies cited above, and others, have shown the usefulness of this kind of limited biomechanical analysis, one key component that they did not consider is the way in which an

¹ Closed skill: “A skill performed in a stable or largely predictable environmental setting. The movement patterns for closed skills can be planned in advance” (Kent, 1998).

athlete moves in order to generate the parameters that they considered. That is, none of them measured the kinematics of the rowers. There have however been several investigations that did consider kinematics in conjunction with other measures in rowing, and commented on the need for monitoring technique on the land to help improve on-water technique and to help prevent injuries (Torres-Moreno et al., 2000). The validity of land based measurement protocols are further supported by Lamb (1989) who measured the kinematic behaviour of rowers' trunk and leg segments on the water and on the ergometer and concluded that they exhibit similar patterns, and furthermore are the prime contributors to the drive phase. Pudlo et al. (2005) cited the role of ergometer studies in the laboratory as facilitating reliable comparison inter and intra rower.

As with the simpler analyses cited above, higher level investigations have been performed with various research goals, such as observing the change in sagittal plane spinal kinematics with increasing exercise intensity, and relating this to the development of low-back pain and acute injury (McGregor et al., 2004a; McGregor et al., 2005). Other studies have described the potential injury relevance of lower limb bilateral asymmetries in movement (Colloud et al., 2006a), and noted the changes that occur in sagittal plane spinal, pelvic and lower limb kinematics of elite individuals during prolonged, fatiguing exertions (Holt et al., 2003). While some have investigated the use of statistical techniques, applied to handle force and kinematics data in developing a model of the rowing stroke that would distinguish variations within and between more or less talented rowers, and those with or without a history of back pain (O'Sullivan et al., 2003).

Hofmijster et al. (2008) measured various force profiles, aerobic capacity and body kinematics to investigate the influence of technical skill on rowing stroke power and efficiency. However, the kinematic measures were only used to calculate a trajectory for the whole body centre of mass. They commented that in order to effectively transfer force from the feet to the hands, an athlete should endeavour to maintain good spinal posture through a stiff connection from the hips upwards. By observing measures of external forces and three-dimensional kinematics Halliday et al. (2004) suggested that the majority of segmental motion in ergometer rowing was exhibited by flexion and extension of the joints, though they did note some levels of abduction/adduction and internal/external rotation. Halliday et al. (2004) provided no indication as to the magnitude of these movements. In their study into the effects of repetitive motion, Caldwell et al. (2003) noted the adverse affect that fatigue can have on maintaining good technique, and cited an awareness of increased lumbar flexion and muscular fatigue as being important for injury prevention. Torres-Moreno et al. (2000) reported that compromising technique in an attempt to maximise stroke power can create instability in the lower back and in fact reduce power output. The authors demonstrated four main characteristics in technique that could potentially compromise an effective and safe performance, highlighting the possibility of

undesirable movements inducing microtrauma in the knee, and the potential for injury to the spine if the lower vertebrae were not adequately stabilised through good postural control in the trunk. The above remarks from Halliday et al. (2004) and Caldwell et al. (2003) are also offered by Bull and McGregor (2000). Bull and McGregor (2000) used a combination of kinematic measurements and magnetic resonance imaging to observe rowers' segment poses at various stages of the rowing stroke. The paper suggested that rowers do not deviate much from a sagittal rowing action, and also reported that spinal kinematics change, possibly for the worse, within rowers, when they are fatigued or asked to simulate some often-seen errors in technique. Hase et al. (2004) considered injury prediction when studying the kinematics and kinetics of a rowing population; the study calculated the musculoskeletal loading of a five university rowers, and five non rowers, finding that the rowing group displayed higher contact forces at the knee and higher peak lumbar and knee flexion moments. However the study by Hase et al. (2004) suffered because of its low number of subjects, and due to the fact that only two rowing strokes were recorded and used a representation of an individual's technique.

Other approaches to solving the problem of describing athletes' motion characteristics in the laboratory include, the use of electrogoniometers, and the implementation of bespoke arrangements of potentiometers. Hawkins (2000) developed a system that provided coaches and athletes with quantitative information concerning kinetics and kinematics during training by employing force transducers, a potentiometer (for handle position), and four electrogoniometers attached to the ankle, knee, hip and elbow. While the conclusion was that the system did permit the assessment of performance, several limitations of the study were apparent: the electrogoniometers were reported to be cumbersome and prone to slippage, the protocol could only evaluate the segment and joint position and angle data in the sagittal plane (this is particularly unsuitable for the elbow joint), large errors in joint angles (10-20°) and position (100-150 mm) were computed, and the study assumed that the entire foot did not move before going on to report that this is not a reasonable assumption to make. Page and Hawkins (2003) observed that the kinematic parameters in Hawkins (2000) were not measured, but inferred. The study from Page and Hawkins (2003) used potentiometers, a linear position-measuring transducer, a load cell, anthropometric measurements, and a system of interconnecting aluminium bars attached to the ergometer seat and the rower's shoulders in an attempt to provide an improvement to the setup described by Hawkins (2000). However, as with the earlier study, assumptions and limitations were apparent. For example, a calculation procedure they used assumed that the positions of the hips and shoulders remained fixed relative to the seat, and that all of the joints evaluated could be described as hinges. Furthermore, during an accuracy assessment of the system it was found that errors in the identification of joint positions were as much as 104 mm (Page and Hawkins, 2003).

One study that provides a more comprehensive analysis of ergometer rowing is Pudlo et al. (2005). Here the objective was to provide information that could be used to quantify internal forces and articular moments using the inverse dynamics method. The work cites other studies that have attempted to explain the spinal injuries common to high level rowers, and reports that compressive load peaks at the junction of the fifth lumbar and first sacral vertebrae can be as high as six times the athlete's body weight. The researchers utilised three-dimensional motion tracking and force transducers at the feet, seat, and handle to provide an original data set, which constituted that required to apply inverse dynamics to body segments including the lumbar spine. No description of this data was presented. In addition to this, pre-manufactured force plates, and the manufacturer's reports on component accuracy were relied upon, and the study used a bespoke handle whose design was quite different to that which an athlete would normally use on a rowing ergometer, the impact of which was not addressed.

As the times and distances achieved on ergometers do not necessarily indicate good rowing technique, developing understanding as to how biomechanical principles can manage effective training in rowing is an important goal. Most of the studies that have been cited in this chapter go only so far as to describe kinetic or kinematic profiles seen during rowing activity, and many of these studies include significant limitations (Table 2.1). These profiles are then occasionally linked to other issues, and discuss how certain parameters may change with, for example, fatigue or training status, whilst at other times there is a leaning towards possible explanations for injury mechanisms, or how measured information may be used in an attempt to improve an athlete's performance. The published literature in this field has provided useful insights into various aspects of the sport of rowing. However, there has been no one body of work that has conducted a comprehensive study of elite rowing technique. In addition to this, many previous studies display room for improvement in their methodology and/or the reliability of their measurements. Based on the literature reviewed, and in the light of the aims of this thesis, the following objectives were established: To provide reliable description of how rowers move and generate force, to investigate the effects of exercise intensity and longitudinal training, to make statements about which aspects of technique make a difference to how well an athlete performs, and to suggest ways in which a rower might use biomechanics to protect themselves from injury. The current research conducted three preliminary optimisation studies. These were done to ensure that the measurements recorded during athlete testing were as accurate and reliable as possible. The next chapter discusses this aspect of the current approach.

Study	Kinematics measured	Other measures	Purpose or aim of study	Most pertinent limitations
Bernstein et al. (2002)		HF, HM	Comparing ergo designs – safety	No kinematics
Caplan and Gardner (2005)		HF, HM	Effect of foot position on mechanical effectiveness	No kinematics
Colloud et al. (2006b)		HF, HM, FF, SF	Ergo design and biomechanics	No kinematics
Hartmann et al. (1993)		HF, HM	How max force effects power	No kinematics
Macfarlane et al. (1997)		HF, HM, FF, hr	Describe rowing performance	No kinematics
Schabert et al. (1999)		P, hr, $\dot{V} O_{2peak}$	Reliability of a rowing test	No kinematics
Shiang and Tsai (1998)		HF	Elite vs <i>general</i> – performance	No kinematics
Smith and Spinks (1995)		HF, HM	Biomechanics – elite/good/novice	No kinematics
Bull and McGregor (2000)	Femoral, pelvic, lumbar flexion		Applicability of an EM tracking system	Ltd variables, sagittal plane only, no intersegmental angles
Caldwell et al. (2003)	Lumbar flexion	EMG erector spinae	Change in lumbar flexion with fatigue	Limited variables, sagittal plane kinematics only
Colloud et al. (2006a)	3D lower limbs	HF, FF, SF	Symmetry of the lower limbs	No discussion of back kinematics, limited results published
Halliday et al. (2004)	3D whole body	HF, FF, EMG lower limbs	Functional stimulation of able bodied technique in a spinal cord injured rower	Only sagittal plane kinematics were reported, small <i>n</i>
Hase et al. (2004)	Whole body	HF, FF, EMG right side	Competitive vs non rowers	Sagittal plane of trunk and knee only, questionable accuracy
Hawkins (2000)	Electrogoniometers for ankle, knee, hip, shoulder, elbow	HF, HM, anthropometrics	Develop a system for instantaneous, & post test biomechanics feedback	Goniometers limited motion and slipped, big errors, poor assumptions
Hofmijster et al. (2008)	Whole body – segments	HF, FF, SF	Effect of skill on power output	Kinematics only used to calculate position of whole body COM
Holt et al. (2003)	Femoral, pelvic, lumbar flexion	HF	Identify injury mechanisms & changes in technique with fatigue	2D of limited segments, no intersegmental angles
Lamb (1989)	Whole body	HM	Comparison of ergometer rowing and on water rowing	Sagittal plane kinematics used
McGregor et al. (2004a)	Femoral, pelvic, lumbar flexion	HF	Technique with changing intensity	Ltd variables, sagittal plane only, no intersegmental angles
McGregor et al. (2005)	Femoral, pelvic, lumbar flexion	HF	Spinal kinematics with change in intensity	Ltd variables, sagittal plane only, no intersegmental angles
O’Sullivan et al. (2003)	3D of lower back	HF	Statistical detection of injury mechanisms and rowing ability	Limited variables, results not clinically significant/usable
Page and Hawkins (2003)	2D whole body	HF, HM, anthropometrics	Develop a system for instantaneous, & post test biomechanics feedback	Large errors – up to 103.9 mm and 20° in joint position & angle
Pudlo et al. (2005)	3D kinematics	HF, HM, FF, SF	Inverse dynamical analysis of rowing	No discussion of segment poses or joint angles
Torres-Moreno et al. (2000)	2D kinematics	HF	Biomechanics for performance and safety	Sagittal plane kinematics only

Table 2.1: Previous research into rowing: measurements, aims, and limitations

HF,FF,SF = Handle, Foot, Seat force, HM = handle motion, P = power, hr = heart rate, $\dot{V} O_{2peak}$ = peak O_2 uptake

Chapter 3

Instrumentation and Configuration

This chapter provides an overview of all of the apparatus used during athlete testing. This is followed by sections describing experiments that were conducted to optimise the system's accuracy.

3.1 Hardware

A direct current based electromagnetic motion analysis system that can measure the position and orientation (six degrees of freedom) of its sensors at any instant in time was used during all testing sessions (Flock of Birds, Ascension Technology, Burlington, USA). This study used an extended range transmitter and four sensors on long leads. Reasons for selecting this measurement system are presented in Section 3.2.

A rowing ergometer was used for all athlete testing sessions (Concept 2 model D indoor rowing machine, Concept Inc, Vermont, USA). This ergometer was modified at the handle, the flywheel and the seat (Figure 3.1). A uniaxial force transducer was introduced in series with the handle and handle chain to measure the pulling (tensile) force exerted by athletes. Two rotary encoders that measured the horizontal and vertical movement of the handle were incorporated into the flywheel. Four uniaxial load cells were mounted on the ergometer slide rail to measure the vertical forces exerted by the athlete at the seat (magnitude and centre of pressure) during rowing exercise. These modifications were performed as part of another research project and aspects relating to how this apparatus was commissioned are not presented here (Chee et al., 2009).

A dedicated PC was used in conjunction with custom written software (Chee et al., 2009). This controlled the acquisition of signals and the display of real-time feedback.

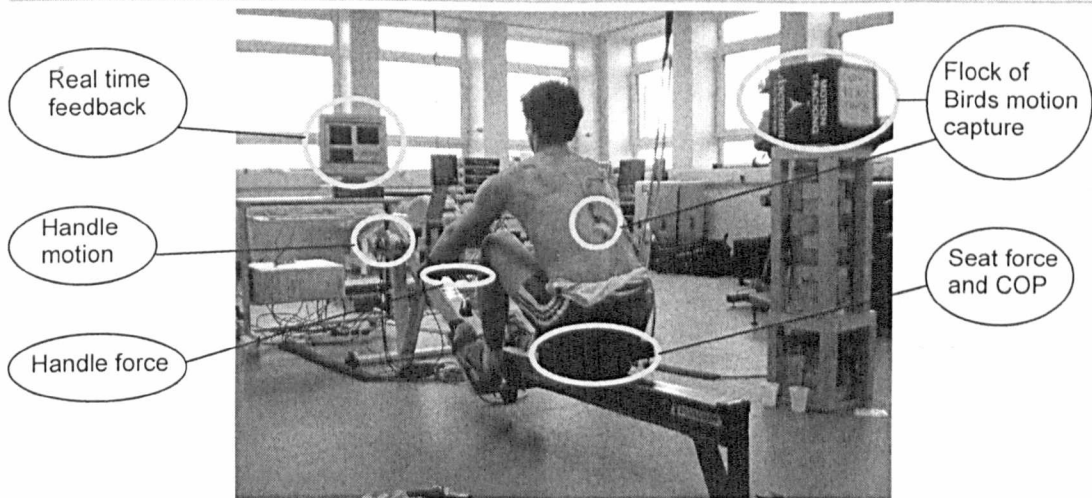


Figure 3.1: The laboratory setup during athlete testing

3.2 Electromagnetic motion tracking and ergometer rowing

Rigid body measurement for human performance analysis has been conducted using accelerometry, goniometry and optical tracking systems. The main disadvantages associated with optical tracking are a requirement to regularly calibrate the experimental volume, and, in three-dimensional assessments, for at least two optical sensors to maintain a line of sight with each of the system's "markers". Accelerometry amplifies translation measurement errors due to the necessity to twice integrate an acquired data set, and while one can assess the motion of whole segments that sensors are attached to, it is difficult to obtain trajectories of specific skeletal landmarks and joint centres of rotation. Goniometry has typically been the preferred method with which to evaluate ranges of motion in the clinical setting. Slobounov et al. (1999) compared range of motion measures in the human knee as recorded through goniometry versus motion analysis by means of electromagnetic (EM) devices. They concluded that the EM system eliminated the problem of goniometer intertester reliability, and it was shown that the EM apparatus provided accurate measurements in all three planes of motion, and detailed movement analysis at complex joints such as the hip and shoulder.

Six degrees of freedom EM tracking is based on the appliance of mutually orthogonal EM fields (Kindratenko, 2001). The measurements are made by utilising low frequency, magnetic field technology and interpreting the interaction of those magnetic fields between three sets of orthogonal coils housed within both a transmitter and its equivalent sensors. The aim of the following review was to examine variables which may be deleterious to accurate performance by EM tracking systems, when used for on-land rowing performance analysis.

3.2.1 Generation of magnetic fields

There are two types of EM trackers: those that use alternating current (AC) and those that use direct current (DC) to generate the required magnetic field. This field generation induces the development of currents in the passive coils contained within the system's sensors. The location and orientation of the sensors are then computed from the resulting currents. AC systems are generally faster with more favourable signal to noise ratios. However, in DC based systems a pulsing sequence is used to generate the magnetic field which is equivalent to regularly turning the transmitter from on to off, this reduces distortion of the field produced by eddy currents which can form in nearby metallic objects. The primary measurements are performed with the three coils in the transmitter emitting no signal; this allows the X, Y and Z components of the Earth's magnetic field to be computed through the sensor. After this, each of the transmitter's three coils are pulsed in sequence and the equivalent current induced in each of the sensor's three coils is recorded. Finally the magnitude of the Earth's magnetic components are subtracted from the measured values and the remaining nine values are transformed into outputs of the location and orientation of the sensor relative to its transmitter (Ascension Technology Corporation, 2002).

3.2.2 Metals and interfering fields

Concept 2 rowing ergometers are constructed from a number of materials including plastic and a significant amount of aluminium. In addition to this the ergometer is a large piece of apparatus, measuring 2.4 m in length with a maximum width of 0.6 m. The aim of this section is to explore and understand the influence that the presence of metals and interfering fields can have on the accuracy of EM motion trackers.

Metallic objects present within an experimental volume can introduce unwanted effects on an EM system's measurement accuracy (Bottlang et al., 1998; Day et al., 2000; McGill, 1997; Meskers et al., 1999; Milne et al., 1996). When a metallic item is present, eddy currents may be generated which in turn can produce secondary magnetic fields. This combination alters the pattern and distribution of intensity of the original field expelled by the EM tracker's source (Jaberzadeh et al., 2005). When a magnetic field is produced by an EM motion tracker it will most likely incorporate various regions of intensity. This could simply be a result of decay with increasing distance from the source, or due to the positioning of sensors. One might expect the deleterious effects of metallic objects to be increased with respect to the intensity of the magnetic field at their location. Indeed, the errors that Jaberzadeh et al. (2005) attributed to field distortion induced by metallic items (0.15-0.36° angular error) was much less than that reported by McGill et al. (1997) (up to 9.35°) where the authors placed metallic objects in the

high concentration zone between source and sensor, while similar items were placed on the lateral borders of the magnetic field by Jaberzadeh et al. (2005). This idea is supported by Bull et al. (1998), who reported that mild steel imparted negative effects on positional accuracy only when the object was positioned between the transmitter and receiver; if the steel was more than 150 mm from both the receivers and transmitter then there was no effect on positional accuracy. In the current study it was specified that during athlete testing the positioning of all of the motion sensors should remain within a constant region of magnetic field intensity, and no metal should be placed between the sensors and the transmitter.

The magnitude of the induced errors due to metallic objects varies with metal type. LaScalza et al. (2003) carried out an investigation into the varying effect of steel and aluminium on the measurement accuracy of a Flock of Birds (FOB) setup. The authors concluded that, in general, error due to steel interference was more pronounced than that of aluminium. The explanation offered for these results concerned the magnetic permeability of the two materials. In short, aluminium is a paramagnetic material, as such the eddy currents formed due to the combination of the DC transmitter's pulses and the aluminium's high conductivity decay quickly. On the other hand, steel is a ferromagnetic material with a much higher magnetic permeability. Thus, eddy currents induced through steel are sustained for longer, and interfere more with the original field generated by the transmitter. This type of distortion is further highlighted by Nixon et al. (1998); here the effects of a wider range of metallic objects on the measurement accuracy of both an AC and a DC EM tracking system were examined. The group investigated mild steel, copper, stainless steel (316), brass, aluminium, and a ferrite. The authors reported that both systems suffered significantly at the hands of the copper, steel, and ferrite; either due to their induction of eddy currents or because of other ferromagnetic effects. One of the main reasons behind the development of DC EM trackers was to attempt to eliminate the unwanted errors imparted by eddy currents. Nixon et al. (1998) state that the AC system was adversely affected by all metals tested, while the DC system (the FOB) was relatively unaffected by eddy currents induced in all metals (with the exception of copper), and subsequently only suffered in performance at the hands of three out of the six materials (copper – eddy currents, steel and ferrite – other ferromagnetic effects). This information supports the choice of the FOB DC system in the current study. Nixon et al. (1998) also investigated the effect of the size of the metal object causing disruption. The important finding here, with respect to the current research, is, that as the surface area of the metal increased beyond 0.2 m^2 the AC device became the worse affected setup. In the current research the main source of metallic interference may be assumed to come from the rowing machine, as this apparatus measures approximately 2.4 by 0.6 m the DC based FOB is more appropriate than an AC system.

The rate at which a DC EM tracking system samples data also has an impact on measurement accuracy in a metallic environment (LaScalza et al., 2003). Due to the pulsating nature of DC devices, measurements can be taken once the eddy currents that have been induced in any nearby metals have begun to decay. LaScalza et al. (2003) found that interference caused by the presence of aluminium increased with sampling rate, whilst steel interference was characterised by the inverse of this relationship. The relevant conclusion of this work was that it is possible to gain some level of control over the negative impact of aluminium in the testing environment by optimising the sampling frequency – explicitly, by lowering the sampling frequency. Mains interference has a significant effect on accuracy (McGill, 1997; Nixon et al., 1998). This relates to sampling frequency as this distortion is most likely due to the potential for aliasing mains interference (Nixon et al., 1998). When in the presence of mains powered appliances the data acquired from an EM tracking system will experience less noise if it is sampled at twice the frequency of the mains. In an attempt to avoid aliasing mains interference one might be wise to select a sampling frequency equal to double that of the mains; 100Hz versus 50Hz (120Hz versus 60Hz in North America). Due to restrictions of the system, in the current study it was not possible to achieve a sampling rate of 100Hz. Thus, in order to minimise the possible negative effect of the mains, the recommendation of Ascension technologies; to have all mains powered appliances separated by at least 1.2 m from the FOB transmitter and sensors was adhered to. Utilizing a lower sampling rate did have a positive influence on the system accuracy regarding the relationship of low sampling rates and the presence of aluminium (above).

A final point concerning interference is the potential noise that can be introduced by the proximity of an EM tracker's receiver leads to the transmitter. Unconsidered arrangement of leads is another source of potential error acquisition when using a particular AC system, but not for the FOB DC system (Nixon et al., 1998).

3.2.3 Transmitter to sensor distance

The use of EM tracking has previously been limited by standard range (SR) systems' short operating ranges, the most popular being effective across transmitter to sensor separations of up to 0.7 m, with errors of less than 2% (Milne et al., 1996). At greater distances increased errors are experienced due to the decay of the magnetic field (Day et al., 2000). One solution to this may lie in the long range (LR) systems that are offered by some manufacturers.

Milne et al. (1996) showed that a FOB device experienced positional measurement error that increased proportionally with the measured distance, 1.80% of stepped displacement size within a pre-defined optimal operating range. A similar assessment of errors was conducted by

Bull et al. (1998), however here the error was found to be 0.23% of a very similar range of step sizes (Milne et al. (1996) = 25 – 152 mm; Bull et al. (1998) = 25 – 200 mm). Périé et al. (2002) noted that the largest source of error in a study investigating the LR MotionStar® system (Ascension Technologies. Inc., Burlington, USA) was magnetic field distortion, and that this increased with the distance between the transmitter and the sensor. Similarly Jaberzadeh et al. (2005) reported the negative effect of increased transmitter to sensor distance when assessing positional accuracy. Furthermore, Jaberzadeh et al. (2005) suggested that the orientation of a sensor with respect to the transmitter impacted negatively on the system's overall positional accuracy. Most other studies in the literature provide results that conflict with Jaberzadeh et al. (2005) on this point, however Day et al. (1998) also eluded to the negative impact of sensor orientation on positional accuracy at extremely high separation ranges. Day et al. (1998) investigated the positional and rotational accuracy of both a SR and a LR Polhemus EM device (Polhemus Incorporated, Colchester, Vermont). The protocol was controlled using a frame and jig and assessed the systems' effectiveness up to transmitter to sensor separation of 2.7 m and 5 m for the SR and LR units respectively. At greater distances the signal deteriorated rapidly. The data collected by the SR set up experienced noise levels more than five times greater than the LR, and while the SR was ineffective beyond 1.5m the long range transmitter operated comparatively well at much greater distances. Day et al. (1998) concluded that the use of LR transmitters would result in decreased noise and orientation errors.

In a multiple sensor set up Bull et al. (1998) stated that in order to avoid saturating any one FOB sensor, the transmitter control unit alters the strength of the magnetic field it produces in response to the distance between the source and the sensor in closest proximity to it. As the closest sensor advances further from the transmitter, the output strength of the field is doubled and redoubled at specified distances, thus if one sensor is much closer to the transmitter than another the distal sensor will suffer in performance. Bull et al. (1998) indicated one must also be aware of the magnitude of distance present between any two sensors. The authors report that having multiple receivers in a system does not markedly reduce overall accuracy. However if two receivers come into very close proximity (≤ 30 mm) there results a significant increase in measurement error.

During rowing exercise athletes utilise their entire body, and it is the overall aim of this research to investigate segmental motion of this activity. The literature can be used to make some methodological decisions. Firstly, the LR version of the FOB is required, secondly the overall positioning of key equipment (the EM transmitter and the ergometer) merits careful consideration, and thirdly the eventual choice of where on the performer the required receivers will be mounted is important, not only to facilitate measurement of the movement under

investigation, but also to avoid any unwanted measurement errors that may be introduced through fixing individual sensors too close to each other.

3.3 Optimisation of the tracking hardware

Having considered all of the information presented in the previous section it was decided to conduct an evaluation of the measurement accuracy of the LR FOB.

3.3.1 Aims

The aims of this study were:

1. To identify an optimal layout for the laboratory.
 - The ergometer is a fixed piece of equipment. Action may occur through the area between the flywheel and the rear of the slider. The most effective way in which the layout of the laboratory could be optimised for FOB performance was to identify the prime location for the transmitter to be positioned in the X,Y,Z directions (Section 3.3.2).
 - After identifying an optimal location for the FOB transmitter a study was carried out to assess the repeatability of transmitter placement.
2. To assess how accurately the LR FOB was able to calculate the orientation and position of its sensors within a relevant experimental volume (Section 3.3.3).

3.3.2 Optimising the laboratory layout

In previous studies into the biomechanics of rowing (Bull and McGregor, 2000; Holt et al., 2003; O'Sullivan et al., 2003) the LR FOB transmitter has been positioned on a $0.4 \times 0.3 \times 0.3$ m (height, length, width) plastic platform. The long axis of the slide on the rowing machine was positioned parallel to the transmitter's Z axis (anterior/posterior) at a distance of 1.25 m from the closest face of the transmitter. The platform was halfway along a line from the rear of the ergometer to the flywheel. The use of long leads for all electrical equipment meant that no electrical apparatus was situated in close proximity to the transmitter (Figure 3.2). In the current study ten transmitter locations were assessed.

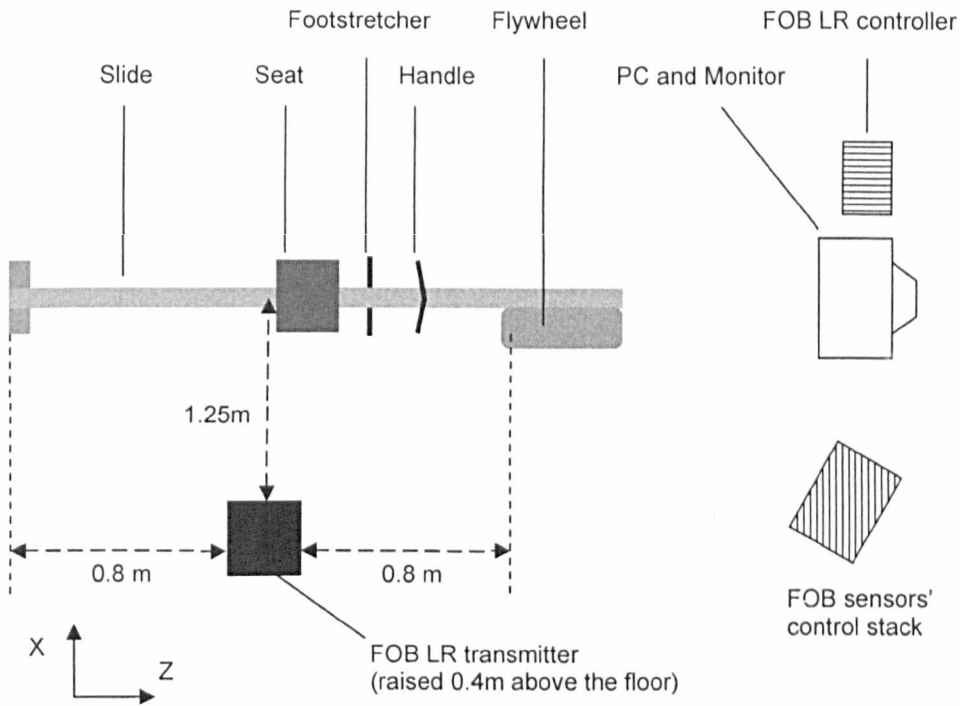


Figure 3.2: Overhead view of the laboratory layout used in previous studies into rowing biomechanics. The axis frame is the FOB transmitter axis system

3.3.2.1 Determination of the aims

In the studies that used the laboratory layout described in Figure 3.2 the midway point from the rear of the ergometer to the flywheel was used because a FOB sensor measured the motion of the ergometer handle. This meant that measurements were recorded from a sensor that moved from the flywheel to the rear of the ergometer in the Z direction. However, in this thesis encoders are used to measure handle travel, thus the furthest point anteriorly that a sensor may travel (whilst attached to an athlete's shank) is approximately in line with the footstretcher. The first direction in which the optimal coordinate for the transmitter was considered was the Z direction. The position of the FOB transmitter was always halfway along a line from the rear of the ergometer to the footstretcher. As stated previously, in order to avoid saturation of any one sensor by the EM field, the field's strength is managed according to the proximity of the sensor closest to the transmitter. Critical ranges reported by Ascension for the LR FOB are 0.61 and 0.76 m transmitter to receiver separation. This means that if all sensors are more than 0.76 m from the transmitter cube then maximum power will be used to generate the magnetic field. This is why 1.25 m separation in the X direction was used in the past. For the purposes of this optimisation it was decided that the performance of the FOB should be assessed with varying magnitudes of transmitter to ergometer x (m). Ascension technologies recommends that in the presence of metal reinforced floors the FOB transmitter should be raised up at least 1m from the

floor. This study tested the performance of the FOB with varying levels of transmitter to floor y (m).

Often in human movement studies the experimental protocol includes a calibration of the experimental volume prior to every kinematic testing session. The purpose of such calibration is to locate the motion tracker's source within a fixed laboratory axis system. The origin and directions of such laboratory axis systems may be defined by other hardware such as force plates, or, by any other permanent feature of the laboratory that does not move over time. This type of calibration was not done during athlete testing sessions in the current study. Kinematic assessment of rowers in the current study involved observing the trajectories of joint centres and intersegment angles (Chapter 4, PART 2, PART 3). Since trajectories were measured within the FOB transmitter's axis frame, it was critical that placement of the transmitter in the laboratory be consistent if comparisons were to be made between testing sessions (Chapter 8, Chapter 9). Furthermore the way in which the ankle joint coordinate system was defined in the current study (Section 4.3) meant that inconsistencies in the orientation of the transmitter could be deleterious to calculations of ankle angles. After identifying the optimal location for the transmitter, a pilot study was conducted to assess the repeatability of transmitter placement.

3.3.2.2 Materials

This study utilised the FOB DC based EM motion tracking system with the extended range transmitter and four sensors on long leads (i,ii,iii,iv). A custom made board, manufactured using medium density fibreboard (MDF), was used throughout all trials as a surface to which the EM sensors were mounted in known positions. The board was $1400 \times 1100 \times 6$ mm, and was backed with six lengths of 75×21 mm wood to ensure a rigid structure. Forty holes were drilled in the main face of the board to provide '*locks*' to the sensors' '*keys*'. The *keys* were small blocks of wood ($35 \times 30 \times 21$ mm) each of which was backed with two 10 mm length, 10 mm diameter chamfered dowels. Each sensor was secured to its *key* and hence could be positioned in any of the twenty *locks* (A-T, Figure 3.3). To prevent ferromagnetic effects being introduced, only PVA wood adhesive and 100% brass fixtures were utilised.

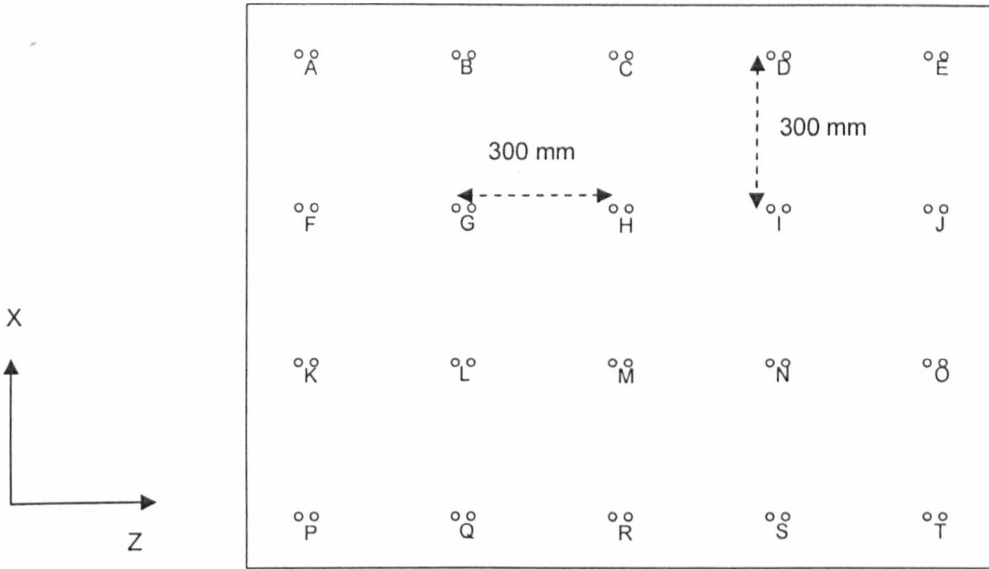


Figure 3.3: The board used during laboratory optimisation trials. The axis frame is the FOB transmitter axis system

3.3.2.3 Experimental methodology

Initially nine positions were used to vary both the height of the transmitter from the floor, and its perpendicular distance from the ergometer slide. During trials the transmitter was 0.95 m, 1.25 m or 1.55 m from the ergometer in the X direction (equal to the location used in previous studies, Figure 3.2, and one transmitter width either side of this baseline). It was elevated 0.40 m, 0.70 m or 1.00 m from the floor (equal to previous investigations, equal to Ascension technologies' recommendation, and the mid point of these two). A tenth position was added after the first results were obtained. This location lifted the transmitter 1.30 m from the floor, and maintained the minimum lateral separation used previously, 0.95 m (Figure 3.4).



Figure 3.4: Location of the FOB transmitter during optimisation trials

In addition to moving the transmitter during the experiment; the board was positioned at three levels of elevation above the ergometer slide. The lowest distance from the ground was 0.43 m; placing the surface of the board just above the ergometer seat, the second height was 0.68 m, and the third was 0.93 m; thus covering a vertical range of 0.50 m (Figure 3.5). The trials were performed with the ergometer in situ, and without.

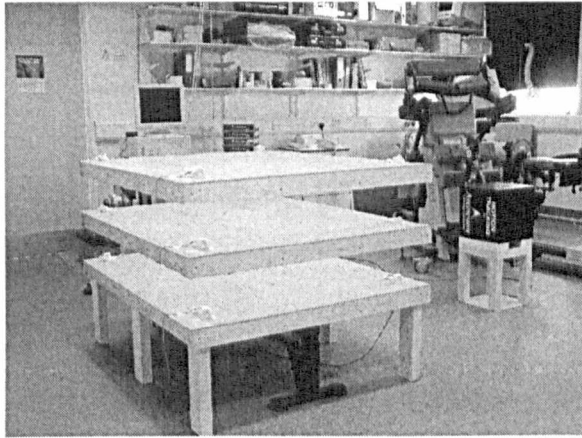


Figure 3.5: Three levels of board positioning during optimisation trials

Using the various transmitter locations (1-10), by raising or lowering the height of the board, by including the ergometer in the laboratory setup or not, and by changing the position of the FOB sensors (during trials sensor i, ii and iii were fixed and sensor iv was moved across the board) 969 arrangements were produced and a recording of the position (X,Y,Z) of each sensor in space logged. The experiment was carried out a total of ten times through which average measurements were computed for each arrangement. Full details of the arrangements used are shown in Appendix 1.

The known vector distance between sensors i & iv, ii & iv, and, iii & iv were compared to their equivalents as measured through the experimental trials, yielding the error of between sensor distance for each arrangement. Because there were 969 arrangements and the distance between sensors i & iv, ii & iv, and, iii & iv was calculated for each, a total of 2,907 values were computed and stored in a 153×19 matrix. Columns 1-10 of the matrix described the errors recorded with the transmitter in locations 1-10 and the ergometer in place, and columns 11-19 of the matrix described the errors recorded with the transmitter in locations 1-9 and the ergometer not in place. For each column the following values were then calculated:

- the average absolute error
- the maximum absolute error
- the sum of the absolute errors

- the sum of the squared errors
- the average error expressed as a percentage of the true inter-sensor distance
- the maximum error expressed as a percentage of the true inter-sensor distance
- the sum of the absolute errors expressed as a percentage of the true inter-sensor distance

In addition to this, independent samples t tests were used to test for differences between the measurements taken using each of the transmitter locations, and the true data set, and also to test for a difference in data produced when the ergometer was in place as to when it was not.

For the analysis into transmitter placement repeatability; a single FOB sensor was positioned in the middle of the *rower* experimental volume. The FOB transmitter and its plinth were then moved in and out of optimal position ten times over a period of four days, during which time the power supply and data acquisition software were switched off and reinitialised several times. When the transmitter was in the optimal location for studying rowing kinematics a recording of the position of the FOB sensor was taken. The average, standard deviation and range of the sensor coordinates in the X,Y,Z directions were used as a measure of the repeatability of transmitter placement. Furthermore, because any deviations in the measured sensor coordinates could have resulted from incorrect positioning of the transmitter in the X,Y,Z direction, or, could have been due to the transmitter being oriented inaccurately, and because of the reliance of ankle joint angles on the direction of transmitter X axis (Section 4.3), the sensor coordinates were used to calculate the maximum mal-orientation of the transmitter that could have induced any measured positional deviations.

3.3.2.4 Results

This section presents the results of the laboratory layout optimisation study, and the analysis of the FOB transmitter placement repeatability. The effect on system performance of the presence of the rowing ergometer, the location of the transmitter, and the global position of FOB receivers is commented on, and the repeatability of transmitter placement is reported.

Effect of the ergometer

The results presented later in this section will show that the maximum and mean errors calculated during this experiment did show some variation when comparing the data logged when the rowing machine was in situ in the laboratory and when it was not. However, the results of independent t tests comparing the data (Table 3.1) show that the performance of the FOB was not significantly affected by the presence of the ergometer for any of the transmitter locations 1-9.

Transmitter location	p-value (ergometer vs no ergometer)
1	.954
2	.973
3	.968
4	.958
5	.974
6	.982
7	.960
8	.965
9	.976

Table 3.1: Effect of the rowing machine on FOB measurement accuracy (independent samples t tests)

Effect of transmitter location

The optimal position for the source is 1.00 m from the floor and 0.95 m lateral to the ergometer slide (location 1, Table 3.2, Figure 3.4). Figure 3.6 shows results of analysis of data collected when the ergometer was in situ in the laboratory. In agreement with the literature, the results obtained show that accuracy of the system is negatively affected when the transmitter is moved further away from the ergometer (and coincidentally, the FOB sensors) and closer to the floor.

	Transmitter location	Average of absolute errors (mm)	Maximum of absolute errors (mm)	Sum of absolute errors (mm)	Sum of squared errors (mm)	Average error as % of true inter-sensor distance	Maximum error as % of true inter-sensor distance	Sum of errors as % of true inter-sensor distance	p-value (observed vs actual)
Ergometer in place	1	8.37	35.59	1280.16	17631.93	1.09	6.15	166.59	0.955
	2	14.53	54.55	2223.73	56218.19	1.94	9.09	296.98	0.788
	3	29.33	89.43	4487.57	211648.98	3.83	14.58	586.37	0.467
	4	11.43	34.26	1749.33	30632.07	1.48	7.49	225.84	0.964
	5	20.26	67.62	3099.94	114324.88	2.68	13.55	410.73	0.652
	6	38.45	116.92	5882.70	366265.91	4.98	19.64	762.57	0.321
	7	16.06	50.64	2457.12	70644.43	2.09	11.94	320.52	0.799
	8	29.12	93.97	4455.31	229618.63	3.82	16.67	585.13	0.481
	9	48.73	142.39	7455.17	573606.83	6.27	21.93	959.41	0.198
	10	7.95	49.64	1216.19	19414.61	1.04	8.17	159.31	0.910
No ergometer	1	7.36	23.60	1126.52	12169.82	1.01	4.02	154.89	1.000
	2	15.30	43.41	2340.78	58361.37	2.07	8.17	317.47	0.762
	3	30.44	83.66	4657.57	226356.37	3.98	13.17	608.55	0.442
	4	11.20	29.54	1713.87	28837.53	1.50	5.90	229.90	0.922
	5	21.30	63.92	3259.38	121014.94	2.82	10.90	432.19	0.629
	6	39.06	112.70	5976.47	379953.67	5.06	16.10	773.99	0.310
	7	16.89	50.17	2584.61	75324.47	2.22	9.13	340.33	0.760
	8	30.16	95.21	4614.27	249062.44	3.93	13.85	601.33	0.454
	9	49.67	144.18	7599.28	605990.72	6.35	18.86	971.01	0.187

Table 3.2: Errors associated with the laboratory optimisation study
The three best performing transmitter locations are in bold type in each column.

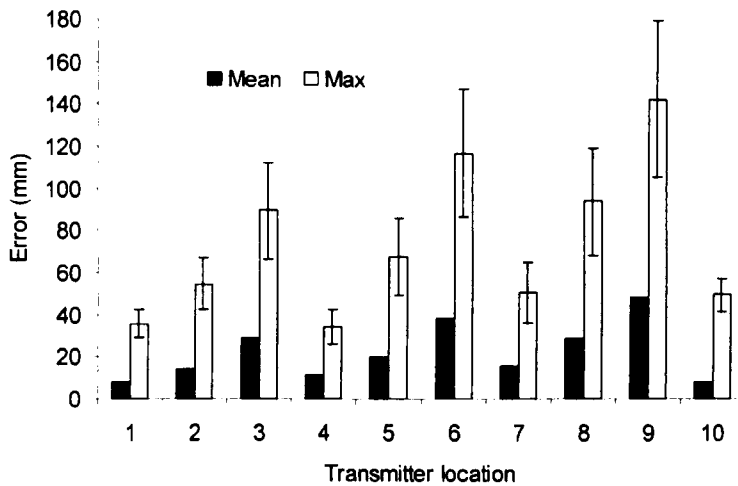


Figure 3.6: Average, maximum and standard deviation of errors recorded during the laboratory optimisation study, with the ergometer in situ
 Measurement error increases as the transmitter is moved laterally further away from the ergometer (and coincidentally, the FOB sensors), and as the transmitter is moved closer to the floor.

Effect of sensor position

The results shown in Table 3.2 represent the data recorded from all 969 arrangements used in the current study. Other data analysis using only the data recorded when the transmitter was in location 1 compared the errors recorded when the board was in its low, middle and high position. The analyses revealed that the vertical sensor coordinate is influential to the system accuracy, with the board in its low (Y) position the average error recorded was between 1.44 and 2.06 times higher than that recorded when the board was at its middle or high elevation (Table 3.3).

Height of the board from the floor	Ergometer in situ: Average error (mm)	No ergometer: Average error (mm)
Low (0.43 m)	12.32	9.49
Middle (0.68 m)	5.97	6.59
High (0.93 m)	6.81	6.00

Table 3.3: The effect of global sensor position of FOB performance

Repeatability of transmitter placement

The maximum, minimum, mean and standard deviations of the sensor coordinates logged during the experiment are shown in Table 3.4. The changes in sensor coordinates calculated could have been the result of incorrect positioning of the transmitter in the X,Y,Z direction, or mal-alignment of the transmitter; application of trigonometry to the FOB sensor coordinates

found that the variations in position could have resulted from up to 1.0° ($\pm 0.3^\circ$) of rotation of the transmitter about its X axis, up to 0.5° ($\pm 0.1^\circ$) of rotation about its Y axis, or up to 0.1° ($\pm 0.0^\circ$) about its Z axis.

Direction	Maximum (mm)	Minimum (mm)	Range (mm)	Average (mm)	Standard deviation (mm)
X	1096.09	1094.53	1.56	1095.21	0.46
Y	-565.46	-566.98	1.53	-566.07	0.49
Z	92.08	82.15	9.93	86.40	2.77

Table 3.4: Sensor coordinates during assessment of the repeatability of transmitter placement
If the repeatability of transmitter placement was perfect, range and standard deviations would be equal to 0.00 mm in all directions.

3.3.2.5 Discussion

The current study used a large experimental volume and considered the accuracy of the FOB system when a rowing ergometer was present in the space and when it was not. The volume utilised provides a good estimation of the space that a person might occupy during a land based rowing task, thus the results presented are valid for the application of analysing rowing activity on an ergometer in the current laboratory.

The most accurate, relative, sensor to sensor position data was obtained with the FOB transmitter positioned 1.00 m from the floor and 0.95 m lateral to the rowing ergometer slide. This conclusion is made despite the average error being 0.42 mm higher for location 1 than location 10 with the ergometer in situ (Table 3.2). The overall variability, and maximum error was less in location 1 than location 10; $p = 0.955$ and $p = 0.910$, and 6.15% and 8.17% of the true inter sensor distance, respectively. With the transmitter in location 1 the FOB performance was never more than 5.26% poorer than any other location, whereas in location 10 the maximum recorded error was 39.48% greater than for location 1. Table 3.2 shows that the data measured when the transmitter was in its optimal location did not vary significantly from the true data series either when the ergometer was absent from the volume or when it was present, $p = 1.000$ and $p = 0.955$, respectively. Of the eight results columns shown in Table 3.2, transmitter location 1 was found to be one of the three best performing locations seven times. Table 3.2 also shows that when considering only the data recorded with the rowing machine in situ, as will be the case during athlete testing, location 1 was always one of the two best performing locations, with locations 4 and 10 being the other, nearly optimal setups.

The negative effect that is shown regarding sensor position (Y) is possibly explained by the influence of metal in the experimental volume. In the current laboratory, as the FOB sensors

were moved closer to the floor they came into closer proximity of the ergometer and the metal reinforcements in the floor. Another possible explanation is that when the sensors were moved across the board at its low elevation the transmitter to sensor separation was greater than when the board was at its middle or high height.

It was found that the transmitter could be positioned in the optimal location with good repeatability. However because of the way in which ankle angles are computed in this work, the small variations in transmitter placement that have been demonstrated may induce small errors in the calculation of joint angles. Chapter 8 looks at the effect of longitudinal training on athlete kinematics; the results of this repeatability study are considered when presenting the findings of the longitudinal investigation.

This study provided no information regarding the FOB ability to measure the orientation of its sensors accurately, or how it would quantify small changes in sensor position. The aim of the next section is to address this point.

3.3.3 Assessing the measurement accuracy of the tracking hardware

In order to evaluate any influence that the orientation of a sensor may have on the measurement accuracy of an EM system Shin (1999) states that one has only to perform experiments for four specific orientations of the sensor; a neutral axis (sensor's axes aligned with that of the transmitter), a 180° elevation, a 180° roll, and a 180° azimuth. Bull et al. (1998) performed an assessment of the accuracy of a short range FOB system using rotational increments of 0.7° to 29.8°. The experimental methodology for the current study was a compromise between such previous research. Furthermore, the way in which rotations in the present experiment were performed permitted analysis of the system's ability to measure small changes in position across a large experimental area. As stated previously, Bull et al. (1998) found that the presence of multiple sensors in a FOB protocol only had a significant effect on the accuracy of the system if two or more sensors were within 30 mm of each other. For ease of data collection, this study utilised only one FOB sensor.

By mounting the FOB sensor in a jig, and taking measurements after rotations about the centre point of this jig, the current experiment aimed to: assess how accurately the LR FOB calculated its sensors' orientation and thus provide a measure of sensor rotation, and, determine how reliably the system could detect small changes in sensor position within a large experimental volume.

3.3.3.1 The experimental volume

By reviewing a database of 774 tests that had previously recorded information on rowing biomechanics, with the laboratory set up as recommended in Section 3.3.2.5, the maximum and minimum x and z coordinates that had been measured by the system in the past were obtained. Due to the detrimental effects on FOB accuracy imparted by transmitter to sensor distance and metal interference reported in the literature, and from the results presented and discussed in Sections 3.3.2.4 and 3.3.2.5 it was only necessary to use the low board height (Figure 3.5). In previous investigations into rowing exercise using this setup and in the accuracy assessment currently under discussion the minimum x coordinates that had been measured by the FOB were 805 and 791 mm respectively. Even if one were to concede that when these measurements were taken the corresponding y and z coordinates were 0 mm and 0 mm, then the displacement along X alone achieves the minimal transmitter to sensor separation required to induce maximal system power output from the FOB (Section 3.3.2.1). Figure 3.7 shows a scale drawing of the current experimental setup. Forty four locations that the FOB sensor was rotated about, the position of the transmitter, the position of the ergometer, and the maximum and minimum historically recorded x and z coordinates are all displayed.

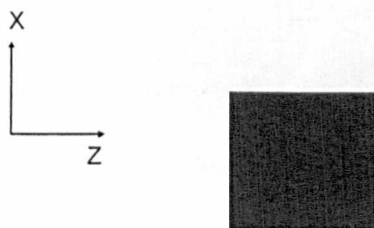
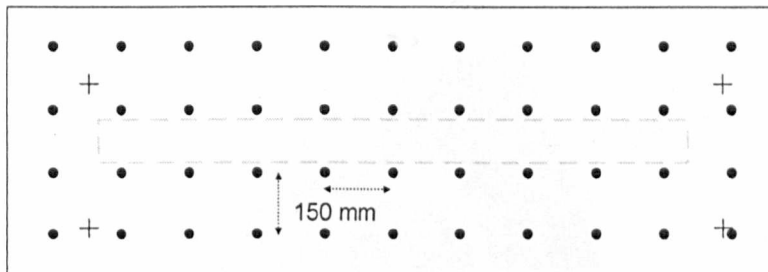


Figure 3.7: Scale view of the experimental setup used during the FOB measurement accuracy assessment

Each circle on the figure shows one of the forty four locations where the FOB sensor was rotated. The large black square is the transmitter, the dashed grey rectangle shows the position of the rowing machine slide rail, and the black crosses illustrate the coordinates of the maximum and minimum x and z positions that have previously been recorded during investigations into rowing ergometry. Overhead view, the axis frame is the FOB transmitter axis system.

3.3.3.2 Materials

This experiment utilised the board that was used in the previous laboratory optimisation study. Additions to this apparatus included adding more holes to the board; this allowed the sensor to be located in increments of 150 mm as opposed to the 300 mm used previously, and the production of a sensor mounting block and block holder to which a FOB sensor was attached.

The mounting block was a plastic cube of side 83.7 mm (Figure 3.8). The sides of the cube were numbered and marked 1-6. A section was cut from the block to allow a FOB sensor to be mounted within the space using two nylon screws, thus the sensor could be rotated about any of the original cube edges by 90° . The only edges that were not usable were those that would have resulted in the extruding sensor cable protruding from the lower most cube surface. The centre of the cube and the origin of the sensor were not coincident. The block holder was a piece of 21.0 mm thick plastic. This item had holes of diameter 10.0 mm drilled through it whose centres were the four corners of a 150.0 mm square, these could be positioned over four holes on the board and secured using wooden dowels. An 84.0 mm square was cut out of the centre of the block holder to accommodate the mounting block. The centres of the 150.0 mm and 84.0 mm squares were coincident and their sides parallel.

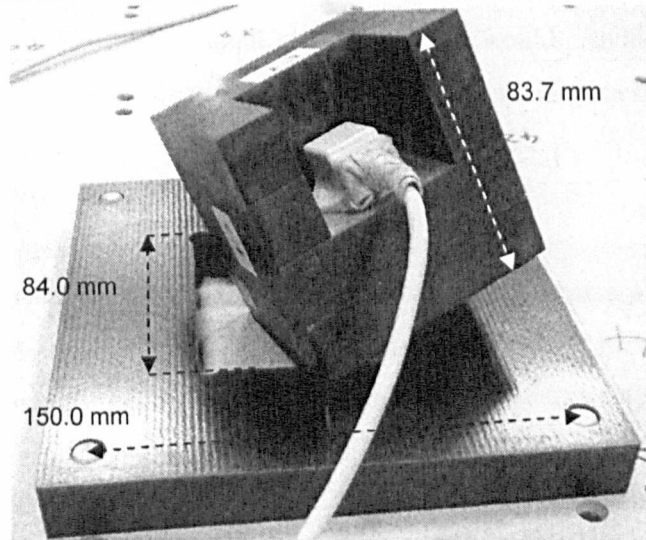


Figure 3.8: Sensor mounting block and block holder used during the FOB accuracy assessment

3.3.3.3 Experimental methodology

The sensor was rotated nineteen times by 90° , from a starting orientation. These rotations were carried out, from the same starting orientation, in the forty four separate locations within the predetermined experimental volume.

Each data point collected was in the form of an x , y and z positional coordinate, and a 3×3 orientation matrix. For each of the forty four locations, twenty recordings were taken; these were the starting position and orientation, and the position and orientation after each of the nineteen rotations. The starting orientation of the sensor was the same for each location and subsequent rotations of 90° were carried out in the same order for each location in the experimental volume. Four recordings were taken with each of the five cube faces matched to the surface of the board, separated by 90° rotations about the global Y axis (one cube face was not usable because of the extruding sensor cable). Thus twenty sets of positional coordinates and twenty orientation matrices (one baseline plus nineteen rotations) were collected with the mounting block and holder in each of the forty four experimental locations.

As the centre of the mounting block and the origin of the sensor were not coincident, when each rotation was made during the trials the sensor shifted in position by a small amount. Thus the change in position was measured nineteen times for each of the forty four locations. It was not possible to determine in advance what the changes in x,y,z magnitude would be as a result of the rotations because the exact vector between the origin of the sensor used in this study and the centre of the mounting cube was unknown (and was not required for the experiments in this thesis). However, because the sequence of rotations was the same for all forty four locations within the experimental space it was known that the change in x,y,z magnitude from one orientation to the next should be the same regardless of the location. It was also known that these changes in position would be small, thus the dataset would provide information on how reliably the FOB could measure small changes in position over a large area.

3.3.3.4 Computations – orientation

An approach using measurements about a helical axis was used to assess the FOB accuracy for the rotations performed during the trials. A helical axis is one about which any combination of three rotations about a typical X,Y,Z axis frame can be expressed as a single rotation of θ° .

The method described by Bull et al. (1998) was used to calculate θ for the 836 rotations involved in the study. The output recorded by the system during the current study comprised an x , y and z coordinate, and a 3×3 orientation matrix (\mathbf{A}), where:

$$\mathbf{A} = \begin{bmatrix} \cos y \cos z & \cos y \sin z & -\sin y \\ -\cos x \sin z + \sin x \sin y \cos z & \cos x \cos z + \sin x \sin y \sin z & \sin x \cos y \\ \sin x \sin z + \cos x \sin y \cos z & -\sin x \cos z + \cos x \sin y \sin z & \cos x \cos y \end{bmatrix}$$

Hence, for any one location the matrix that describes the rotation from \mathbf{A}_n to \mathbf{A}_{n+1} can be found by the equation:

$$\mathbf{A} = \mathbf{A}_n \mathbf{A}_{n+1}^{-1}$$

subsequently:

$$\cos \theta = \frac{1}{2} [(\mathbf{A}_{11} + \mathbf{A}_{22} + \mathbf{A}_{33}) - 1]$$

3.3.3.5 Computations – position

In order to measure the change in position induced by rotations; x_n, y_n, z_n were subtracted from $x_{n+1}, y_{n+1}, z_{n+1}$, for $n=0:18$ rotations, for each of the forty four locations. A 3×19 matrix consisting of $\Delta x, \Delta y, \Delta z$ for each of the rotations was calculated for each location. The 3×19 average and standard deviation matrices were then calculated for these forty four datasets to give a measurement of how robust the system’s measurement of sensor position was across the entire volume.

3.3.3.6 Results – orientation

Table 3.5 shows that on average the FOB was capable of measuring the magnitude of a rotation to within 0.10% of the true rotation, in this case equivalent to 0.10° , with a maximum error of 0.85° . With reference to this level of error it should be remembered that the mounting block was of side 83.70 mm and the block holder was of side 84.00 mm. An analysis of these dimensions and the application of trigonometry tell us that it is conceivable that despite the current study’s assumption that all rotations were 90.00° exactly, this number could be incorrect by up to 0.21° .

True θ ($^\circ$)	Max θ measured ($^\circ$)	Min θ measured ($^\circ$)	Ave θ measured ($^\circ$)	SD ($^\circ$)
90.00	90.58	89.15	89.99	0.25

Table 3.5: FOB system accuracy for orientation

Figure 3.7 illustrated the laboratory layout that was utilised during this accuracy assessment. The forty four locations used in the experiment can be described by eleven columns of four elements, for example locations 1-4 are the furthest to the right in Figure 3.7 with 1 being closest to the transmitter and 4 being the furthest away. Furthermore we can see that in any one of these columns the middle two locations are closer to the ergometer slide than are the first and

the last location on the column. Figure 3.9 shows the maximum error recorded for any one rotation at each of the locations used during the experiment, and Figure 3.10 illustrates the magnitude of all of the errors calculated from the data.

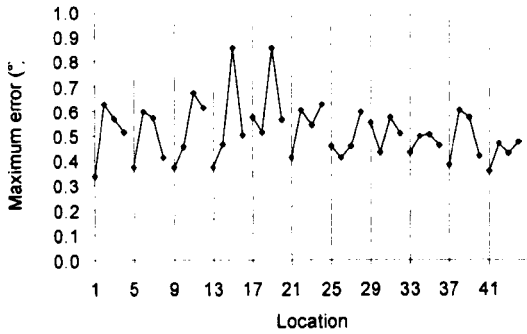


Figure 3.9: FOB system accuracy for orientation. Maximum measurement errors
The eleven series shown indicate the maximum deviation from $90^\circ (\pm)$ that occurred during data acquisition. Data describes all forty four locations used in terms of eleven columns of four locations.

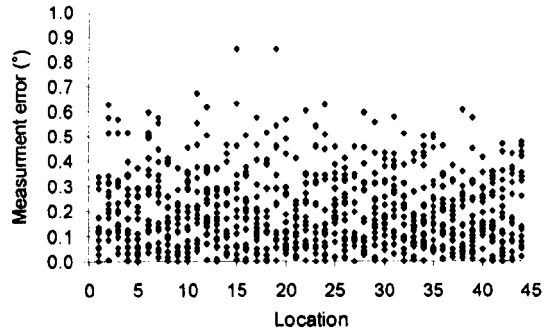


Figure 3.10: FOB system accuracy for orientation. Measurement error for all sensor rotations
Data is shown for all 836 rotations (44 locations with 19 rotations each) performed in the current study.

3.3.3.7 Results – position

The data presented in Table 3.6 and Figure 3.11 shows that the FOB has good repeatability when measuring small changes in the position of the system sensors in the X, Y and Z directions. The relative variability of measurements may be slightly higher when considering very small changes in coordinate ($<$ approximately 4 mm); on average the magnitude of the standard deviations in such cases are 1.78 mm.

Rotation	Average (\pm SD) Δx		Average (\pm SD) Δy		Average (\pm SD) Δz	
1	4.43	(1.38)	-0.85	(1.65)	21.72	(1.78)
2	24.22	(1.58)	1.97	(2.69)	-0.60	(2.04)
3	-4.46	(1.68)	1.42	(3.37)	-25.81	(2.23)
4	-9.66	(1.40)	-9.77	(1.29)	-0.83	(1.19)
5	-13.00	(1.48)	-2.18	(1.62)	14.42	(2.80)
6	14.40	(1.86)	1.83	(1.73)	15.62	(2.93)
7	11.98	(1.63)	0.18	(1.49)	-13.98	(1.51)
8	-0.05	(1.61)	8.26	(1.77)	-11.45	(1.29)
9	-23.70	(1.87)	-0.93	(2.45)	-3.53	(1.67)
10	-3.44	(1.68)	-1.85	(1.69)	21.24	(1.78)
11	23.66	(2.11)	1.25	(2.30)	7.42	(1.67)
12	-9.66	(2.34)	10.28	(1.35)	-2.85	(1.76)
13	14.97	(1.70)	1.65	(1.36)	-12.18	(2.93)
14	-14.15	(2.26)	0.68	(2.10)	-12.59	(3.13)
15	-15.96	(1.56)	-3.60	(1.75)	11.85	(1.46)
16	25.52	(1.71)	7.00	(2.20)	0.87	(1.30)
17	-10.86	(1.11)	-0.86	(1.10)	-10.16	(1.97)
18	-10.40	(1.10)	-1.75	(1.27)	8.84	(0.87)
19	11.56	(0.82)	1.81	(1.20)	10.35	(0.90)

Table 3.6: FOB system accuracy for position

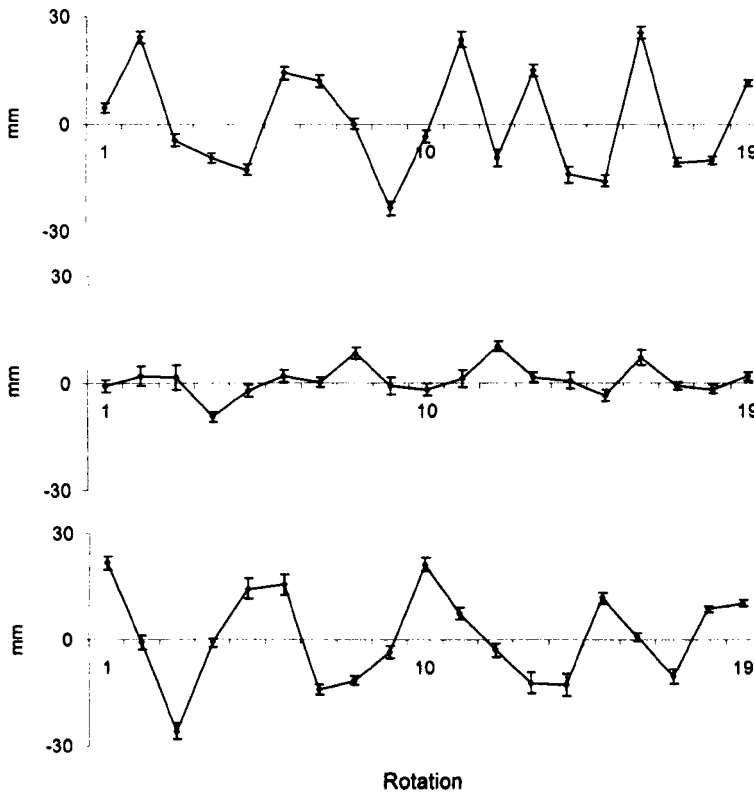


Figure 3.11: FOB system accuracy for position

The top graph shows the change in x , the middle shows change in y and the bottom shows change in z position. Each point on a graph is the average of the change in position recorded for the forty four locations, in the appropriate direction that was induced by the n th rotation. The errors bars show the standard deviation of the measurements.

3.3.4 Discussion and conclusions

The results of the current optimisation study show that in a working laboratory with a large experimental volume, and with careful examination of the space, the LR FOB is capable of measuring the relative position of multiple sensors to within 6.15% of the true inter-sensor distance, and are accurate to 8.37 mm. The patterns of data shown in Figure 3.6 and Figure 3.9 show that maximum FOB measurement errors increase with increasing transmitter to sensor distance, and when sensors are in closer proximity to metallic objects; this is in agreement with the literature. Considering overall system performance, Figure 3.11 shows that there was no particular location in the experimental volume that was repeatedly more deleterious to the accuracy of the FOB. The results presented in Section 3.3.3.6 show that the FOB can measure rotations accurately within the laboratory involved in the current study, and furthermore is capable of consistent detection of small changes in the position of the system sensors.

Often when manufacturers assess the quality of their systems, the work is conducted in an idealised environment that is not applicable to clinical or applied situations. It was deemed not to be necessary for the current study to evaluate the LR FOB system in an ideal environment, before progressing to a more realistic and meaningful one. This decision was made because the system under investigation would not be used in an ideal environment during athlete testing, and was supported by the work presented by Périé et al. (2002). A literature search suggested that the results obtained by Périé et al. (2002) exhibit the most accurate performance of an extended range electromagnetic motion tracking system previously evaluated in an applied setting. By utilising a wooden frame and jig, and with a view to developing a recommendation for an EM system's suitability for measuring action during lifting tasks, Périé et al. (2002) examined the measurement accuracy of the LR Motion Star® across a volume of $1.4 \times 0.8 \times 1.2$ m. In a laboratory, with computer hardware, and a force platform (both initialised and turned off) in situ in the measurement space, and after performing a calibration procedure based on the work by Day et al. (2000) the authors achieved overall positional and rotational accuracy of less than 20 mm and 2° respectively. The internal hardware of the FOB extended range setup is identical in function to the Motion Star® extended range setup¹.

The results of the experiments presented in this section describe the measurement accuracy of the LR FOB as in keeping with, or better than that reported in the literature. The system is a suitable technology for measuring the trajectory of moving body segments and thus the kinematics of rowers during ergonomic training.

¹ e-mail communication with Ascension Technology Corporation.

3.4 Seat instrumentation calibration

Force plates are a standard tool for the measurement of kinetic information related to human movement. They are generally used to measure the three-dimensional characteristics of the magnitude, direction and position, or in the case of distributed masses the centre of pressure (COP) of loads applied to them during activity. However, in previous experiments with traditional piezoelectric force plates, errors of up to ± 30 mm in determining the position of force application have been reported (Bobbert and Schamhardt, 1990). This issue has been addressed by attempting to calibrate specific laboratory's equipment in situ (Bobbert and Schamhardt, 1990; Cappello et al., 2004; Fairburn et al., 2000; Gill and O'Connor, 1997; Schmiedmayer and Kastner, 2000), by providing recommendations on quality control procedures (Browne and O'Hare, 2000; Fleming et al., 1997; Rabuffetti et al., 2003), and by implementing "spot check" protocols (Baker, 1997). The current study investigated the accuracy of a bespoke arrangement of force transducers designed to measure the magnitude and COP of the vertical component of force on the seat of an instrumented rowing ergometer.

3.4.1 Equipment and laboratory setup

The ergometer used for testing was instrumented with four uniaxial load cells mounted on the ergometer slide rail (Figure 3.12). The development of the instrumentation used a redundant approach, and also provided a bracket to which the seat could be attached in the usual way. In this case the redundancy of the design refers to the fact that the system could have used only three load cells. Shear forces were assumed to be negligible and thus were not measured (Pudlo et al., 2005). This setup was designed to provide information on the vertical component of force, and position of the COP of an athlete whilst they performed rowing exercise.

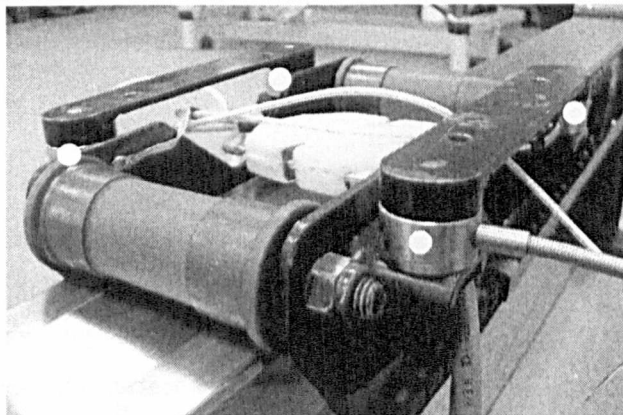


Figure 3.12: Ergometer seat bracket and force transducers
The position of the transducers is highlighted by the white circles.

Several weights of known mass were utilised and a “vertical point loading apparatus” (PLA) was designed and built. The PLA included three sections of box steel: two supports and a cross beam. A circular hole was machined through the cross beam and a linear bearing assembly mounted in the space. A collar and loading platform were also produced; these items were bolted together and provided a mechanism whereby loads could be added incrementally. A hole of diameter 11 mm was drilled orthogonally into the end face of the bearing shaft, and a tight fitting ball bearing was then half sunk into this hole to minimise the footprint of the PLA (Figure 3.13). The design was based work by Hall et al. (1996).

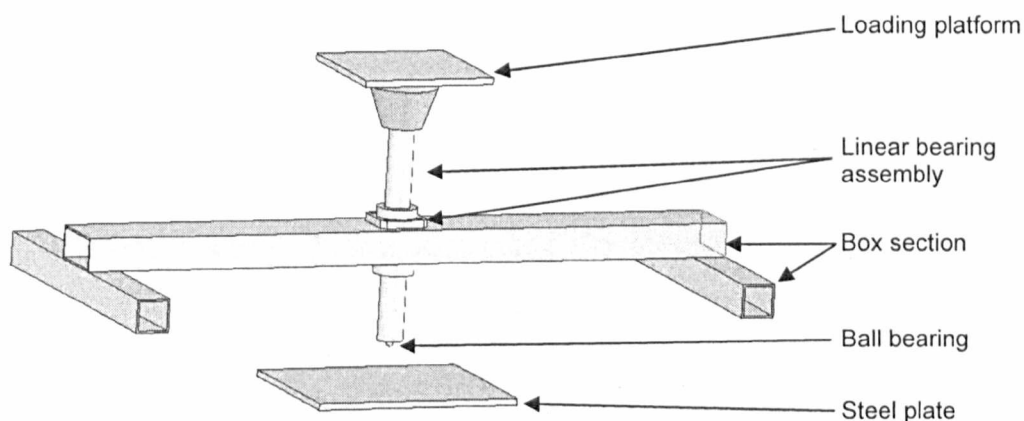


Figure 3.13: Vertical point loading apparatus for seat force calibration

An MDF template whose dimensions were equal to those of the steel plate shown in Figure 3.13 was produced. Multiple holes were drilled through its main face at regular intervals, the diameter of which were less than that of the PLA’s end ball bearing. This grid was used for alignment of the PLA. The steel plate was attached to the ergometer in place of the usual seat and the PLA was positioned above this. Spirit levels were then used to ensure that both the ergometer and the PLA were mounted horizontally and thus the steel plate and loading platform were orthogonal to the bearing shaft. The aim of the current study was to quantify the measurement accuracy of the instrumented seat and, if necessary, perform a calibration.

3.4.2 Experimental methodology

Eleven loading conditions ranging from 0 N to 940 N were applied at twenty five locations (30 mm increments covering -60 mm to 60 mm anterior/posterior (Z) and -60 mm to 60 mm medial/lateral (X)) across the surface of the plate. Thus twenty five trials were conducted, one for each position. Prior to each trial precise positioning of the PLA was ensured by attaching the alignment grid to the steel plate and then matching the PLA’s half sunk ball bearing with the appropriate drilled hole for the current trial. After this the loading platform, bearing shaft and

alignment grid were removed and the load cells zeroed. The duration of each trial was 7 min 20 s. First data was sampled under no force application for 20 s, then a 20 s period was allowed during which time a load was added to the system, this was followed by 20 s uninterrupted data collection, before another load was added to the previous level. Of the 20 s periods during which there was no addition of force only the data collected during the middle 10 s (500 data points) was selected for analysis. This was to ensure against any sway induced in the setup through the application of weight. Table 3.7 describes one full trial. When the practical aspect of the experiment had been completed the measured force and COP values were compared to the true values.

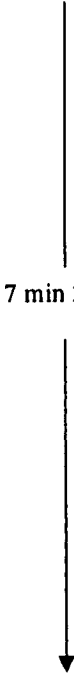
N applied = 0	
20 s data collection	
Addition of load, N = 33.35	
20 s data collection	
Addition of load, N = 100.06	
20 s data collection	
Addition of load, N = 211.90	
20 s data collection	
Addition of load, N = 323.73	
20 s data collection	
Addition of load, N = 435.56	
20 s data collection	
Addition of load, N = 547.40	
20 s data collection	
Addition of load, N = 645.50	
20 s data collection	
Addition of load, N = 743.60	
20 s data collection	
Addition of load, N = 841.70	
20 s data collection	
Addition of load, N = 939.80	
20 s data collection	

Table 3.7: Experimental trial protocol during seat calibration

3.4.3 Computations

Initial calculation of force and COP from the transducers' voltage outputs were performed based on principles outlined in Winter (2005). It was assumed that the arrangement of equipment qualified the instrumentation as a traditional force platform. The vertical component of force and position of COP were calculated using the equations:

$$F_Y = F_{OO} + F_{XO} + F_{OZ} + F_{XZ}$$

Where F_Y is the vertical component of force exerted on the system, and F_{OO} , F_{XO} , F_{OZ} and F_{XZ} are the forces measured by the individual transducers (Figure 3.14).

$$z = \frac{Z}{2} \left[1 + \frac{(F_{OZ} + F_{XZ}) - (F_{OO} + F_{XO})}{F_Y} \right]$$

Where z is one component of COP position and Z is the distance in the Z direction between the central axes of transducers (Figure 3.14).

$$x = \frac{X}{2} \left[1 + \frac{(F_{XO} + F_{XZ}) - (F_{OO} + F_{OZ})}{F_Y} \right]$$

Where x is one component of COP position and X is the distance in the X direction between the central axes of transducers (Figure 3.14).

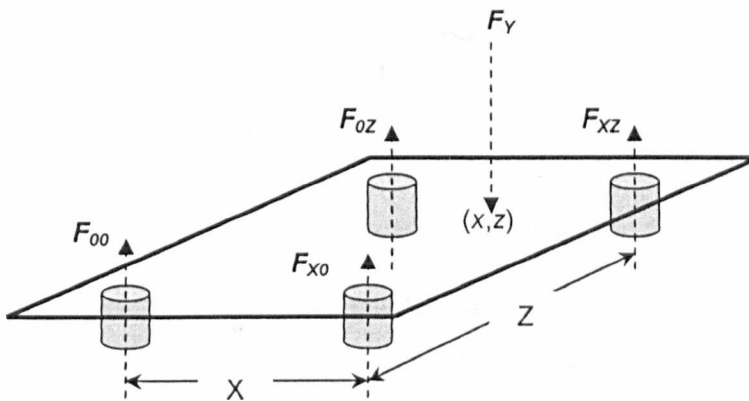


Figure 3.14: Ergometer seat instrumentation schematic

The information calculated by manipulating the transducers' signals as described by Winter (2005) was unacceptably imprecise. Hence a new method was devised to compute force and COP based on the values output by each of the transducers. This was conducted using Matlab (The MathWorks, Inc, Natick, Massachusetts, USA), was implemented with the software's left divide function, and included a minimisation of errors process based on a least squares solution. As twenty five trials were conducted, each of which included eleven loading conditions, and five hundred data samples were collected for analysis during each of these intervals, 137,500 (n_1) individual recordings were made of the voltage output by each of the four transducers.

The force magnitude was computed as shown below:

1. Create an $n_1 \times 4$ matrix containing the raw transducer signals (A)
2. Create an $n_1 \times 1$ matrix containing the known force values ($F_{y \text{ known}}$)
3. Calculate the solution in the least squares sense to

$$A \times C_1 = F_{y \text{ known}}$$
4.
$$C_1 = A \setminus F_{y \text{ known}}$$
5.
$$A \times C_1 \approx F_{y \text{ known}} = F_{y \text{ calculated}}$$

Where C_1 is a 1×4 matrix of unchanging multiplication constants. A measure of how effective C_1 was at predicting the true magnitude of the vertical component of force was found by comparing the descriptive statistics of $F_{y \text{ calculated}}$ and $F_{y \text{ known}}$.

The z component of COP was calculated as shown below:

1. Create an $n_1 \times 4$ matrix containing the raw transducer signals (A)
2. Create an $n_1 \times 1$ matrix containing the known force values ($F_{y \text{ known}}$)
3. Create an $n_1 \times 1$ matrix containing the known z positions (z_{known})
4.
$$F_{y \text{ known}} \times z_{\text{known}} = M_{a/p \text{ known}}$$
5.
$$C_2 = A \setminus M_{a/p \text{ known}}$$
6.
$$A \times C_2 \approx M_{a/p \text{ known}} = M_{a/p \text{ calculated}}$$
7.
$$M_{a/p \text{ calculated}} / F_{y \text{ calculated}} = z_{\text{calculated}}$$

$M_{a/p}$ is the anterior/posterior moments that were applied to the system as a result of the coordinate at which F_y was exerted. A measure of how effective C_2 was at computing the true z position was found by comparing $z_{\text{calculated}}$ with z_{known} . x was computed by the same process as for z , but using the appropriate known x values in place of z .

Initial results showed improvement on the previous technique. However, errors were still present in the calculated data. Hence a second and a third calibration were completed using the same data set, minus that which was recorded when the applied force was less than 100.06 and 211.90 N, respectively. That is, the steps outlined above were completed for a second and a third time with n_1 substituted for n_2 and n_3 respectively ($n_2 = 112,500$, $n_3 = 100,000$).

3.4.4 Results

The errors that led to the second and third calibrations were increasingly variable when the applied load was less. In this results section only the results of data analyses using the Winter (2005) method, on the data set where n_3 was relevant is used for comparative purposes. The maximum and mean system errors realised by the Winter (2005) computation method were equal to 4.45% and 2.41% of the applied load, and 31.37 mm and 17.77 mm for force magnitude and COP respectively. The post calibration maximum and mean system errors were equal to 2.95% and 0.51% of the applied load, and 3.43 mm and 1.10 mm for force magnitude and COP respectively. These errors in COP location are the resultant error in the plane of the loading platform, in the anterior/posterior direction the maximum and mean post calibration errors were 2.57 mm and 0.72 mm, and in the medial/lateral direction were 3.38 mm and 0.67 mm. Figure 3.15 shows that the calibration decreased the average error of force measurement by between 80% and 85%. This improvement achieved accuracy to ± 2 N. Figure 3.15 also shows that after calibration procedure 3 the magnitudes of error reported for COP measurement had decreased by more than 90% (anterior/posterior) and 95% (medial/lateral). This development provided computations to within 1.10 mm of the true position. The improvement in COP calculation is further highlighted by Figure 3.16 where the direction and magnitude of the errors using the Winter (2005) method and the new method are illustrated.

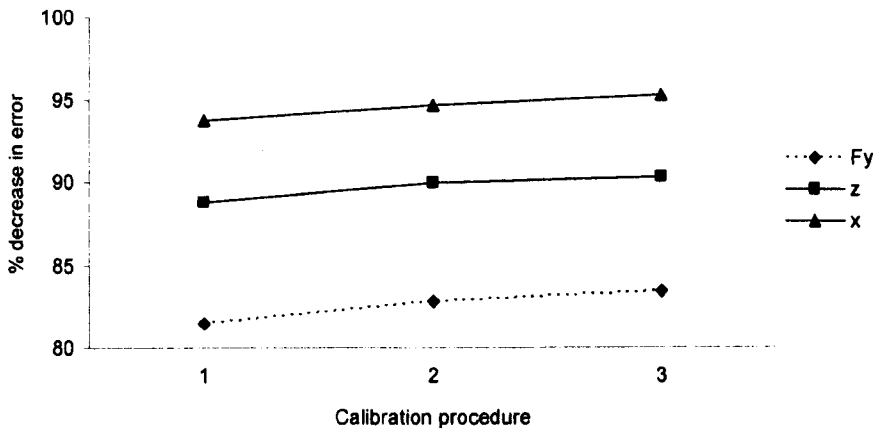


Figure 3.15: Reduction in measurement error from the seat calibration experiment

The figure shows the reduction in the magnitude of average errors resulting from the three calibration procedures, as compared to the computations performed using the method described by Winter (2005). The dashed line shows the results for vertical force magnitude, and the results for z and x coordinate of COP are shown by the solid lines.

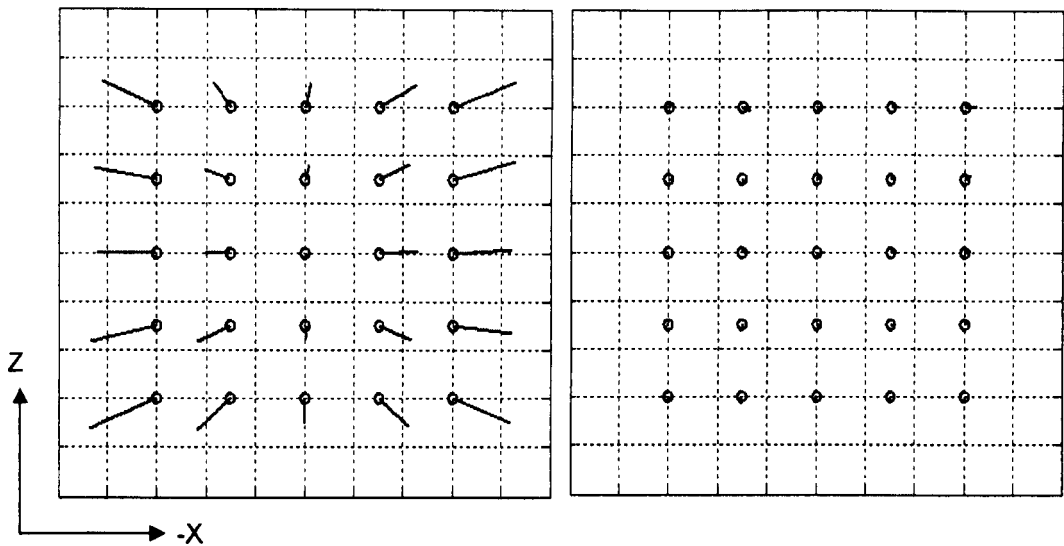


Figure 3.16: Impact of the seat calibration study on COP measurement

Each of the dashed squares in the figure is of side 20 mm. The circles show the true position of the applied load, and the solid lines show the magnitude and the direction of the error in the calculated value. The results displayed on the left are pre calibration, and on the right is post calibration.

3.4.5 Discussion and conclusions

Bobbert and Schamhardt (1990) state that strain-gauge and piezoelectric force platform manufacturers detail the accuracy of their systems as being within 2% for force measurement, and up to ± 30 mm in determining the position of force application. The instrumentation calibrated in the current study achieves mean accuracy of force measurement and maximum and mean calculation of COP location to well within these standards. Table 3.8 details results concerning the accuracy of force and COP measurement systems from two previous studies and the current study.

	Equipment assessed	Mean error in vertical force (%)		Mean error in COP location (mm)	
		Pre-calibration	Post-calibration	Pre-calibration	Post-calibration
Current study	See Chee et al. (2009)	2.41	0.51	6.9(z), 14.7(x)	0.7(z), 0.7(x)
Bobbert and Schamhardt (1990)	KISTLER type 9287	NA	NA	3.5(x), 6.3(y)	1.3(x), 1.6(y)
Gill and O'Connor (1997)	AMTI OR6-6-1000	2.80	NA	Reports "comparable" results to Bobbert and Schamhardt (1990)	

Table 3.8: Comparison of measurement errors relevant to the seat instrumentation

The linear nature of the errors reported pre calibration (Figure 3.16) suggests that the problem with the system may have been that the original software was not set up accurately enough. More specifically, this is likely to have been an error in defining where in space each of the force transducers were in relation to each other and hence the origin of the system. That is, referring to Figure 3.14, Z and X might have been set at too high a magnitude. Similarly, the force transducers' original calibration may have had errors.

This study has provided an effective method of transforming the signals obtained from an innovative application of force transducers to provide meaningful and valid information on the magnitude and position of forces exerted on the apparatus. The instrumented seat is suitable for research into rowing technique.

3.5 Summary

This chapter has shown how the environment in which motion tracking is conducted can influence the performance of electromagnetic systems. It has demonstrated that factors such as the presence of metallic items and the distance between EM source and sensors can impart negative effects on the accuracy of measurement systems. In response to this, experiments were carried out to optimise the layout of a human performance laboratory and to evaluate the measurement accuracy of the extended range FOB EM motion tracking system. It was found that the positioning of key equipment in the laboratory did affect the measurement accuracy of the system, and furthermore that the position and orientation of sensors could be reliably tracked in the same, optimised laboratory. Previous work has demonstrated the suitability of the FOB for measuring spinal and lower limb motion (Bull et al., 1998; Bull and McGregor, 2000). It is a conclusion of this thesis that the FOB apparatus is suitable for measuring human movement during ergometer rowing. This chapter also conducted a calibration procedure on a bespoke arrangement of force transducers housed under the seat of the rowing ergometer in the same human performance laboratory. It was found that after calibration the system was able to accurately report the magnitude and position of force application on the apparatus.

The experiments presented in this chapter were completed in preparation for conducting research into the technique and athletic performance of elite rowers. Chapter 4 addresses the other preparatory steps that were taken in designing the protocol that was used during athlete testing.

Chapter 4

Methodology

In this chapter the methods used for testing athletes are presented. Initially the body segments that are required to fully represent human movement from the volar foot to the lumbar spine are introduced; this is followed by a description of how each of these segments, and anatomical landmarks thereon were tracked during athlete testing. After this the coordinate systems used in the study are presented. The final section of this chapter describes the test protocol that each athlete was subject to during laboratory sessions.

4.1 Recording three-dimensional kinematics

The data acquisition program that was designed for and used during athlete testing was capable of recording the signals of four FOB sensors in an extended range setup (Section 3.1). As such the current protocol was able to track the motion of the right foot, right leg, pelvis and lower back. The motion of this region of the body was defined by the position and orientation of six body segments. All of the body segments were tracked via anatomical landmarks, or directly by a FOB sensor. The six segments were:

1. The lumbar region of the spine (BACK)
2. The pelvis (PELVIS)
3. The thigh (FEMUR)
4. The shank (TIBIA)
5. The posterior portion of the foot (POSFOOT)
6. The anterior portion of the foot (ANTFOOT)

The foot was split into two sections as the nature of ergometer rowing sees the front of the foot and the back of the foot flexing and extending relative to each other about an axis that can be identified at the level of the metatarsal heads and the ergometer foot strap (Figure 4.12, Page 79). The lumbar region of the spine was described as a single segment; this was done as it was not deemed possible or necessary to define each vertebral body as an individual segment in the current study.

Following the definition of six body segments, five joint centres were identified:

1. The junction of the fifth lumbar and first sacral vertebrae (LSJ)
2. The hip joint centre (HJC)
3. The knee joint centre (KJC)
4. The ankle joint centre (AJC)
5. The point of rotation of the rear of the foot about the front of the foot (FJC)

In order to construct a model of these segments, joint centres and the corresponding axis systems, several locations on and within the body had to be identified; these are introduced later in this chapter. The current study utilised three techniques common to motion analysis. These techniques allow the spatio-temporal behaviour of discrete points on the body that do not have a sensor attached specifically to them to be monitored. The techniques can be referred to as: digitisation of anatomical points, functional assessment for the identification of joint centres, and anthropometric based prediction of position. These techniques are incorporated into investigations of motion prior to the main kinematic performance and are described below.

4.1.1 Digitisation of anatomical points

The FOB allows the motion of any object or body segment to be tracked with six degrees of freedom by attaching only one sensor to it (Section 3.1). Digitisation of anatomical points on a body segment involves the use of a sensor that is fixed somewhere on the segment, palpation of the anatomical point(s) of interest and a second FOB sensor which is mounted on a stylus. First the anatomical point is identified through palpation; the stylus with sensor attached is then used to digitise the space. This involves the tip of the stylus being aligned with the landmark and a recording being made while the stylus is rotated about its tip. This rotation of the stylus sensor about one co-ordinate in space generates a three-dimensional (3D) cloud of data which is the history of the position and orientation of the stylus sensor as it is moved about the anatomical point. Using this data an iterative approach which involves a minimisation of errors in a sphere fitting procedure is used to calculate the magnitude of the offset from the FOB stylus sensor to the tip of the stylus. This offset is then combined with the data that was collected during the digitisation procedure and thus the position of the palpated anatomical landmark can be obtained, this point is stored as a rigid offset from the FOB sensor that has been attached to the body segment throughout. Using the FOB this process has previously been utilised by Bull et al. (2002). In the current study digitisation was used to determine several “virtual” points, and is illustrated by Figure 4.1.

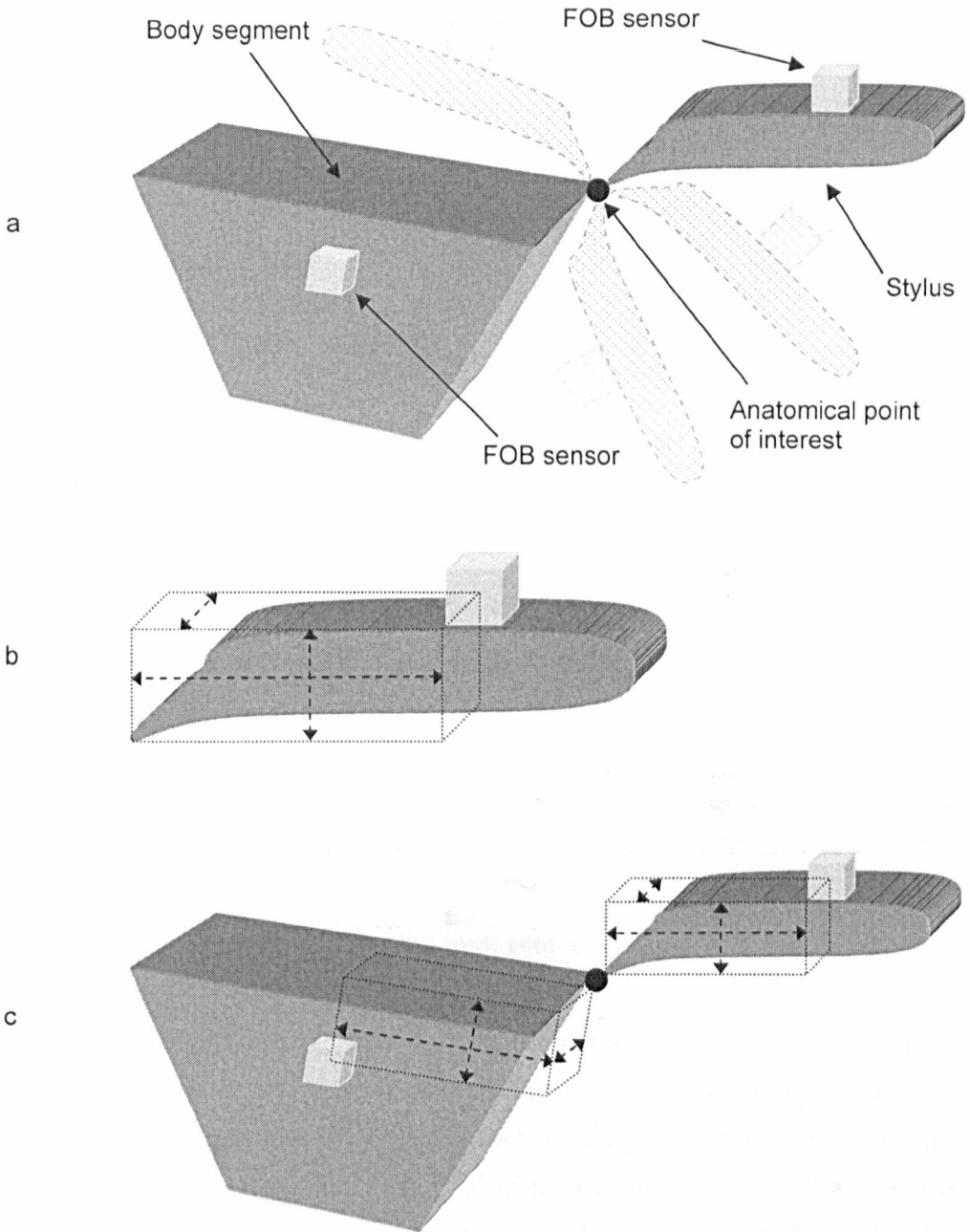


Figure 4.1: Digitisation of an anatomical point schematic

The stylus tip is aligned with the required anatomical point (a), from here the stylus is rotated about its tip whilst a recording of the sensor coordinates and orientation are made. The recorded data is used to calculate the x,y,z offset from the sensor origin to the stylus tip (b). The recorded data and the newly calculated stylus offset are used to store the position of the landmark relative to the sensor that is fixed to the body segment (c).

4.1.2 Digitising in the current study

The methodology used in the current study required nine anatomical landmarks to be digitised in preparation for athlete testing (Table 4.1).

Anatomical position	Abbreviation
Right posterior superior iliac spine	RPSIS
Left posterior superior iliac spine	LPSIS
Right anterior superior iliac spine	RASIS
Left anterior superior iliac spine	LASIS
Lateral femoral epicondyle	LEPI
Medial femoral epicondyle	MEPI
Distal apex of the lateral malleolus	LMAL
Distal apex of the medial malleolus	MMAL
Dorsal aspect of the fifth metatarsal head	METS

Table 4.1: Digitised anatomical points

4.1.3 Functional identification of joint centres

The functional method is well described in the literature (Camomilla et al., 2006; Cappozzo et al., 1995; Cereatti et al., 2004; Piazza et al., 2001; Piazza et al., 2004). It is a similar process to that of digitisation and identifies the joint centre as the centre of rotation of one segment relative to another during an ad hoc movement. Comparing the method to digitisation, one of the segments would be the stylus whilst the ad hoc movement would be the rotation of the stylus. This method was used to identify the position of the HJC.

4.1.4 Identifying the location of the hip joint centre

Camomilla et al. (2006) states that the functional method for the HJC identifies the joint centre as the centre of rotation of the femur relative to the pelvis. Camomilla et al. (2006) investigated various factors that contribute to optimising the accuracy of the functional method when locating the HJC. They found that optimised experimental and analytical approaches could identify the position of the joint centre to within 1 mm of its true location. Errors in this process can be deleterious to both hip and knee kinematic measurements. Camomilla et al. (2006) described the effect of the type and amplitude of the ad hoc movement of the femur relative to the pelvis, the positioning of motion sensors on the femur and the number of data samples recorded during the ad hoc movement on the accuracy of estimating the position of the HJC within a pelvis local axis frame. They showed that errors in HJC location were significantly decreased by performing a combination of flexions, extensions, abductions, and circumductions of the femur, completing these movements with as wide a range of movement as possible (amplitude of movement), by positioning femur motion sensors proximally on the segment, and, either through slower movement or higher sampling frequency, recording more than 500 data samples during the ad hoc movement. It was offered that performing a variety of movement types was preferable to any one movement type when all other parameters were the same

because the more complex movement sequence fully explored the degrees of freedom of the hip, and thus acquired additional relevant information. Camomilla et al. (2006) also noted that the recommendation of proximally mounted femur sensors was in conflict with the more generally adhered to control of fixing motion sensors on the part of the segment with least potential to introduce soft tissue artefacts; in the case of the thigh this is the distal region. They did not include any control for soft tissue interference in any of their simulations, experimental work or calculations.

In this study, athletes were required to perform several flexions, extensions, abductions and circumductions of the thigh, across as wide a range as comfortably possible, for a sufficient time period that over 500 data samples could be recorded. Positioning of a FOB sensor to track the movement of the thigh is discussed in Section 4.2.1.

4.1.5 Anthropometric based prediction of position

The anthropometric based method has been shown to be effective in identifying the position of joint centres. The prediction approach uses regression equations whose independent variables describe the geometry of body segments, which are then multiplied by pre-determined coefficients to identify an internal point of interest as an offset from a palpable landmark. In the literature this technique has previously been demonstrated and used in order to describe the geometry of the pelvis and subsequently determine the position of the HJC (Andriacchi et al., 1980; Bell et al., 1989; Bell et al., 1990; Seidel et al., 1995; Tylkowski et al., 1982). The next section describes an experiment that was carried out in order to identify the position of LSJ.

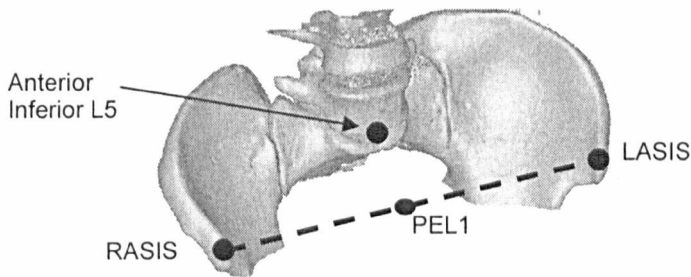
4.1.6 Identifying the location of the lumbosacral junction

An analysis of CT data was completed to ascertain the position of the junction between the fifth lumbar and first sacral vertebrae, within a predefined pelvic local axis system. It was proposed that it would be possible to use individuals' pelvic geometry to control the magnitude of the X,Y,Z offsets from a segment origin, to the joint centre of interest.

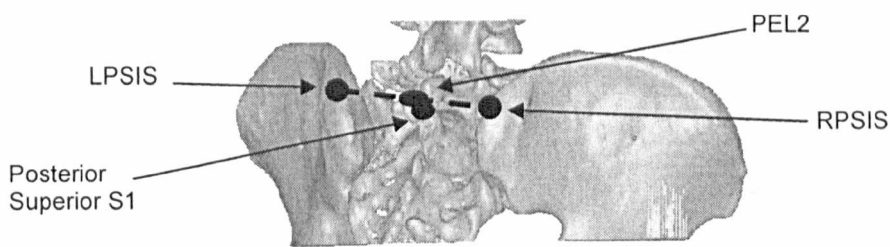
4.1.6.1 Obtaining data

Sixteen sets of CT pelvis scans from Dandachli et al. (2009) were segmented using Mimics software (Materialise, Heverlee, Belgium). For each pelvis the software scanned the image stacks and its default thresholds for bone CT were applied, thus a mask of each pelvis could be reconstructed as a digital 3D object. After this, the X,Y,Z coordinate of the right and left anterior superior iliac spine (ASIS) and posterior superior iliac spine (PSIS), the most anterior and inferior point on the fifth lumbar vertebra, and the most posterior and superior point on the

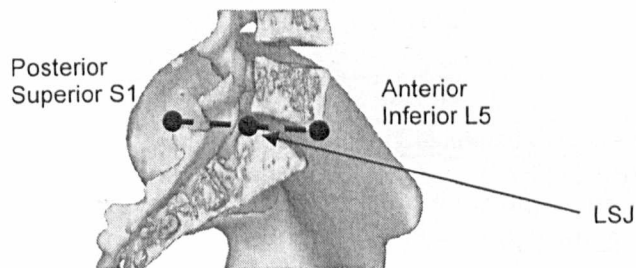
first sacral vertebra were logged. This allowed the coordinate of the midpoint of the lines RASIS-LASIS (PEL1) and RPSIS-LPSIS (PEL2) to be computed. The midpoint of the line connecting the anterior inferior lumbar spine and posterior superior sacral spine was LSJ (Figure 4.2).



Oblique view of the anterior pelvis



Oblique view of the posterior pelvis



Sagittal cross section of the pelvis

Figure 4.2: Anatomy used for regression identification of LSJ

A local axis system whose directions were dictated by features of the pelvis was defined. The origin of the local axis system was PEL1, the X axis was defined by the line RASIS-LASIS, the Y axis was orthogonal to the plane formed by RASIS-LASIS and PEL2, and was positive in the coronal direction, and the Z axis was mutually perpendicular to the X and Y axes and positive anteriorly (Figure 4.3).

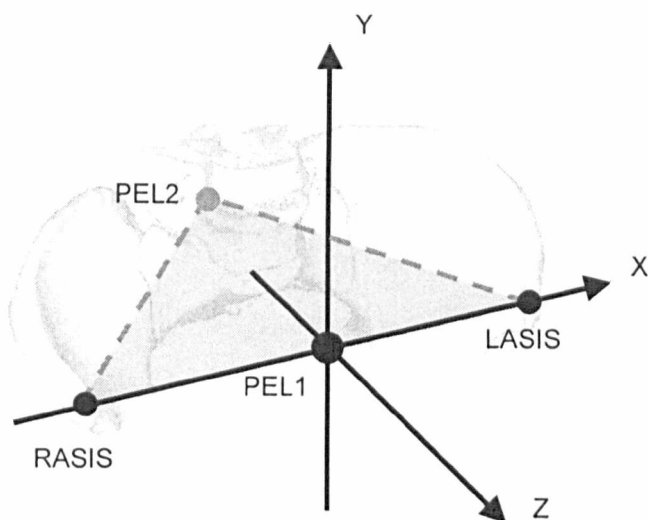


Figure 4.3: Pelvis local axis system used for regression identification of LSJ

The origin was PEL1, the X axis was defined by the line RASIS-LASIS, the Y axis was orthogonal to the plane formed by RASIS-LASIS and PEL2, and was positive in the coronal direction, and the Z axis was mutually perpendicular to the X and Y axes and positive anteriorly.

4.1.6.2 Computations

Once the positions of key anatomy were known within the pelvis coordinate frame the distances between pertinent points were calculated. Table 4.2 details the positions and distances used for further analysis.

Coordinate known in pelvis axis frame	Calculated distance between points
RASIS	RASIS-LASIS
LASIS	RPSIS-LPSIS
RPSIS	PEL1-PEL2
LPSIS	
PEL1 (origin)	
PEL2	
LSJ	

Table 4.2: Anatomy and measurements used for regression identification of LSJ

The coordinate of each pelvis' LSJ could then be expressed as a percentage of the interASIS, interPSIS and interPEL distances. For example, if in mm, LSJ was situated (2,5,-100) from PEL1 (0,0,0), and the interASIS distance was 200 mm, then the position of LSJ could be expressed as:

$$x = \frac{2}{200} \times 100 \qquad y = \frac{5}{200} \times 100 \qquad z = \frac{-100}{200} \times 100$$

$x = 1\%$	$y = 2.5\%$	$z = -50\%$
interASIS distance	interASIS distance	interASIS distance

For each pelvis the magnitude of LSJ x,y,z were converted to percentages of interASIS, interPSIS and interPEL. These were used to compute an average ($n = 16$) offset which described the position of LSJ within the pelvis. The average offset was used to calculate the position of LSJ for each of the pelvises used in the study. These values were compared to the coordinates that had previously been identified in Mimics, thus a measurement of error in LSJ position (mm) prediction was calculated for each pelvis. Maximum, average and standard deviation of these error levels provided information on which inter anatomy distance was the most effective predictor for LSJ position. Once this optimal inter anatomy distance had been identified a leave one out analysis was conducted in which the data obtained from each individual pelvis was removed in turn (control pelvis), and a new average ($n = 15$) offset was calculated. These new offsets were used to predict the position of LSJ within the control pelvis, and the result compared to the known location. This technique showed how an approximation of the above described average offset predicted the position of LSJ in a pelvis whose geometry was not utilised in the computation of the offset. A repeatability analysis was conducted by repeating the entire method two weeks later.

4.1.6.3 Results

This section provides information on the offsets calculated to predict the position of LSJ, the errors involved in this prediction, the identification of an optimal method for prediction and the repeatability of the process. Table 4.3 shows that on average the technique of anthropometric based prediction of position provided the location of LSJ to within 8.36 mm of its true coordinate within the pelvis. Noting that there were six anatomical points identified using Mimics for each of the sixteen pelvises (Section 4.1.6.1), and an X,Y,Z coordinate was logged for each; 288 individual components of position were observed during the initial and repeated tests. The maximum discrepancy in any logged component of position between the initial trial and the repeated trial was 3.72 mm, the average discrepancy was 0.38 mm and the standard deviation

was 0.57 mm. Both the initial and the repeated experiment found that the most effective way to predict the position of LSJ as an offset from a pelvic landmark was to describe the location as an X,Y,Z offset whose magnitude was expressed as a percentage of the distance between PEL1 and PEL2.

	Position of LSJ (mm) and offsets (%)			Errors in position identification through applying the offsets (mm)			
	X	Y	Z	X	Y	Z	resultant
Initial measurement							
Average							
Coordinate (mm)	0.55	8.12	-102.86				
using interASIS	0.31	3.57	-45.85	2.85	4.70	11.02	13.42
using interPSIS	0.70	8.47	-106.41	2.86	4.86	6.93	9.95
using interPEL	0.41	5.57	-70.01	2.85	4.86	4.20	8.14
St Dev							
Coordinate (mm)	3.74	6.27	-7.93				
using interASIS	1.81	2.76	-6.53	2.34	3.92	8.06	7.45
using interPSIS	3.75	6.46	-8.81	2.33	3.95	4.71	4.77
using interPEL	2.51	4.31	-3.65	2.32	3.87	3.25	3.60
Maximum							
using interASIS				7.26	13.74	27.35	27.46
using interPSIS				7.11	13.67	15.52	18.02
using interPEL				7.21	13.85	10.86	17.63
Repeated measurement							
	X	Y	Z	X	Y	Z	resultant
Average							
Coordinate (mm)	0.62	7.76	-102.92				
using interASIS	0.36	3.41	-45.78	3.03	4.88	10.95	13.47
using interPSIS	0.75	8.06	-105.69	3.02	5.03	6.58	9.91
using interPEL	0.48	5.32	-70.10	3.01	5.00	4.23	8.36
St Dev							
Coordinate (mm)	3.89	6.30	-7.88				
using interASIS	1.92	2.78	-6.40	2.38	3.76	7.83	7.11
using interPSIS	3.86	6.51	-8.79	2.36	3.81	5.12	4.95
using interPEL	2.65	4.33	-3.68	2.37	3.72	3.29	3.33
Maximum							
using interASIS				8.14	12.99	26.72	26.95
using interPSIS				7.92	12.95	15.91	18.74
using interPEL				8.08	13.19	10.78	17.03

Table 4.3: Offsets and associated errors for prediction of LSJ position (n = 16)

The average and standard deviation of x,y,z coordinates for LSJ is shown for the initial and repeated observations. The associated offsets and resulting prediction error of those offsets are also included. The offsets that induced the least error are highlighted.

Table 4.3 shows that in the initial analysis the offset of LSJ from PEL1 was 0.41%, 5.57% and -70.01% of the interPEL distance in the X,Y,Z directions respectively. Table 4.3 also shows that in the repeated analysis this offset was 0.48%, 5.32% and -70.10% of the interPEL distance. It is recommended that the average of these two be used for the identification of athletes' LSJ. That is, the location of LSJ can be found by gaining the coordinate of PEL1 and PEL2 and then moving 0.45% of the interPEL distance to the left, 5.45% of the interPEL distance superiorly,

and 70.06% of the interPEL distance posteriorly, from PEL1, along a pelvis axis system defined as described in Figure 4.3. Table 4.4 shows that 94% of the time an approximation of the offsets calculated from all sixteen pelvis predicted the position of LSJ, in a pelvis not used during computation of offsets to within 13.22 mm. Table 4.4 also shows that reducing the number of datasets used in calculation of an offset by only one pelvis scan results in increased error of approximately 6.78%.

n		Initial trial Error, in mm				Repeated trial Error, in mm			
		X	Y	Z	resultant	X	Y	Z	resultant
16	Max	7.21	13.85	10.86	17.63	8.08	13.19	10.78	17.03
16	Mean	2.85	4.86	4.20	8.14	3.01	5.00	4.23	8.36
16	SD	2.32	3.87	3.25	3.60	2.37	3.72	3.29	3.33
Control									
15	Pelvis 1	4.07	1.15	5.16	6.68	4.61	0.25	5.24	6.98
15	Pelvis 2	0.87	0.10	5.26	5.33	0.99	1.03	5.64	5.81
15	Pelvis 3	1.56	1.06	5.41	5.73	2.34	0.73	5.15	5.71
15	Pelvis 4	2.16	3.18	0.66	3.90	2.70	3.57	0.68	4.53
15	Pelvis 5	0.81	8.69	1.17	8.81	1.51	7.59	0.36	7.74
15	Pelvis 6	3.43	3.07	0.24	4.60	2.39	5.46	0.35	5.97
15	Pelvis 7	4.88	2.36	7.01	8.86	4.52	1.86	7.33	8.81
15	Pelvis 8	6.44	0.42	2.30	6.85	7.03	0.07	2.38	7.42
15	Pelvis 9	1.14	9.32	4.47	10.40	2.34	9.57	4.76	10.94
15	Pelvis 10	0.60	4.37	2.60	5.43	0.53	5.81	2.01	6.17
15	Pelvis 11	0.59	3.89	9.41	10.20	0.46	4.94	9.53	10.74
15	Pelvis 12	3.88	4.78	3.91	7.30	3.24	5.38	4.30	7.61
15	Pelvis 13	7.49	8.89	0.33	11.62	6.87	8.30	0.31	10.78
15	Pelvis 14	7.69	7.90	2.72	11.35	8.81	7.89	3.53	12.34
15	Pelvis 15	1.95	8.69	9.46	13.00	3.15	8.98	9.17	13.22
15	Pelvis 16	1.04	14.77	11.59	18.80	0.07	14.03	11.47	18.12
	Max	7.69	14.77	11.59	18.80	8.81	14.03	11.47	18.12
	Mean	3.04	5.19	4.48	8.68	3.22	5.34	4.51	8.93
	SD	2.47	4.12	3.47	3.84	2.55	3.97	3.50	3.56
% Increase in error when prediction offset is computed from 15 datasets as opposed to 16 datasets									
	Max	6.66	6.64	6.72	6.64	9.03	6.37	6.40	6.40
	Mean	6.67	6.79	6.67	6.63	6.98	6.80	6.62	6.82
	SD	6.47	6.46	6.77	6.67	7.59	6.72	6.38	6.91

Table 4.4: Leave one out analysis validation of the LSJ offset

The top section shows the errors associated with the original calculations with 16 pelvis, the middle section shows the errors associated with the leave one out analysis, and the bottom section shows the increase in error associated with the leave one out analysis compared to the original analysis.

4.1.6.4 Discussion and conclusions

Table 4.3 shows that when using the interPEL distance to calculate offsets, compared to either the interASIS or interPSIS distances, the associated errors are similar in both the medial/lateral and coronal directions; it is only in the anterior/posterior direction (and subsequently the resultant error) where a marked improvement in error levels is noted. This is likely due to the

fact that the largest displacement that any offset considers is in the Z direction, and the interPEL distance is the only one of the three distances used which is sensitive to changes in this aspect of pelvic geometry. It is possible that variably accurate prediction methods would occur in response to changing the definition of the pelvis axis system, and more specifically its origin. It can also be noted from both Table 4.3 and Table 4.4 that when considering the offsets calculated using interPEL distance, the greatest associated errors occur in the coronal direction. Table 4.4 shows that six out of the eight reported maximum errors in the control section were procured when pelvis 16 was used as the control, indeed there is a marked increase in maximum errors when considering this control to any other in the group. It is possible that this particular pelvis exhibited some more unusual coronal geometry than the other pelvises used in the study, and thus the errors observed were greater than for any other of the controls. The results in Table 4.4 also show that an approximation of the method of predicting the position of LSJ that has been presented here is, 94% of the time, accurate to less than 13.22 mm, and on average will predict the position of LSJ to within 8.93 mm

4.2 Athlete preparation

Before commencing any recordings of athletic performance and technique it was necessary to complete steps that would allow each of the segments and joint centres previously introduced to be reconstructed in a kinematic model. This section first describes how each of the FOB sensors used in the current research were employed, and mounted on the body. This is followed by description of how, using the position of various landmarks, relevant coordinate frames were established in order to calculate 3D joint angles.

4.2.1 The electromagnetic sensors

The four FOB sensors used during all testing sessions served three purposes; the first was to provide information on the position and orientation of the BACK, the second was to track the movement of a digitising stylus and, in turn, the thigh whilst preparing an athlete for testing, and the third purpose was as reference for digitised anatomical points.

FOB sensor 1 (S1) was attached to the back at the junction of the twelfth thoracic and first lumbar vertebrae (Figure 4.4). Correct positioning of the sensor was obtained by palpation of the lumbar vertebrae. This sensor was used to track the position and orientation of the BACK. FOB sensor 2 (S2) was attached to the pelvis at the junction of the fifth lumbar and first sacral vertebrae (Figure 4.4). Correct positioning was obtained by palpation. This sensor was used as a reference for the position of ten anatomical landmarks.

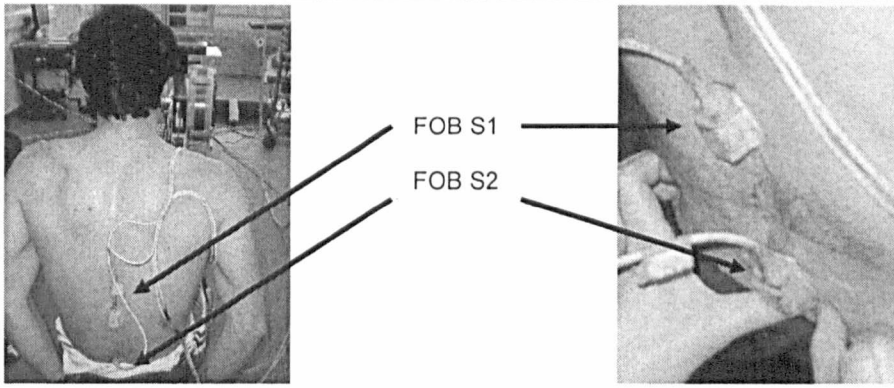


Figure 4.4: Location of FOB sensor 1 (S1) and sensor 2 (S2) during athlete testing

FOB sensor 3 (S3) was used as the stylus mounted digitising sensor, and during functional assessment of the HJC. Using nylon screws S3 was fixed to a piece of moulded plastic (Figure 4.5, Figure 4.6), this was used as a stylus when digitising the anatomical points identified in Table 4.1, and subsequently was attached to the lateral side of the thigh approximately half way between the greater trochanter and femoral epicondyles using elasticated Velcro straps. The exact location of the sensor (distal vs proximal) was dictated by individual's varied musculature. Fixing S3 to the thigh allowed the functional HJC assessment to be carried out and provided data that was used in a real time bio-feedback system during testing (Chee et al., 2009).

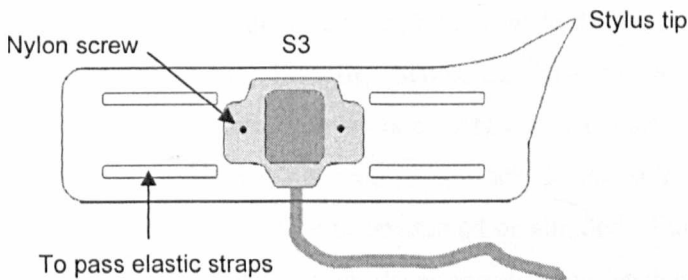


Figure 4.5: FOB sensor 3 (S3), mounting block and stylus complex

FOB sensor 4 (S4) was inserted into a custom cuff: The cuff was fixed to the anterior distal shank using elasticated Velcro straps (Figure 4.6). Cappozzo et al. (1995) showed that sufficiently wide elasticated bands help to reduce soft tissue movements, without restricting action. This sensor was used as a reference for the position of six anatomical landmarks.

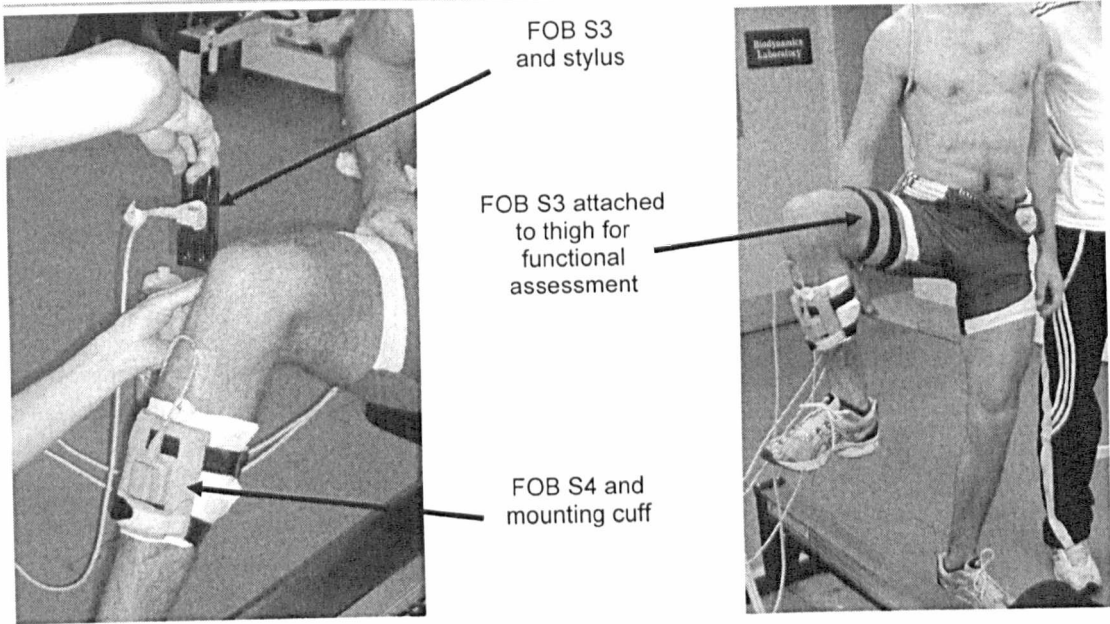


Figure 4.6: Digitisation and functional assessment of anatomical locations

The picture on the left shows S3 being used to digitise the position of the right lateral femoral epicondyle, and the picture on the right shows an athlete performing the ad hoc movement required for functional identification of the HJC.

In previous studies into rowing on an ergometer (Bull and McGregor, 2000; Holt et al., 2003; O'Sullivan et al., 2003) participants occasionally reported irritation at the site of marker adhesion, and FOB sensors have been damaged by the adhesives used.¹ In response to this issue, in this study S1 and S2 were fixed to the skin by utilising adhesive patches that were specifically designed to adhere small devices to the human body during activity. PALstickies™ were chosen (PAL Technologies Ltd, Glasgow, Scotland); these patches employ a dual layer hydrogel to provide optimum skin adhesion on one surface and device adhesion on the other. The dual layer gel allows the skin contact side to conform to the skin surface and provides adhesion without requiring the skin surface to be shaved or abraded. Furthermore the patches are durable to the high levels of perspiration produced during exercise that has previously led to the failure of other adhesives.

4.2.2 Non-performance trials

To facilitate analysis into the motion of BACK, PELVIS, FEMUR, TIBIA, POSFOOT and ANTFOOT, about the joint centres LSJ, HJC, KJC, AJC and FJC; ten recordings were made using the FOB prior to all rowing trials. S1, S2, and S4 were attached to the participant as described previously. After this the athlete was asked to sit on the ergometer and the stylus and S3 were used to digitise nine anatomical landmarks (Table 4.1), S3 was then attached to the thigh of the athlete and an ad hoc movement provided data from which the position of HJC

¹ Private communication with the authors.

could be extracted. Figure 4.6 illustrated the digitisation method and functional assessment used, and Table 4.5 details all of the anatomical points that were required by the kinematic model for identification of the location of LSJ within the pelvis segment, and for 3D movement analysis in the current study.

Anatomical point	Abbreviation	Notes	Stored as a vector offset from FOB:
Junction of twelfth thoracic and first lumbar vertebrae	BACK	Tracked by S1	NA
Right posterior superior iliac spine	RPSIS	Digitised	S2
Left posterior superior iliac spine	LPSIS	Digitised	S2
Right anterior superior iliac spine	RASIS	Digitised	S2
Left anterior superior iliac spine	LASIS	Digitised	S2
Lateral femoral epicondyle	LEPI	Digitised	S4
Medial femoral epicondyle	MEPI	Digitised	S4
Distal apex of the lateral malleolus	LMAL	Digitised	S4
Distal apex of the medial malleolus	MMAL	Digitised	S4
Dorsal aspect of the fifth metatarsal head	MET5	Digitised	Transmitter
	PEL1	Midpoint of RASIS-LASIS	S2
	PEL2	Midpoint of RPSIS-LPSIS	S2
	PEL3	Midpoint of LASIS-LPSIS	S2
	PEL4	Midpoint of RASIS-RPSIS	S2
Junction of fifth lumbar and first sacral vertebrae	LSJ	Anthropometric prediction	S2
Hip joint centre	HJC	Functionally identified	S2
Knee joint centre	KJC	Midpoint of LEPI-MEPI	S4
Ankle joint centre	AJC	Midpoint of LMAL-MMAL	S4
Foot joint centre	FJC	Offset from MET5	Transmitter
	distFOOT	Offset from FJC	Transmitter

Table 4.5: Anatomical points used in the kinematic model

4.3 Coordinate systems

In this study there were four different types of axis system: The global/laboratory system, local axis frames whose directions were dictated by FOB sensors, local coordinate frames that were defined for individual segments in the system, and joint centre axis frames, from which intersegmental angles were computed. Figures 4.7 to 4.12 illustrate the various axis systems that were used in the current study.

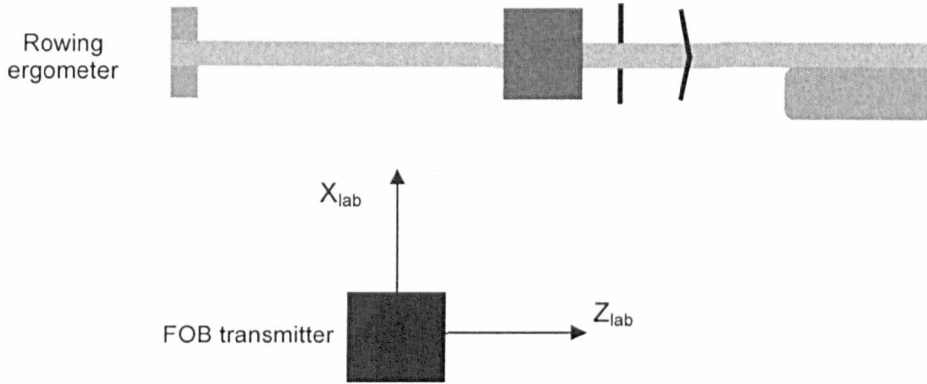


Figure 4.7: Global/laboratory axis system used during athlete testing

The laboratory axis system follows a right hand triad, thus Y_{lab} is positive vertically upwards.

The intersegmental angles contributing to the kinematic output of the current research were obtained using the floating axis theory described by Grood and Suntay (1983), and, for the calculation of flexion and extension about FJC; the application of trigonometry. The Grood and Suntay (1983) technique was used to construct a joint coordinate system between two adjacent body segments by using the medial/lateral axis of the superior segment (F_{sup}), the coronal axis of the inferior segment (F_{inf}) and a floating axis (F_{cross}) whose direction was the cross product of F_{sup} and F_{inf} . Joint flexion/extension was about F_{sup} and was the angle between the superior segment's coronal/long axis and F_{cross} . Abduction/adduction or eversion/inversion occurred about F_{cross} and was the angle between the superior segment's medial/lateral axis and the inferior segments long axis. Internal/external rotation occurred about F_{inf} , and was the angle between F_{cross} and the inferior segments medial/lateral axis. From this point, all flexion/extension angles are identified as alpha (α), trunk side flexion, hip abduction/adduction and ankle eversion/inversion are beta (β), and internal/external rotation are gamma (γ). Because both the femoral epicondyles, and the lateral and medial malleoli were stored as offsets from the S4 it was not possible to compute β or γ for the KJC.

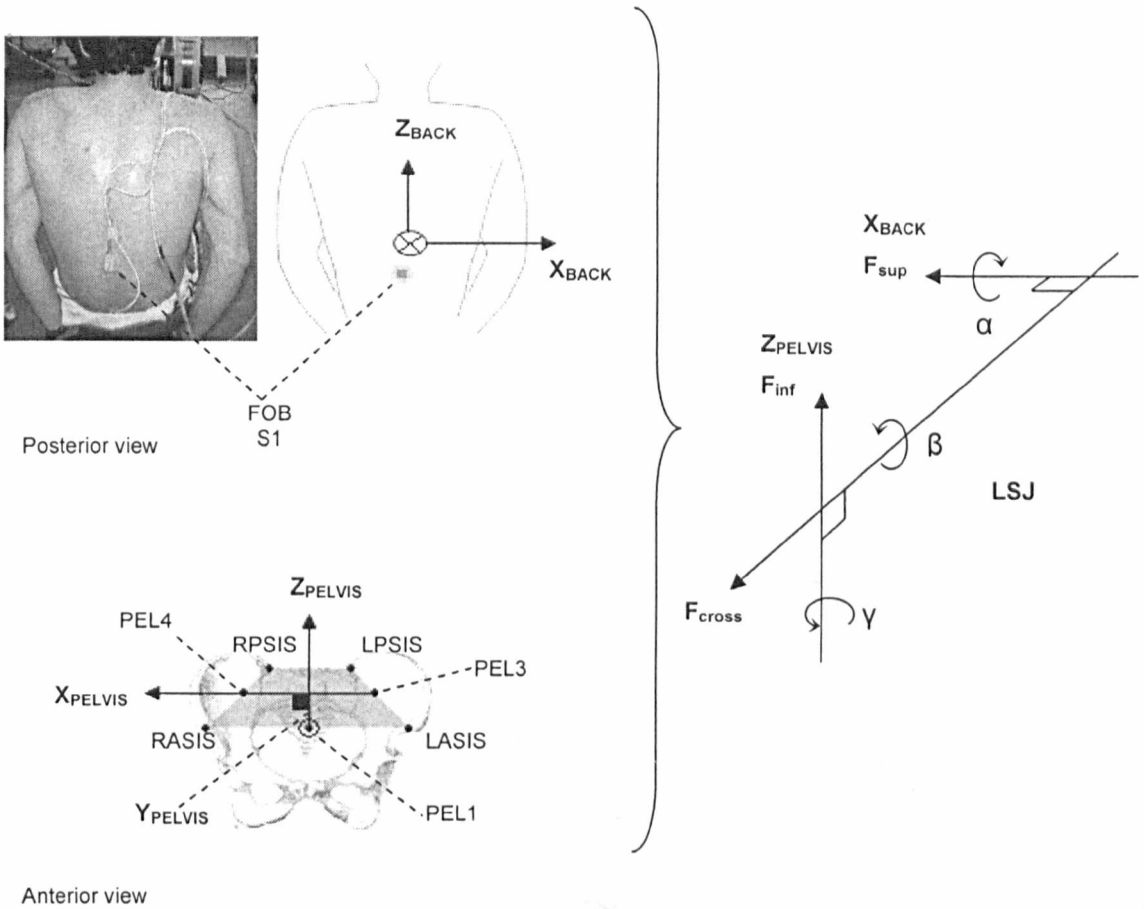


Figure 4.8: BACK, PELVIS and LSJ coordinate frames

The orientation of the BACK was considered to be coincident with the orientation of FOB S1. The X_{BACK} axis was positive from left to right, Y_{BACK} was positive anteriorly, and Z_{BACK} was positive in the coronal direction. X_{PELVIS} was defined by the line PEL3-PEL4, and was positive from left to right, Y_{PELVIS} was perpendicular to X_{PELVIS} , intersected PEL1 and was positive anteriorly, and Z_{PELVIS} was mutually perpendicular to the X_{PELVIS} and Y_{PELVIS} axes following the right hand rule.

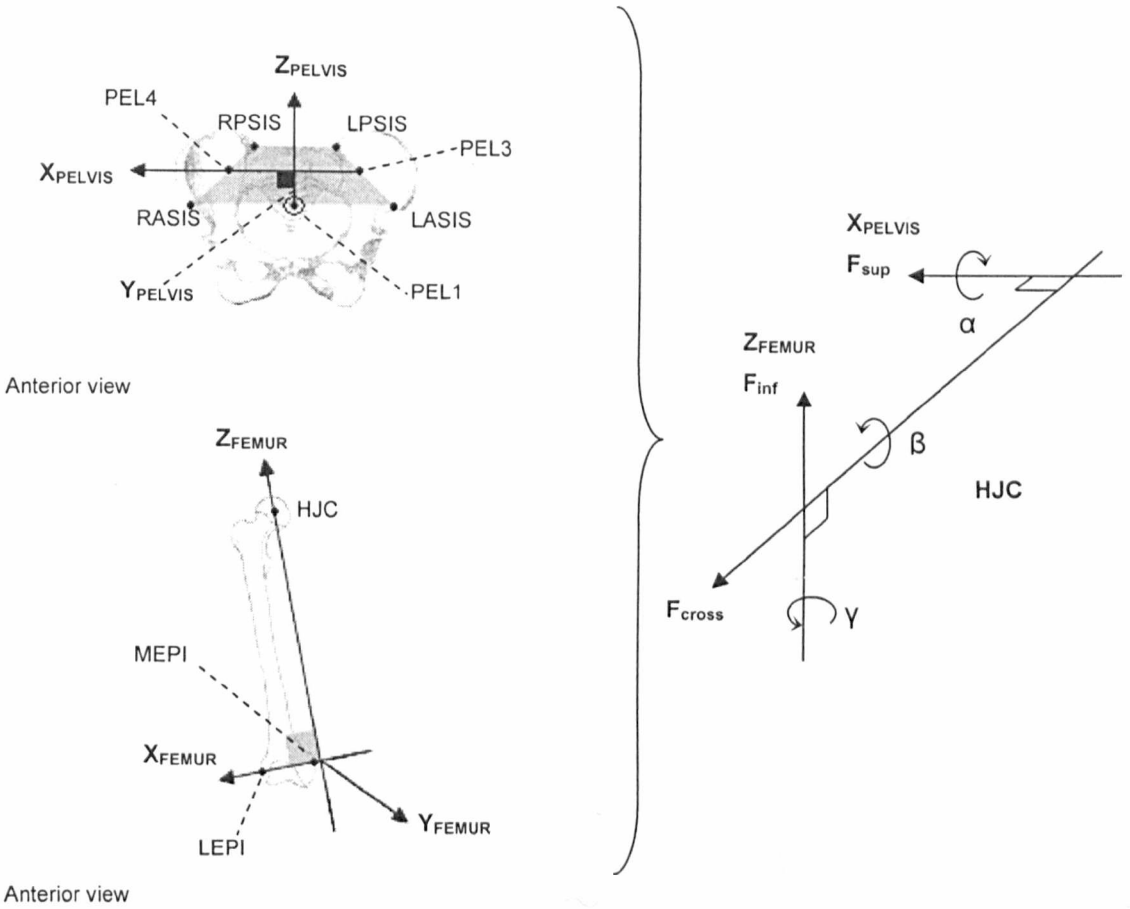


Figure 4.9: PELVIS, FEMUR and HJC coordinate frames

X_{PELVIS} was defined by the line PEL3-PEL4, and was positive from left to right, Y_{PELVIS} was perpendicular to X_{PELVIS} , intersected PEL1 and was positive anteriorly, and Z_{PELVIS} was mutually perpendicular to the X_{PELVIS} and Y_{PELVIS} axes following the right hand rule. X_{FEMUR} intersected the points MEPI and LEPI and was positive from left to right, Z_{FEMUR} was perpendicular to X_{FEMUR} , intersected HJC and was positive in the proximal direction, and Y_{FEMUR} was mutually perpendicular to X_{FEMUR} and Z_{FEMUR} and was positive anteriorly.

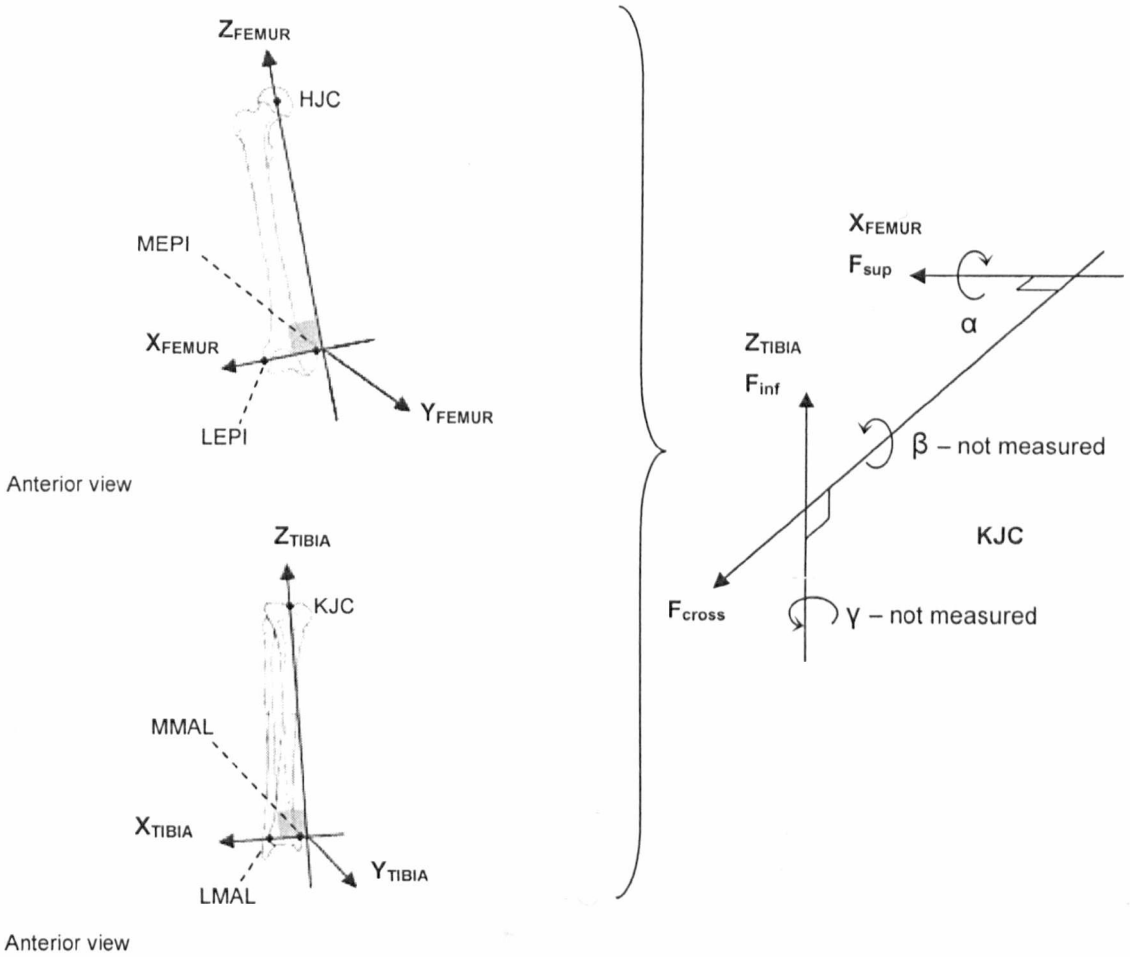


Figure 4.10: FEMUR, TIBIA and KJC coordinate frames

X_{FEMUR} intersected the points MEPI and LEPI and was positive from left to right, Z_{FEMUR} was perpendicular to X_{FEMUR} , intersected HJC and was positive in the proximal direction, and Y_{FEMUR} was mutually perpendicular to X_{FEMUR} and Z_{FEMUR} and was positive anteriorly. X_{TIBIA} was positive from left to right and was defined by MMAL to LMAL, Z_{TIBIA} was perpendicular to X_{TIBIA} , intersected the point KJC and was positive in the proximal direction, and Y_{TIBIA} was mutually perpendicular to X_{TIBIA} and Z_{TIBIA} and was positive anteriorly.

When representing POSFOOT for calculation of angles at AJC, some assumptions had to be made regarding the orientation of the segment within the FOB transmitter axis frame. This was because no FOB sensor was available to directly track the motion of the segment, or to store digitised anatomical locations such as MET5 or the calcaneus. Therefore, as shown in Table 4.5, the position of MET5 was stored in reference to the FOB transmitter, and was assumed not to move during rowing trials. The unit vector from MET5 to FJC was then assigned X,Y,Z components (1,0,0). That is, the direction of the line MET5 to FJC, which was X_{POSFOOT} , was coincident with the FOB transmitter X axis. The vector components of the line FJC to AJC considered only the Y and Z laboratory axes; the sagittal plane. Thus the vector from FJC to AJC (Y_{POSFOOT}) was (0,FJC_y-AJC_y,FJC_z-AJC_z). The cross product of these two axes was Z_{POSFOOT} .

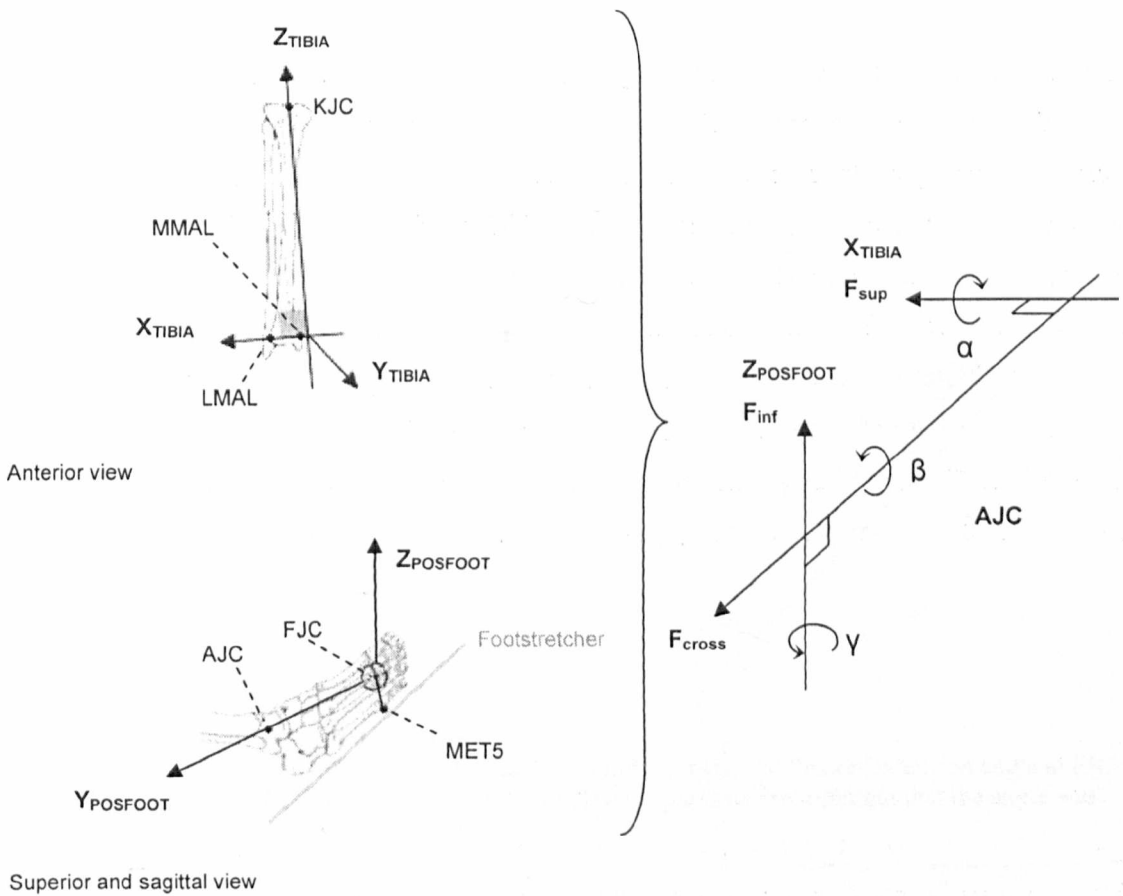


Figure 4.11: TIBIA, POSFOOT and AJC coordinate frames

X_{TIBIA} was positive from left to right and was defined by MMAL to LMAL, Z_{TIBIA} was perpendicular to X_{TIBIA} , intersected the point KJC and was positive in the proximal direction, and Y_{TIBIA} was mutually perpendicular to X_{TIBIA} and Z_{TIBIA} and was positive anteriorly. FJC was offset from the position of MET5 and was coincident with the FOB transmitter X axis (X_{POSFOOT}). Y_{POSFOOT} was positive from FJC to AJC and was defined in the sagittal plane of the FOB transmitter, and Z_{POSFOOT} was the cross product of X_{POSFOOT} and Y_{POSFOOT} .

ANTFOOT was defined by the anatomical locations distFOOT and FJC (Figure 4.12). The strap that holds a person's foot in place on a rowing ergometer traverses the foot at the level of MET5, hence the current study assumed that once the athlete's foot had been strapped into the ergometer distFOOT could be described as a constant offset from FJC in global space. Moreover distFOOT was offset in Y_{lab} and Z_{lab} only. As the footstretcher in the current study forms a 45° angle with Z_{lab} distFOOT was described as having equal offsets in the Y_{lab} and Z_{lab} directions ($\tan^{-1} 1/1 = 45^\circ$). Using the $x_{lab}, y_{lab}, z_{lab}$ coordinates of AJC, FJC and distFOOT it was possible to calculate a quasi flexion/extension angle between POSFOOT and ANTFOOT (FJC α , Figure 4.12).

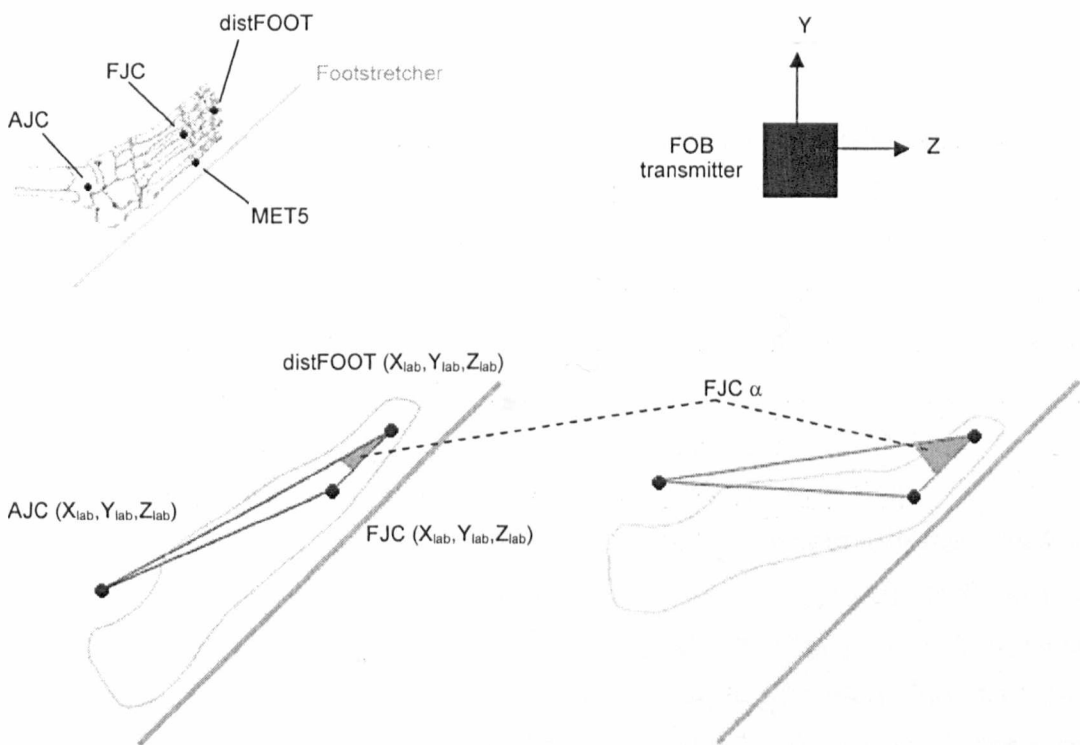


Figure 4.12: Calculation of the angle at FJC

The figure shows the anatomical locations that were used to calculate the flexion/extension angle at FJC. Two indicative poses of the foot during ergometer rowing are presented to highlight that the angle was offset due to the use of AJC instead of calcaneus.

As it was not possible to track the motion of the calcaneus there was an offset in the calculation of AJC α and FJC α which was dependent on individual's anthropometrics (Figure 4.12). That is, even if the athlete's foot was flat on the footstretcher AJC α measurements were offset in the direction of plantar flexion, and FJC α measurements were offset and suggested that the heel had been raised a little from the footstretcher. This offset was typically between 6° and 10° . When reviewing the results of kinematics calculations the magnitude and direction of change of AJC α and FJC α were more important than the magnitude of the angles.

4.4 The ergometer test

So far this chapter has explained the different ways in which all of the relevant anatomical points were tracked during testing, and has described how local axis systems for segments and joints were defined. This section describes the experimental protocol that was followed during athlete testing sessions.

There were nine separate testing sessions in the current research, the first of these was at the start of the rowing season in the year 2006, and the last was in February 2009. The athletes tested were all members of the Great Britain rowing squad, and were classified into four boat classes (Chapter 1); heavyweight women scullers (HWW-SCULL), heavyweight sweep women (HWW-SWEEP), lightweight men (LWM), and lightweight women (LWW). Athletes were classified as a HWW-SCULL or HWW-SWEEP based on the manner in which they had been regularly training in the months leading up to the laboratory test; as such there were 7 individuals who were classified as HWW-SCULL in some testing sessions and HWW-SWEEP in others. The maximum number of athletes tested during any one session was 26, and the minimum was 15. Moreover, 42 individuals were tested at least once, 4 athletes attended all nine sessions, and 2 rowers completed a full test at all nine sessions. A detailed description of the scope of data collected between December 2006 and February 2009 is presented in Section 6.1.

All testing was performed on the modified ergometer that was introduced in Chapter 3. The first thing that was done on a test day was to record the mass of the athletes. As stated in Section 4.2 a process of preparing the athlete for performance was then undertaken; taking approximately fifteen minutes the FOB sensors were fixed to the appropriate body segments and the digitisations and functional HJC assessment completed. The athlete was then asked to stretch and perform a warm up in final preparation for the main body of the test. The ergometer protocol required each participant to perform six pieces of work and is commonly known as an incremental “Step test”. This test format is routinely used in the rowing world to establish individualised training levels and also allows athlete’s fitness and health status to be monitored longitudinally (McGregor et al., 2005). The first five Steps required the athlete to row for four minutes at intensities equal to 55%, 60%, 65%, 70% and 75% of a predetermined maximum that is described below. The final Step required the athlete to row a distance of 500 m at maximal intensity. The predetermined maximum was used to individualise the intensities for each athlete; prior to testing, the athletes’ personal best (PB) 2000 m time was obtained from the squad’s support staff. This time was divided by four and a 500 m *race split* that reflected the 500 m average of the PB was determined. It was this 500 m race split that was used to calculate the Step intensities. Table 4.6 describes the calculated Step splits for a hypothetical athlete with

a PB of 6 minutes. The athletes who participated in this study were all capable of controlling their split to tenths of a second.

PB for 2000 m	360.0 s		
Average 500 m / race split	90.0 s		
	Split	Duration	Approx m rowed
Step 1 – intensity = 55%	163.6 s	4 min	733
Step 2 – intensity = 60%	150.0 s	4 min	800
Step 3 – intensity = 65%	138.5 s	4 min	866
Step 4 – intensity = 70%	128.6 s	4 min	933
Step 5 – intensity = 75%	120.0 s	4 min	1000
Step 6 – intensity = race pace	90.0 s	≈90 s	500

Table 4.6: Structure of an ergometer Step test

Between Steps the athletes received 30 s to 150 s of rest, during which time coaches and others would provide feedback on the technique that had been exhibited during the previous effort. In addition to the feedback discussed between Steps, and post-test, each athlete was provided with information on their technique in real-time using a bespoke biofeedback package (Chee et al., 2009). This test was familiar to all of the athletes who participated, it allowed kinematic data to be recorded at different training intensities, and was a repeatable way to monitor athletes' performance longitudinally. In addition to this, because the intensity of effort was individualised for each athlete it was possible to make comparisons inter rower, and also, by taking averages of multiple rowers' data, to describe the technique of specific groups of rowers. If FOB sensors were observed to have loosened or slipped at any point during a test the data for that test was discarded.

This chapter has detailed how each of the relevant body segments was represented for kinematic analysis in the current study, and has presented the format of athlete testing sessions. The next chapter describes the processes that were used post test to treat and analyse the experimental data.

Chapter 5

Data Processing and Error Analysis

The aim of this chapter is to describe the data processing and statistical techniques that were used in the analysis of rowing data. First the data processing stages are described. There is then a section discussing why some of the dependent variables were chosen, and in some cases, how they were calculated. Following this is an error analysis associated with the calculation of three dimensional kinematics in the current setup. The discussion of statistical methods is limited in this chapter and further information is presented at appropriate points in Chapters 6-9.

The data that was acquired during each of the athlete preparation stages and the Steps for all testing sessions were logged in the form of a matrix whose dimensions were forty four columns by a variable number of rows. For each athlete test there were ten files that constituted the preparation stage (nine digitisations, and one functional HJC), and up to six Step files. The data columns contained information regarding the output of the ergometer handle (force and position) and seat (force, centre of pressure), the FOB sensors' global position and orientation, and a time series extracted from the acquisition computer's internal clock (seconds past midnight). In order to extract useful numbers and trends from the raw data, the test files were subject to three processing sequences. These were implemented in Labview, C/C++ and Matlab, and hereafter are referred to as the kinematics program (Labview), the normalisation program (C/C++), and the data extraction programs (Matlab). After relevant data had been extracted, feedback was delivered to the athletes and coaches, and statistical analyses were carried out in Matlab and SPSS (SPSS Inc, Chicago , Illinois).

5.1 Acquisition of 3D kinematics

The kinematics program worked in two stages, first the program accessed a user specified athlete's preparation files, and used the FOB position and orientation data columns to calculate the stylus offset, offsets from the digitised anatomical points to their reference FOB sensor, and the offset of the HJC to its FOB reference sensor.

After this the user was prompted to input the directory and name of an appropriate Step file, and the athlete's body mass; the previously calculated offsets and the FOB position and orientation information contained within the Step file were used to calculate a new output file that included the 3D kinematics of the athlete during the specified Step. The output file also contained the columns of data describing the output of the various transducers used in the experiment, the seconds past midnight column, and a record of the athlete's body mass. The files output by this

program were of identical dimensions to the raw Step file and are described in full in Chee et al. (2009).

5.2 Data normalisation

To allow features of rowing strokes to be identified, compared to each other, and in order that an average/representative stroke for a Step could be calculated, it was necessary to treat the raw kinematics data in such a way as to represent it as n individual strokes. That is, individual strokes were identified within the raw matrix, and linear interpolation utilised to normalise i rows of data per stroke to 101 rows of data per stroke (0-100%). The current study defined the beginning of the n^{th} stroke to be at the n^{th} catch, and the end to be the beginning of the $n+1^{\text{th}}$ catch.

An algorithm was derived and used to identify observations in the raw kinematic data that represented a catch. This algorithm observed the series of data logged from the handle force transducer, scanning through the rows until it located four sequentially logged data points that satisfied six conditions. The four data points were the first in groups of ten observations (Figure 5.1). The six conditions specified that: a particular relationship must exist between the magnitudes of the four values, that the first and fourth value must be respectively below and above relevant thresholds, and that the $n+1^{\text{th}}$ catch could not occur within ten rows of the n^{th} catch. Once a kinematic file had been scanned and all of the catch rows identified, rowing strokes of i rows in length were defined as occurring between the two rows of data; catch row n to catch row $(n+1)-1$. The data representing each stroke was placed in an array and linear interpolation was used to transform strokes of length i rows into strokes of length 101 rows. Figure 5.1 shows an example of two strokes being identified from a data series, the figure includes information on the pertinent values of handle force, and a short description of exactly how the stroke identification algorithm was designed (Figure 5.2) and put into practice follows.

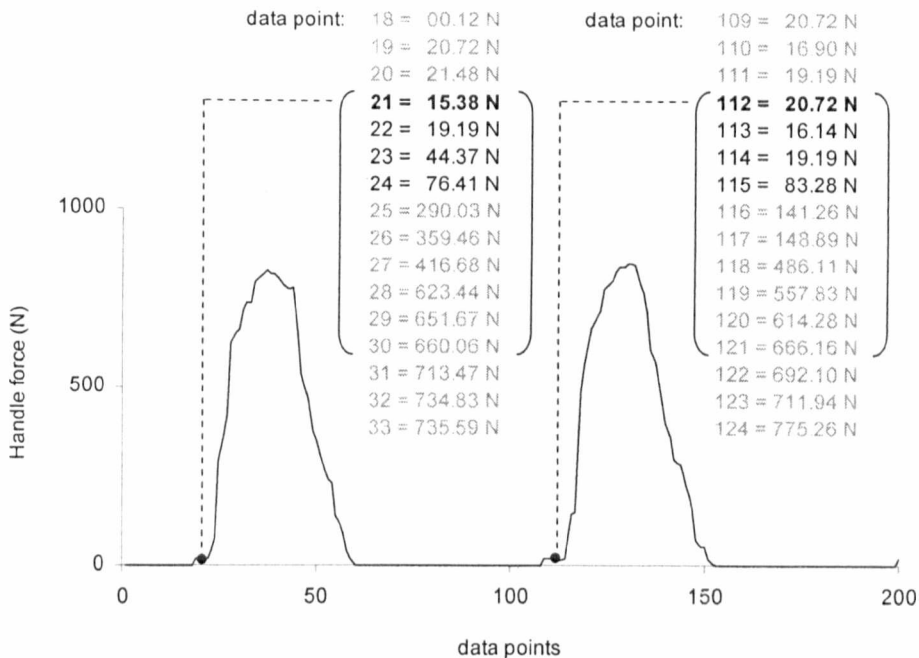


Figure 5.1: Identification of individual rowing strokes within raw data

The figure shows two strokes being identified from athlete data. The pertinent values that met the six conditions of the stroke recognition algorithm are presented in black type, and the data points that were identified as being the catch of a stroke are in bold type. Once data points 21 and 112 had been identified as catch rows the program did not allow any of the rows 22-30 or 113-121 to be considered as catch rows (the observations in brackets).

```

datacount = length (data);
catchpoints = zeros(datacount,1);
i = 10;

while i <= datacount

    if (data(i-9,1) - data(i-8,1)<5) && ...
       (data(i-8,1) - data(i-7,1)<5) && ...
       (data(i-7,1) - data(i-6,1)<5) && ...
       (data(i-6,1)>75) && ...
       (data(i-9,1)<40)

        catchpoints(i-9,1) = 1;
        i = i + 10;
    else
        i = i + 1;
    end
end

```

Figure 5.2: Pseudocode used for stroke identification

The choice of the thresholds 75 N and 40 N was based on the results of an optimisation pilot study in which several thresholds were tested to find the lowest values that could be used whilst maintaining a robust stroke identifier. This was carried out by using Matlab to visualise the data in plots and filtering by eye. In the example shown in Figure 5.1, the first catch was identified

at data point 21. It was not identified earlier than this because the value of data point 20 minus data point 21 was greater than 5 N, and because it was not until data point 24 that handle force exceeded 75 N. Neither data point 113 nor 114 were identified as a catch row because there was less than 10 rows between them and a previously defined catch; they were within the brackets shown in Figure 5.1. Once the Step files had been normalised their dimensions were equal to forty five columns and 101 times the number of individual strokes rows. Five additional columns were then calculated from the existing data and appended to the matrix. The new columns described the length of the rowing stroke (mm), the stroke rate (per minute), the work done (J), and the power output (W). Stroke length was calculated using the output from the rotary encoders that tracked handle motion (i.e. the chain length from the catch point to the maximum chain excursion), stroke rate utilised the seconds past midnight column of data, work was calculated incrementally as the product of handle force and handle motion, and power output was calculated by numerically integrating the work curve. The output file from the normalisation program consisted of a matrix whose dimensions were fifty columns and, 101 times the number of individual strokes rows (Table 5.1).

Each raw data file contained:	Each raw kinematics file contained:	Each normalised kinematics file contained:
Ergometer handle transducers' signals	Ergometer handle transducers' signals	Ergometer handle transducers' signals
Ergometer seat transducers' signals	Ergometer seat transducers' signals	Ergometer seat transducers' signals
FOB sensors' global position and orientation	FOB S1 and S2 global orientation	FOB S1 and S2 global orientation
Seconds past midnight	Seconds past midnight	Seconds past midnight
	Global position of LSJ, HJC, KJC, AJC, FJC	Global position of LSJ, HJC, KJC, AJC, FJC
	Intersegmental angles at LSJ, HJC, KJC, AJC, FJC	Intersegmental angles at LSJ, HJC, KJC, AJC, FJC
	Athlete's body mass	Athlete's body mass
		Stroke length
		Stroke rate
		Work done
		Stroke power output

Table 5.1: The content of raw and processed Step test files

5.2.1 Additional considerations for data normalisation

The data shown in Figure 5.1 shows that the stroke identification algorithm did not always record the beginning of a rowing stroke exactly where one might by visual observation of the same data. That is, in the example shown in Figure 5.1 a visual assessment of the data would probably find the second stroke to begin at data point 114, two data points after the current stroke identification algorithm. It was recognised that this could be an area of potential error particularly as data would subsequently be used to generate average/representative strokes intra and inter athlete (Section 5.3). It was thought that the impact of this effect would be small and this was tested in a pilot study to assess two different mechanisms for stroke identification.

5.2.1.1 Validation of stroke identification

These first of these methods used the handle force data and specified that a catch occurred when the force data recorded during the recovery phase increased above the mean of the recovery forces plus one standard deviation from the same mean (Figure 5.3). The method also used the same thresholds as the current algorithm for the catch point (< 40 N), and fourth stroke data point (> 75 N):

```
datacount    = length (data);
catchpoints  = zeros (datacount, 1);
i            = 20;

while i      <= datacount

    if      (data(i-9,1) > (mean(data(i-19:i-14,1)) +
std(data(i-19:i-14,1))))    && ...
        (data(i-6,1) > 75)    && ...
        (data(i-9,1) < 40)

        catchpoints(i-9,1) = 1;
        i = i + 10;
    else
        i = i + 1;
    end
end
```

Figure 5.3: Pseudocode rejected for use in stroke identification – version 1

The method produced exactly the same results as the algorithm described in Section 5.2. An attempt was then made to improve this standard deviation method by adjusting the lower threshold either through increasing it or removing it completely; this endeavour resulted in many incorrect strokes being identified, and strokes being identified noticeably after the onset of handle force (Figure 5.4). This delay would have been unfamiliar to the rowing community,

and would also have caused significant decreases in work and power calculations for the drive phase of the stroke.

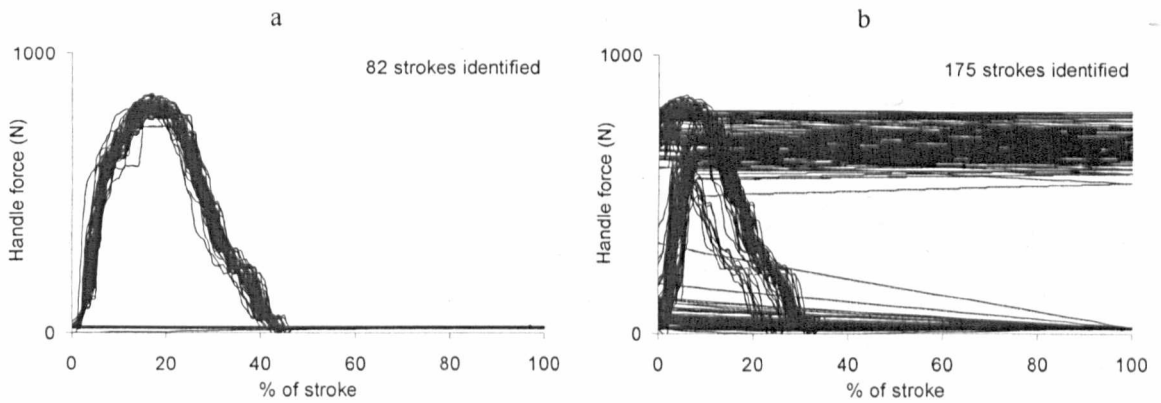


Figure 5.4: Strokes identified using different algorithms

Using a sample of data from HWW SCULL during moderate intensity exercise; the strokes identified by the algorithm that was used throughout the project (a), and the rejected pseudocode version 1 with thresholds removed (b). The average number of data points that contributed to the construction of a normalised stroke in (a) was 125, and in (b) was 59.

The second new method that was assessed used data concerning the trajectory of the ergometer handle. This algorithm simply identified the rows in a data set where the handle reversed its direction of travel at the stern of the ergometer (Figure 5.5):

```

datacount = length (data);
catchpoints = zeros (datacount, 1);
i = 10;

while i <= datacount

if      data(i-9,43)>data(i-8,43)&&...
      data(i-8,43)>data(i-7,43)&&...
      data(i-7,43)>data(i-6,43)&&...
      data(i-5,43)>data(i-6,43)&&...
      data(i-4,43)>data(i-5,43)&&...
      data(i-3,43)>data(i-4,43)

      catchpoints(i-9,1) = 1;
      i = i + 10;
else
      i = i + 1;
end
end
end

```

Figure 5.5: Pseudocode rejected for use in stroke identification – version 2

This algorithm consistently underestimated where the catch occurred. That is the “slippage” mentioned above in relation to the optimal algorithm was noticeably accentuated; catch rows

were identified an average of 4.6 ± 1.1 data points earlier. It is possible that other methods for stroke identification could have been explored, for example Bull and McGregor (2000) used maximal femoral flexion to identify the timing of the catch. However the example shown in Figure 5.5 suggests that the use of spatial data can be unsuitable for this purpose.

5.2.1.2 Effect of stroke identification inaccuracy

Having decided that the stroke identification algorithm presented in Section 5.2 could not be easily improved upon a pilot study was carried out to assess the potential effect of it occasionally finding the beginning of a stroke up to 2% prior to a visual assessment of the same data. The 168 dependent variables considered in this thesis are introduced in Section 5.3. When a 2% change in the timing of identified strokes was applied to pilot data it was found that the largest change in any measurement of three-dimensional kinematics was 2.0 mm and 0.3° , and that across all measurements the average change in an observed value was 0.1 ± 0.3 mm and $0.0 \pm 0.0^\circ$. It was concluded that any apparent weakness of the current stroke identification algorithm would not induce significant errors in the measurement and analysis of elite rowers' technique and performance.

5.3 Data extraction

In Matlab there were three main stages of data analysis. First of all each of the normalised files were analysed by a program which used the handle force column of data, relevant thresholds and graphs to ensure that all of the strokes that had previously been identified by the normalisation program were valid (Appendix 2). This was completed because preliminary investigations found that the normalisation program would occasionally (<1% of the time) identify a stroke incorrectly (Figure 5.6). This was in part due to the stroke identification algorithm not being absolutely infallible, and also because occasional random spikes in handle force data were observed (Figure 5.6). It was discovered that these spikes in the handle force data were caused due to wiring issues in the hardware setup; this was corrected and was not an issue subsequently.

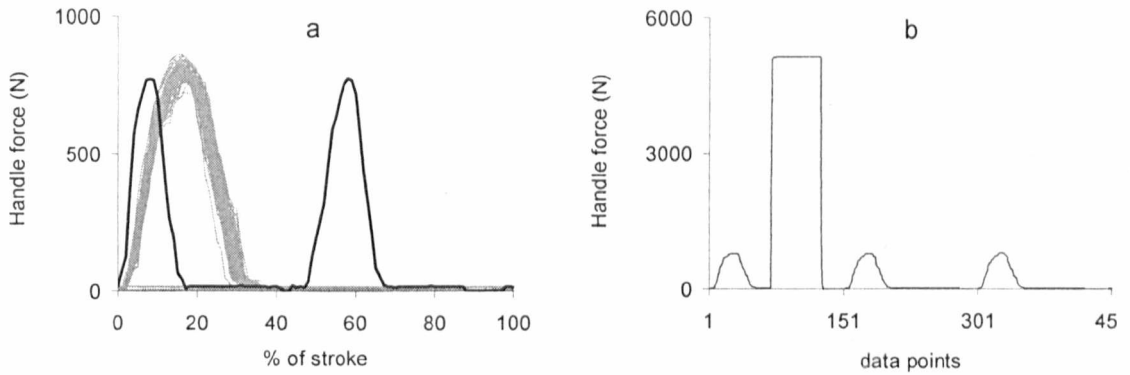


Figure 5.6: Errors in stroke identification

Every stroke that was identified from a raw data file (grey) is plotted below one particular stroke that should have been identified as two strokes (a). A random spike in handle force that occurred during data collection (b).

After confirming the validity of all of the strokes that were to be used for further analysis each Step file of interest was processed by a second Matlab program (Appendix 3). This program calculated an average stroke for the Step. It was then possible to calculate further average strokes for groups of athletes (Appendix 4). Once all of the average strokes of interest had been calculated a third Matlab program was run in order to extract dependent variables from each stroke matrix (Appendix 5). The variables that were logged are presented in Table 5.2. There were 138 variables that pertained to three-dimensional body kinematics; describing the X,Y,Z position of joint centres and the flexion/extension (α), side flexion, abduction/adduction or eversion/inversion (β), and twist or internal/external rotation (γ) intersegmental angles. Each of these kinematic data were logged six times per stroke; i. the maximum value, ii. the minimum value, iii. the value at the catch of the stroke, iv. the value at the point in the stroke when maximum force was being exerted on the handle, v. at the finish of the stroke (the instant in the stroke, after peak handle force was observed, when handle force dropped below 50 N), and vi. at the point in the stroke when the knees started to rise during the stroke recovery (knees break/knees up). This data was collected so that a full description of the kinematic behaviour of elite rowers could be produced, and also because it was hypothesised that some variables would change with increasing exercise intensity, or over time (rowing season). Furthermore, it was thought that some kinematic parameters may be linked with rowing performance or injury mechanisms. The other dependent variables were derived from the data recorded via the handle instrumentation and the seat instrumentation, and measured the timing of key stroke events, and parameters such as stroke length and power output. All of the variables considered are presented in Table 5.2 and are examined in PART 2.

Non 3D kinematic variables	Kinematic data*
COP drift – MHF (mm)	LSJ X
COP drift – Finish (mm)	LSJ Y
COP drift, MHF-Fin (mm)	LSJ Z
COP drift, Recovery (mm)	LSJ alpha
COP drift, Stroke (mm)	LSJ beta
COP Z @ Catch	LSJ gamma
COP Z @ MHF	HJC X
COP Z @ Finish	HJC Y
Quality COP X @ Catch	HJC Z
Quality COP X @ Finish	HJC alpha
Quality COP X @ MHF	HJC beta
	HJC gamma
Max handle force (%)	KJC X
Finish (%)	KJC Y
Knees up (%)	KJC Z
	KJC alpha
Max handle force (N)	AJC X
Max H Force/BM (N/kg×100)	AJC Y
Slope of handle force	AJC Z
Max seat force (N)	AJC alpha
Min seat force (N)	AJC beta
Seat force @ MHF (N)	AJC gamma
	FJC alpha
Suspension 1 (BW(s))	
Suspension 2 (BW(s))	
Power output (W)	
Stroke length (mm)	
Stroke rate (/min)	
Work done (J)	
Quality LP ratio @ Catch	
Quality LP ratio @ MHF	
Quality LP ratio @ Finish	
Z handle minus Z KJC	

Table 5.2: Dependent variables extracted from experimental data

It was this data upon which descriptive and statistical analyses were carried out.

* Kinematic data was logged six times; maximum, minimum, and at four stroke events (Section 5.3).

5.3.1 Description of the variables

From this point any variable which appears in column one of Table 5.2 may be referred to as a “stroke profile” variable, whilst the others are referred to as kinematic variables. The variables in Table 5.2 that relate to the timing of key events within the rowing stroke were measured in percentages and are often useful in determining when to look at other parameters. In addition to this, the timing of a stroke may in itself be a good performance indicator. The timing of the maximum force exerted on the handle during the stroke (Max handle force, MHF %), the timing of the finish of the stroke (Finish %), and the timing when the knees break in the recovery (Knees Up %) were logged. The slope of handle force was the magnitude of the peak force divided by the timing of peak handle force. Seat force @ MHF referred to the force that was exerted on the seat at the time point of maximum handle force.

The suspension variables noted in Table 5.2 were calculated using the seat force data. A key coaching principle in rowing is for an athlete to *suspend* their body between their feet and hands during the propulsive part of the stroke, the legs should exert pressure on the footstretcher and activation of the latissimus dorsi muscles will facilitate suspension (Thompson, 2005). The level that an athlete suspended during the current study was defined using the seat force data and the athlete's body weight (BW). The area under the seat force curve was calculated and this magnitude was divided by the athlete's BW, this yielded a normalised score for suspension in BWs. Suspension 1 refers to the level of suspension achieved from the catch to the occurrence of maximum handle force, and Suspension 2 refers to the level of suspension achieved throughout the entire drive phase.

The lumbopelvic (LP) ratio refers to the magnitude of the extension or flexion of the lumbar and sacral regions of the spine. In the sagittal plane the LP ratio can be used to describe how the BACK and PELVIS move in relation to each other. For example, if towards the finish of a stroke an athlete's pelvis was found to be in 20° of extension, and their lumbar spine was found to be in 30° of extension, the LP ratio would be 1.5 ($30^\circ/20^\circ = 1.5$). In some specific cases the angle between the two segments and not the lumbar angle divided by the pelvic angle was said to be the LP ratio. For example; if the lumbar spine was found to be in 5° of flexion, and the pelvis was found to be in 0.2° of flexion the LP ratio would have been 4.8 (the angle between the segments), not 25 ($5^\circ/0.2^\circ = 25$). The LP ratio is calculated using the orientation output of the FOB sensors attached to the body segments, can be used as a coaching tool, and has previously been shown to aid in understanding low back pain in rowers (McGregor et al., 2002; McGregor et al., 2005). The drive phase of the rowing stroke may be likened to a high pull, or to some extent a leg press in weightlifting, and lifting coaches recommend "*pull against the bar so that the arms are straight and the low back is flat*".¹ Deviations from alignment of the two spinal segments (deviation from a ratio of 1) were said to be of lower quality than sagittal coordination, thus the quality LP ratio scores seen in Table 5.2 refer to the distance of the measured ratios from 1.

Z handle minus Z KJC was a measure of where in space the ergometer handle was (in the anterior/posterior direction) in relation to the position of the KJC at the point in the stroke where the knees break in the recovery. This measure was included as another key aspect of rowing technique is that the handle should be distal to the KJC before the knees break.

Forces exerted in the direction of gravity on the seat were recorded as negative values. Because contact at the seat is supported over a varying surface area with different pressures at each part, the centre of pressure (COP) can be used to describe how the rower is moving their weight

¹ www.healthline.com, accessed June 2008.

across the surface of the seat. In Table 5.2 the variables that are labelled “COP drift * ” refer to the trajectory of the athletes’ COP on the seat during certain parts of the stroke. COP trajectory was measured with a medial/lateral coordinate (X) and an anterior/posterior coordinate (Z). The drift measurement is the sum of the absolute values of the COP coordinate in the X direction as recorded between the catch and the occurrence of maximum handle force (COP drift – MHF), the catch and the finish (COP drift – Finish), the occurrence of maximum handle force and the finish (COP drift, MHF-Fin), from the finish to the instant before the subsequent catch (COP drift, Recovery), and during the entire stroke (COP drift, Stroke). These measurements were made because it was theorised that deviations medially or laterally from the centre line of the ergometer seat would be deleterious to rowing performance, and that they might be related to aspects of body kinematics. The X and Z coordinate for COP was also logged at the catch, at maximum handle force, and at the finish of the stroke. These measurements were again hypothesised to be linked with improving rowing performance and body kinematics. Note that the X coordinate of COP is logged as a “Quality” score; this is the absolute number of the coordinate as the number would be negative on one side of the seat and positive on the other, and, as with the “drift” scores it was thought that minimising the X coordinate of COP in either direction may be linked to rowing performance. The Z coordinate was also either negative or positive, however, it was not necessary to use the absolute value as it was thought that an “ideal” rowing performance would include some anterior/posterior displacement of COP on the seat. Figure 5.7 illustrates how some of the COP measurements were calculated.

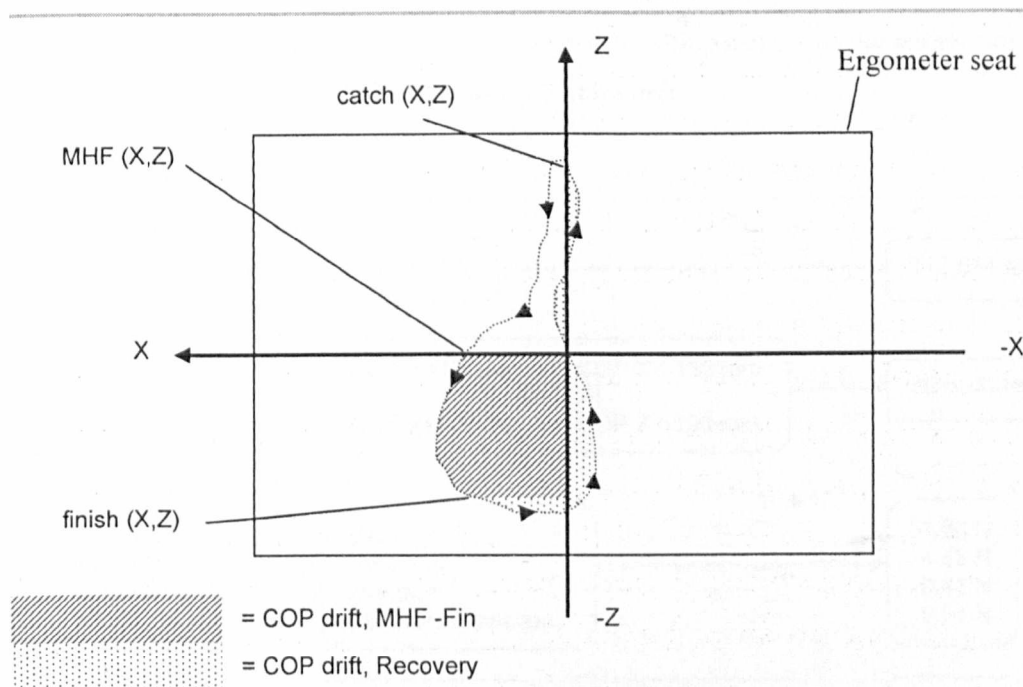


Figure 5.7: Example of how centre of pressure data was used

The dashed black line represents an indicative trajectory, in the direction indicated by the arrow heads, of COP for a rowing stroke. Computations of two of the “drift” scores are illustrated.

5.3.1.1 Additional considerations for centre of pressure

Initial data analysis revealed that occasionally the coordinates logged for COP were unreliable. The ergometer seat measured 300 mm (X) by 250 mm (Z), thus even if it was assumed that an athlete's COP could be on the very edge of the seat, the coordinates could not lie out with the range -150 to 150 mm (X) and -125 to 125 mm (Z). It was found that, occasionally, and always when less negative magnitudes of force were being applied to the seat, the measured COP lay outside of the border of the seat. That is, when some athletes approached complete suspension during the drive, and therefore as 0 N of downwards force on the seat was neared, the coincident COP information became erroneous. It was decided that a low pass filter based on the instantaneous magnitude of vertical force on the seat should be applied to the COP data. A pilot study was conducted to determine the threshold of the filter. This is described below.

After normalisation of athlete data, but before any average strokes were calculated, the current study had obtained 7,754,982 pairs of COP coordinates (X,Z) from athlete Step tests, and the coincident values for the magnitude of vertical force on the seat. This data represented 76,782 individual rowing strokes, and was contained within 1,115 normalised Step files. These normalised matrices were reduced to 1,115 average stroke matrices using one of the Matlab programs that have already been introduced. Hence, there were 112,615 sets of COP coordinates and seat force data contained within the average strokes (1,115 average strokes \times 101 rows per average stroke = 112,615 rows). This data was put into a matrix of 112,615 rows by 3 columns (A). A was analysed to provide a magnitude for the required filter threshold (Figure 5.8). This magnitude was then validated by comparing it to the entire, normalised but not averaged, dataset, B (7,754,982 rows by 3 columns).

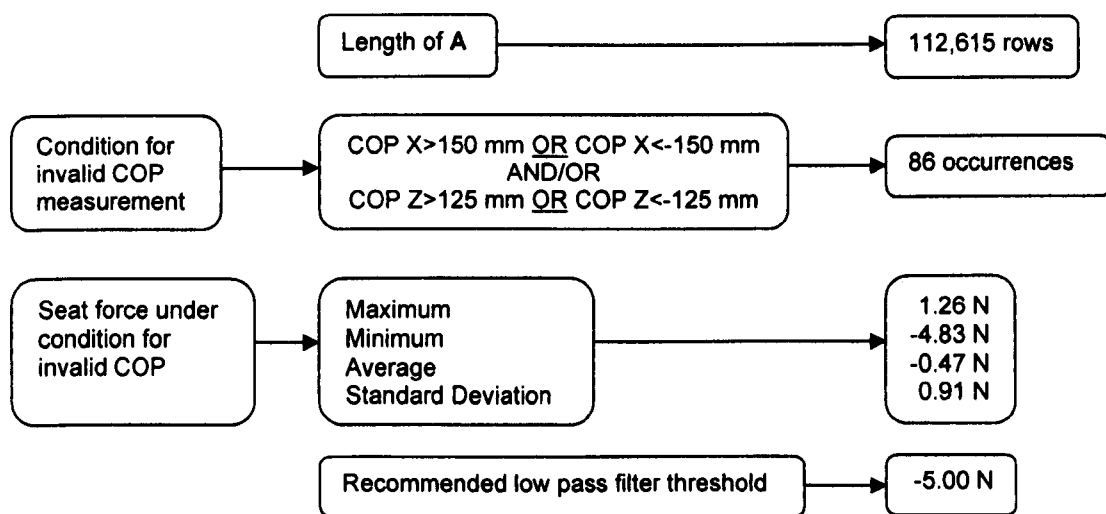


Figure 5.8: Determination of COP filter magnitude

The magnitude of the filter was set to -5 N. It was thought that the unexpected maximum seat force shown in Figure 5.8 (>0 N) may have occurred as a result of the inertial effects associated with rapid unloading of the seat. The filter worked by scanning logged seat force data, identifying when its magnitude was greater than -5 N and automatically reassigning the coincident COP coordinate to 0,0 (X,Z). After applying the filter to **A** the average absolute coordinate in the X direction was 7.87 mm, and in the Z direction was 19.06 mm. Figure 5.9 illustrates all of the COP data contained in **A**.

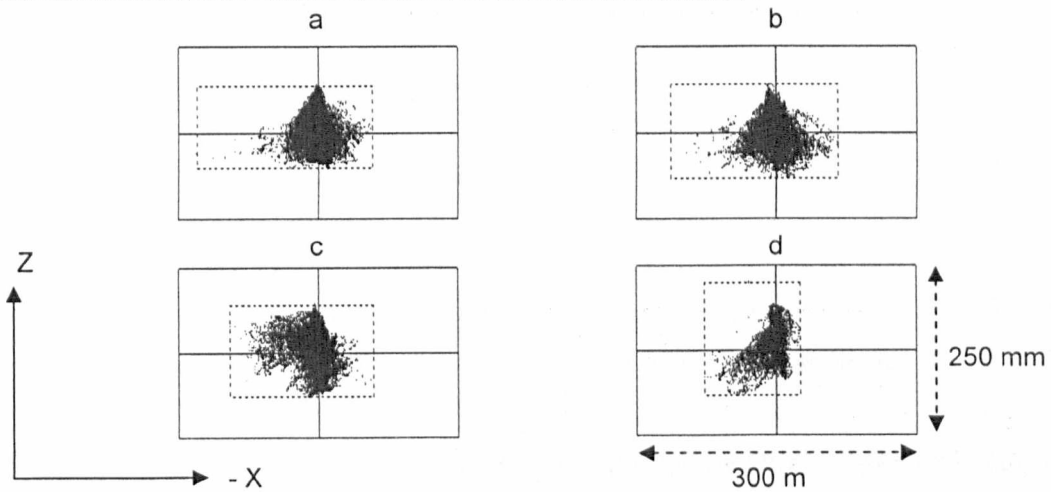


Figure 5.9: Filtered centre of pressure coordinates

The COP data recorded from HWW-SCULL (a), HWW-SWEEP (b), LWM (c), and LWW (d). The scatter plots highlight the position of 34037, 33027, 36158 and 9393 pairs of COP coordinates respectively. The solid black lines represent the borders of the ergometer seat. The dashed black rectangles highlight the maximum COP coordinates logged.

The strength of the choice of -5 N was further tested by observing the 7,754,982 rows of data in **B**. It was found that 0.23% of the unfiltered data met the condition for invalidating COP (condition shown in Figure 5.8). Of these 17,671 invalid coordinates 214 had coincident seat force values of less than -5 N. Thus the total probability of -5 N not being an appropriate filter to be applied to **B** was 2.8×10^{-5} . The 17,671 invalid coordinates found in **B** are shown in Figure 5.10.

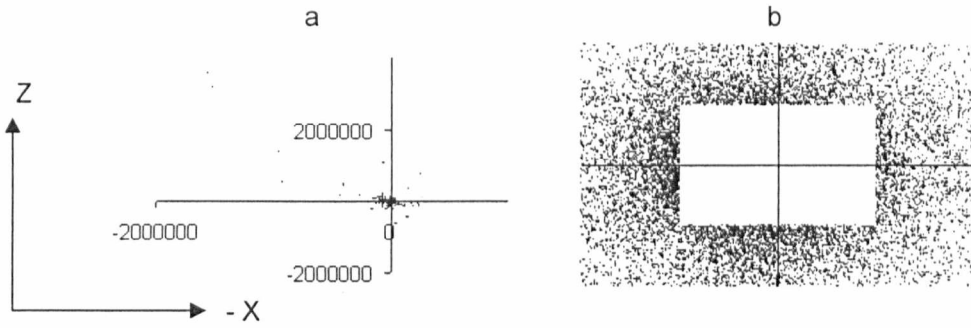


Figure 5.10: All invalid, unfiltered centre of pressure coordinates

All of the data that was found to meet the condition for invalidating a COP measurement (a), the scale is in mm. Magnified view of the same data, the chart area is twice the size of the ergometer seat, with the ergometer seat in the middle (b).

5.3.1.2 Three dimensional kinematics and associated errors

In order to assess the validity of any subsequent measures of changes in kinematics and to quantify errors associated with the measurement system, the aim of this section is to quantify the uncertainty associated with three dimensional kinematics in the current setup.

In this application measured kinematics are dependent upon multiple sources of independent uncertainty (FOB motion tracker, manual palpation, regression equation to identify the location of L5S1), hence the total system uncertainty must be determined in order to validate observed differences in kinematics with factors such as increasing exercise intensity. In such cases it is possible for separate uncertainties to partially cancel each other out; by using the standard error of the mean to represent uncertainty in a measured value the following method may be used to calculate the net uncertainty in the current system (Kirkup, 1994):

$$V = FOB + palp + reg \quad \text{Equation 5.1}$$

V is the quantity of a measured kinematic variable

FOB is the measured position and orientation of one or more FOB sensors

$palp$ is the act of manually palpating an anatomical landmark

reg is the influence of the regression equation used in determining the location of L5S1

(Section 4.1.6)

$$\sigma_{\bar{V}} = \sqrt{\left(\frac{\partial V}{\partial FOB}\right)^2 \sigma_{FOB}^2 + \left(\frac{\partial V}{\partial palp}\right)^2 \sigma_{palp}^2 + \left(\frac{\partial V}{\partial reg}\right)^2 \sigma_{reg}^2} \quad \text{Equation 5.2}$$

$\sigma_{\bar{x}}$ is the standard error of the mean/the uncertainty of the associated measurement.

Thus

$$\sigma_{\vec{V}} = \sqrt{\sigma_{\text{FOB}}^2 + \sigma_{\text{palp}}^2 + \sigma_{\text{reg}}^2} \quad \text{Equation 5.3}$$

In this case it is assumed that tracking the location of L5S1 is associated with greater uncertainty than any other of the anatomical joint centres due to the involvement of the regression equation used in identifying the location of L5S1 within a pelvic axis system. It may be argued that other factors contribute uncertainty to the current system; soft tissue artefact has not been addressed and it is outwith the scope of this study, and any errors associated with the actual process of digitisation or functional assessment of the hip joint centre location are assumed to be covered by the FOB uncertainties. Some of the previously described experiments (Chapter 3 and 4), and some data extracted from the literature were used to calculate values to substitute into Equation 5.3.

The uncertainty associated with the motion tracking system was derived from data logged during the experiments presented in Section 3.3. With the FOB transmitter in its optimal location within the current laboratory, and with the ergometer in place the average discrepancy in the measured vector between two sensors was 8.37 mm, the standard deviation for this data was 6.75 mm and the associated standard error of the mean was 0.55 mm. A similar standard error associated with the repeatability of transmitter placement was 0.39 mm. Concerning orientation, data collected during the experiment presented in Section 3.3 provided an uncertainty measurement of less than 0.01°; the latter source of uncertainty was ignored. Both 0.55 mm and 0.39 mm will be entered into Equation 5.3 to represent the uncertainty associated with the FOB motion tracker.

In a study quantifying sources of variability associated with three dimensional human kinematics, De Groot (1997) concluded that palpation of anatomical landmarks is an accurate method of recording the orientation of body segments. However, Della Croce et al. (2005) stated that because such palpable landmarks are often the pinnacle of larger curved areas, their identification by manual palpation is subject to inter and intra examiner variability. In order to provide a number representing the uncertainty associated with manual palpation of anatomical landmarks the current study used data presented in the literature (Morton et al., 2007) and received from personnel communications with the authors of published studies (Moriguchi et al., 2009). These studies considered the variability in anatomical landmark location and the repeatability of inter and intra examiner palpation of upper limb, pelvic and lower limb body segments. The data provided a measure of 1.1 mm to be entered into Equation 5.3.

The final source of uncertainty currently being considered when measuring a kinematic displacement is associated with the regression equation that identifies the location of L5S1 within a pelvic axis frame (Section 4.1.6). The data collected during this experiment provided a standard error of the mean identification of L5S1 in three dimensions of 0.87 mm; this too will be entered into Equation 5.3:

$$\sigma_{\bar{V}} = \sqrt{\sigma_{\text{FOB}}^2 + \sigma_{\text{palp}}^2 + \sigma_{\text{reg}}^2} \quad \text{Equation 5.3}$$

$$\sigma_{\bar{V}} = \sqrt{0.55^2 + 0.39^2 + 1.10^2 + 0.87^2}$$

$$\sigma_{\bar{V}} = 1.56 \text{ mm}$$

It is concluded that there is uncertainty associated with measurements of kinematics in the current setup, however the magnitude of uncertainty is small and will only be referred to in PART 2 if a statistically significant difference in a variable is found at very low magnitudes of change (< 1.56 mm). Furthermore, due to the systemic nature of EM system errors reported in the literature (Section 3.2), and found in Chapter 3 of this thesis, it is reasonable to assume that because all pertinent anatomical landmarks will be displaced a similar distance from the EM source in the medial lateral direction, any errors in the identification of anatomical points will occur in consistent directions and with similar magnitudes; therefore it is unlikely that the measured orientation of body segments will be imprecise, and thus calculated intersegmental angles will be appropriate.

5.4 Statistics

After processing data as described above, various statistical methods were employed using Matlab and SPSS (Figure 5.11). In addition to calculating the descriptive statistics of the data, and providing graphical representations of its trends, some other statistical techniques provided insight into changes in the magnitude of, and relationships between the dependent variables that have been introduced (Table 5.2), and some other variables that are discussed in Chapter 9 and Chapter 10. These statistics included general linear models with repeated measures (ANOVA with repeated measures), correlation analyses and linear regression analysis. The SPSS functions utilised were primarily parametric tests; in order to ensure the validity of all statistical analyses the data that was used and the residuals of regression analyses were assessed for normality of distribution, and appropriate examinations of homogeneity of variance and sphericity of data were conducted.

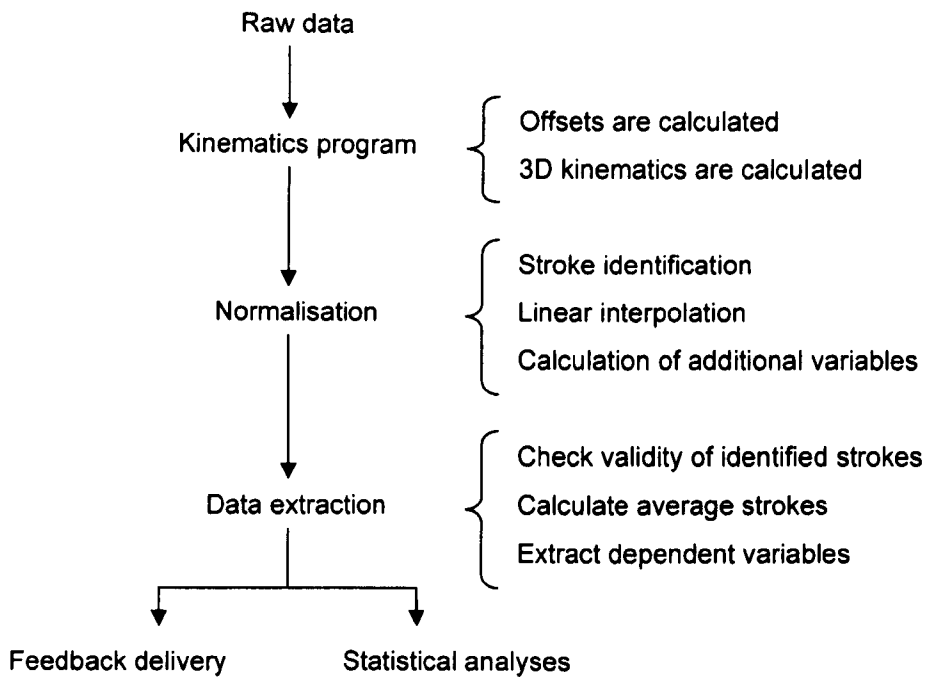


Figure 5.11: The data analysis process

ANOVA with repeated measures (ANOVA RM) was conducted in order to understand the effect that increasing intensity (Steps 1-6) had on the dependent variables, and also to observe changes in measured data over the course of many months. Each test was assessed for sphericity and significance before appropriate pairwise comparisons were made post hoc to identify where differences lay.

Correlation analyses were used in order to identify those dependent variables which accounted for the majority of the variability in the dataset, and to provide information on which variables were related to each other. This process was conducted in Matlab and helped in the process of regression analyses.

5.5 Summary and hypotheses

This chapter has illustrated the work that was carried out in order to gather and interpret the data logged during athlete testing. It has been shown that the raw data collected during laboratory sessions could be manipulated and reduced to provide information on the technique and performance of elite rowers. As a result of this data reduction it was possible to formulate hypotheses that could be tested using statistical modelling. The hypotheses offered were:

1. That a full description of the stroke profile and three-dimensional kinematics of elite rowers could be produced (Chapter 6).

2. That some aspects of elite rowers' technique and performance would be affected by the intensity of their exertions (Chapter 7).
3. That some aspects of elite rowers' technique and performance would change with longitudinal training (Chapter 8).
4. That high levels of performance could be predicted by aspects of athletes' technique and rowing kinematics (Chapter 9).
5. That some aspects of elite rowers' technique, performance and rowing kinematics could be exploited to reduce the risk of injury and pain (Chapter 9).

Throughout PART 2 there is further description of the statistics employed and the meaning of the results gathered.

PART 2

Results of analysis of the stroke profile and 3D kinematics of elite rowers

Chapter 6

Descriptive Results

This chapter includes three distinct sections; Section 6.1 specifies the number of athletes that were tested during each session, along with providing information on which Steps were completed by whom, and how many rowing strokes were used during data analysis. In Section 6.2 there is a reminder of the laboratory setup and axis systems that were used in the current research, and a guide to interpreting intersegmental angles. Section 6.3 is presented in response to the first hypothesis listed in Section 5.5; describing the stroke profile and kinematic behaviour of elite HWW-SCULL, HWW-SWEEP, LWM and LWW rowers, and includes graphical representations of their ergometer performances with accompanying dialogue of the graph trends and features.

6.1 Scale of athlete testing

Forty two individual athletes attended at least one testing session, and completed up to six Steps during each visit. In total 1,115 Steps were recorded over a period of 26 months, and the average number of individual strokes recorded during each Step was 68 (Table 6.1 and Table 6.2). On average the largest group of athletes was the HWW-SWEEP (Table 6.1), and two athletes completed all Steps at every testing session (athlete 7 and athlete 32, Table 6.3).

Number of:	Dec-06	Apr-07	Jul-07	Oct-07	Dec-07	Mar-08	Jun-08	Dec-08	Feb-09	Total	Average
HWW-SCULL tested	4	4	5	7	6	6	6	10	11	59	7
HWW-SWEEP tested	8	14	4	9	10	9	8	-	-	62	9
LWM tested	6	6	5	5	5	8	7	8	6	56	6
LWW tested	1	2	1	1	1	2	2	3	3	16	2
All athletes	19	26	15	22	22	25	23	21	20	193	21
Steps by HWW-SCULL	23	24	28	38	36	36	36	55	61	337	37
Steps by HWW-SWEEP	48	84	24	44	60	51	47	-	-	358	51
Steps by LWM	34	36	30	29	28	48	42	44	36	327	36
Steps by LWW	6	12	5	6	6	10	12	18	18	93	10
All Steps recorded	111	156	87	117	130	145	137	117	115	1115	124

Table 6.1: Number of athletes tested and Steps completed during each session

Number of:	Step 1	Step 2	Step 3	Step 4	Step 5	Step 6	Total	Average
Steps by HWW-SCULL	58	58	57	58	56	50	337	56
Steps by HWW-SWEEP	62	62	62	62	61	49	358	60
Steps by LWM	55	56	55	56	54	51	327	55
Steps by LWW	16	16	16	16	15	14	93	16
All Steps recorded	191	192	190	192	186	164	1115	186
Maximum number of strokes per Step	84	84	91	92	110	63	-	87
Minimum number of strokes per Step	30	11	18	19	18	18	-	19
Average number of strokes per Step	66	68	71	76	82	47	-	68
Standard Deviation strokes per Step	10	12	13	14	14	6	-	12

Table 6.2: All Steps recorded and number of individual rowing strokes therein

6.2 Laboratory setup and directions of movement

Figure 6.1 illustrates the laboratory setup used during athlete testing, and includes information on the direction of global and seat axis systems. Table 6.4 details what the output of the kinematics program was in terms of clinically relevant joint rotations, for example, in the current study knee flexion was characterised by KJC alpha values greater than zero degrees.

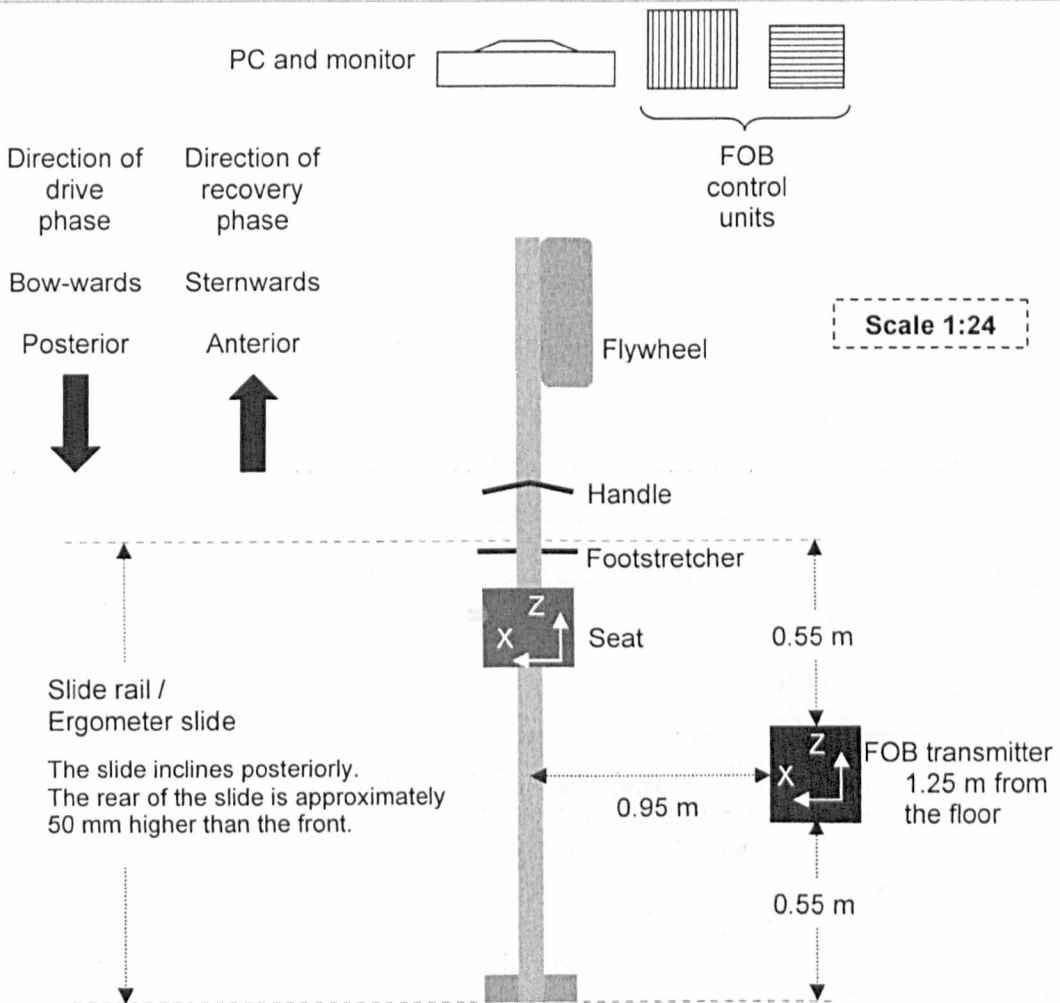


Figure 6.1: Overhead view of the laboratory setup used during athlete testing sessions

Illustrating the location of all of the key equipment used in the current research. The origin of the laboratory/FOB axes was in the centre of the FOB transmitter cube, its X axis was medial/lateral to performance and positive in the direction shown in the figure, the Y axis was superior/inferior and positive in the superior direction, and the Z axis was anterior/posterior and positive in the anterior direction. The origin of the ergometer seat axis system was in the centre of the seat and X and Z were positive in the directions shown in the figure.

Clinical rotation	Measured within	Value of output angle (°)
Flexion of the lumbar spine	LSJ alpha	< zero
Extension of the lumbar spine	LSJ alpha	> zero
Lumbar side flexion to the right	LSJ beta	> ninety
Lumbar side flexion to the left	LSJ beta	< ninety
Lumbar twist to the right	LSJ gamma	< zero
Lumbar twist to the left	LSJ gamma	> zero
Hip flexion	HJC alpha	< zero
Hip extension	HJC alpha	> zero
Hip abduction	HJC beta	> ninety
Hip adduction	HJC beta	< ninety
Internal hip rotation	HJC gamma	< zero
External hip rotation	HJC gamma	> zero
Knee flexion	KJC alpha	> zero
Knee extension	KJC alpha	< zero
Dorsi flexion	AJC alpha	< minus ninety
Plantar flexion	AJC alpha	> minus ninety
Eversion of POSFOOT	AJC beta	> ninety
Inversion of POSFOOT	AJC beta	< ninety
Internal rotation of POSFOOT	AJC gamma	< zero
External rotation of POSFOOT	AJC gamma	> zero
Flexion between POSFOOT and ANTFOOT caused by the athletes' right heel lifting from the footstretcher	FJC alpha	Increasing magnitudes. Offset by use of AJC and not calcaneus to define POSFOOT

Table 6.4: Clinical rotations measured in the current study

The table explains the relevance of the angles that were measured in the current study. All of the angles measured at HJC, KJC, AJC and FJC were from the athletes' right limb.

6.3 How athletes row and move

In this section the first hypothesis that was presented in Section 5.5 is addressed; that a full description of the stroke profile and three-dimensional kinematics of elite rowers could be produced. The graphs and description of the trends presented in this section show the stroke profile, three-dimensional kinematics, and performance of elite rowers. All of the data that was collected between December 2006 and February 2009 was used to calculate an average stroke for each group of athletes during each Step. Thus, for each Step, an average of 56 (HWW-SCULL), 60 (HWW-SWEEP), 55, (LWM), and 16 (LWW) performances were condensed to a single representative stroke for each boat class.

In rowing, the intensity of an athlete's effort is often categorised into one of up to six zones: oxygen utilisation 3 (U3), oxygen utilisation 2 (U2), oxygen utilisation 1 (U1), anaerobic threshold (AT), transport (TPT), and anaerobic (AN) (Thompson, 2005). These categories relate to the physiological cost, and associated energy systems that are required to maintain a specific intensity of exercise. Table 6.5 describes some of the features of the six intensity zones.

	Stroke rate (/min)	Heart rate (% of maximum)	Individual's rating of perceived exertion	Physiological definition
U3	<18	65-75	1-2	Below the onset of blood lactate accumulation
U2	17-18	65-75	2-4	Below the onset of blood lactate accumulation
U1	19-23	70-80	5-6	Above onset of blood lactate accumulation but below onset of metabolic acidosis
AT	24-28	82-86	7-8	Just below the onset of metabolic acidosis
TPT	28-36	87-95	9	Above the onset of metabolic acidosis
AN	>36	Maximum	10 (Maximum)	Maximum effort

Table 6.5: Zones of exercise intensity

Adapted from Thompson (2005) and www.concept2.co.uk (accessed 16/03/09).

The head coach of the athletes involved with this research advised that in the ergometer Step test used: Steps 1-2 could be classified as U2, Steps 3-4 are within U1, Step 5 is AT, and Step 6 is TPT. With a view to facilitating easier description and understanding of technique and performance, only data associated with Step 2, Step 4 and Step 6 are presented in the scatter plots in this section. All of the scatter graphs show one complete, representative stroke (0-100%). Descriptive statistics such as the calculation of means and standard deviations were carried out in this chapter; when reference is made to differences between athlete groups or changes observed with increasing exercise intensity it is observational and for descriptive purposes only, it does not indicate statistical significance. Higher order statistics are carried out in subsequent chapters.

6.3.1 Athletes' stroke profile

The figures and accompanying descriptions in this section show the data logged for variables such as handle force, seat force and centre of pressure trajectory, and power output. For Steps 1-6 the average stroke rate observed per minute was 18-31 for HWW-SCULL, 18-30 for HWW-SWEEP, 19-31 for LWM, and 18-32 for LWW. Figure 6.2 shows the timing of the maximum recorded handle force, the finish of the stroke, and the instant when the athletes' knees began to rise during the stroke recovery. The figure shows that these timing measures were least variable for the HWW-SWEEP and LWW groups.

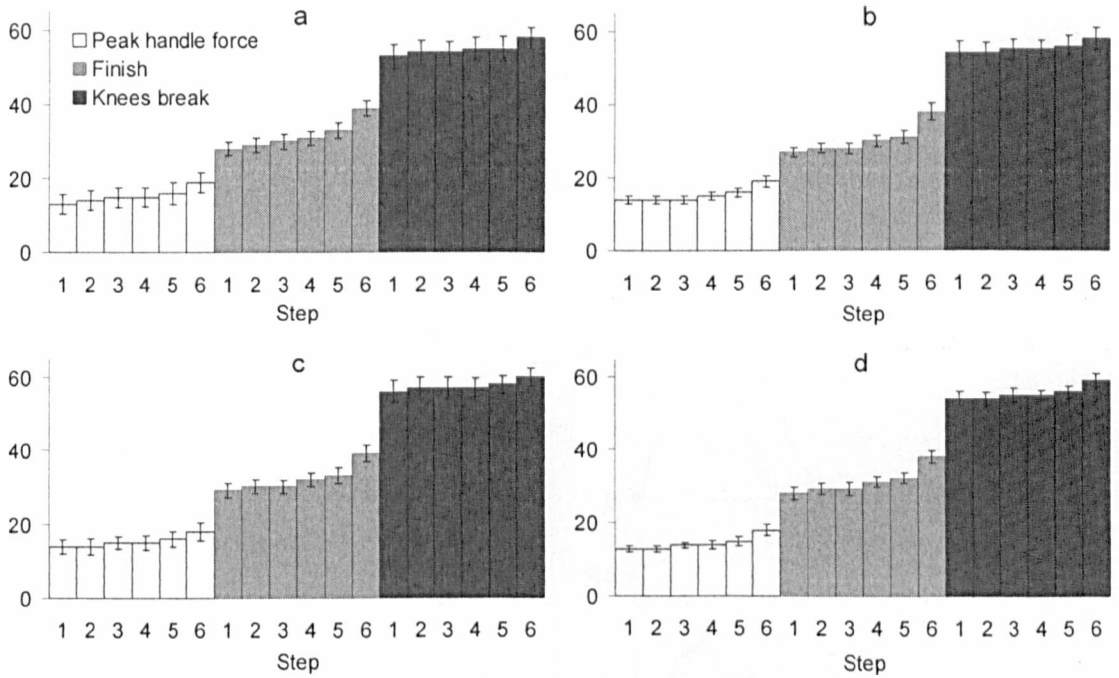


Figure 6.2: Mean and standard deviation of the timing of stroke events for all athlete groups
a. is HWW-SCULL, b. is HWW-SWEEP, c. is LWM, d. is LWW. All measurements are as a percentage of the rowing stroke. The columns show the average measurement for the timing of peak handle force, the finish of the stroke, and the instant when the athletes' knees began to rise during the stroke recovery of each Step. The error bars show associated standard deviations.

Figure 6.3 shows that all handle force series began with a roughly symmetrical bell shaped curve; the time from peak handle force to the finish was less than the time from the catch to peak handle force by 1%, 0%, 2%, and 2% for HWW-SCULL, HWW-SWEEP, LWM and LWW respectively (average asymmetry of bell shaped curve over all Steps). All athlete groups showed increasing peak force and decreasing drive:recovery duration ratio as intensity increased. Within each Step, the time at which each boat class exerted peak force on the handle, reached the finish of the stroke, and broke the knees during the recovery was respectively within 1%, 2%, and 3% of each other (Figure 6.2). The LWW produced the lowest peak pulling force through the handle (731.75 N in Step 6), followed by the HWW-SWEEP (781.71 N in Step 6), HWW-SCULL (795.39 N in Step 6), and LWM produced the highest handle forces (913.76 N in Step 6). As a result of this the rate at which force was produced was: in Step 6: 38.51 N/% \approx 1962 N/s (LWW), 39.09 N/% \approx 2041 N/s (HWW-SWEEP), 39.77 N/% \approx 2296 N/s (HWW-SCULL), and 48.10 N/% \approx 2669 N/s (LWM).

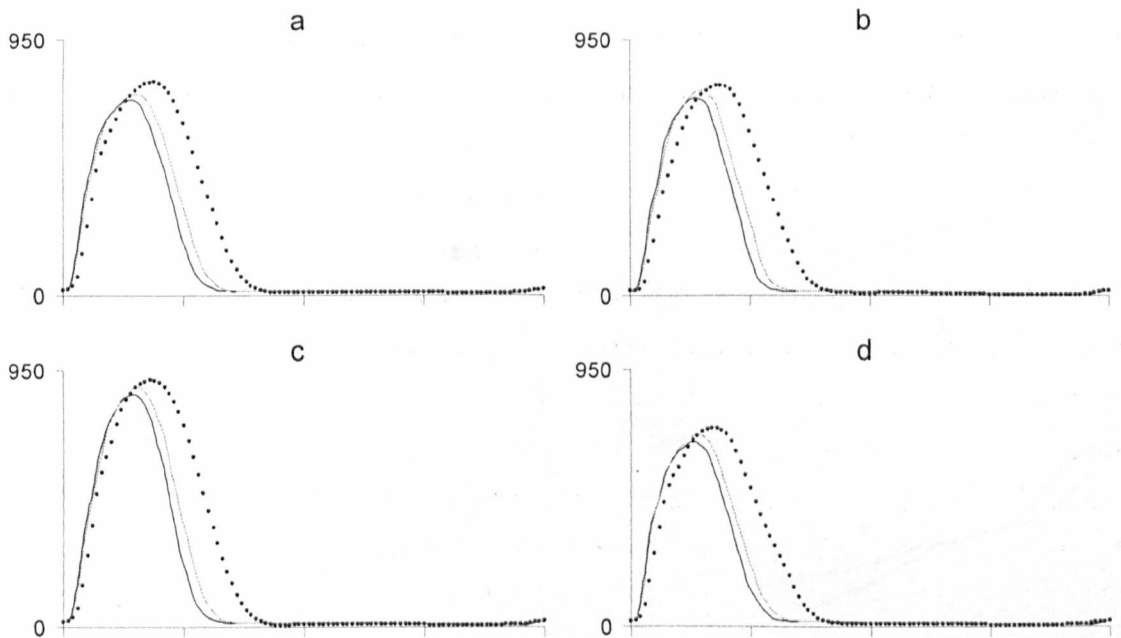


Figure 6.3: Handle force for all athlete groups

a. is HWW-SCULL, b. is HWW-SWEEP, c. is LWM, d. is LWW. The X axis is 0-100 percent of a representative rowing stroke. The Y axis is handle force in Newtons. The solid black line is Step 2, the semi solid grey line is Step 4 and the dotted black line is Step 6. Standard deviations for this data ranged from ± 4.86 to ± 104.59 N (a), ± 4.09 to ± 93.35 N (b), ± 4.51 to ± 139.16 N (c), and ± 4.28 to ± 85.65 N (d).

HWW-SCULL and HWW-SWEEP show fairly even suspension away from the seat during the first 10-20% of the stroke, never achieving complete suspension and continuing the stroke with a sharp increase in force applied to the seat as they move towards the finish (Figure 6.4). On the other hand LWW and, to a greater extent, LWM achieve peak suspension after at least 5% of the stroke has been completed; well into the initial portion of the drive phase, and, also hold good suspension for 10-20% at the start of the stroke (Figure 6.4). During Steps 1-5, on average, the greatest magnitude of force exerted onto the seat was 1.2 times the athletes' body weight (BW), rising to 1.3 times BW in Step 6 (all boat classes). After peak force had been exerted on the seat the athletes moved past the finish of the stroke and, as BW was returned to the feet in preparation for the next stroke, force was once again removed from the seat throughout the stroke recovery. For all athletes the relief of force from the seat appears to occur in three stages, beginning quickly as the athletes' flexed their trunk about their hips away from the finish position (rockover), then slowing through the middle of the recovery before increasing in gradient in the final fifth of the stroke.

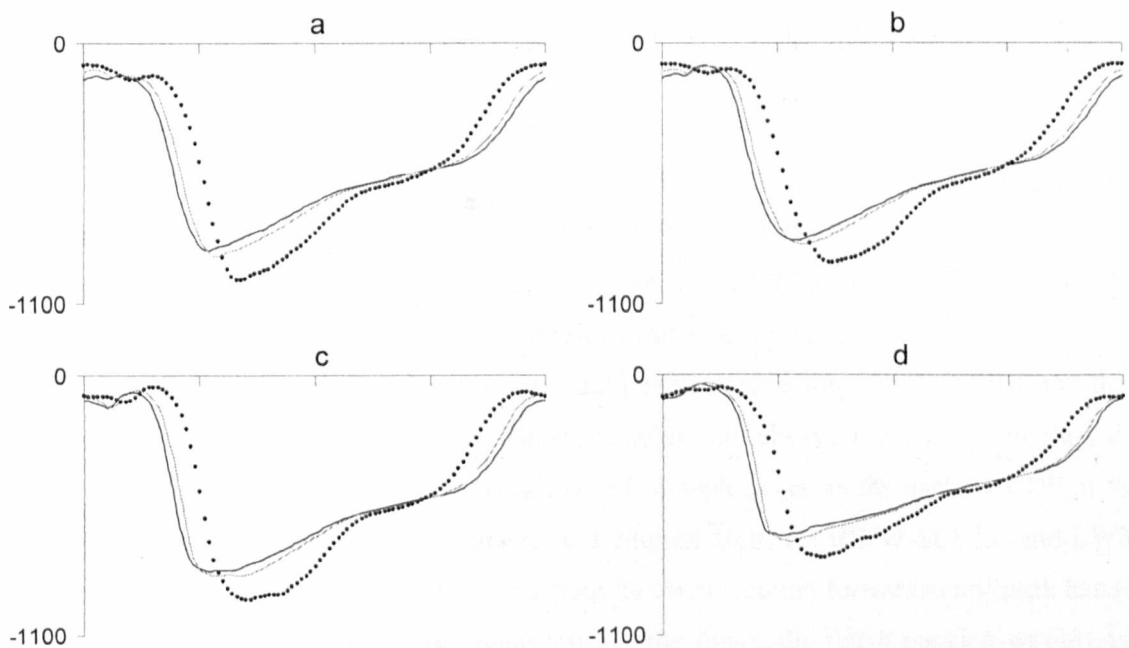


Figure 6.4: Seat force for all athlete groups

a. is HWW-SCULL, b. is HWW-SWEEP, c. is LWM, d. is LWW. The X axis is 0-100 percent of a representative rowing stroke. The Y axis is seat force in Newtons. The solid black line is Step 2, the semi solid grey line is Step 4 and the dotted black line is Step 6. Standard deviations for this data ranged from ± 27.24 to ± 211.34 N (a), ± 20.65 to ± 157.73 N (b), ± 18.09 to ± 201.73 N (c), and ± 11.63 to ± 189.99 N (d).

All of the COP coordinates presented in Figure 6.5 were within 40 mm anterior/posterior or left/right from the centre of the ergometer seat. All athlete groups moved left or right to a greater degree during the early phases of the stroke and less during the recovery phase of the stroke. HWW-SCULL and HWW-SWEEP athletes displayed less movement medially and laterally than both the LWM and LWW, and all boat classes showed increasing levels of left/right COP displacement as the intensity of exercise progressed. During the drive in all Steps, from the catch to peak handle force then from peak handle force to the finish HWW-SCULL COP was displaced right then right, HWW-SWEEP moved right then left, LWM moved right then right, and LWW moved left then right (low intensity) or right then right (high intensity). Considering only the medial/lateral COP coordinate at the catch and at the finish, during all Steps, all boat classes COP moved to the right; the magnitude of rightwards COP motion during the drive was greater in Step 6 than in earlier Steps; in Step 6 COP was 7.9 mm further to the right at the finish than at the catch for HWW-SCULL, 6.9 mm for HWW-SWEEP, 11.6 mm for LWM, and 23.5 mm for LWW.

There was a general shift posteriorly in COP displacement range as Step increased; all boat classes achieved less anterior displacement and more posterior displacement. The location of COP was more posterior at the catch as intensity increased; COP Z at the catch for HWW-SCULL was 13.7 mm more posterior in Step 6 than in Step 2, 8.9 mm for HWW-SWEEP, 9.1 mm for LWM, and 13.3 mm for LWW. The location of COP was also more posterior at the finish as intensity increased; COP Z at the finish for HWW-SCULL was 5.9 mm more posterior in Step 6 than in Step 2, 8.6 mm for HWW-SWEEP, 8.7 mm for LWM, and 15.5 mm for LWW. In the anterior/posterior direction, during all Steps, HWW-SWEEP COP moved from its catch location forwards until peak handle force was applied and then backwards again towards the finish; the finish position was always more posterior than the location when peak handle force was being exerted, though never as far back as COP at the catch. Again in the anterior/posterior direction, during all Steps for HWW-SCULL and LWM and during Steps 4 and 6 LWW, COP moved from its catch location forwards until peak handle force was applied and then backwards again towards the finish; the finish position was always more posterior than both the location when peak handle force was being exerted, and the location at the catch.

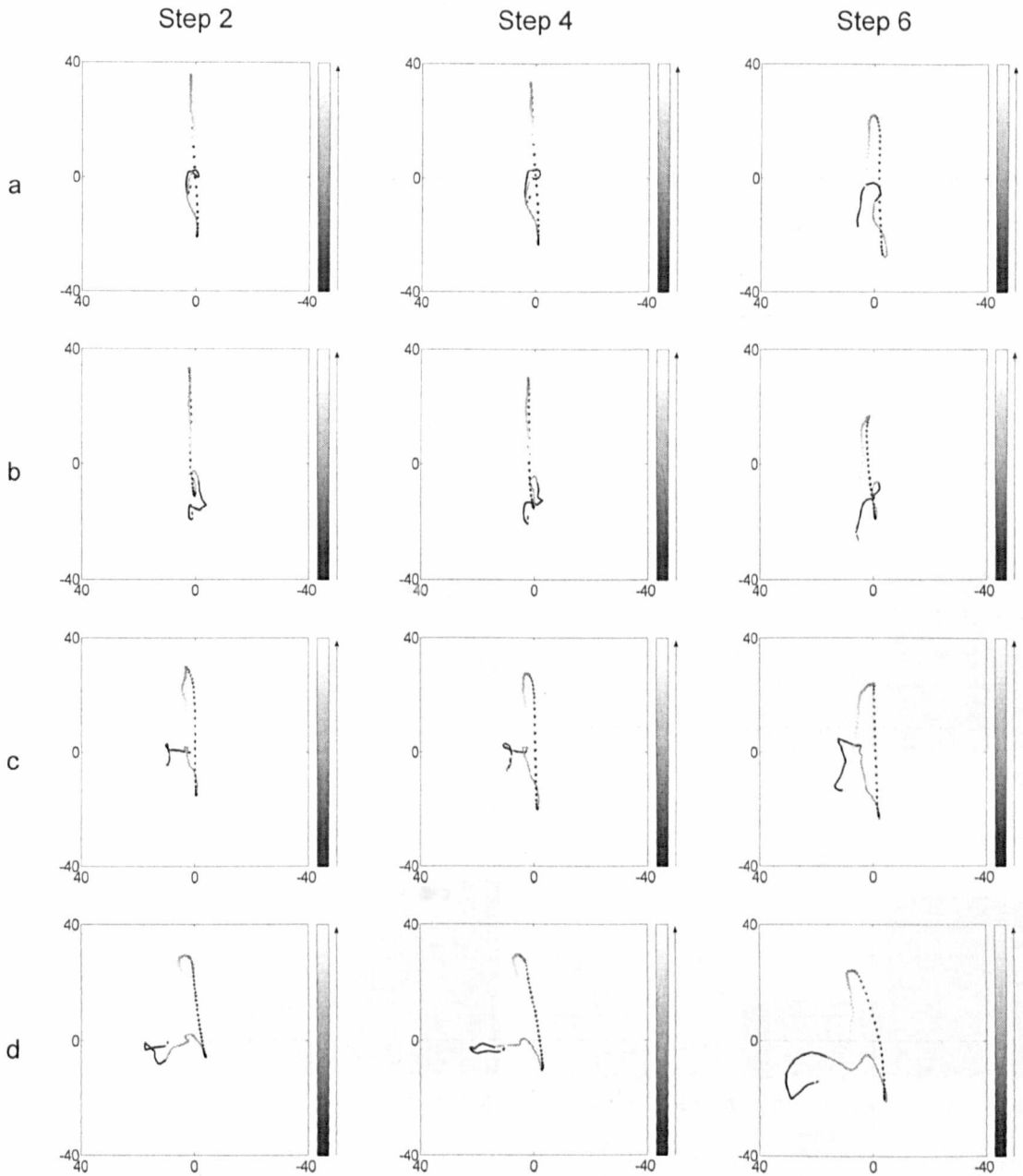


Figure 6.5: Centre of pressure trajectory for all athlete groups

a. is HWW-SCULL, b. is HWW-SWEEP, c. is LWM, d. is LWW. In each graph the horizontal axis shows COP displacement left (+^{ve}) and right (-^{ve}) on the seat and the vertical axis shows COP displacement anteriorly (+^{ve}) and posteriorly (-^{ve}). The units for both the horizontal and the vertical axes are mm. The solid black series represents COP trajectory from the catch until maximum force was exerted on the handle, the solid grey series is from peak handle force until the finish of the stroke, and the graduated dotted series with the colour bar to the right of the graphs illustrates COP progression during the recovery phase of the stroke. Standard deviations for medial/lateral data ranged from ± 4.8 to ± 25.6 mm (a), ± 4.2 to ± 25.8 mm (b), ± 3.5 to ± 30.5 mm (c), and ± 2.1 to ± 30.3 mm (d). Standard deviations for anterior/posterior data ranged from ± 10.4 to ± 20.6 mm (a), ± 10.1 to ± 23.1 mm (b), ± 14.7 to ± 25.3 mm (c), and ± 12.2 to ± 34.3 mm (d).

Figure 6.6 shows that all athlete groups produced progressively more power as the intensity of exercise increased; power output in Step 6 was 78%, 77%, 79%, and 77% greater than in Step 1 for HWW-SCULL, HWW-SWEEP, LWM and LWW respectively. All groups produced similar amounts of work per stroke regardless of the Step; all measurements were within 8% of the associated work maximum (for example LWM Step 1 vs LWM Step 6). All groups exhibited a shorter rowing stroke during Step 6 than Steps 1-5 (Chapter 7 describes a statistical evaluation of changes observed in technique and performance with increasing exercise intensity). The lowest variability in power output was recorded from the HWW-SWEEP, who, along with LWW exhibited the least variability for all three of the measures presented below (Figure 6.6).

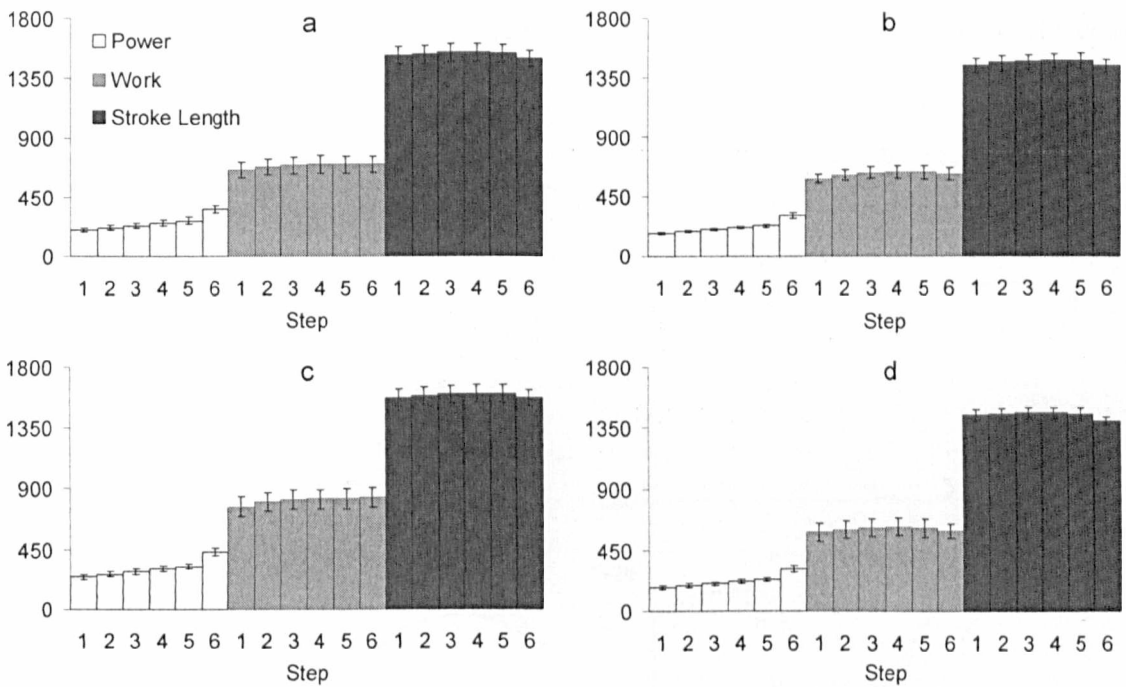


Figure 6.6: Stroke; Power Output, Work Done, and Length for all athlete groups
a. is HWW-SCULL, b. is HWW-SWEEP, c. is LWM, d. is LWW. The units for Power are Watts, for Work are Joules, and for Stroke Length are mm. The columns show the average measurement for each Step and the error bars show the standard deviation.

The data calculated for Z handle minus Z KJC (Section 5.3.1) between December 2006 and February 2009 was found to be prone to error and is not presented for this reason. The measurement error occurred because displacement of the handle was measured by the encoders introduced in Chapter 3, not by the FOB, and the method used to calculate a trajectory for handle motion within the global (FOB) coordinate frame was found to be unreliable.

6.3.2 Athletes' kinematics

The figures and accompanying descriptions in this section illustrate the data logged for all of the 3D kinematic variables that have previously been introduced (Table 5.2). In addition to this, there is some information regarding the measured lumbopelvic (LP) ratios. As in the scatter plots presented in the previous section, for clarity, Steps 1, 3 and 5 have not been included.

The trends shown in the Figure 6.7 are similar for all athlete groups, and during all Steps. The position of LSJ seems to move slightly to the athletes' left from the catch until maximum handle force is exerted, it then reverses its direction of motion until the finish of the stroke; moving to the athletes' right. A similar waveform is seen during the recovery phase of the stroke. The magnitude of displacement for HWW-SCULL and HWW-SWEEP is no more than 15 mm and for LWM and LWW is up to 35 mm. There may be a slight increase in the magnitude of medial and lateral motion of LSJ as intensity increases.

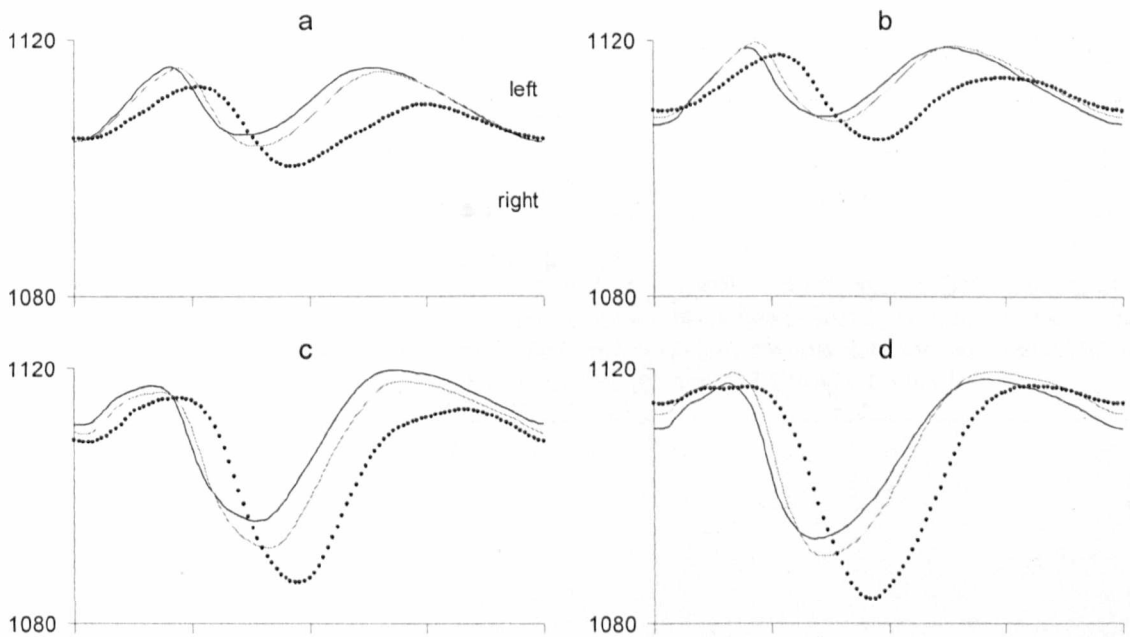


Figure 6.7: Trajectory of LSJ X for all athlete groups

a. is HWW-SCULL, b. is HWW-SWEEP, c. is LWM, d. is LWW. The X axis is 0-100 percent of a representative rowing stroke. The Y axis is in mm. The solid black line is Step 2, the semi solid grey line is Step 4 and the dotted black line is Step 6. Standard deviations for this data ranged from ± 10.3 to ± 18.0 mm (a), ± 11.5 to ± 15.0 mm (b), ± 8.8 to ± 24.2 mm (c), and ± 11.1 to ± 18.6 mm (d).

The trajectory of HJC in the X direction was found to be extremely similar to the trajectory of LSJ for all athlete groups (Figure 6.8). After the catch of the stroke a shift to the athletes left was followed by motion to their right hand side, then left, then right again as the stroke progressed. Again similar to LSJ, and especially considering the maximum shifts to the athletes' right hand side, the magnitude of motion was less for the HWW-SCULL and HWW-SWEEP than it was for LWM and LWW.

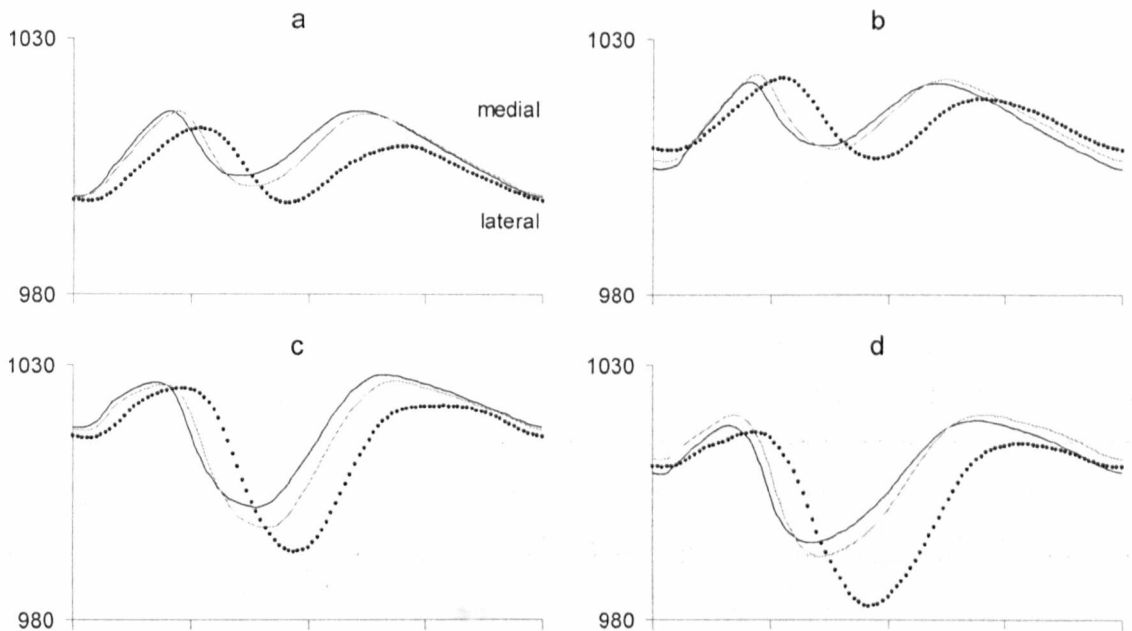


Figure 6.8: Trajectory of HJC X for all athlete groups

a. is HWW-SCULL, b. is HWW-SWEEP, c. is LWM, d. is LWW. The X axis is 0-100 percent of a representative rowing stroke. The Y axis is in mm. The solid black line is Step 2, the semi solid grey line is Step 4 and the dotted black line is Step 6. Standard deviations for this data ranged from ± 13.7 to ± 19.9 mm (a), ± 13.6 to ± 17.2 mm (b), ± 10.8 to ± 23.5 mm (c), and ± 12.6 to ± 21.1 mm (d).

Displacement of all athletes' KJC in the X direction followed a fairly consistent pattern, however there were noticeable differences in trend comparing Step 6 to earlier Steps, and there were also differences in the magnitude of motion when considering different boat classes (Figure 6.9). In general the KJC was positioned laterally at the catch of the stroke (most laterally was HWW-SCULL Steps 2,4, and least was LWW), it then moved medially during the drive phase of the stroke, before going laterally again during the recovery. During all Steps for the lightweights, and during Step 6 for the heavyweights, medial displacement during the drive was interrupted by short sharp lateral movements and short plateaus respectively; it is possible that this may be related to instability or weakness around the hip and gluteals at high intensity, indeed Figure 6.26 (Page 132) shows slightly reduced rates of HJC abduction at this point in the stroke during Step 6, and Figure 6.29 (Page 135) shows that this point in the stroke is also a point of inflexion considering internal/external rotation of HJC. Where the other athlete groups completed the medial aspect of KJC translation by the time the finish of the stroke was reached, HWW-SCULL were found to continue medial KJC displacement during the finish and early stroke recovery. Continuous lateral displacement during the recovery was often followed by a very short period of medial displacement at the end of the stroke.

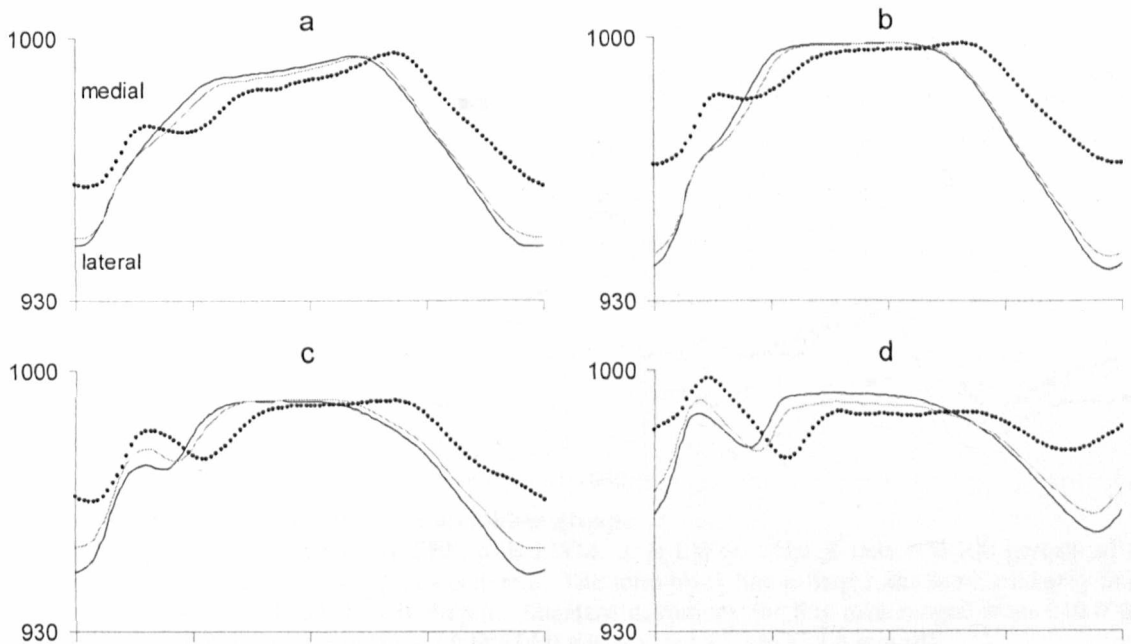


Figure 6.9: Trajectory of KJC X for all athlete groups

a. is HWW-SCULL, b. is HWW-SWEEP, c. is LWM, d. is LWW. The X axis is 0-100 percent of a representative rowing stroke. The Y axis is in mm. The solid black line is Step 2, the semi solid grey line is Step 4 and the dotted black line is Step 6. Standard deviations for this data ranged from ± 8.0 to ± 27.0 mm (a), ± 8.8 to ± 29.0 mm (b), ± 8.7 to ± 36.3 mm (c), and ± 6.0 to ± 32.6 mm (d).

Figure 6.10 shows that the displacement of AJC for HWW-SCULL and HWW-SWEEP is reminiscent of that for KJC; in general, as the stroke progresses there is motion from a lateral position to a more medial position followed by a return laterally, there is then a repeat of this lateral to medial to lateral motion at a lower magnitude within the final third of the stroke. LWM show a different pattern of movement during their stroke than the heavyweight women; their AJC begins the stroke medially at the catch and moves to its most lateral position in three stages from the catch to the early recovery; initially there is a small lateral shift, followed by a plateau, before another lateral movement. The position of LWM AJC in the X direction continually moves medially during the final third of the stroke. The most variability in motion behaviour between low intensity Steps was seen for the LWW; the trend of motion was similar for all Steps, however the overall position of AJC was more medial as the Steps increased. For all athlete groups the AJC was found to be more medial at the catch during Step 6 than during lower intensity efforts.

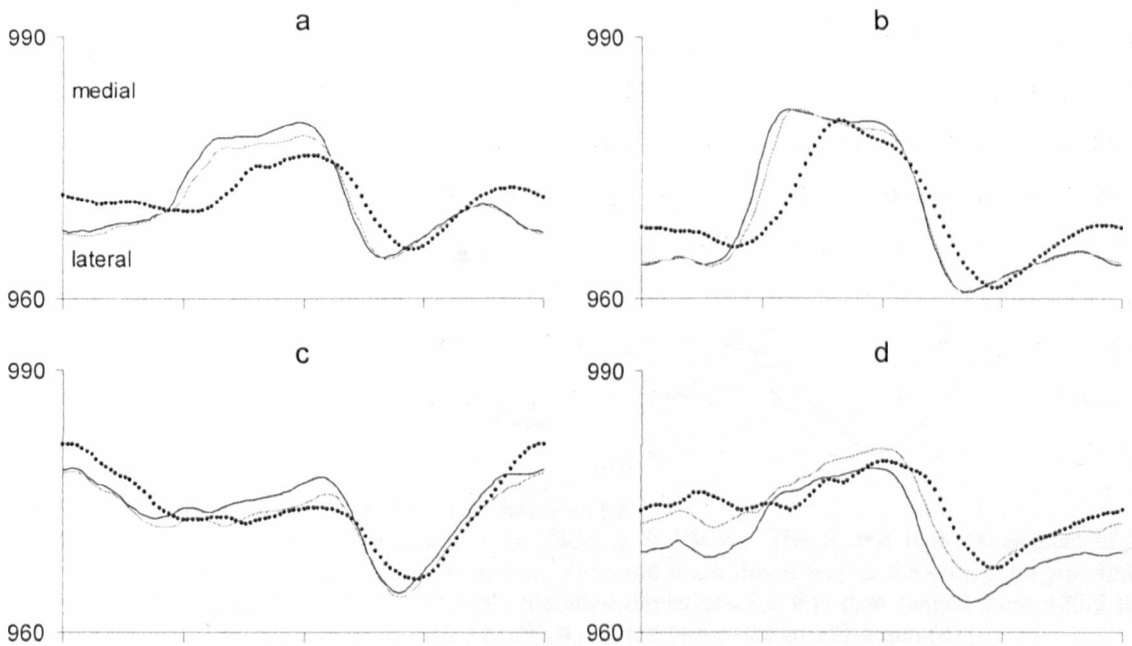


Figure 6.10: Trajectory of AJC X for all athlete groups
 a. is HWW-SCULL, b. is HWW-SWEEP, c. is LWM, d. is LWW. The X axis is 0-100 percent of a representative rowing stroke. The Y axis is in mm. The solid black line is Step 2, the semi solid grey line is Step 4 and the dotted black line is Step 6. Standard deviations for this data ranged from ± 10.6 to ± 16.0 mm (a), ± 10.8 to ± 17.1 mm (b), ± 7.9 to ± 14.0 mm (c), and ± 5.3 to ± 14.8 mm (d).

LSJ at the catch is highest for HWW-SCULL, followed by HWW-SWEEP and LWW, and is lowest for LWM (Figure 6.11). All athlete groups begin the stroke with LSJ translating upwards during the first half of the drive phase before it drops again through to the finish. In part due to the athletes' movement, and in part because the rowing ergometer has inbuilt rearwards incline along its length (Figure 6.1, Page 104), the position of LSJ in the Y direction is similar at the catch and at the finish. After the finish, the athlete should lead with the pelvis and rock up and over, rotating about their hips to commence the recovery phase, thus LSJ again gains superior vertical displacement; this gain is less at higher intensity. During the final one third to one quarter of the stroke LSJ gradually declines in height, again this will be linked to both athlete motion and the geometry of the rowing ergometer.

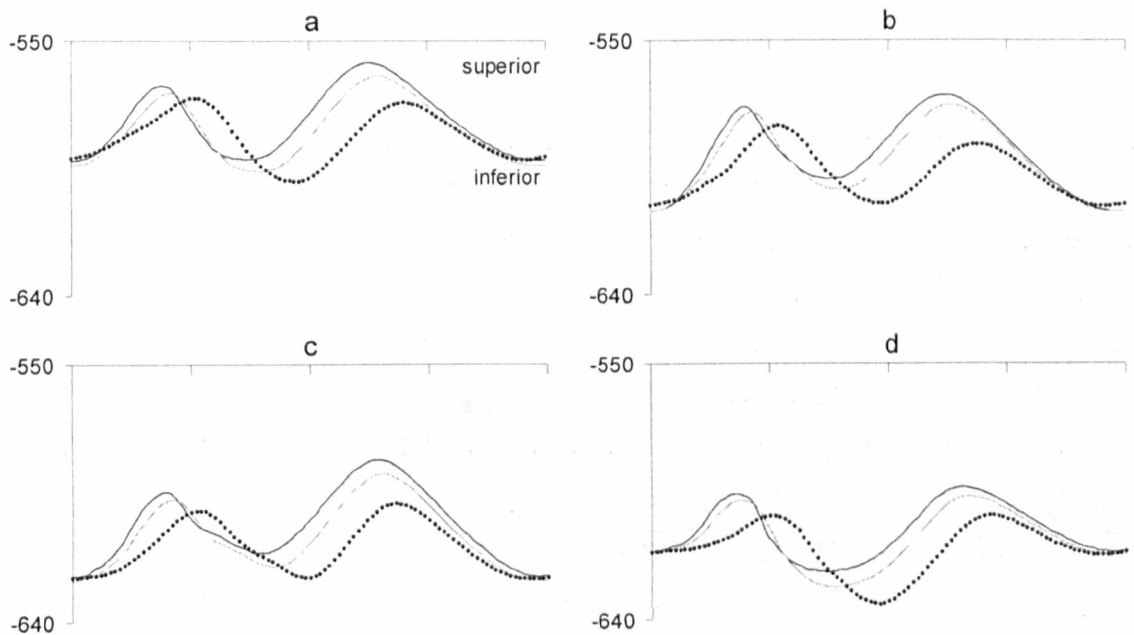


Figure 6.11: Trajectory of LSJ Y for all athlete groups

a. is HWW-SCULL, b. is HWW-SWEEP, c. is LWM, d. is LWW. The X axis is 0-100 percent of a representative rowing stroke. The Y axis is in mm. The solid black line is Step 2, the semi solid grey line is Step 4 and the dotted black line is Step 6. Standard deviations for this data ranged from ± 20.5 to ± 24.7 mm (a), ± 19.3 to ± 25.8 mm (b), ± 18.3 to ± 31.4 mm (c), and ± 14.6 to ± 23.4 mm (d).

In the Y direction HJC for all athletes became gradually higher up as the drive phase progressed (Figure 6.12). Some of this rise will be explained by the physical incline of the ergometer (≈ 50 mm) however much of it will also be linked to the activation of muscle groups such as the gluteals and large abdominals raising the position of the pelvis. Figure 6.12 shows the range of HJC trajectory in the Y direction varies with changes in Step; this is particularly clear as being lower at the finish for HWW-SCULL as intensity increased, and lower at the catch for LWW when intensity was less. Figure 6.12 also reveals that downwards motion of the athletes' HJC occurred more slowly in the early recovery than it did in the second part of the recovery phase. At the finish, HJC Y was found to be within 35 mm of LSJ Y for all athlete groups during Step 6.

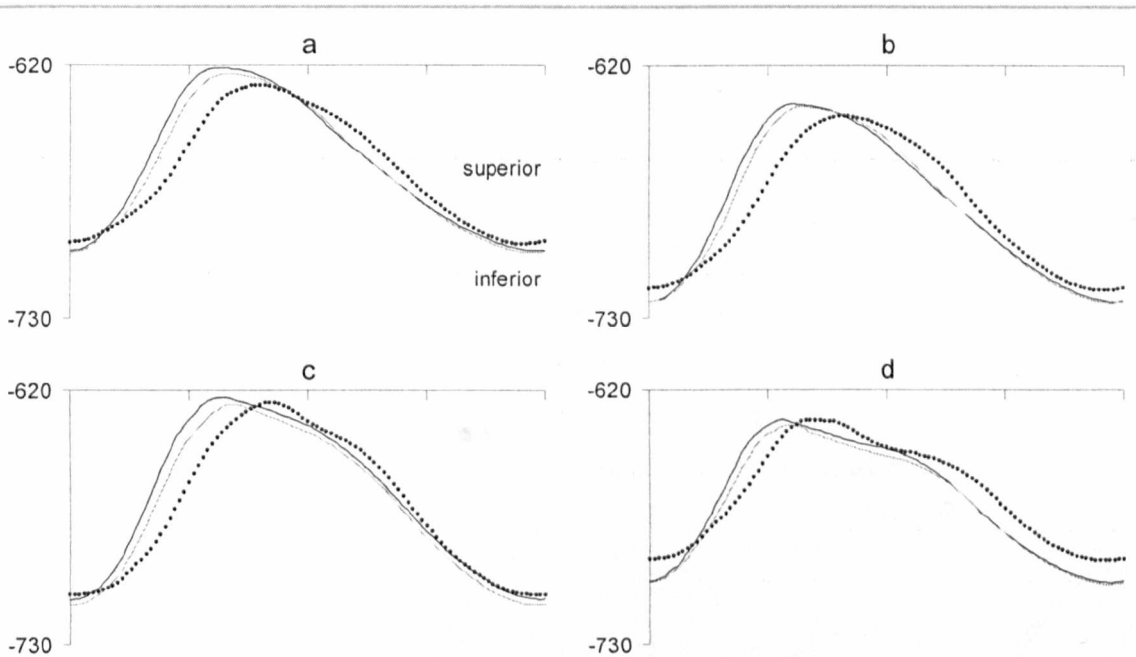


Figure 6.12: Trajectory of HJC Y for all athlete groups
 a. is HWW-SCULL, b. is HWW-SWEEP, c. is LWM, d. is LWW. The X axis is 0-100 percent of a representative rowing stroke. The Y axis is in mm. The solid black line is Step 2, the semi solid grey line is Step 4 and the dotted black line is Step 6. Standard deviations for this data ranged from ± 14.1 to ± 27.0 mm (a), ± 12.8 to ± 18.6 mm (b), ± 20.8 to ± 29.8 mm (c), and ± 19.0 to ± 30.7 mm (d).

All athlete groups show the same general movement pattern for the KJC in the Y direction (Figure 6.13). The KJC is at its highest at the catch of the stroke, it remains at a fairly constant high level for approximately 5% of the stroke at the beginning of the drive before moving downwards at a constant rate throughout the remainder of the propulsive phase. The KJC remains at its lowest level during the finish and rockover and then, in preparation for the next stroke, returns to a higher position during the recovery. All athletes' were found to move their KJC to a lower position at the finish during lower intensity exercise, and with the exception of HWW-SWEEP, to a higher position at the catch during higher intensity exercise. In Step 2 and Step 4 the position of KJC reached its lowest point approximately 30% of the way through the stroke, its Y coordinate did not then change for a further 15% of the stroke before it started a smooth rise again. In Step 6 however we see that after reaching its lowest point the KJC begins to rise very gradually for 10-15% before commencing its main, more rapid rise back to the catch position.

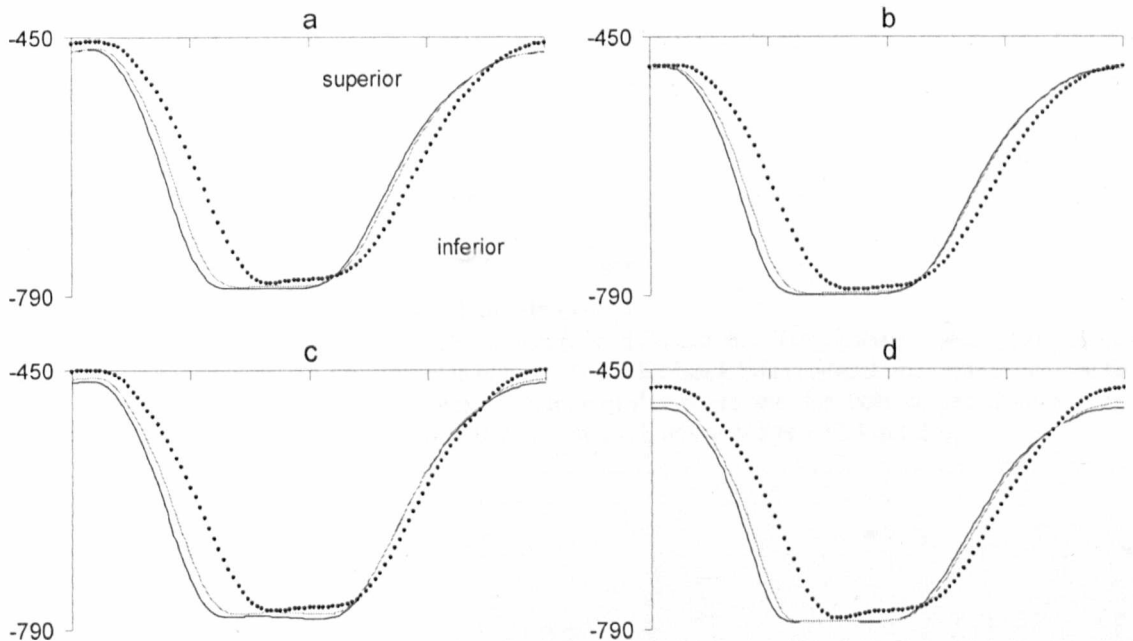


Figure 6.13: Trajectory of KJC Y for all athlete groups

a. is HWW-SCULL, b. is HWW-SWEEP, c. is LWM, d. is LWW. The X axis is 0-100 percent of a representative rowing stroke. The Y axis is in mm. The solid black line is Step 2, the semi solid grey line is Step 4 and the dotted black line is Step 6. Standard deviations for this data ranged from ± 15.7 to ± 41.9 mm (a), ± 14.3 to ± 34.5 mm (b), ± 19.4 to ± 46.5 mm (c), and ± 13.5 to ± 27.4 mm (d).

For all athlete groups and during all Steps, movement of the AJC in the Y direction was fairly consistent (Figure 6.14). At the catch the AJC was found to be at its highest point vertically, it then moved downwards during the first half of the drive and upwards during the second half of the drive phase. After reaching a peak in the Y direction at the finish the AJC gradually descended during the majority of the stroke recovery, then with around 20% of the stroke remaining AJC again rose to a high Y peak in preparation for the next rowing stroke.

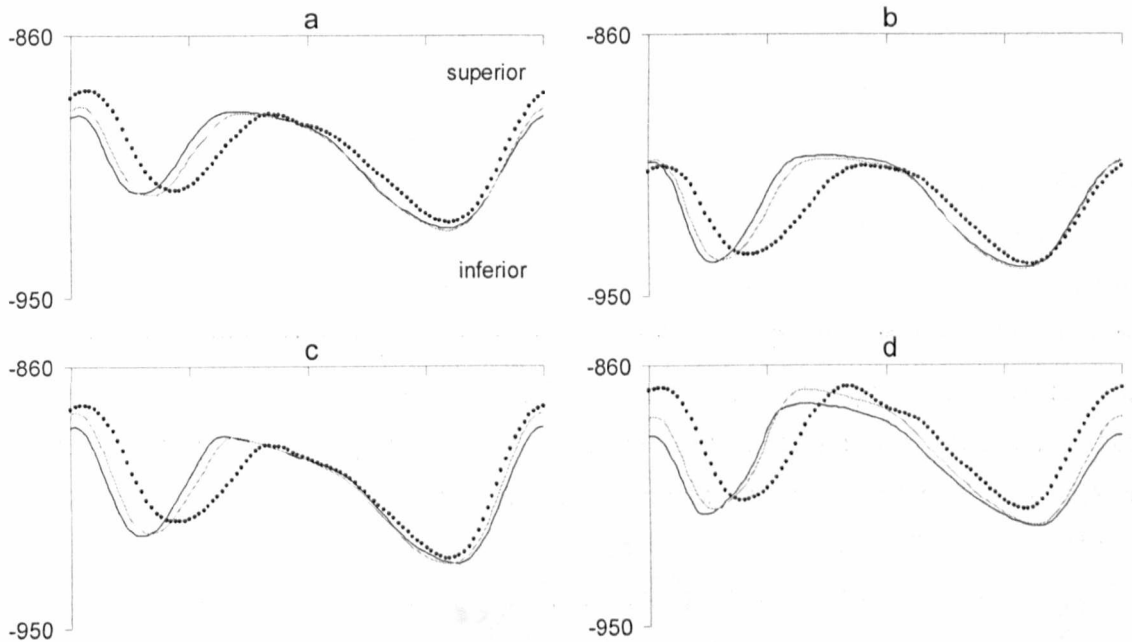


Figure 6.14: Trajectory of AJC Y for all athlete groups

a. is HWW-SCULL, b. is HWW-SWEEP, c. is LWM, d. is LWW. The X axis is 0-100 percent of a representative rowing stroke. The Y axis is in mm. The solid black line is Step 2, the semi solid grey line is Step 4 and the dotted black line is Step 6. Standard deviations for this data ranged from ± 15.2 to ± 26.2 mm (a), ± 9.6 to ± 21.7 mm (b), ± 16.9 to ± 31.3 mm (c), and ± 19.5 to ± 32.4 mm (d).

Predictably, the motion of LSJ in the Z direction was constantly bow-wards during the drive phase of the stroke, and constantly sternwards during the recovery phase of the stroke (Figure 6.15). The lowest values recorded (occurring at the finish) remained virtually unchanged as Step increased, however there was a noticeable difference in the anterior position of LSJ at the catch in Steps 2,4 compared to Step 6; in Step 6 there was 54 mm less anterior displacement of LSJ for HWW-SCULL, 60 mm less for HWW-SWEEP, 61 mm less for LWM, and 65 mm less for LWW. LWM were found to exhibit the largest total displacement range, followed by both HWW-SCULL and HWW-SWEEP, and finally with the least total displacement, LWW. The difference noted in range for LWW compared to all other athletes is easily explained by leg length differences. The average leg length for each athlete group was found by examining the logged X,Y,Z catch coordinates for the HJC, KJC and AJC; the HWW-SCULL and HWW-SWEEP leg length was 8% longer than LWW, and the LWM leg length was 10% longer than LWW. While the HWW-SCULL and HWW-SWEEP groups were found to exhibit similar total range for LSJ in the Z direction, HWW-SWEEP were found to come a little further forward at the catch, and HWW-SCULL were found to move a little further backwards at the finish of the stroke.

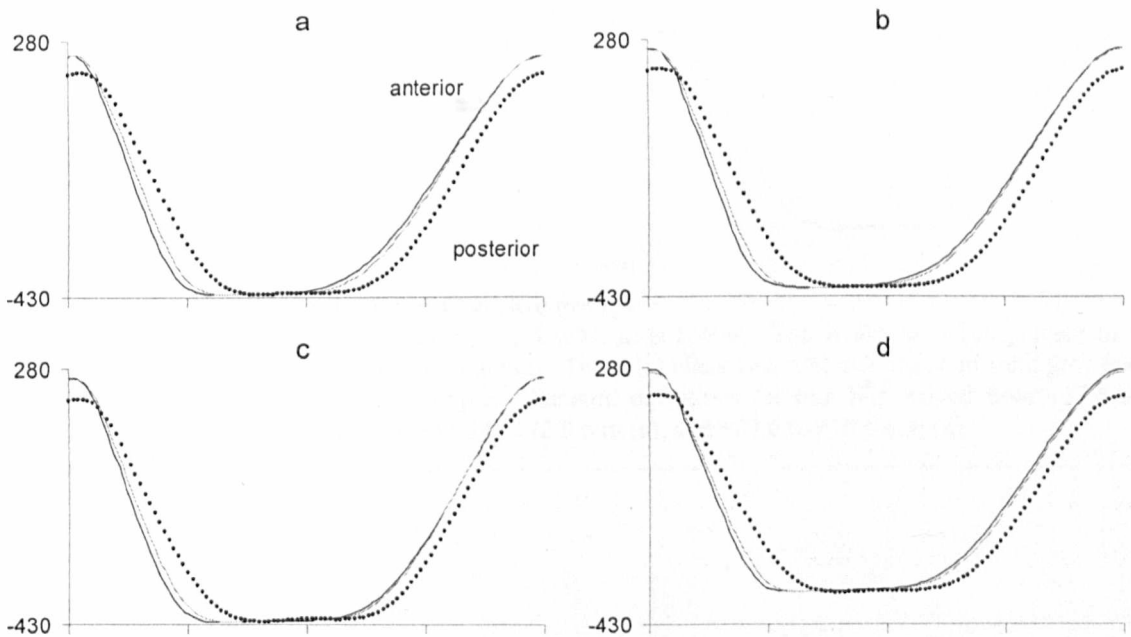


Figure 6.15: Trajectory of LSJ Z for all athlete groups

a. is HWW-SCULL, b. is HWW-SWEEP, c. is LWM, d. is LWW. The X axis is 0-100 percent of a representative rowing stroke. The Y axis is in mm. The solid black line is Step 2, the semi solid grey line is Step 4 and the dotted black line is Step 6. Standard deviations for this data ranged from ± 34.4 to ± 68.1 mm (a), ± 27.8 to ± 69.6 mm (b), ± 34.7 to ± 67.1 mm (c), and ± 26.0 to ± 67.4 mm (d).

The trend observed for HJC Z (Figure 6.16) is very similar to the trend observed for LSJ Z; the motion is rearwards from the catch position to a maximum posterior displacement at the finish, then anterior displacement during the recovery phase of the stroke. On this occasion there is noticeably less anterior displacement of the HJC at the catch during Step 6 than in earlier Steps (50 mm HWW, 55 mm LWM and LWW). In addition to this the two lightweight groups were found to displace their HJC between 15 and 25 mm more anteriorly at the catch than either of the heavyweight groups regardless of the Step being rowed; this may be linked to the shear bulk of the heavyweights and the corresponding impact on achievable knee and hip flexion at the catch (Section 6.3.4.2, Page 140)

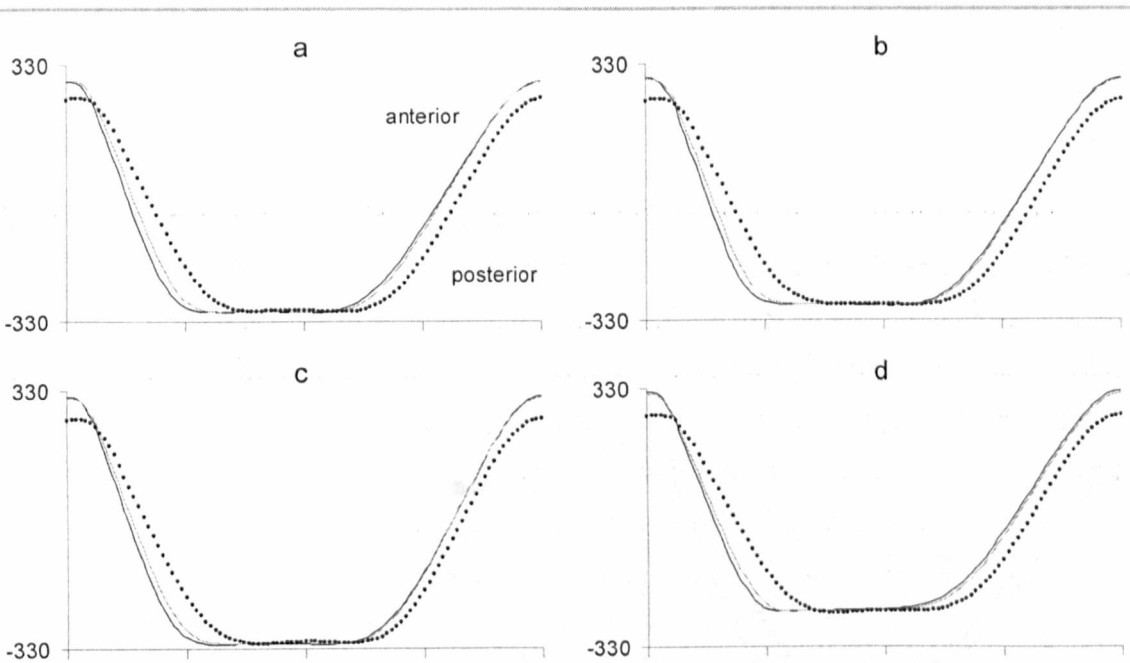


Figure 6.16: Trajectory of HJC Z for all athlete groups
 a. is HWW-SCULL, b. is HWW-SWEEP, c. is LWM, d. is LWW. The X axis is 0-100 percent of a representative rowing stroke. The Y axis is in mm. The solid black line is Step 2, the semi solid grey line is Step 4 and the dotted black line is Step 6. Standard deviations for this data ranged from ± 37.6 to ± 67.5 mm (a), ± 28.0 to ± 71.3 mm (b), ± 37.3 to ± 72.9 mm (c), and ± 27.6 to ± 70.8 mm (d).

In the Z direction KJC moved progressively and smoothly from its most anterior coordinate to its most posterior coordinate during the drive phase, it remained at its most posterior coordinate whilst the legs were locked in full extension at the finish of the stroke before commencing anterior displacement during the stroke recovery (Figure 6.17). The rate at which KJC moved posteriorly was greater than the rate at which it moved anteriorly in Steps 2 and 4, though was comparable in Step 6 (reflecting the reduction in drive:recovery duration ratio as intensity increased, Section 6.3.1). All athlete groups also showed that when exercising at race pace in Step 6 the position of their KJC at the catch was noticeably less anterior than it was in earlier Steps. The differences in total Z range between HWW-SCULL, HWW-SWEEP, LWM and LWL are explained by leg length differences.

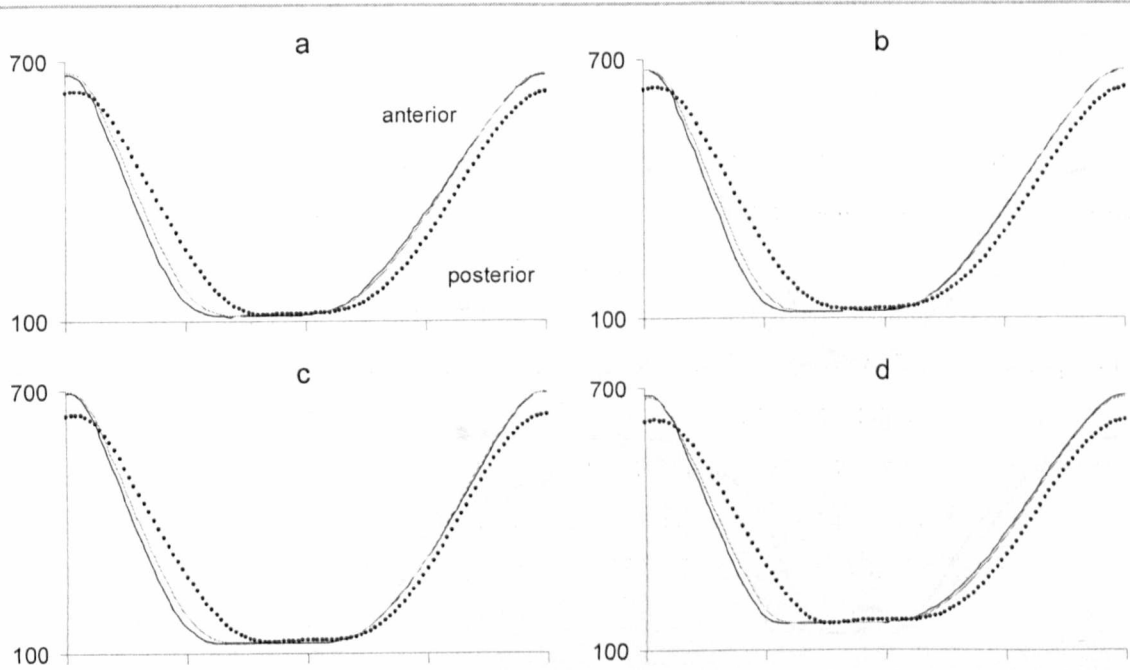


Figure 6.17: Trajectory of KJC Z for all athlete groups
 a. is HWW-SCULL, b. is HWW-SWEEP, c. is LWM, d. is LWL. The X axis is 0-100 percent of a representative rowing stroke. The Y axis is in mm. The solid black line is Step 2, the semi solid grey line is Step 4 and the dotted black line is Step 6. Standard deviations for this data ranged from ± 31.1 to ± 56.5 mm (a), ± 25.5 to ± 57.4 mm (b), ± 27.7 to ± 61.4 mm (c), and ± 18.1 to ± 49.1 mm (d).

Figure 6.18 shows that HWW-SWEEP and LWW had a larger range of AJC movement in the Z direction than HWW-SCULL or LWM (68 and 67 mm respectively versus 59 and 57 mm respectively). As with the other joint centres' trajectories in the anterior/posterior direction, motion is consistently rearwards during the drive phase, followed by a plateau lasting for around 30-35% of the stroke, followed by consistent displacement anteriorly during the stroke recovery. The rate of posterior motion during the early drive was lower than posterior motion in the late drive, and the rate of anterior motion in the late recovery was lower than anterior motion during the early recovery. In Step 6, to a larger extent than other boat classes, LWW exhibited an extra spike of anterior AJC motion between 38% and 44% of the stroke (LWW finish in Step 6 = 38%); it is likely that this is related to the athletes' heel lifting from the footstretcher at the finish of the stroke (Figure 6.24, Page 130).

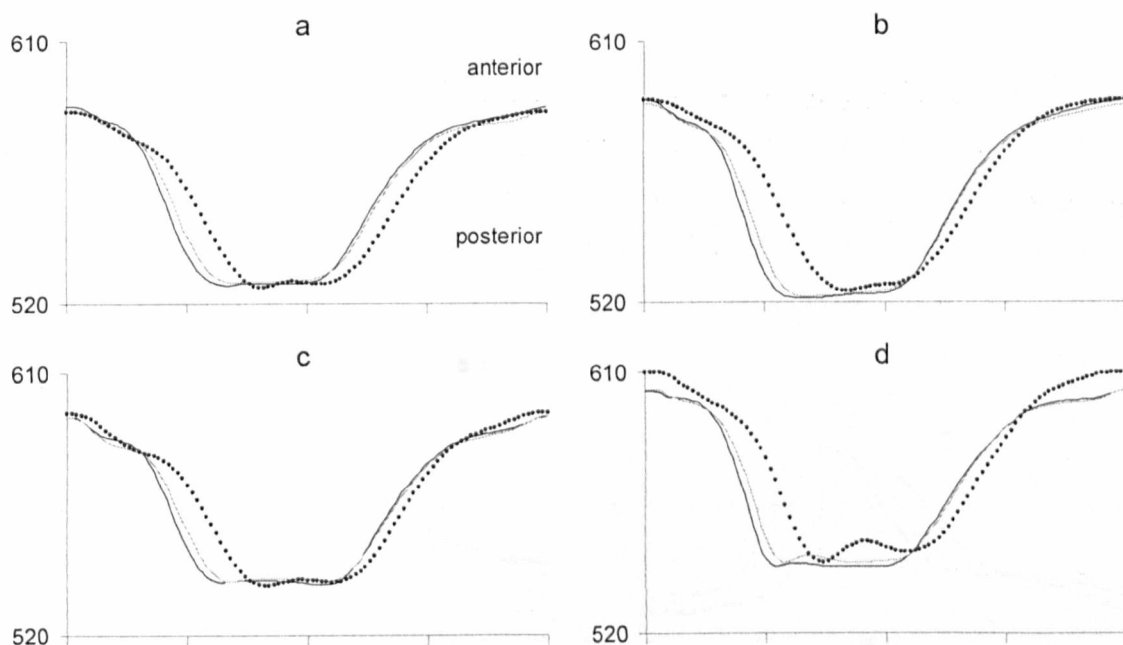


Figure 6.18: Trajectory of AJC Z for all athlete groups

a. is HWW-SCULL, b. is HWW-SWEEP, c. is LWM, d. is LWW. The X axis is 0-100 percent of a representative rowing stroke. The Y axis is in mm. The solid black line is Step 2, the semi solid grey line is Step 4 and the dotted black line is Step 6. Standard deviations for this data ranged from ± 15.4 to ± 24.2 mm (a), ± 10.8 to ± 19.1 mm (b), ± 16.8 to ± 22.7 mm (c), and ± 15.6 to ± 22.6 mm (d).

Figure 6.19 shows that at the catch there was significant flexion of the lumbar spine, this was greatest for LWW (up to 17°) and least for HWW-SWEEP (up to 10°). During the drive phase of the stroke the lumbar spine remained flexed about the pelvis segment (kyphotic pose) until close to the finish when it moved into an orientation extending it beyond the pelvis segment (lordotic pose). At the finish the maximum amount of lumbar extension was for LWM in Step 4 (7°) and the minimum was for HWW-SCULL, also in Step 4 (0°). Beyond the finish the maximum amount of lumbar extension noted was for HWW-SWEEP (up to 12°) and the least was for HWW-SCULL (up to 6°). For all athlete groups the maximum level of lumbar flexion was noted during Step 6, and for HWW-SCULL and LWM the maximum level of lumbar extension also occurred in Step 6. During stroke rockover and recovery the flexion/extension angle of the lumbar spine about LSJ returned to neutral and then back into lumbar flexion.

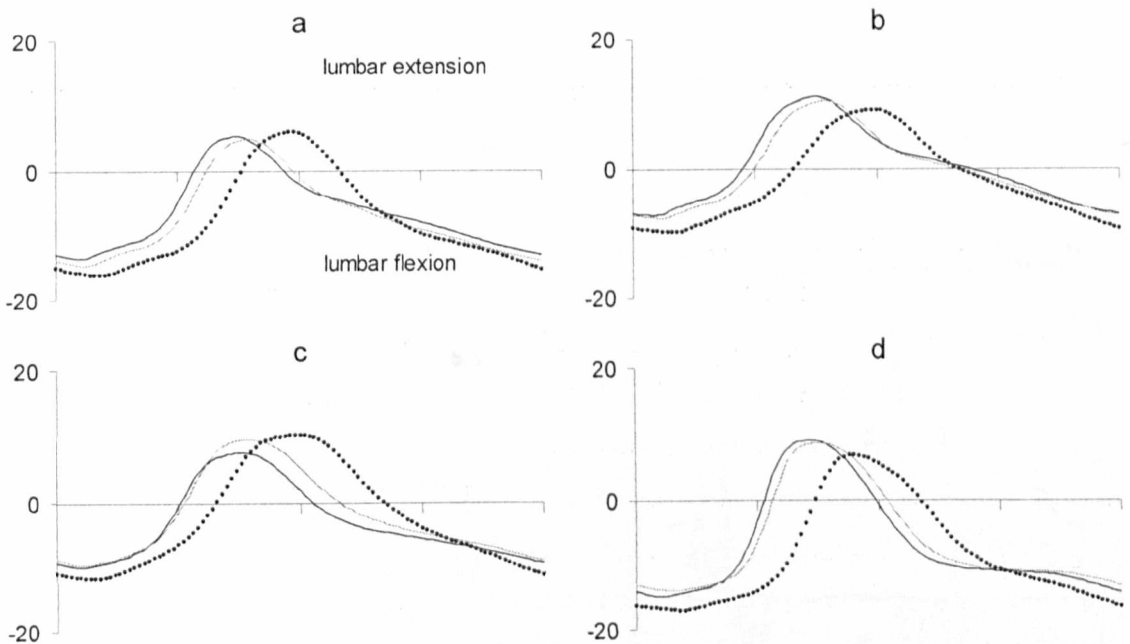


Figure 6.19: LSJ alpha angle for all athlete groups

a. is HWW-SCULL, b. is HWW-SWEEP, c. is LWM, d. is LWW. The X axis is 0-100 percent of a representative rowing stroke. The Y axis is in degrees. The solid black line is Step 2, the semi solid grey line is Step 4 and the dotted black line is Step 6. Standard deviations for this data ranged from ± 9.1 to $\pm 11.8^\circ$ (a), ± 10.4 to $\pm 12.2^\circ$ (b), ± 8.4 to $\pm 10.5^\circ$ (c), and ± 9.4 to $\pm 14.4^\circ$ (d).

In most instances the LP ratio was calculated as the BACK angle divided by the PELVIS angle (Section 5.3.1), and, considering the data presented in Figure 6.19 we might expect all of the data series shown in Figure 6.20 to consistently not be equal to 1. Indeed 89% of the data shown in Figure 6.20 is <0.9 or >1.1 , however all athlete groups appear to have quite good alignment of the body segments around the finish of the stroke; while this is not in total agreement with the results shown in Figure 6.19 we do see for example, that, similar to LSJ alpha, at the finish HWW-SCULL have better alignment than HWW-SWEEP (1.01 to 1.03 and 1.06 to 1.12 respectively). Considering the entire stroke HWW-SWEEP displayed ratios closest to 1, this was followed by HWW-SCULL with the lightweight athletes showing the highest mal-alignment of segments (particularly at the catch) and the greatest variability in scores. The seemingly inconsistent results shown in Figure 6.19 and Figure 6.20 can be explained by considering the global orientation of the segments, as opposed to just their relative alignment. This is discussed in more detail in Section 6.3.4.1.

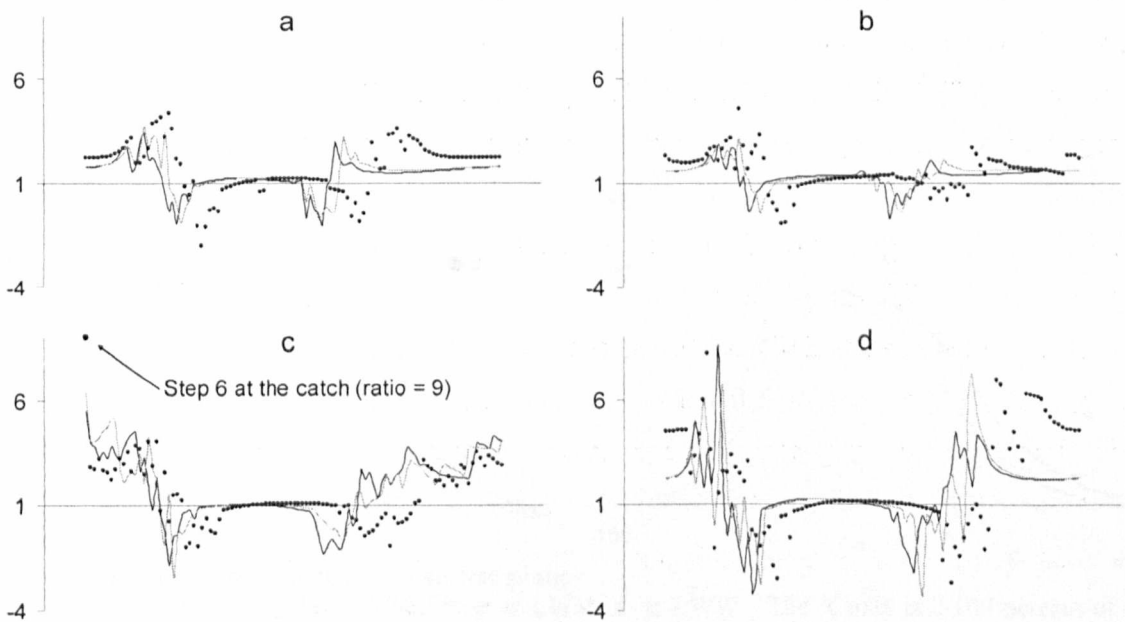


Figure 6.20: Lumbopelvic ratio for all athlete groups

a. is HWW-SCULL, b. is HWW-SWEEP, c. is LWM, d. is LWW. An entire representative stroke (0-100%) is shown, there is additional blank space on either side of the data series so that values at the catch of the stroke can be more easily seen. The Y axis is the LP ratio. The solid black line is Step 2, the semi solid grey line is Step 4 and the dotted black line is Step 6. Standard deviations for this data ranged from ± 0.3 to ± 8.4 (a), ± 0.4 to ± 7.5 (b), ± 0.2 to ± 10.1 (c), and ± 0.3 to ± 13.3 (d).

Figure 6.21 shows that at all times all athletes' were found to be in some degree of HJC flexion; 35-142° (HWW-SCULL), 42-143° (HWW-SWEEP), 33-142° (LWM) and 29-135° (LWW). Maximum flexion occurred around the catch of the stroke and was up to 5° less for all athlete groups during Step 6 than it was during lower intensity efforts; this change in hip flexion angle at the catch was more noticeable for HWW-SWEEP and LWW than it was for HWW-SCULL and LWM. Hip flexion gradually became less as the legs and pelvis were extended through the drive of the stroke, and minimal hip flexion was noted around the finish of the stroke. The low rate increase in flexion seen after the finish (approximately 35-55% of the Step 2,4 stroke cycle) will have occurred as a result of the pelvis flexing forwards during rockover, and acceleration of this rate of flexion occurred as the knees broke and started to rise during the recovery phase of the stroke (>55% of the Step 2,4 stroke cycle).

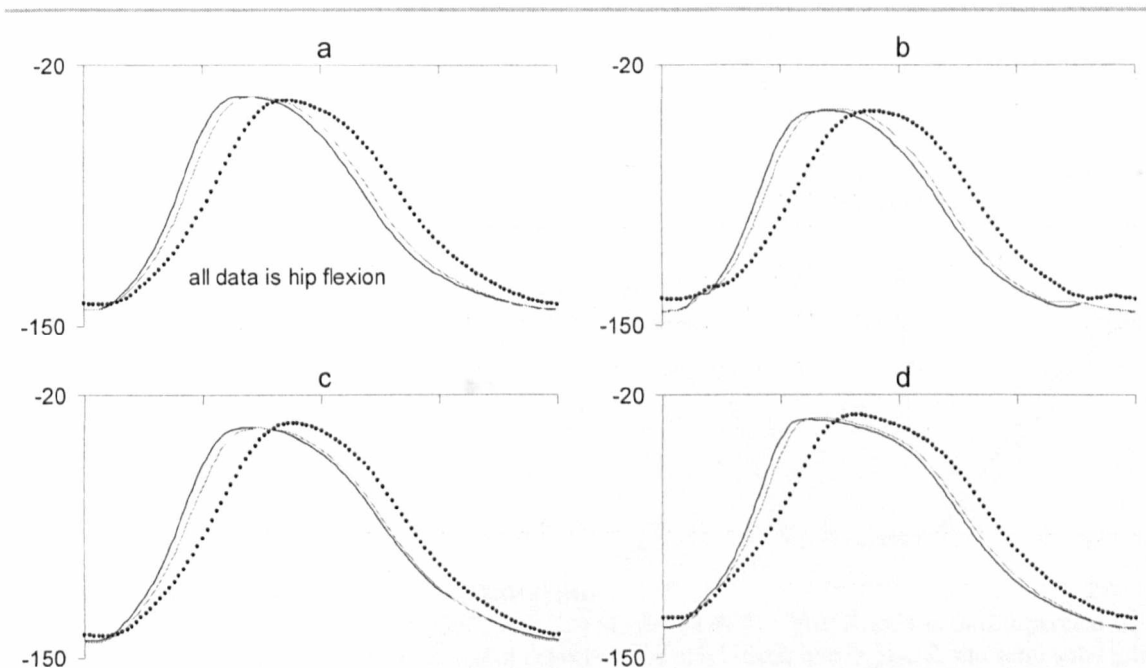


Figure 6.21: HJC alpha angle for all athlete groups
 a. is HWW-SCULL, b. is HWW-SWEEP, c. is LWM, d. is LWW. The X axis is 0-100 percent of a representative rowing stroke. The Y axis is in degrees. The solid black line is Step 2, the semi solid grey line is Step 4 and the dotted black line is Step 6. Standard deviations for this data ranged from ±10.9 to ±15.6 ° (a), ±10.3 to ±46.9 ° (b), ±10.8 to ±15.2 ° (c), and ±10.3 to ±16.1 ° (d).

Figure 6.22 shows that maximum levels of knee flexion were observed around the catch of the stroke for all athlete groups; 133° (HWW-SCULL), 133° (HWW-SWEEP), 137° (LWM) and 130° (LWW). This level of knee flexion at the catch was up to 8° less during Step 6 than it had been during other Steps in the test, and this intensity related reduction in maximum knee flexion was least evident in HWW-SCULL. The knee was rapidly moved from deep flexion towards a neutral position during the drive phase, and further into knee hyper extension by the finish of the stroke; up to 6° knee hyper extension (HWW-SCULL), 5° (HWW-SWEEP), 4° (LWM) and 7° (LWW). For all groups other than LWW the magnitude of maximum knee extension became noticeably less as the intensity of exercise was increased.

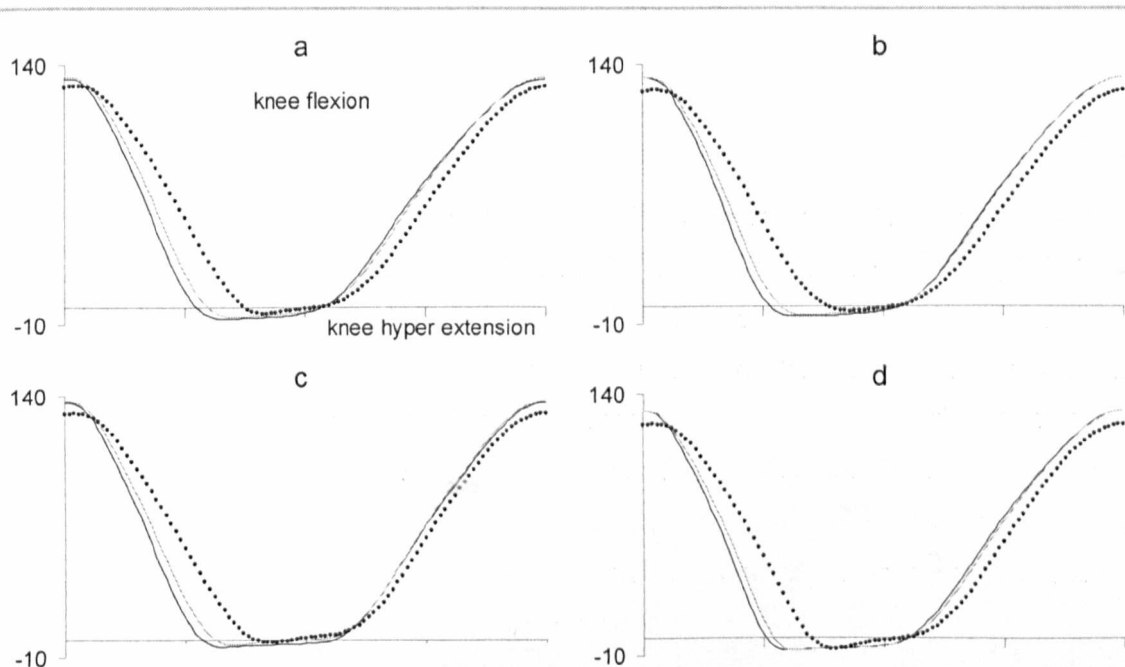


Figure 6.22: KJC alpha angle for all athlete groups

a. is HWW-SCULL, b. is HWW-SWEEP, c. is LWM, d. is LWW. The X axis is 0-100 percent of a representative rowing stroke. The Y axis is in degrees. The solid black line is Step 2, the semi solid grey line is Step 4 and the dotted black line is Step 6. Standard deviations for this data ranged from ± 3.3 to $\pm 14.0^\circ$ (a), ± 5.7 to $\pm 12.7^\circ$ (b), ± 4.8 to $\pm 14.2^\circ$ (c), and ± 2.6 to $\pm 9.9^\circ$ (d).

Figure 6.23 shows that during Steps 2 and 4 all athletes exhibited dorsi flexion at the catch of the stroke; up to 11° (HWW-SCULL), up to 11° (HWW-SWEEP), up to 9° (LWM) and up to 7° (LWW). HWW-SCULL and HWW-SWEEP were also found to dorsi flex at the catch in Step 6 (2° and 8° respectively), though LWM were found to be in 4° of plantar flexion and LWW in 7° of plantar flexion at the catch during Step 6. After the catch HWW-SCULL, HWW-SWEEP and LWM either maintained a constant AJC alpha for 10-15% of the stroke, or moved towards plantar flexion, before exhibiting rapid increases in plantar flexion throughout the remainder of the drive. On the other hand, LWW increased their level of dorsi flexion within the first 10-15% of the stroke before making rapid gains in plantar flexion. After the finish, the level of plantar flexion achieved by all athletes steadily decreased during the stroke recovery. And, just before the end of the stroke, after reaching a peak of dorsi flexion, tended towards plantar flexion. The total range of motion recorded from HWW-SCULL was 92° , HWW-SWEEP 89° , LWM 91° , and LWW 104° . Recall that these values are offset in the plantar direction (typically 6° to 10° , Section 4.3). Considering this offset, the dashed horizontal axis shown in Figure 6.23 may better approximate the proper value at which to distinguish between dorsi and plantar flexion; adding 8° to each dorsi flexion angle, and subtracting 8° from each plantar flexion angle presented above.

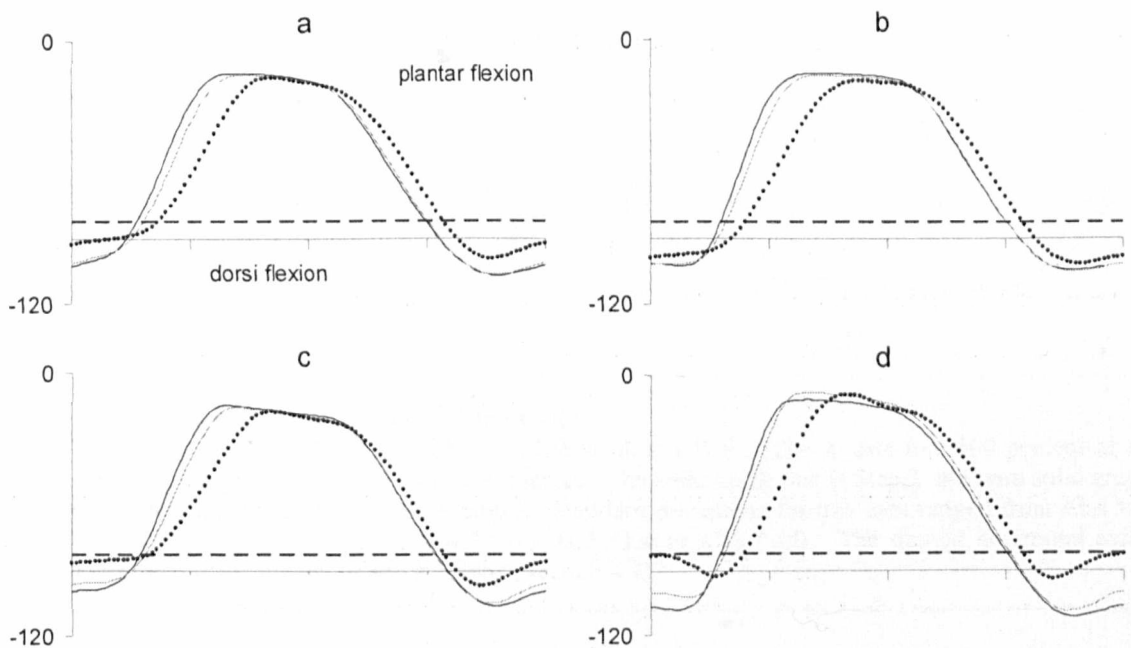


Figure 6.23: AJC alpha angle for all athlete groups

a. is HWW-SCULL, b. is HWW-SWEEP, c. is LWM, d. is LWW. The X axis is 0-100 percent of a representative rowing stroke. The Y axis is in degrees. The solid black line is Step 2, the semi solid grey line is Step 4 and the dotted black line is Step 6. Standard deviations for this data ranged from ± 7.6 to $\pm 19.0^\circ$ (a), ± 6.5 to $\pm 18.3^\circ$ (b), ± 6.1 to $\pm 18.5^\circ$ (c), and ± 4.1 to $\pm 18.6^\circ$ (d). The dashed horizontal axis approximates the offset in calculated AJC alpha (Section 4.3).

Recall that the values shown in Figure 6.24 are offset by the sagittal angle between AJC, FJC and the calcaneus (Section 4.3). Figure 6.24 shows the magnitude of the angle between POSFOOT and ANTFOOT that occurred due to the athletes' heel rising from the footstretcher during the stroke; the dashed horizontal axis shown in the figure may better approximate the proper value at which to distinguish between the heel being flat on the footstretcher, and the heel being raised away from the footstretcher (8°). At the catch of the stroke the angle at FJC, was greatest for HWW-SWEEP and LWW, the angles for HWW-SCULL and LWM were respectively 3° and 1° less. As the drive phase progressed the heel was returned to the footstretcher as the athletes' pressed out through their legs and, in line with coaching philosophy, tried to keep their heels down. Figure 6.24 may suggest that only the LWW showed noticeable separation of the heels from the footstretcher as they reached the finish of the stroke.

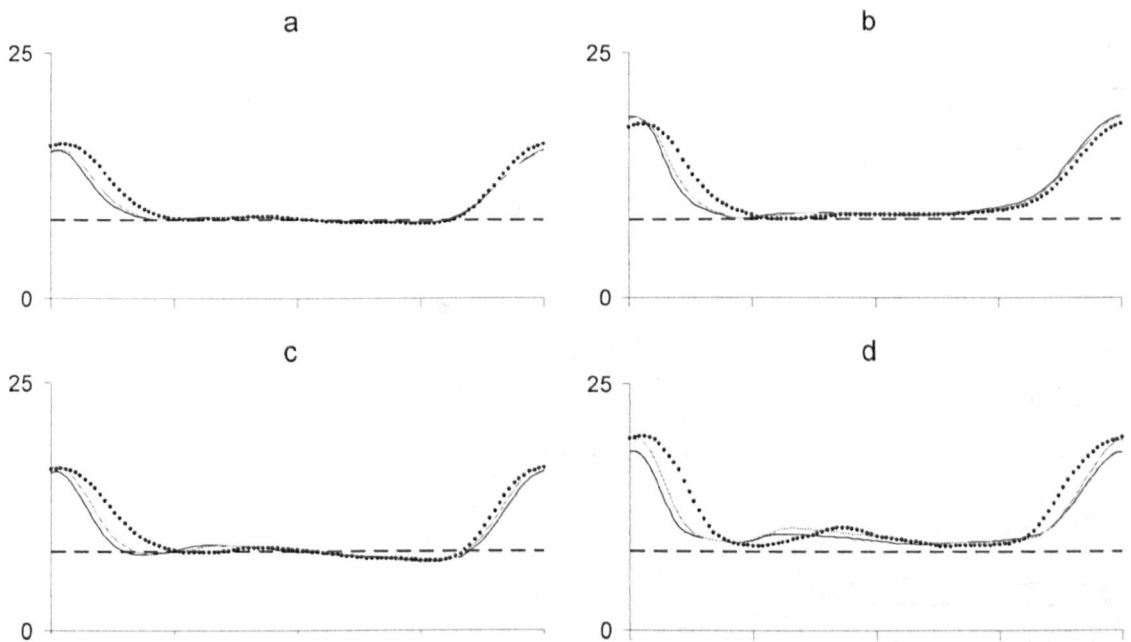


Figure 6.24: FJC alpha angle for all athlete groups

a. is HWW-SCULL, b. is HWW-SWEEP, c. is LWM, d. is LWW. The X axis is 0-100 percent of a representative rowing stroke. The Y axis is in degrees. The solid black line is Step 2, the semi solid grey line is Step 4 and the dotted black line is Step 6. Standard deviations for this data ranged from ± 1.4 to $\pm 4.5^\circ$ (a), ± 1.0 to $\pm 4.5^\circ$ (b), ± 1.1 to $\pm 4.7^\circ$ (c), and ± 1.4 to $\pm 7.9^\circ$ (d). The dashed horizontal axis approximates the offset in calculated FJC alpha (Section 4.3).

In general, all athlete groups exhibited some degree of lumbar side flexion to the right at the catch of the stroke. This decreased throughout the drive, rockover, and the beginning of the stroke recovery, before increasing again in preparation for the next catch. Figure 6.25 shows that all of the lumbar side flexion exhibited by athletes during the current study was to the right. Within any one Step, the range of rotation was $\leq 2.1^\circ$, 2.1° , 2.5° and 3.5° for HWW-SCULL, HWW-SWEEP, LWM and LWW respectively, and maximum ranges of lumbar rotation always occurred in Step 6; furthermore, for HWW-SCULL, HWW-SWEEP, LWM and LWW the magnitude of the ranges recorded during Step 6 were up to 8.1%, 33.3%, 3.7% and 161.9% greater than the ranges for Step 2 or Step 4. This data shows that changes in this kinematic aspect with increasing exercise intensity, were least for the LWM, and by a considerable order of magnitude, greatest for LWW. This result may be related to the higher muscular strength that males are known to have over females, and heavyweight females are known to have over lightweight females (McGregor et al., (2004b); Figure 6.3, Page 108).

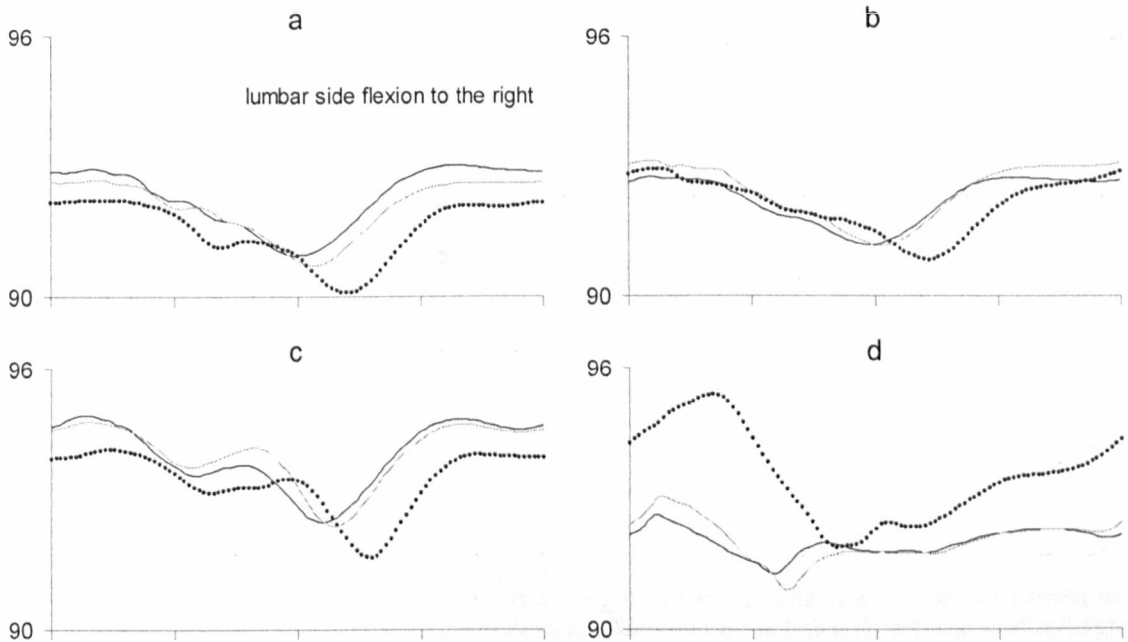


Figure 6.25: LSJ beta angle for all athlete groups

a. is HWW-SCULL, b. is HWW-SWEEP, c. is LWM, d. is LWW. The X axis is 0-100 percent of a representative rowing stroke. The Y axis is in degrees. The solid black line is Step 2, the semi solid grey line is Step 4 and the dotted black line is Step 6. Standard deviations for this data ranged from ± 4.3 to $\pm 5.5^\circ$ (a), ± 3.4 to $\pm 4.9^\circ$ (b), ± 3.7 to $\pm 5.3^\circ$ (c), and ± 3.2 to $\pm 5.4^\circ$ (d).

Figure 6.26 shows that all athlete groups exhibited similar movement patterns for all Steps, with the most striking visual similarities coming between HWW-SWEEP and LWM. The HJC was found to be in up to 6.1° , 5.2° , 5.1° and 6.2° of adduction at the catch of the stroke, and progressed into up to 5.3° , 5.3° , 6.7° and 7.7° of abduction during the drive, rockover and recovery phases (HWW-SCULL, HWW-SWEEP, LWM, LWW). The HWW-SCULL exhibited a fairly smooth transition from adduction to abduction and back again, whilst, just after the knees broke in the recovery, the other groups (particularly HWW-SWEEP and LWM) showed a noticeable increase in abduction compared to the mid-stroke plateau. Only the HWW-SWEEP showed a considerable change in rotation at the catch as exercise intensity increased. Immediately prior to, and immediately following a catch there was often a period of 5-15% of the stroke where HJC rotation did not change.

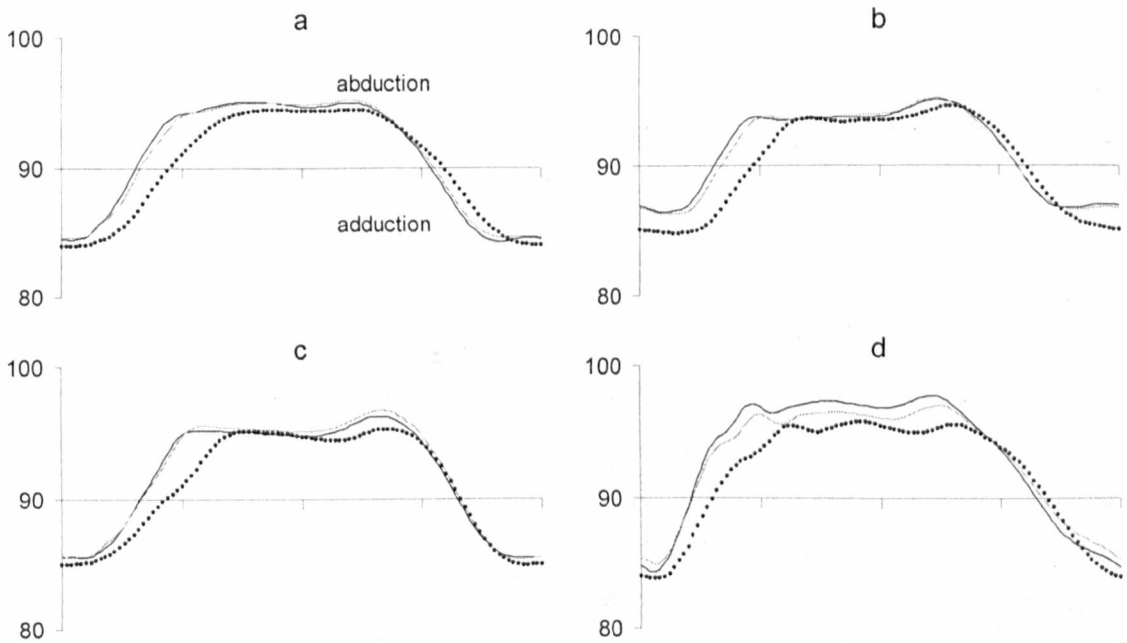


Figure 6.26: HJC beta angle for all athlete groups

a. is HWW-SCULL, b. is HWW-SWEEP, c. is LWM, d. is LWW. The X axis is 0-100 percent of a representative rowing stroke. The Y axis is in degrees. The solid black line is Step 2, the semi solid grey line is Step 4 and the dotted black line is Step 6. Standard deviations for this data ranged from ± 5.8 to $\pm 8.6^{\circ}$ (a), ± 5.4 to $\pm 7.4^{\circ}$ (b), ± 5.2 to $\pm 8.4^{\circ}$ (c), and ± 3.2 to $\pm 8.4^{\circ}$ (d).

For all athlete groups, and in all Steps (excluding LWW Step 6) POSFOOT was in eversion about AJC at the catch of the stroke. For HWW-SWEEP, this level of eversion was 0.1° more in Step 6 than in Step 2, though for all other athlete groups, minimum eversion at the catch occurred in Step 6. Figure 6.27 shows the intersegmental angle progressed from eversion to inversion during the drive phase of the stroke, and remained in this pose during rockover, and the beginning of the recovery. After the knees broke, the ankle once again moved towards eversion in preparation for the next catch. Within any one Step the LWW showed the greatest range of angles (15.4°), this was followed by the HWW-SWEEP, LWM and HWW-SCULL (14.0° , 13.7° and 11.7° respectively). The smallest range of motion always occurred in Step 6, and was 13.1%, 6.0%, 24.1% and 39.6% less than any other Step for HWW-SCULL, HWW-SWEEP, LWM and LWW respectively. Depending on the orientation of the FOB transmitter these angles may be incorrect by approximately 1° (repeatability of transmitter placement, Section 3.3.2).

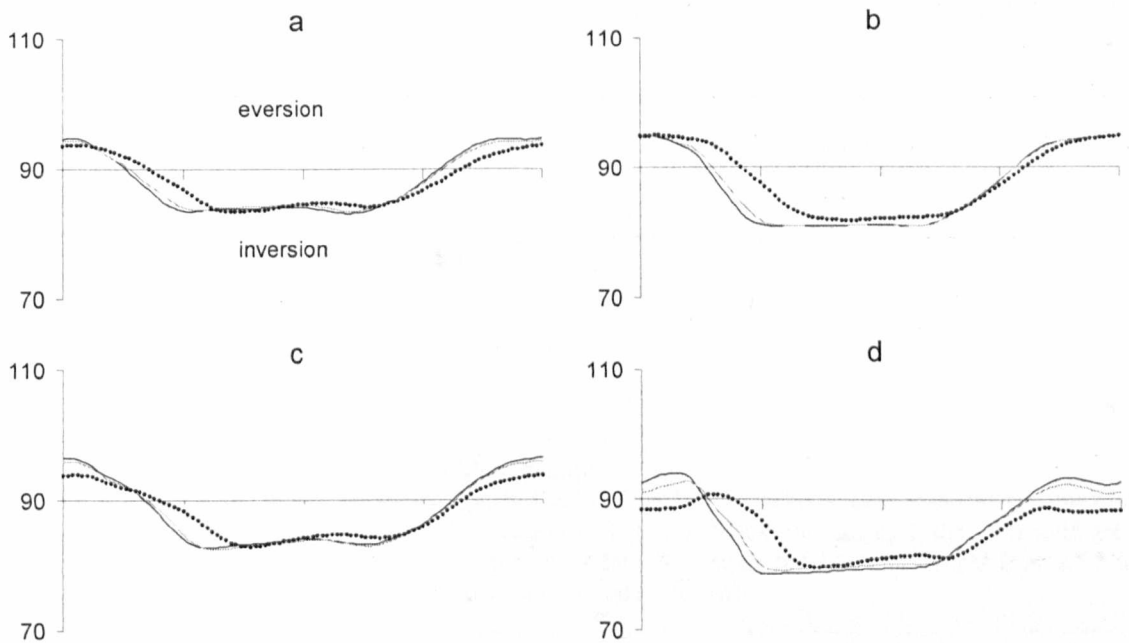


Figure 6.27: AJC beta angle for all athlete groups

a. is HWW-SCULL, b. is HWW-SWEEP, c. is LWM, d. is LWW. The X axis is 0-100 percent of a representative rowing stroke. The Y axis is in degrees. The solid black line is Step 2, the semi solid grey line is Step 4 and the dotted black line is Step 6. Standard deviations for this data ranged from ± 4.2 to $\pm 7.7^\circ$ (a), ± 5.8 to $\pm 7.8^\circ$ (b), ± 4.7 to $\pm 8.1^\circ$ (c), and ± 4.2 to $\pm 11.2^\circ$ (d).

Figure 6.28 shows that all of the data calculated for LSJ gamma was equal to or greater than 0° . Hence the athletes consistently showed twisting rotation of the BACK to the left about the PELVIS. Within any one Step the lowest range of angles was recorded for HWW-SCULL (1.2° to 1.6°), followed by HWW-SWEEP (1.3° to 1.8°), LWM (2.4° to 3.8°) and LWW showed the greatest range of rotation (3.1° to 5.4°). This trend of rotation range magnitude between athlete groups is similar, if slightly amplified, to that for LSJ beta. Furthermore, the shape of the series shown below for LWM and LWW is reminiscent of those for LSJ beta (Figure 6.25). It is possible that the level of right-wards lumbar side flexion exhibited by athletes is related to the amount of left-wards lumbar twist.

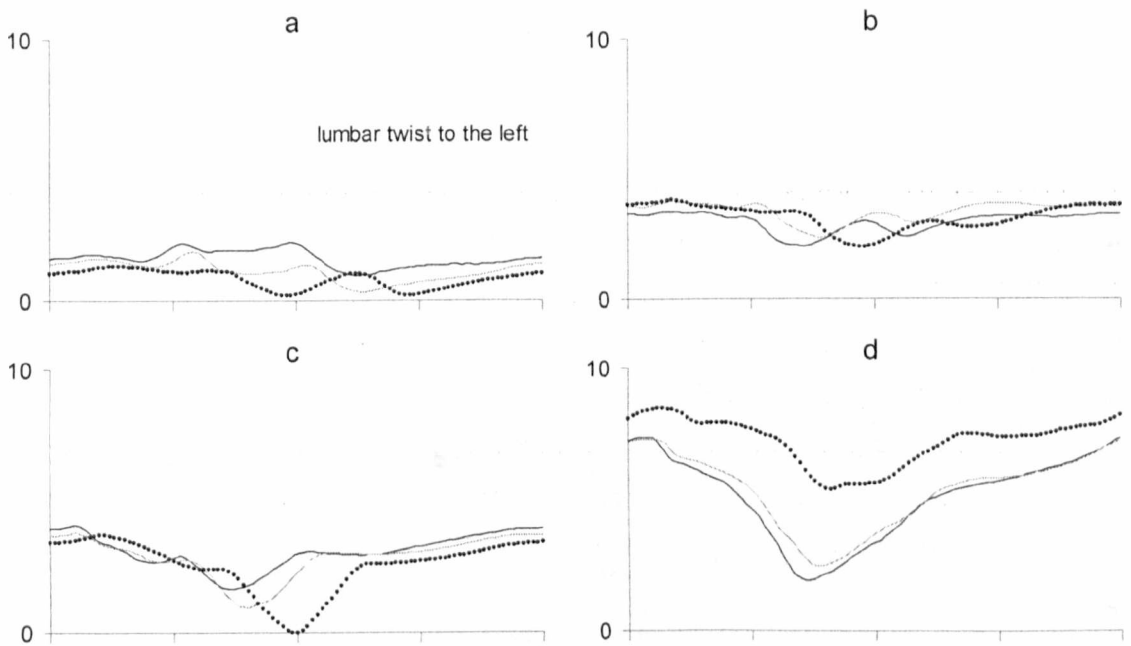


Figure 6.28: LSJ gamma angle for all athlete groups

a. is HWW-SCULL, b. is HWW-SWEEP, c. is LWM, d. is LWW. The X axis is 0-100 percent of a representative rowing stroke. The Y axis is in degrees. The solid black line is Step 2, the semi solid grey line is Step 4 and the dotted black line is Step 6. Standard deviations for this data ranged from ± 3.9 to $\pm 6.2^\circ$ (a), ± 4.3 to $\pm 6.9^\circ$ (b), ± 4.3 to $\pm 8.1^\circ$ (c), and ± 4.0 to $\pm 7.9^\circ$ (d).

Figure 6.29 shows that the HWW-SCULL, HWW-SWEEP and LWM externally rotated their HJC at the catch of the stroke for all Steps. The magnitude of this external rotation was always less as exercise intensity increased; the change into Step 6 being particularly noticeable for HWW-SWEEP. Throughout the drive and rockover HJC moved from external to internal rotation and then reversed its direction of change for the second half of the stroke. The change in angle throughout the stroke was reasonably smooth for HWW-SCULL and HWW-SWEEP, and less so for LWM; this may be indicative of muscular weakness around the hip and gluteals. Despite beginning the stroke in slight internal rotation, LWW did, as did the other athlete groups, move towards increased internal rotation for the first 10-15% of the stroke. However between 20-60% of the stroke the kinematics of the LWW were almost the mirror image of the HWW-SCULL. Within any one Step the HWW-SCULL exhibited the largest range in angles (16.4°); this was followed by LWW, LWM and HWW-SWEEP (12.1° , 11.9° and 10.5° respectively).

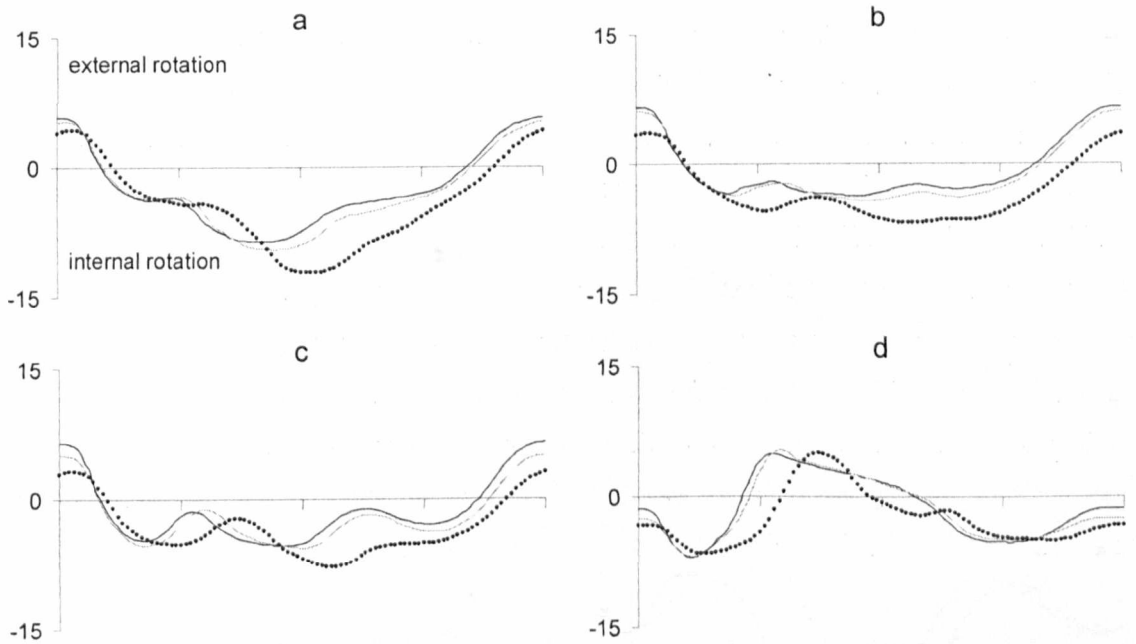


Figure 6.29: HJC gamma angle for all athlete groups

a. is HWW-SCULL, b. is HWW-SWEEP, c. is LWM, d. is LWW. The X axis is 0-100 percent of a representative rowing stroke. The Y axis is in degrees. The solid black line is Step 2, the semi solid grey line is Step 4 and the dotted black line is Step 6. Standard deviations for this data ranged from ± 5.4 to $\pm 9.6^{\circ}$ (a), ± 6.5 to $\pm 10.0^{\circ}$ (b), ± 5.9 to $\pm 9.9^{\circ}$ (c), and ± 5.7 to $\pm 10.4^{\circ}$ (d).

At the catch HWW-SCULL, HWW-SWEEP and LWM externally rotated their foot more as the intensity of exercise increased; Step 6 was greater than Step 2 by 3.0°, 3.2° and 4.3° for HWW-SCULL, HWW-SWEEP and LWM respectively. Excluding the values calculated for a few percentage points during Step 2, Figure 6.30 shows that HWW-SCULL, HWW-SWEEP and LWM consistently exhibited external AJC rotation throughout the entire rowing stroke. Despite always being in external rotation the groups mentioned above did move towards internal rotation during the second half of the drive phase; this trend is shown and amplified by the LWW. The LWW AJC was on average found to be in 6.7° of external rotation at the catch, during the first half of the drive phase, roughly until the point in the stroke when maximum handle force was being exerted, they moved into further external rotation (increasing by an average of 3.8°), after this, between the occurrence of maximum handle force and the finish of the stroke, they rotated rapidly into internal rotation, the angle changing by an average of 14.2°. From the finish all athletes increased external rotation during the first half of the recovery phase, and increased internal rotation during the second half of the recovery. Depending on the orientation of the FOB transmitter these angles may be incorrect by approximately 1° (repeatability of transmitter placement, Section 3.3.2).

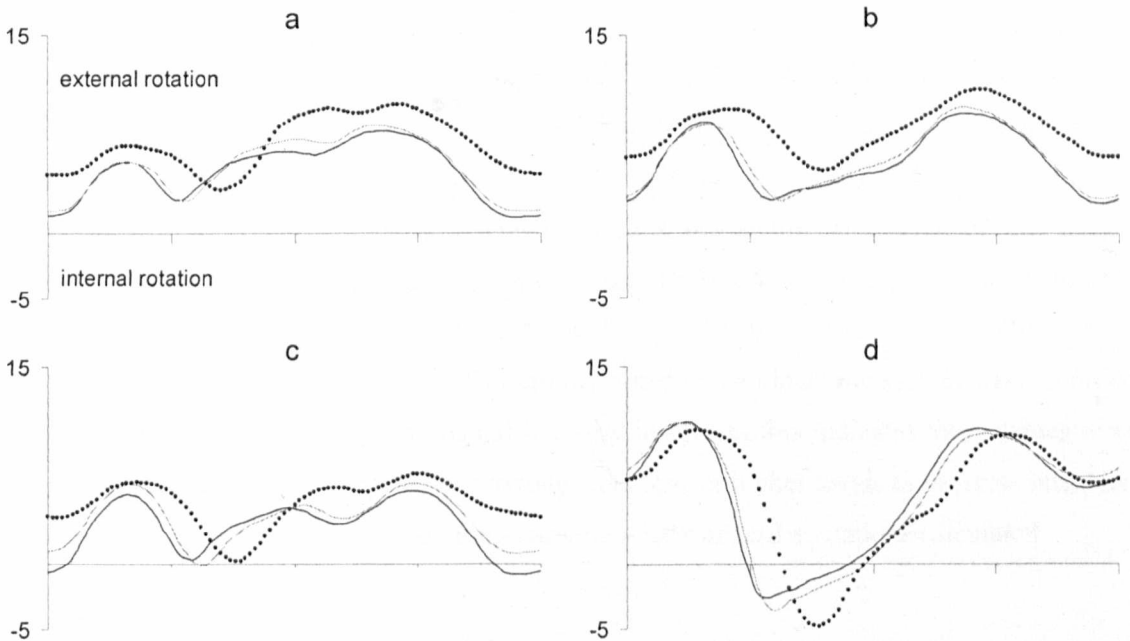


Figure 6.30: AJC gamma angle for all athlete groups

a. is HWW-SCULL, b. is HWW-SWEEP, c. is LWM, d. is LWW. The X axis is 0-100 percent of a representative rowing stroke. The Y axis is in degrees. The solid black line is Step 2, the semi solid grey line is Step 4 and the dotted black line is Step 6. Standard deviations for this data ranged from ± 5.3 to ± 8.6 ° (a), ± 6.7 to ± 10.0 ° (b), ± 4.0 to ± 7.2 ° (c), and ± 4.7 to ± 9.5 ° (d).

6.3.3 Variability of kinematics

In order to show the results as clearly as possible, comprehensive measures of data variability were omitted from the graphs presented in the previous section. This section presents information regarding the variability of measured three-dimensional kinematics.

When the average strokes presented in Section 6.3.1 and Section 6.3.2 were calculated it was also possible to calculate a standard deviation stroke. For example; the grand average stroke that was calculated to be representative of HWW-SCULL during Step 1 was computed from all of the individual Step 1 average strokes gathered from HWW-SCULL data between December 2006 and February 2009, this was 58 average strokes. Thus the representative stroke was a matrix of dimensions; 50 columns and 101 rows, each element of which was the average of 58 values. The standard deviation stroke was a similar matrix of 50 columns by 101 rows, each element of which was the standard deviation of 58 values. Thus for each column of data (e.g. LSJ X) a measure of the standard deviation of the variable was computed for each percentage point in the stroke (101 rows), finally the average, and maximum of these 101 values was computed for each column. The most variable displacement kinematic measurement was the position of the HJC in the Z direction, and the least variable was the position of the AJC in the X direction. The most variable rotational kinematic measurement was HJC alpha, and the average and maximum standard deviations for HWW-SWEEP were far higher than for any other boat class. The least variable rotational kinematic variable was FJC alpha. When considering the variability of kinematic data under different Steps, Table 6.6 shows that for HWW-SCULL 43% of the largest average standard deviations, and 43% of the largest maximum standard deviations occurred in Step 6, for HWW-SWEEP these margins were 65% and 57%, for LWM they were 61% and 52%, and for LWW they were 52% and 48%. Thus over half (53%) of all of the extremes of variability noted in the kinematic system were recorded when athletes were performing at maximal intensity in Step 6, this indicates that athletes were less able to maintain consistency in their rowing technique at higher levels of exercise intensity. Table 6.6 shows the average and maximum variable-wise standard deviations calculated.

move across a greater global range; for example the HJC data had higher standard deviations than the AJC and FJC where the AJC and FJC were nearer to the point at which the athletes' body was restrained at the footstretcher. The data presented in Sections 6.3.1, 6.3.2 and 6.3.3 represents the fullest description of elite athletes' stroke profile and three-dimensional kinematics that is currently available in the literature.

6.3.4.1 Explanation of seemingly inconsistent results

Figure 6.19 showed that all athlete boat classes exhibited small amounts of lumbar extension at the finish of the stroke, and considerable amounts of lumbar extension beyond the finish of the stroke. From the finish to the finish plus 15% stroke duration, intersegmental angles between the pelvis and the lumbar spine were between 0° and 12°. However, the LP ratios shown in Figure 6.20 appeared to show that there was good alignment of the segments during this period of the stroke. In order to connect these seemingly discordant results consider the following: around the finish of the stroke it was not uncommon to coincidentally measure the BACK segment to be in 40° of extension, whilst the PELVIS segment was in 30° of extension in the FOB sagittal plane. In this situation one could expect LSJ α to be close to 10° of lumbar extension; the LP ratio for this posture would be 1.3. An LP ratio of 1.3 may at first appear to suggest good alignment of the two body segments, but this example shows that it does not. In the current research, when feedback was delivered to athletes and coaches only LP ratios that were greater than 0.9 and less than 1.1 were considered to be of high quality.

The other seemingly conflicting results presented in Figure 6.19 and Figure 6.20 concerned LSJ α and postural control at the catch. For example, Figure 6.19 showed that LWM generally had a lower intersegmental angle at the catch than HWW-SCULL. However, Figure 6.20 highlighted that HWW-SCULL had consistently better LP ratios at the catch. This illusory disagreement is again explained by considering the global orientation of the segments. Typically a HWW-SCULL athlete might move their BACK into 30° and their PELVIS into 15° of flexion about the global X axis at the catch; this would result in LSJ α being close to 15° of lumbar flexion about the pelvis, and an LP ratio of 2.0. On the other hand an example of a typical orientation of LWM body segments at the catch is; BACK = 14° flexion and PELVIS = 3.5° flexion; this would result in LSJ α being close to 10.5° of lumbar flexion about the pelvis (less than HWW-SCULL), and an LP ratio of 4.0 (twice as big as HWW-SCULL). Considering the average of all Steps HWW-SWEEP achieved the most flexion of PELVIS (22°). This was 22% more flexion than HWW-SCULL, 64% more flexion than LWM, and 148% more flexion than LWM, and, while this had a significant effect on the calculation of LP ratios, it did not, on its own, impact upon LSJ α .

6.3.4.2 Differences between athlete groups

The way in which athletes suspended away from the seat during the early portion of the drive phase was different for the heavyweight boat classes compared to the lightweight. Figure 6.4 showed that, depending on the Step, during the first 20% of the stroke the magnitude of suspension achieved by HWW-SCULL and HWW-SWEEP did not vary too much, and increased very little, if at all, from the catch. On the other hand the LWW and to an even greater extent the LWM showed noticeable increases on the suspension they achieved at the catch as the first half of the drive phase progressed. This may be related to the posture that each group exhibited at the catch of the stroke. The higher quality LP ratios (closer to 1) and increased pelvis flexion at the catch shown by the heavyweight groups, may suggest that they were in a stronger position at the catch, thus providing a more rigid lever that was more easily suspended away from the seat as forces developed at the footstretcher and the handle were transmitted through the body. Concurrently, it may also be that it was not until the lightweight groups had moved posteriorly from the catch and were in a more balanced and comfortable position that they were able to achieve their best suspension. Another explanation might be that the lightweight groups activated the main push through their legs slightly later than the heavyweight rowers did. That is, it is possible that during the first few percent of the stroke, instead of pressing through the legs only, whilst maintaining a strong and rigid trunk with straight arms (Chapter 1), lightweights may have actively pulled more through the handle using the torso, shoulders and arms than HWW-SCULL or HWW-SWEEP did.

Again comparing heavyweight athletes to lightweights Sections 6.3.1 and 6.3.2 showed that there were some noticeable differences in the magnitude and trend of motion trajectory in the X direction for COP, LSJ, HJC and AJC. The LWM and LWW generally exhibited greater COP deviations on the seat in the medial and lateral directions, and greater medial and lateral displacement of LSJ and HJC than their heavyweight counterparts. The magnitude of LSJ gamma was also higher for lightweights than for heavyweights. In addition to this, heavyweight women and lightweights displaced their AJC in different ways throughout the rowing stroke, whilst the magnitude of these movements was small, the variations were consistent (Figure 6.10) and the variability of data was small (Section 6.3.3).

Figure 6.16 showed that, independent of Step, lightweight athletes displaced their HJC more anteriorly at the catch of the stroke than heavyweights. Because knee flexion was similar for heavyweights and LWW at the catch (Figure 6.22), and the position of ANTFOOT was the same for all athletes the additional anterior HJC displacement seen for LWW is probably explained by lower leg length; HWW leg length was 8% longer than LWW, ≈ 66 mm. In the case of LWM versus HWW-SCULL and HWW-SWEEP, where leg length was more

comparable (LWM leg length was 2% longer than HWW, ≈ 16 mm), the additional anterior HJC displacement seen for LWM is possibly explained by the coincidentally observed greater magnitude of knee flexion (Figure 6.22). Lightweights and HWW-SWEEP displaced their LSJ more anteriorly than HWW-SCULL; this is consistent with the additional displacement of the HJC seen for LWM and LWW, and may be explained by spinal posture for HWW-SWEEP versus HWW-SCULL. As mentioned previously, at the catch HWW-SWEEP flexed their pelvis anteriorly 22% more than HWW-SCULL, and they also achieved consistently better LP ratios than any other boat class; the next best were HWW-SCULL who were between 0.2 and 0.4 further from the ideal ratio of 1.0 for all Steps. This combination of increased anterior pelvic tilt with coincident higher quality postural control would displace HWW-SWEEP LSJ more anteriorly than HWW-SCULL LSJ at the catch.

There were also some noticeable differences in the measurements of HJC gamma and AJC gamma comparing the LWW to the other athlete groups. These differences are hard to explain, though may simply be a product of fewer LWW being included in the current research. Thus the data may be slightly skewed in favour of a particular athlete's technique.

6.3.4.3 Other results

Figure 6.12 showed that the rate at which HJC Y was displaced upwards was less in the first half of the drive than it was in the later portion of the drive. The KJC was consistently displaced less inferiorly at the finish of Step 6 than earlier Steps and did not remain fully extended during rockover in Step 6, concurrently; Figure 6.22 showed that Step 6 was the only Step when three out of the four boat classes did not hyper extend their knee at the finish. In addition to this, Figure 6.11 showed that all athlete groups exhibited less upwards displacement of LSJ during the stroke rockover in Step 6 than in earlier efforts. This may indicate that the quality of athletes' rockover was not as good at higher intensity, and that the rowers were not getting "up and over" their hips as effectively when moving into the recovery phase during Step 6. Also at the rockover, Figure 6.18 showed that all athletes, though particularly LWW showed a peak of upwards motion of the AJC; this is explained by noting the athletes' heels' departure from the footstretcher that occurred at the same time ($\approx 40\%$ of the stroke, Figure 6.24).

All boat classes achieved more AJC Y, similar levels of AJC Z, less LSJ Z, less HJC Z, less KJC Z, and less COP Z at the catch during Step 6 than in earlier Steps; hence there was also less dorsi flexion, less knee flexion and less hip flexion. This may have been responsible for the additional lumbar flexion at the catch during Step 6; which was required in order to maintain

some degree of stroke length at the front of the stroke at high intensity. The magnitudes of the reductions in KJC Z and in dorsi flexion were greater for lightweights than for heavyweights.

Chapter 7

Effect of Exercise Intensity

The data used in this investigation was obtained during the testing session of June 2008. This data was selected because the athletes in the group were coming to the peak of their rowing ability in the run up to the Olympic Games in Beijing, and hence the best picture of elite rowing was available from this testing session. A total of 22 athletes completed all six Steps; 6 were HWW-SCULL, 7 were HWW-SWEEP, 7 were LWM and 2 were LWW (Table 6.3, Page 103). Due to an insufficient number of LWW no analysis was completed on their data. Unless otherwise specified, all statistical tests were conducted with a significance level of 0.05. The analyses and results in this chapter are presented in response to the second hypothesis listed in Section 5.5; that some aspects of elite rowers' technique and performance would be affected by the intensity of their exertions.

After organising the data into an appropriate format the Kolmogorov-Smirnov (KS) and Shapiro-Wilk (SW) tests were used to assess the normality of the data, and subsequent ANOVA RM was conducted on 168 dependent variables for each of the three athlete groups (Table 5.2, Page 90). The output of the general linear model was comprised of descriptive statistics for the dependent variable, four multivariate tests; Pillai's Trace, Wilks' Lambda, Hotellings's Trace, Roy's Largest Root, there was also Mauchly's test of sphericity, and the results of the ANOVA RM. In order to conduct pairwise comparisons a post hoc procedure with Bonferroni adjustment was included in the analysis. In this chapter the term pairwise refers to a comparison of a dependent variable between any two individual Steps.

7.1 Interpreting the test results

For the results of ANOVA RM to be considered valid, data must be normally distributed and meet an acceptable level of sphericity. The KS and SW tests must yield a p-value of more than 0.05 (a non-significant result) if a dataset is to be considered to be parametrically distributed. Mauchly's test of Sphericity (MS) provides an analysis of the variability of data, similar to homogeneity of variance seen in non repeated measures ANOVA which states that the variance within each experimental group should be similar. The p-value obtained from MS must be greater than 0.05 if one is to assume sphericity of a dataset. However, even if the assumption of sphericity is violated, SPSS provides two techniques by which the data's degrees of freedom, and resulting F ratio may be adjusted in order to proceed validly; these are the Greenhouse-Geisser (GG) adjustment, and the Huynh-Feldt (HF) adjustment. Providing the

assumptions of normality and sphericity of data are met the result of the ANOVA RM can be observed to find if a significant change occurred in the dependent variable under different experimental conditions, post hoc analysis may then be used to identify exactly which pairwise comparisons show significant change.

7.2 Results

3% of the dependent variables were found to be not normally distributed for the HWW-SCULL group, 4% were not normal for the HWW-SWEEP group and 8% for the LWM. These deviations from normality were only considered pertinent, and hence referred to, if they coincided with variables that significantly varied with exercise intensity.¹ The results of MS tests dictated that all of the variables that are presented in this chapter as exhibiting significant change met the assumption of sphericity. The results of ANOVA RM were grouped into four categories; firstly; where there was no significant difference found with increasing Step, secondly; where there was significant change in the dependent variable as the intensity of exercise changed, thirdly; where a significant difference was noted but Bonferroni post hoc analysis did not identify where the difference lay, and fourthly; where the GG and HF p-values in the ANOVA RM results disagreed (these were flagged and are discussed in due course). Table 7.1 shows the number of variables that were found to fall within each category.

	Number of variables (out of 168)			Flagged
	Non-significant ($p > 0.05$)	Significant ($p < 0.05$)	Significant with failed Bonferroni	
HWW-SCULL	91	44	30	3
HWW-SWEEP	114	23	27	4
LWM	116	26	19	7
Common to all athlete groups	64	10	0	0
Common to HWW-SCULL and HWW-SWEEP	74	13	3	0

Table 7.1: Results of ANOVA RM with changing exercise intensity

Tests conducted on the dependent variables were found to show no significant change, to show significant change, to show significant change with failed Bonferroni post hoc analysis, or were flagged because the results were ambiguous.

It was decided that because none of the athlete groups' data was found to vary for 64 of the 168 original variables only the remaining 104 would be considered in any further analysis. In an attempt to further reduce the dataset recall that each of the 23 kinematic variables were logged

¹ SPSS has the facility to perform some analyses of variance on nonparametric data, however not with repeated measures. Furthermore the output offered by SPSS is limited. No nonparametric tests were conducted on the data that was found to be not normally distributed.

six times (Table 5.2). After reviewing the data presented in Section 6.3.2 it was thought to be likely that the values measured as maximum and minimum would be highly correlated with those recorded at either the catch or the finish of the stroke. Table 7.2 shows the results of a Pearson correlation analysis carried out to test this theory.

Variable	Pearson correlation (r) of the; Value recorded at the CATCH, and the		Pearson correlation (r) of the; Value recorded at the FINISH, and the	
	MAX value	MIN value	MAX value	MIN value
LSJ X	.891**	.359**	.386**	.937**
LSJ Y	.925**	.867**	.879**	.924**
LSJ Z	.996**	.474**	.479**	.994**
HJC X	.907**	.677**	.693**	.894**
HJC Y	.468**	.998**	.991**	.527**
HJC Z	.997**	.320**	.298**	.984**
KJC X	.577**	.982**	.350**	.070
KJC Y	.994**	.340**	.387**	.917**
KJC Z	.997**	.427**	.401**	.983**
AJC X	.771**	.850**	.695**	.650**
AJC Y	.927**	.490**	.577**	.717**
AJC Z	.998**	.534**	.518**	.977**
LSJ alpha	.861**	.990**	.975**	.908**
LSJ beta	.969**	.898**	.922**	.977**
LSJ gamma	.796**	.803**	.822**	.868**
HJC alpha	.698**	.999**	.958**	.718**
HJC beta	-.217*	.846**	.817**	-.154
HJC gamma	.594**	-.065	.146	.639**
KJC alpha	.995**	.195*	.157	.933**
AJC alpha	.214*	.813**	.951**	.414**
AJC beta	.942**	.129	-.080	.843**
AJC gamma	.779**	.626**	.730**	.905**
FJC alpha	.997**	.560**	-.045	-.166

Table 7.2: Correlations between extremes of kinematic measurements and at the stroke catch and finish

** Correlation is significant at the 0.01 level (2-tailed)

* Correlation is significant at the 0.05 level (2-tailed)

Table 7.2 shows that the maximum and minimum values of all of the kinematic parameters under consideration were significantly correlated with the values calculated for the catch and the finish of the stroke. As it is often useful to use these key stroke events when describing rowing activity it was decided that there would be no further need for the maximum or minimum values to be numerically analysed. Where previously completed ANOVA RM tests had shown there to be a significant difference in a maximum or minimum kinematic value, it is discussed if the corresponding catch or finish value was not significant or it is presented in conjunction with the appropriate catch and finish values.

7.2.1 Significant results for more than one athlete group

Table 7.3 identifies the dependent variables that were found to vary significantly with a change in exercise intensity for more than one athlete group, and the figures in this section illustrate the means and standard deviations for selected data. There were 10 variables that varied significantly with changes in Step for all three of the athlete groups tested, and there were a further 3 variables that were common to the HWW-SCULL and HWW-SWEEP groups only. The results of post hoc analyses carried out with the ANOVA RM tests for the variables shown in Table 7.3 are described below, and can be seen in full in Table 7.4, Page 153.

Common to all athlete groups	Common to HWW-SCULL and HWW-SWEEP
Max handle force (%)	Max handle force (%)
Finish (%)	Finish (%)
Max H Force/BM (N/kg×100)	Max handle force (N)
Slope of handle force	Max H Force/BM (N/kg×100)
Min seat force (N)	Slope of handle force
Suspension 2 (BW(s))	Min seat force (N)
Power output (W)	Suspension 2 (BW(s))
	Power output (W)
	Stroke length (mm)
Stroke rate (/min)	Stroke rate (/min)
	Work done (J)
max HJC Z (mm)	max HJC Z (mm)
max KJC alpha (°)	max KJC alpha (°)

Table 7.3: Significant dependent variables common to more than one athlete group

The column graphs that are presented in this section show the mean and standard deviation of dependent variables. When viewing these graphs pairwise comparisons that showed significant changes are identified by the numbers listed vertically above the columns. For example, if for a particular dependent variable HWW-SCULL athletes were found to score significantly higher in Step 6 than they did in Step 5 then the number “5” would be listed above the column describing the mean and standard deviation of the HWW-SCULL result for Step 6. The column value for a Step is always significantly greater than the Steps identified by the numbers listed above it.

Both the timing of the peak handle force and the finish during the stroke were found to occur later as exercise intensity increased (Figure 7.1). The most noticeable result was that all athlete groups showed significantly later maximum handle force and finish events during Step 6 when compared to all the earlier Steps, in addition to this the HWW-SCULL group showed the largest number of significant pairwise comparisons for both of the timing variables. The results shown in Table 7.4 for the HWW-SWEEP group should be viewed with caution as the some of the data for this group of athletes was found to exhibit non parametric distribution.

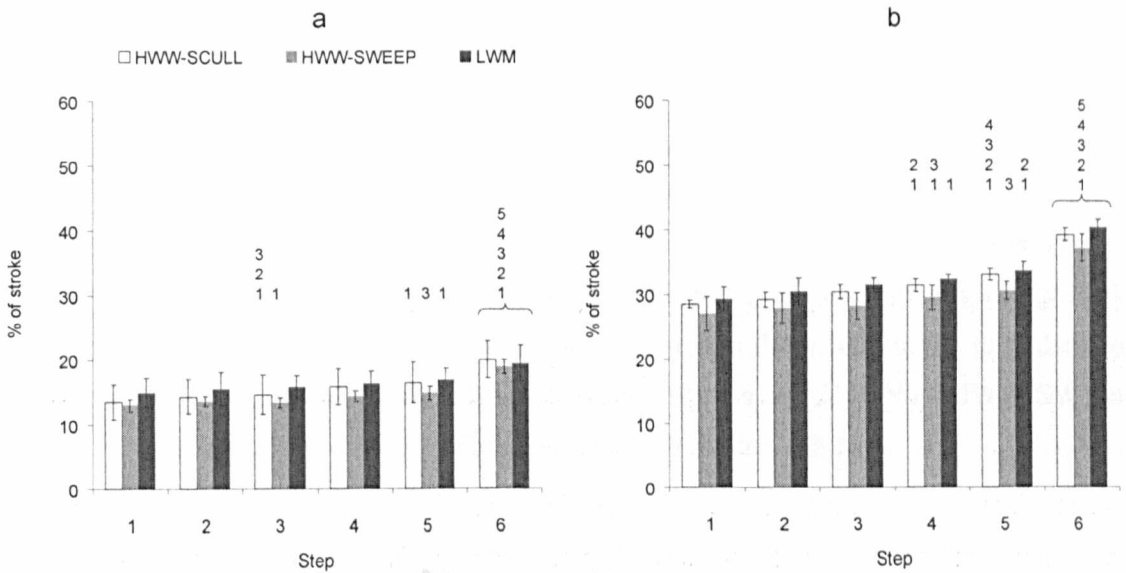


Figure 7.1: The mean and standard deviation of timing of peak handle force (a) and timing of the finish (b) for all athlete groups, for all Steps

The numbers above the columns are the Steps that the column value was significantly greater than ($p < 0.05$).

Whilst the HWW-SCULL and HWW-SWEEP groups both showed differences in the amount of raw force they exerted on the handle as Step changed, the LWM did not exhibit this feature until the raw force values were normalised by body mass. Again, post hoc analysis showed the HWW-SCULL group to have the largest number of significant pairwise comparisons by Step with the HWW-SWEEP and the LWM each only showing one significant difference; that more force was produced per kg of body mass in Step 3 than in Step 1 (Figure 7.2). Because the HWW-SCULL showed increases in the peak forces applied through the ergometer handle and because this peak occurred progressively later in the stroke as intensity increased there were few significant differences noted in terms of the rate of handle force production; as intensity was raised the HWW-SWEEP and LWM groups showed a peak force of similar magnitude occurring later in the stroke, therefore, more often than the HWW-SCULL, the slope of their handle force curves became gradually less steep as Step increased. Figure 7.2 shows that on average HWW-SCULL produced between 40 N and 54 N per stroke percentage until they reached peak pulling force, this was also 40 N to 54 N for HWW-SWEEP, and was 45 N to 54 N for LWM. Considering the athletes' average stroke rate (Figure 7.4) it was also possible to approximate the rate at which force was produced through the handle in the time domain. Depending on the Step, HWW-SCULL achieved 1703 N/s to 2168 N/s, HWW-SWEEP produced 1682 N/s to 2136 N/s, and LWM produced 1799 N/s to 2486 N/s.

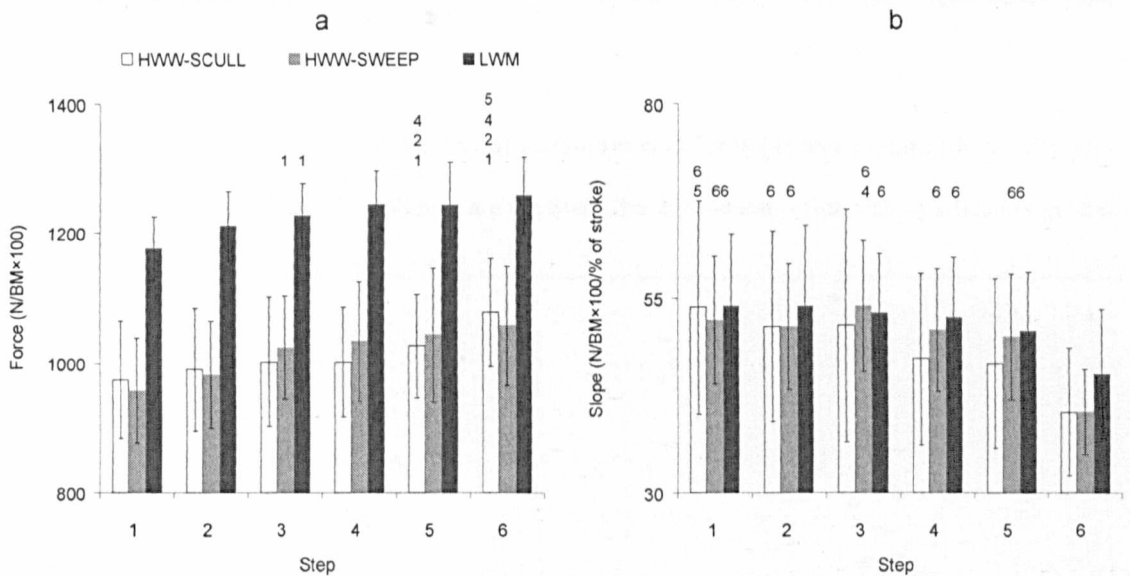


Figure 7.2: Mean and standard deviation of normalised maximum handle force (a) and rate of force production (b) for all athlete groups, for all Steps
 The numbers above the columns are the Steps that the column value was significantly greater than ($p < 0.05$).

The minimum seat force was observed to be lower during higher intensity exercise for all of the athlete groups with the HWW-SWEEP and LWM groups showing more pairwise changes than the HWW-SCULL rowers (Figure 7.3). That is, the peak force exerted onto the seat was of a greater magnitude at higher intensities. The results in Table 7.4 (Page 153) also show that the value logged for suspension during the entire drive, from the catch to the finish, was greater at higher intensity indicating that the magnitude of suspension between the feet and hands was less for all groups over this phase of the stroke (more emphasis was placed on the seat for weight bearing hence a larger score was logged).

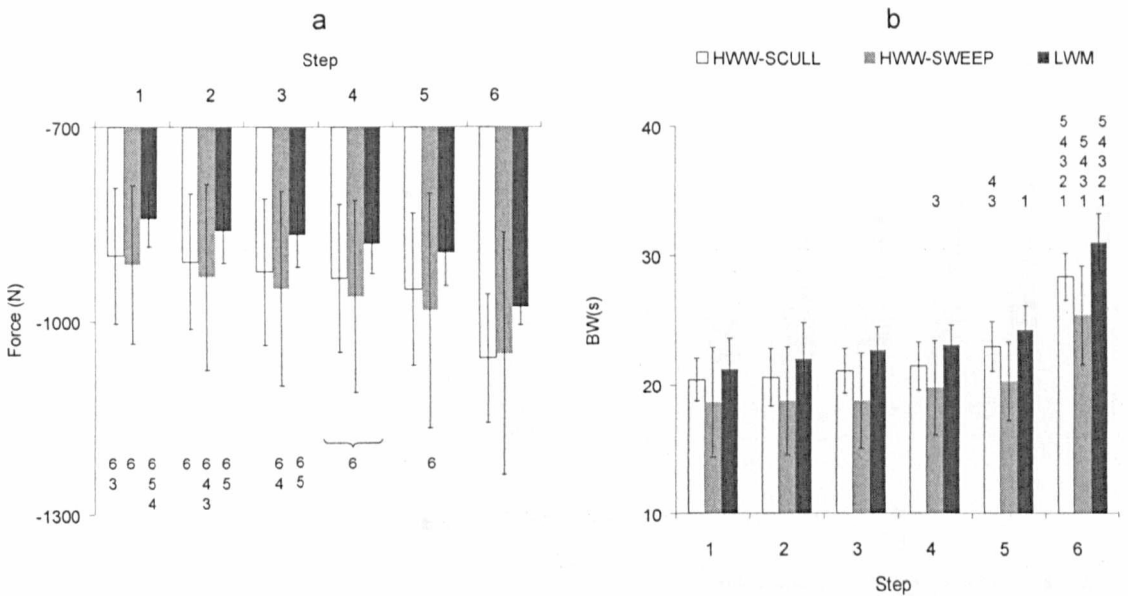


Figure 7.3: Mean and standard deviation of minimum seat force (a) and magnitude of suspension (b) for all athlete groups, for all Steps

The numbers below and above the columns are the Steps that the column value was significantly greater than ($p < 0.05$).

For all groups, power output increased significantly with every Step up in intensity ($p < 0.05$); however data for Steps 3 and 5 were found to be not normal for the HWW-SWEEP rowers. For the HWW-SCULL and HWW-SWEEP there were also some small increases in stroke length with increasing Step (Step 4 vs Step 2, and Steps 3,4 vs Step 1 respectively). All groups showed an increase in the number of strokes they performed each minute as intensity was raised (Figure 7.4). Probably linked to the extra stroke length cited above; the female athletes showed some increases in the amount of work they achieved as Step increased.

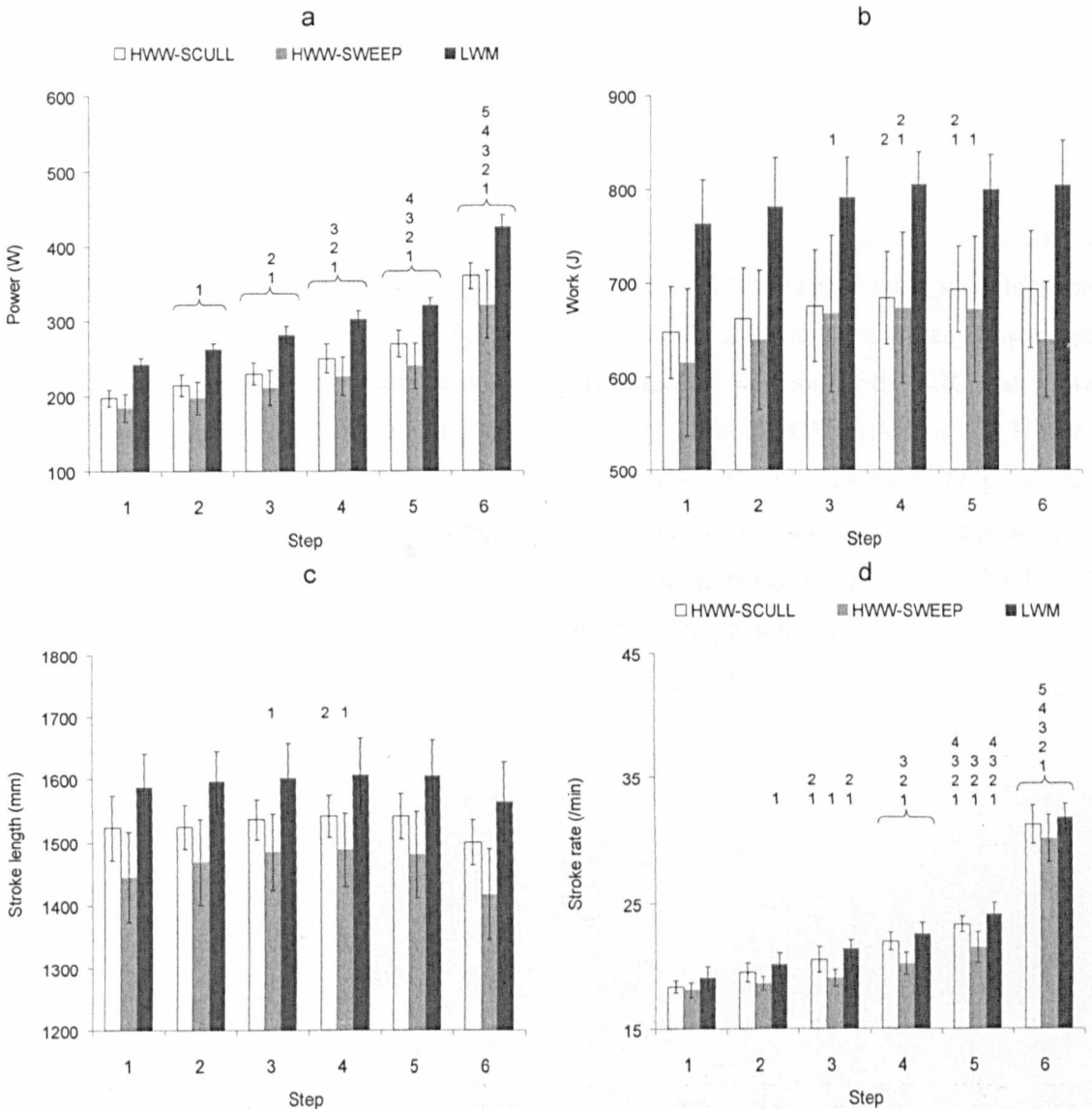


Figure 7.4: Mean and standard deviation of power (a), work (b), stroke length (c) and stroke rate (d) for all athlete groups, for all Steps
 The numbers above the columns are the Steps that the column value was significantly greater than ($p < 0.05$).

Two kinematic variables that were found to change significantly with varying exercise intensity for all athlete groups were the trajectory of the HJC in the Z direction and the magnitude of knee flexion. Figure 7.5 and Table 7.4 show that during Steps 3,4,5 the LWM achieved more anterior displacement of their HJC and, in Steps 2,3,4,5, exhibited significantly more knee flexion than they did when they rowed at race pace in Step 6. The same pattern can be seen for HWW-SCULL during Steps 4,5 vs Step 6 for both variables, and for Step 3, and Step 4 vs Step 6 for the HWW-SWEEP group, for the two variables respectively. These changes in measurement reveal that the athletes *compressed* less during higher intensity exercise. Table 7.3 tells us that it was the maximum value noted for each of these kinematic variables that was found to vary with Step changes for all groups; because we know from Table 7.2 that max HJC Z and max KJC α are highly correlated with HJC Z and KJC α at the catch ($r = .997$ and $.995$ respectively) it is worth examining the behaviour of these dependent variables for the different athlete groups at the catch. At the catch, the HWW-SCULL group show significant changes with Step difference in the anterior position of the athletes' HJC and the magnitude of knee flexion they achieve that exactly matches the results seen for the maximum scores logged in Table 7.4. This agreement in results between the maximum score and the scores at the catch is also true for the LWM, with one addition; at the catch the position of the HJC was more anterior during Step 2 compared to Step 6. The results of the ANOVA RM for the HWW-SWEEP group also show a significant p-value for the two variables at the catch, however, the post hoc procedure failed to identify where the difference lay in both cases. Less anterior displacement of HJC and reduced KJC flexion in Step 6 suggests that the athletes probably had to flex more through their spine in order to maintain stroke length at the front of the stroke.

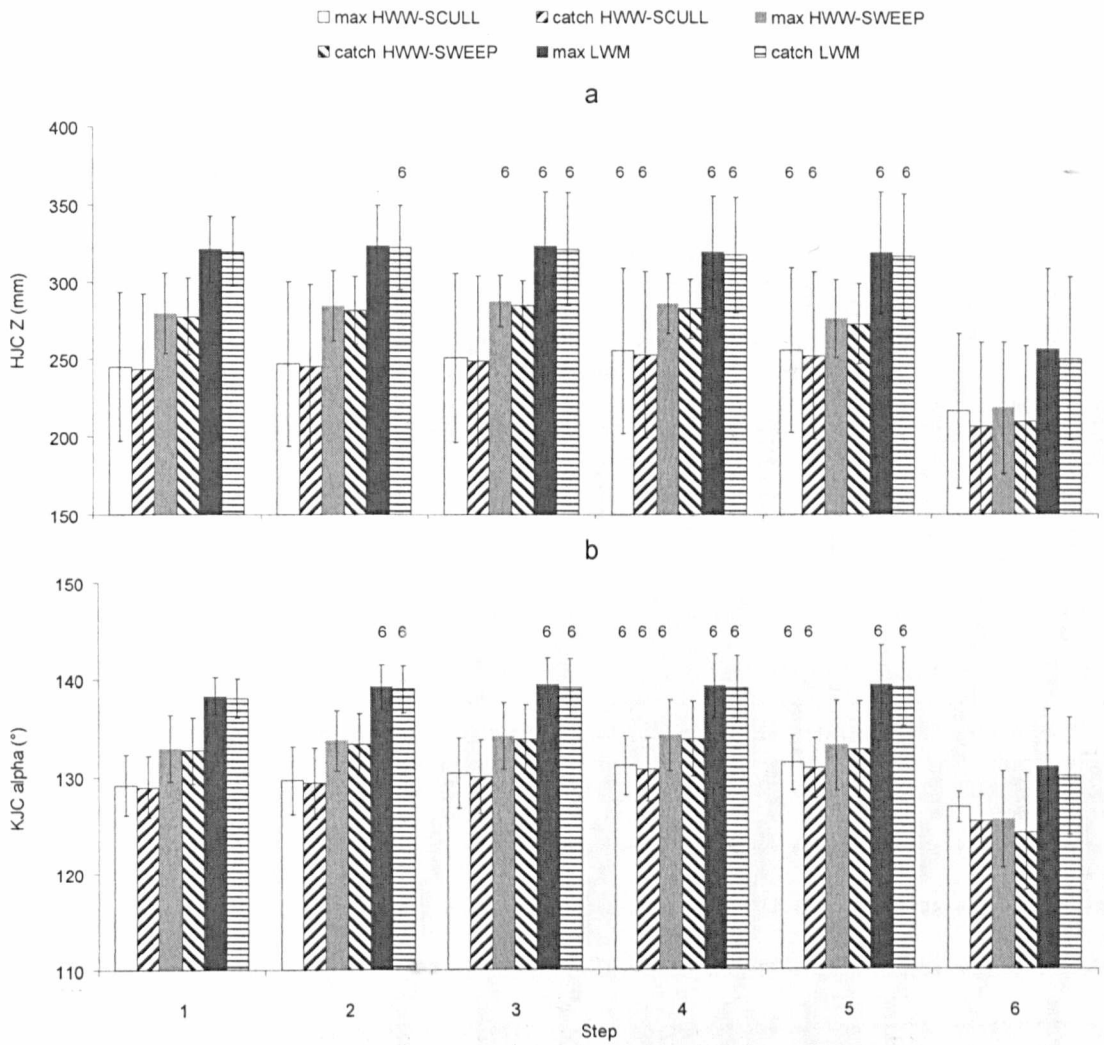


Figure 7.5: Mean and standard deviation of maximum and catch position of the HJC in the Z direction (a) and Maximum value, and value at the catch for KJC α (b) for all athlete groups, for all Steps
 The numbers above the columns are the Steps that the column value was significantly greater than ($p < 0.05$).

7.2.2 Significant results for HWW-SCULL

Table 7.5 identifies the 44 dependent variables that were found to vary significantly with a change in exercise intensity for the HWW-SCULL group, the results of 15 of these were presented in Section 7.2.1. Of the remaining 29 variables; 3 refer to the maximum value recorded and 6 refer to the minimum value recorded, 6 of these 9 are also found in either the catch or finish columns. These 6 variables are identified by the superscripts in Table 7.5 and are not expanded upon for the remainder of this results section, instead only the results from the catch and finish are described. The rest of this section is dedicated to presenting the results of the post hoc analyses carried out for the enduring 23 variables shown in Table 7.5.

Non 3D kinematic variables	Maximum values of 3D kinematic data	Minimum values of 3D kinematic data	3D kinematic data at the catch of the stroke	3D kinematic data at maximum handle force	3D kinematic data at the finish of the stroke	3D kinematic data at knees up during the recovery
Max handle force (%)	HJC Z	-	HJC Z	-	-	-
Finish (%)	KJC alpha		KJC alpha			
Max handle force (N)						
Max H Force/BM (N/kg×100)						
Slope of handle force						
Min seat force (N)						
Suspension 2 (BW(s))						
Power output (W)						
Stroke length (mm)						
Stroke rate (/min)						
Work done (J)						
COP drift – MHF (mm)	LSJ Z ¹	HJC Y ⁴	LSJ Z ¹	LSJ gamma	KJC Y ⁵	LSJ Z
COP drift – Finish (mm)	KJC Z ²	KJC Y ⁵	LSJ gamma	HJC gamma	KJC alpha ⁶	KJC Y
COP Z @ Catch	AJC X ³	KJC Z	HJC Y ⁴	AJC Z	AJC X ³	KJC alpha
COP Z @ Finish		KJC alpha ⁶	KJC Z ²			AJC X
Max seat force (N)		AJC Y				AJC alpha
		AJC alpha				

Table 7.5: Significant dependent variables for the HWW-SCULL group

The variables in the top section of the table are the ones that have previously been presented. *r* values from Table 7.2; ¹ = .996**, ² = .997**, ³ = .695**, ⁴ = .998**, ⁵ = .917**, ⁶ = .933**. **Correlation is significant at the 0.01 level (2-tailed). The 23 variables discussed in this section are highlighted.

Post hoc analysis revealed that during Step 6 the HWW-SCULL athletes' COP on the ergometer seat was medio-laterally displaced up to 100% more than it was during lower Steps in the propulsive phase of the rowing stroke. In addition to this, the group moved their COP up to 22.9 mm further forward on the seat during lower intensity exercise at the catch than they did during higher Steps, and they produced greater posterior COP displacement at the finish when rowing at higher intensity (6.1 mm). There was also one significant pairwise comparison concerning the maximum force that the athletes exerted on the seat; this value was significantly higher in Step 3 than in Step 2. The force value exerted on the seat is recorded as a negative value in the current setup, hence the fact that the maximum force in Step 2 (-86.07 N) was lower

than that in Step 3 (-67.94 N) means that the athletes' were exerting more force on the seat during Step 2.

The minimum value logged for KJC Z revealed that during Step 6 the athletes KJC was in a more anterior position around the finish of the stroke than it was in Step 1 (+4.3 mm). Also during Step 6, the AJC was elevated more than in Steps 3,4,5 at its highest point, and there was a significant extra 1° of dorsi flexion in Step 2 compared with Step 1.

At the catch of the stroke the HWW-SCULL moved their LSJ further anterior during Steps 4,5 than in Step 6 (56.9 and 54.4 mm respectively), concurrently there was significantly 1.3 and 1.8° less twist about LSJ during Step 6. The HJC was found to be significantly lower down in Step 4 vs Step 6, and the KJC was significantly more anterior in Steps 4,5 than it was in Step 6 (43.3 and 43.0 mm respectively).

Approximately half way through the propulsive phase of the stroke, when peak force was being exerted on the handle, there was significantly more lumbar twist to the left about LSJ during lower intensity exercise. Furthermore, at this point in the stroke the HJC was found to be between 1.2 and 2.4° internally rotated during Steps 1-5, however in Step 6 this had become 1.7° of external rotation. The position of the AJC was more posterior during Step 6 than it was in Step 1.

At the finish of the drive, and before the recovery phase of the stroke commenced, the athletes' KJC was between 9.1 and 12.9 mm higher during Step 6 than it was during the lower intensity exertions. In addition to this, Step 6 was the only Step where the athletes did not hyper extend about KJC at the finish and as a result there was significantly more knee flexion in Step 6 than there was in Steps 2,3. One further significant result revealed that during Step 6 the AJC was shifted significantly further laterally during Step 6 than it was in Step 1 (+7.4 mm).

During the recovery phase of the stroke, and just as the athletes' knees began to rise their LSJ was significantly further forward during lower Steps than high, with differences as high as 19.0 mm. In addition to this their AJC was positioned more laterally and exhibited 2.5° less plantar flexion at higher intensity. The statistics also suggest that when the knees broke during the recovery the KJC was higher from the floor at increased levels of intensity, however the KS and SW tests indicated that this data was not normally distributed so should be viewed cautiously. The final finding at "knees up" was that the magnitude of knee flexion increased as in line with Step progression. Descriptive statistics for KJC α are shown in Figure 7.6.

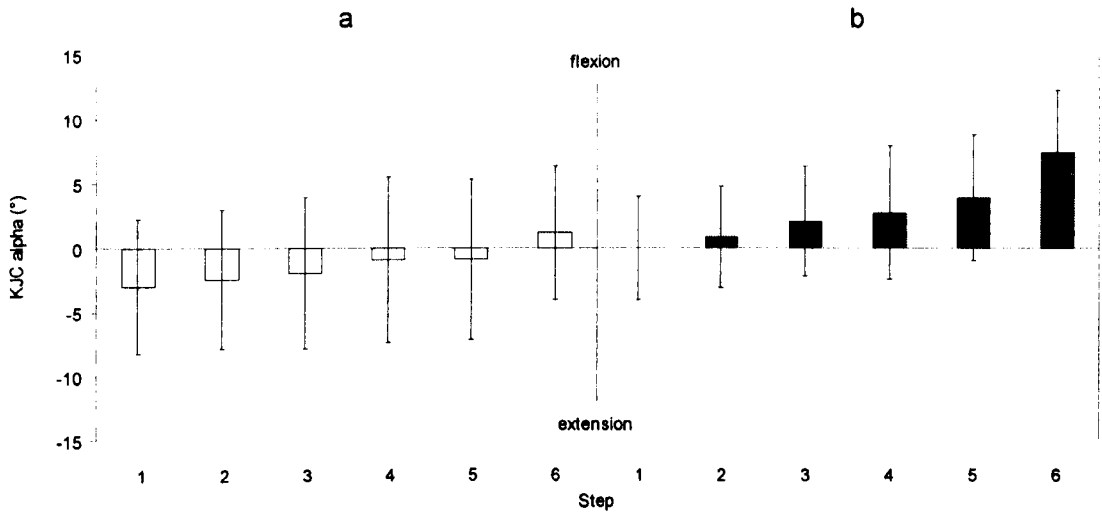


Figure 7.6: Mean and standard deviation for KJC α at the finish (a) and during the recovery (b)

7.2.3 Significant results for HWW-SWEEP

Table 7.6 shows the 23 dependent variables that were found to vary significantly with a change in exercise intensity for the HWW-SWEEP rowers, the results of 13 of these were presented in Section 7.2.1. Of the remaining 10 variables; 1 refers to the maximum value recorded and 2 refer to the minimum value recorded, and 1 of these (the position of KJC in the X direction) is also found in the catch column. This variable is identified by the superscript in Table 7.6 and is not expanded upon for the remainder of this results section, instead only the results from the catch will be described. The rest of this section is dedicated to presenting the results of the post hoc analyses carried out for the enduring 9 variables shown in Table 7.6.

Non 3D kinematic variables	Maximum values of 3D kinematic data	Minimum values of 3D kinematic data	3D kinematic data at the catch of the stroke	3D kinematic data at maximum handle force	3D kinematic data at the finish of the stroke	3D kinematic data at knees up during the recovery
Max handle force (%)	HJC Z	-	-	-	-	-
Finish (%)	KJC alpha					
Max handle force (N)						
Max H Force/BM (N/kg*100)						
Slope of handle force						
Min seat force (N)						
Suspension 2 (BW(s))						
Power output (W)						
Stroke length (mm)						
Stroke rate (/min)						
Work done (J)						
-	LSJ Y	KJC X ¹ AJC gamma	KJC X ¹	LSJ Z HJC Z KJC alpha AJC gamma	-	LSJ Y HJC gamma

Table 7.6: Significant dependent variables for the HWW-SWEEP group

The variables in the top section of the table are the ones that have previously been presented. *r* values from Table 7.2; ¹ = .996**. **Correlation is significant at the 0.01 level (2-tailed). The 9 variables discussed in this section are highlighted.

The trajectory of LSJ was found to vary in both the Y and Z directions at different stages in the stroke, and the maximum value recorded shows that during Step 6 LSJ was positioned lower down than it was in Steps 1,2,3. During the drive the coordinate of LSJ moved posteriorly more quickly during higher intensity exercise, so that by the time peak force was being applied through the handle LSJ was up to 28.0 mm further back than it was in earlier Steps. In addition to this LSJ was significantly lower down at knees up in Step 6 than it was during Step 1. At high intensity the HJC was found to behave in the same way as LSJ, moving 25.6 mm more rearward by mid drive than at lower intensity, and when the knees broke during the recovery there was significantly more external hip rotation in Step 6 than in earlier Steps (4.4° vs 7.5°). The KJC was found to be pushed out more laterally at the catch in Steps 1,2,3 than it was in Step 6, and there was more knee flexion when maximum handle force was being applied during

Step 3 than there was in Step 6 (+3.5°). The minimum recorded values show that there was also less external rotation of the foot about the AJC at higher intensity, and during the drive there was 1.4° more internal rotation in Step 6 than there was in Step 4.

7.2.4 Significant results for LWM

Table 7.7 identifies the 26 dependent variables that were found to vary significantly with a change in exercise intensity for the LWM, the results of 10 of these were presented in Section 7.2.1. Of the remaining 16 variables; 3 refer to the maximum value recorded and 3 refer to the minimum value recorded, 2 of these 6 are also found in the catch column. These 2 variables are identified by the superscripts in Table 7.7 and are not expanded upon for the remainder of this results section, instead only the results from the catch will be described. The rest of this section is dedicated to presenting the results of the post hoc analyses carried out for the enduring 14 variables shown in Table 7.7.

Non 3D kinematic variables	Maximum values of 3D kinematic data	Minimum values of 3D kinematic data	3D kinematic data at the catch of the stroke	3D kinematic data at maximum handle force	3D kinematic data at the finish of the stroke	3D kinematic data at knees up during the recovery
Max handle force (%)	HJC Z	-	-	-	-	-
Finish (%)	KJC alpha					
Max H Force/BM (N/kg*100)						
Slope of handle force						
Min seat force (N)						
Suspension 2 (BW(s))						
Power output (W)						
Stroke rate (/min)						
-	LSJ Y LSJ Z ¹ KJC Z ²	LSJ X LSJ Y AJC Y	LSJ Z ¹ HJC Z KJC Z ² KJC alpha	-	-	LSJ X LSJ Y LSJ alpha HJC X HJC gamma KJC Y

Table 7.7: Significant dependent variables for the LWM group

The variables in the top section of the table are the ones that have previously been presented. *r* values from Table 7.2; ¹ = .996**, ² = .997**. **Correlation is significant at the 0.01 level (2-tailed). The 16 variables discussed in this section are highlighted.

The maximum recorded value for the Y coordinate of LSJ indicates that at some point in the stroke LWM achieved a higher position from the floor during lower intensity Steps the maximum (up to 12.3 mm): catch correlation ($r = .925, p < 0.01$) in Table 7.2 suggests that this kinematic difference probably occurred around the catch of the stroke. The minimum kinematics variables that were found to vary with Step changes showed that there was a small amount of extra lateral motion at the level of LSJ in Step 4 compared to Step 3, again that in

higher intensity efforts LSJ was lower to the floor than it was during Step 1, and that AJC was positioned higher from the floor as the Steps increased.

At the catch; Step 6 consistently saw the position of LSJ, HJC and KJC greater than 70 mm, 66 mm and 65 mm respectively more posterior than in all other Steps. Furthermore it was found that when taking the catch LWM exhibited up to 9.3° less knee flexion during Step 6 than in lower intensity pieces. These measures are further indication of athletes' compressing less at the catch during high intensity work.

The position of LSJ was displaced to the athletes' right and was higher from the ground at lower intensity Steps when in the recovery phase of the stroke, and there was up to 5.9° more extension of the lumbar spine in Step 5 than in Step 2 as the knees broke. At this point in the stroke the medio-lateral position of the HJC followed a similar pattern to LSJ with increasing intensity, and this was accompanied by an extra 2.5° of external hip rotation in Step 6 than in Step 5. The coordinate of the KJC was found to be significantly 7.9 mm to 12.7 mm higher during Step 6 than Steps 4,5 at this stage in the stroke.

7.2.5 All athletes: significant ANOVA RM, non-significant post hoc

Table 7.1 (Page 144) showed that of the 168 variables (for each boat class) that were originally tested for change with increasing exercise intensity 30, 27 and 19; HWW-SCULL, HWW-SWEEP and LWM respectively, resulted in a p-value of significance for the ANOVA RM output, but that the Bonferroni post hoc failed to identify the specific, significant pairwise comparisons. These 76 variables are listed in Table 7.8. SPSS offers the use of a Bonferroni adjustment, a Sidak adjustment, or Tukey's Least Significant Difference (LSD) for post hoc analysis. Field (2000) recommends against the use of the LSD technique as it provides no true adjustment whatever and thus is highly vulnerable to type I errors, and it should definitely not be used if sphericity has been violated (whether subsequent GG or HF adjustments have been used or not). Bonferroni is recommended as it guarantees protection against type I error, and the Sidak test is also suggested to be a valid test by Field (2000), though again is somewhat susceptible to type I error. In an attempt to identify the specific changes seen for the variables shown in Table 7.8 new ANOVA RM were run and the Sidak post hoc analysis was utilised.

Non 3D kinematic variables	Maximum values of 3D kinematic data	Minimum values of 3D kinematic data	3D kinematic data at the catch of the stroke	3D kinematic data at maximum handle force	3D kinematic data at the finish of the stroke	3D kinematic data at knees up during the recovery
HWW-SCULL						
COP Z @ MHF	LSJ Y	LSJ Y	HJC alpha	KJC X	HJC alpha	LSJ Y
Quality COP X @ Catch	KJC Y	LSJ gamma	KJC X	AJC gamma	HJC beta	HJC Y
Knees up (%)	AJC Y	HJC gamma	KJC Y			HJC alpha
Quality LP ratio @ Catch	AJC gamma	KJC X	AJC X			HJC gamma
Quality LP ratio @ MHF			AJC Y			KJC Z
			AJC alpha			AJC Z
						AJC gamma
HWW-SWEEP						
Max seat force (N)	LSJ Z	LSJ Z	LSJ Y	LSJ Y	LSJ Z	LSJ Z
	KJC Z	HJC alpha	LSJ Z	HJC Y		KJC Y
	AJC Z		HJC Z	AJC Z		AJC X
	AJC gamma		HJC alpha			
	FJC alpha		HJC beta			
			HJC gamma			
			KJC Z			
			KJC alpha			
			AJC Y			
			AJC Z			
			AJC gamma			
			FJC alpha			
LWM						
COP drift – Finish (mm)	-	HJC Y	LSJ Y	KJC Y	LSJ X	LSJ Z
COP drift, MHF-Fin (mm)		HJC gamma	HJC Y			HJC Z
Quality COP X @ Catch		AJC alpha				HJC alpha
Max handle force (N)						KJC Z
Stroke length (mm)						KJC alpha
						AJC alpha
						AJC gamma

Table 7.8: Exercise intensity: Significant variables from ANOVA RM with non-significant Bonferroni post hoc

For each of the general linear models run using ANOVA RM and the Sidak correction, 15 pairwise comparisons were made; and because there were 76 variables tested the resulting number of pairwise comparisons was 1,140. Of these 1,140 only 2 identified a significant effect that had been missed by the previously conducted Bonferroni investigations. According to the Sidak post hoc analyses there was a significant difference in the level of hip abduction between Steps 2 and 3 for the HWW-SWEEP group ($p < 0.05$), and there was significantly more force developed through the handle when comparing Step 3 to Step 1 for the LWM ($p < 0.05$). For all of the other variables it was not possible to identify why the ANOVA RM provided a significant result.

7.2.6 Flagged variables

The fourth category into which the results of the ANOVA RM were grouped specified that the assumption of sphericity had been violated, the data was corrected using the GG or HF adjustment and the resulting GG and HF p-values in the ANOVA RM results output disagreed as to whether a significant difference existed. Field (2000) states that when this occurs one may consider the average of the two p-values in conjunction with the significance of the multivariate tests provided in the SPSS output (Pillai's Trace, Wilks' Lambda, Hotellings's Trace, Roy's Largest Root). Table 7.1 (Page 144) showed that in the current study 14 variables fell into this category, 3 for HWW-SCULL, 4 for HWW-SWEEP and 7 for LWM. The category four variables are shown in Table 7.9.

Non 3D kinematic variables	Maximum values of 3D kinematic data	Minimum values of 3D kinematic data	3D kinematic data at the catch of the stroke	3D kinematic data at maximum handle force	3D kinematic data at the finish of the stroke	3D kinematic data at knees up during the recovery
HWW-SCULL						
-	LSJ gamma	HJC alpha	AJC gamma	-	-	-
HWW-SWEEP						
Suspension 1	-	-	-	KJC X KJC Y	HJC alpha	-
LWM						
COP drift – Finish COP Z @ Finish Work	AJC beta	HJC X	KJC X	-	LSJ Y	-

Table 7.9: Category four variables for all athlete groups

For HWW-SCULL LSJ gamma maximum, and HJC alpha minimum the GG and HF p-values were 0.065, 0.060 and 0.033, 0.041 respectively. This yielded average scores of 0.049 for LSJ gamma and 0.051 for HJC alpha. These may then have been considered to be on the verge of being significant, however the multivariate p-values were 0.396 and 0.405, respectively. As the multivariate statistics were so high, and because in the case of HJC alpha minimum the average of GG and HF was greater than 0.05, it was decided that these variables should be treated as non-significant. The third flagged variable for the HWW-SCULL was AJC gamma at the catch. In this case the GG and HF p-values were 0.053 and 0.032 providing an average of 0.043. Furthermore the multivariate p-values for this variable were 0.049 indicating that a significant difference may exist. However, neither a Bonferroni nor a Sidak post hoc analysis identified any significant pairwise comparisons for AJC gamma at the catch. For the HWW-SWEEP

group the results for suspension 1, KJC X during the drive and HJC alpha at the finish yielded average p-values of 0.052, 0.049 and 0.056 (GG+HF/2), and multivariate p-values of 0.164, 0.208 and 0.103 respectively. As such these three variables were deemed to show no significant change with varying exercise intensity. On the other hand, the GG and HF p-values for KJC Y position when maximum handle force was being exerted were 0.067 and 0.031, yielding an average of 0.049. Combined with a multivariate result of 0.011 it was thought that this may be a significant variable; the Bonferroni post hoc procedure found that the position of the HWW-SWEEP groups' KJC was significantly different when comparing Steps 2,3 and 6, and with normality of data confirmed by the KS and SW tests it may be assumed that the vertical position of HWW-SWEEP rowers KJC varies during the propulsive phase of their stroke as intensity of effort changes. Of the 7 variables that were grouped into this category for LWM only the maximum value for AJC beta obtained an average p-value from the ANOVA RM of less than 0.05 (GG+HF/2=0.049), and a multivariate p-value of less than 0.05 (0.01). However, because no significant pairwise comparisons were noted from a Bonferroni or a Sidak post hoc analysis no further information was discovered regarding this variable's tendency to vary with exercise intensity.

7.3 Summary of results regarding exercise intensity

Thirteen of the measured dependent variables were found to vary significantly for both the HWW-SCULL and the HWW-SWEEP groups; ten of which were also common to LWM. A further thirty one variables were found to change significantly with exercise intensity for the HWW-SCULL group only, an additional ten for HWW-SWEEP only, and sixteen dependent variables were significantly affected by Step for LWM only. A short summary of the results and some thoughts on the relevance of the findings are presented here.

Exercise intensity had a significant effect on the timing of key stroke events, with them occurring later in the stroke as intensity was increased. Peak tensile forces exerted on the ergometer handle were found to increase with Step, and this occurred more often for the HWW-SCULL than the other athlete groups. As a result of this the rate of handle force production was found to be less steep more often for the HWW-SWEEP and LWM athletes than the HWW-SCULL. A greater number of pairwise Step comparisons were found to be significant considering the minimum force exerted on the seat by HWW-SWEEP and LWM, than HWW-SCULL. The results also showed that the magnitude of all athletes' suspension away from the seat during the entire drive phase of the stroke became less as Step increased. Stroke rate and power output significantly increased for almost all pairwise comparisons as Step increased. More surprising was the occasional increases in stroke length and work that were noted for the HWW-SCULL and HWW-SWEEP as intensity increased from Steps 1-5. All

athletes were found to displace their HJC less anteriorly (sternwards), and flex their knee less around the catch in Step 6 than they did during lower intensity efforts. Considering that stroke length in Step 6 was not found to be significantly shorter than any other Steps (Figure 7.4, Table 7.4) it may be that at higher intensities the athletes in this study used increased lumbar and thoracic flexion in order to maintain stroke length at the front of the stroke.

7.3.1 HWW-SCULL only

HWW-SCULL exhibited additional sideways COP trajectory as Step increased, and their maximum seat force was greater in Step 3 than in Step 2; this may indicate that this group did not particularly utilise *suspension* during relatively low intensity efforts. Indeed the HWW-SCULL suspended less during the drive than their HWW-SWEEP counterparts during all Steps (Figure 7.3, Page 149). HWW-SCULL moved their COP further sternwards at the catch during low Steps, and further bow-wards during higher Steps. These changes may be linked to the way in which the pelvis and spine are flexed and extended during the stroke. At the finish of the stroke HWW-SCULL exhibited more knee flexion, and a more superior and anterior KJC position. This should be explained by the fact that Step 6 was the only one where no extension of the knee was observed. LSJ and KJC were further posterior at the catch in Step 6 than Steps 4 and 5. In the middle of the drive phase the HJC was slightly internally rotated in Steps 1-5, though slightly externally rotated in Step 6, and the position of the AJC was further posterior at race pace than it was at low intensity. As the athletes' knees broke during the recovery, LSJ was significantly further forward during lower intensity exercise, and they exhibited greater plantar flexion and lower knee flexion during lower intensity Steps.

7.3.2 HWW-SWEEP only

The trajectory of LSJ reached a higher, vertical, peak during lower intensity efforts than it did at Step 6 which was reflected in the change in coordinate as the knees broke during the stroke recovery. This may be linked to the quality of the athletes' *rock over* about the hips, after the finish. LSJ also moved further posterior, faster, during the drive of Step 6 than the drive of earlier Steps. The behaviour of HJC was similar to LSJ during the drive at high Steps as compared to lower Steps. During the recovery there was significantly more external hip rotation in Step 6 than in earlier Steps, and at the catch the KJC was pushed out further laterally at lower intensity. Step 6 also saw less knee flexion in the middle of the drive, and less external but more internal rotation of the foot.

7.3.3 LWM only

The range of Y coordinates for LSJ varied by approximately 12 mm between Steps, though was consistently lower down during higher intensity efforts. At the catch Step 6 consistently saw LSJ, HJC and KJC more posterior than at lower intensity, and, also at the catch, LWM exhibited up to 9.25° less knee flexion. This may indicate a more slumped, or flexed and compressed posture through the lumbar spine as intensity increased. Perhaps due to the heel rising from the footstretcher at the finish of the stroke, the AJC was a little higher from the floor as the Steps increased. The position of LSJ was lower down during the recovery at high intensity, which, similar to the HWW-SWEEP could be related to a *rock over* of lower quality about the hips. There were also some discreet, but significant increases in the range of the medial/lateral coordinate of LSJ and HJC during the recovery phase of the stroke.

7.3.4 Other results

Of all of the dependent variables considered for all athlete groups, 15% varied significantly as exercise intensity changed, and a Bonferroni adjustment yielded no additional information. These variables were assessed using new models with a Sidak post hoc adjustment; two previously unidentified significant pairwise comparisons were highlighted. There was a significant difference in the level of hip abduction between Steps 2 and 3 for the HWW-SWEEP group, and there was significantly more force developed through the handle when comparing Step 3 to Step 1 for the LWM. For all of the other variables it was not possible to identify why the ANOVA RM provided a significant result. Initially, another 2.8% of all variables were found to provide ambiguous results as to whether a significant effect had been observed or not. Of these fourteen observations eleven were categorised as non significant after further analysis, two showed possible significant change with intensity; though no significant pairwise comparisons were found, and additional analysis of the final variable revealed that the position of HWW-SWEEP athletes' KJC may vary in the Y direction as a result of increasing intensity during the drive phase.

The next chapter considers the effect of longitudinal training on many of the dependent variables that were considered in this chapter.

Chapter 8

Effect of Longitudinal Training

The data used in this investigation was obtained during the testing sessions conducted in July 2007 (i), October 2007 (j), December 2007 (k), March 2008 (l) and June 2008 (m). These months were chosen because they allowed progress to be assessed in an Olympic season, it was possible to compare the results obtained at the same point in the season two years running (July 2007 and June 2008), and these months allowed the greatest number of athletes' data to be included in the analyses. The limitation on athlete data was because, not all of the forty two athletes assessed were present for every testing session, and, those who were present did not always complete every Step; only the data collected from a select group could be assessed with repeated measures across several months. The data collected during Steps 2,4,6 was assessed for changes in stroke profile and three-dimensional kinematics.

Eleven athletes completed both Step 2 and Step 4 in all of the testing sessions listed above; three HWW-SCULL, four HWW-SWEEP, and four LWM; athlete numbers 7,9,12,14,18,25,27,29,30,32,42 (Table 6.3, Page 103). Step 6 data was only available for comparison across July 2007, December 2007, March 2008 and June 2008, and data collected from seven athletes was included; two HWW-SCULL, two HWW-SWEEP, and three LWM; athlete numbers 7,9,14,25,27,32,42. The athletes used to assess changes were considered as a single group, not as three groups according to boat class. All statistical tests were conducted with a significance level of 0.05. The analyses and results in this chapter are presented in response to the third hypothesis listed in Section 5.5; that some aspects of elite rowers' technique and performance would change with longitudinal training.

The KS and SW tests were used to assess the normality of the data, and subsequent ANOVA RM was conducted on 121 dependent variables for Step 2, Step 4 and Step 6 (Table 8.1). The output of the general linear model was comprised of descriptive statistics for the dependent variable, the four multivariate tests cited in Chapter 7, Mauchly's test of sphericity, and the results of the ANOVA RM. Pairwise comparisons were conducted using a post hoc procedure with Bonferroni adjustment. In this chapter the term pairwise refers to a comparison of a dependent variable between any two individual testing sessions. When significant change was observed in any pairwise test of kinematics measures, the test was only considered valid if the difference in the average score between testing sessions was greater than the change in kinematics that could have occurred as a result of inconsistent transmitter placement (repeatability of transmitter placement, Section 3.3.2). For example if the position of a joint centre was found to be more superior at the catch in summer 2008 than it was in

summer 2007, the significance of the pairwise comparison was only considered valid if the change in inferior/superior location was greater than 1.53 mm (Table 3.4, Page 43).

Non 3D kinematic variables	Kinematic data*
COP drift – MHF (mm)	LSJ X
COP drift – Finish (mm)	LSJ Y
COP drift, MHF-Fin (mm)	LSJ Z
COP drift, Recovery (mm)	LSJ alpha
COP drift, Stroke (mm)	LSJ beta
COP Z @ Catch	LSJ gamma
COP Z @ MHF	HJC X
COP Z @ Finish	HJC Y
Quality COP X @ Catch	HJC Z
Quality COP X @ Finish	HJC alpha
Quality COP X @ MHF	HJC beta
	HJC gamma
Max handle force (%)	KJC X
Finish (%)	KJC Y
Knees up (%)	KJC Z
	KJC alpha
Max handle force (N)	AJC X
Max H Force/BM (N/kg×100)	AJC Y
Slope of handle force	AJC Z
Max seat force (N)	AJC alpha
Min seat force (N)	AJC beta
Seat force @ MHF (N)	AJC gamma
	FJC alpha
Suspension 1 (BW(s))	
Suspension 2 (BW(s))	
Power output (W)	
Stroke length (mm)	
Stroke rate (/min)	
Work done (J)	
Quality LP ratio @ Catch	
Quality LP ratio @ MHF	
Quality LP ratio @ Finish	

Table 8.1: Dependent variables considered during longitudinal analysis

* Kinematic data was logged four times: The value at the catch, at the point in the stroke when maximum force was being exerted on the handle, at the finish, and at the point in the stroke recovery when the knees started to rise.

In the same way as was introduced in Chapter 7, the results of the ANOVA RM were grouped into four categories; firstly; there was no significant difference found between testing sessions, secondly; there was some significant change in the dependent variable, thirdly; a significant difference was noted but Bonferroni post hoc analysis did not identify where the difference lay, and fourthly; the GG and HF p-values in the ANOVA RM results output disagreed (these results were flagged and are discussed in due course). Table 8.2 shows the number of variables that were found to fall within the four categories listed above.

	Number of variables (out of 121)			
	Non-significant ($p > 0.05$)	Significant ($p < 0.05$)	Significant with failed Bonferroni	Flagged
Step 2	64	43	14	0
Step 4	59	52	9	1
Step 6	75	27	19	0
Common to all Steps	52	23	1	0

Table 8.2: Results of ANOVA RM regarding longitudinal training

Tests conducted on the dependent variables were found to show no significant change, to show significant change, to show significant change with failed Bonferroni post hoc analysis, or were flagged because the results were ambiguous.

6% of the dependent variables were found to be not normally distributed for the data recorded during Step 2, Step 4 and Step 6. These deviations from normality were only considered pertinent, and hence referred to, if they coincided with variables that significantly varied between testing sessions. The results of MS tests dictated that all of the variables that are presented here as exhibiting significant change met the assumption of sphericity. In this chapter: firstly all data that was found to vary across testing sessions for all of the Steps that were considered is presented, followed by an examination of each of the Steps individually, and after this there is information regarding dependent variables that were allocated to groups three and four (Table 8.2).

8.1 Significant results for all Steps

Table 8.3 shows the twenty three dependent variables that were found to significantly vary between testing sessions conducted over a period of one year. Two of the variables were stroke profile (the peak pulling force exerted on the handle, and stroke length), and the other twenty one were three-dimensional kinematic variables; sixteen trajectory and five rotational. The figures in this section illustrate selected data associated with the variables presented in Table 8.3, and the results of post hoc analyses are presented.

Stroke profile	Three-dimensional kinematics			
	at the catch	at peak handle force	at the finish	at knees up
Max handle force (N)	LSJ X	LSJ Y	LSJ Y	LSJ Y
Stroke length (mm)	LSJ Y	LSJ alpha	LSJ Z	LSJ Z
	LSJ alpha	KJC X	LSJ alpha	LSJ alpha
	KJC X	AJC Y	KJC X	KJC X
	AJC Y		AJC Y	AJC Y
	AJC Z		FJC alpha	

Table 8.3: Dependent variables that showed significant change across several testing sessions during Step 2, Step 4 and Step 6

The column graphs that are presented in this section describe the mean and standard error of dependent variables. When viewing these graphs pairwise comparisons that were found to show significant change are identified by the letters listed vertically above or below the columns (i-m representing July 2007-June 2008). For example, if athletes were found to score significantly higher for a particular dependent variable in March 2008 (l) than they did in July 2007 (i) then the letter “i” would be listed above or below the column with the mean and standard error of the result for March 2008. The column value for a testing session is always significantly greater than the testing session identified by the letters listed above or below it.

8.1.1 Stroke profile

Figure 8.1 shows that in the year between July 2007 and June 2008 the group of athletes under consideration significantly increased the peak pulling forces that they exerted on the handle during all Steps in the test protocol. In Steps 2 and 4 June 2008 saw the best performance, and in Step 6 the best performance was in December 2007 (2 N more tensile force on the ergometer handle than in June 2008). For all Steps, peak forces logged in the pre Olympic test in 2008 were 5-7% greater than the forces logged in summer 2007. Unexpectedly the stroke length measured during the testing sessions under consideration became gradually less as months passed. Indeed the longest stroke lengths recorded were in July 2007 for all Steps, and these were significantly longer than all of the other testing sessions in one Step or another. For all Steps, stroke length in June 2008 was equal to 98% of the stroke length achieved the year before. In all testing sessions the highest pulling forces and shortest stroke lengths were logged from Step 6 data, Step 4 gave the longest stroke lengths, and Step 2 the lowest pulling forces.

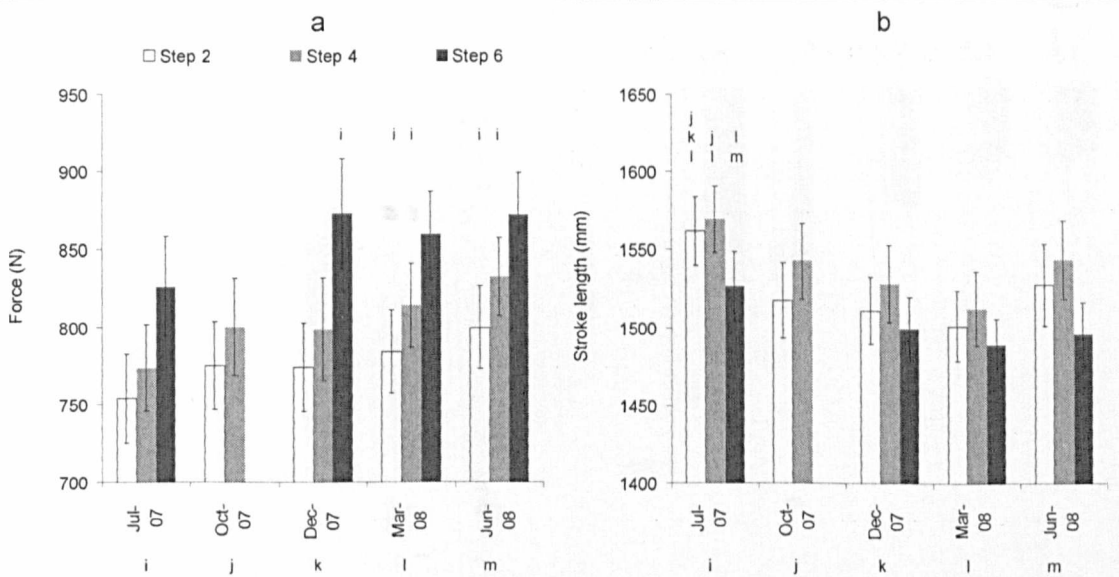


Figure 8.1: Mean and standard error for peak handle force (a) and stroke length (b) Jul-07(i), Oct-07(j), Dec-07(k), Mar-08(l), Jun-08(m). The letters above the columns are the testing sessions that the column value was significantly greater than ($p < 0.05$).

8.1.2 Kinematics at the catch of the stroke

Figure 8.2a has been included because some significant pairwise comparisons were found, however the data logged for LSJ X during Step 6 in December 2007 was found to be not normally distributed, and hence three of the significant pairwise comparisons described in the figure should be viewed with caution. The X position of LSJ at the catch was found to significantly vary between different testing sessions, however over the year was always within 1103 mm to 1121 mm from the FOB transmitter. There were more noticeable changes seen in the Y direction for LSJ between July 2007 and June 2008; Figure 8.2b shows that in each testing session the location of LSJ at the catch was higher from the ground than it was in the previous test (location was up to 47 mm higher in June 2008 than in July 2007), and that several significant pairwise comparisons were discovered. This increased height of LSJ may be an indicator of better posture being achieved at the catch of the stroke.

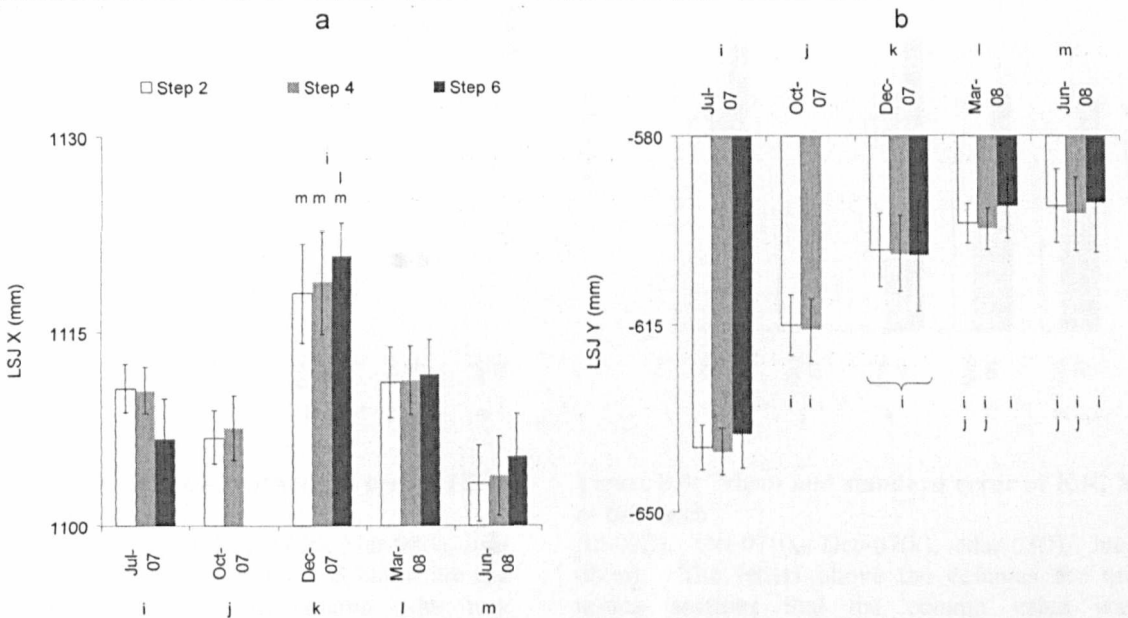


Figure 8.2: Mean and standard error for LSJ X at the catch (a) and LSJ Y at the catch (b) Jul-07(i), Oct-07(j), Dec-07(k), Mar-08(l), Jun-08(m). The letters above and below the columns are the testing sessions that the column value was significantly greater than ($p < 0.05$).

Figure 8.3 shows that as the 2007/2008 rowing season progressed there was sustained improvement in postural control of the lumbar and sacral spinal complex at the catch of the stroke. In the summer of 2007 the group of athletes under consideration were found to exhibit considerable flexion of their lumbar spine about the junction of the fifth lumbar and first sacral vertebrae (LSJ), the magnitude of this was shown to significantly decrease in the following twelve months. This is considered an improvement and will be discussed in Chapter 10. The tests completed in December 2007, March 2008 and June 2008 all showed that the athletes were flexing their lumbar spine significantly less than they had previously done at the catch of the stroke, and is in agreement with the suggested improvement in postural control highlighted by Figure 8.2b.

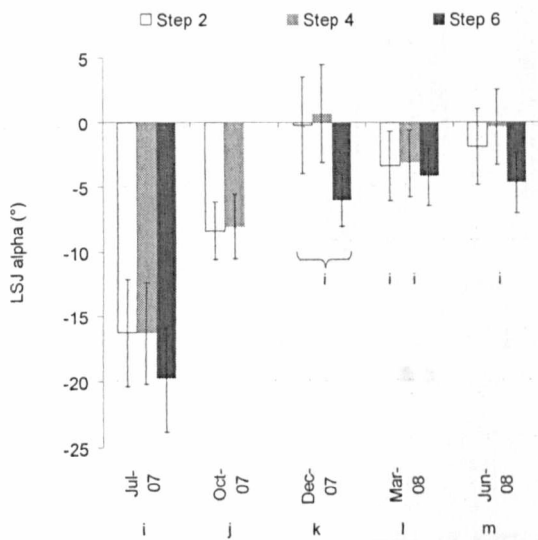


Figure 8.3: Mean and standard error of LSJ alpha at the catch

Jul-07(i), Oct-07(j), Dec-07(k), Mar-08(l), Jun-08(m). The letters below the columns are the testing sessions that the column value was significantly greater than ($p < 0.05$).

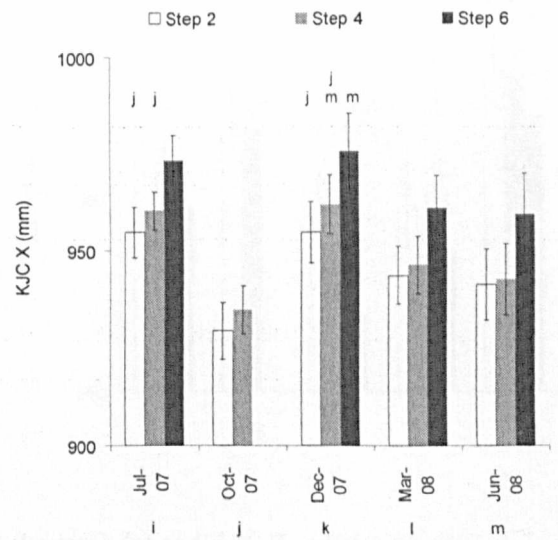


Figure 8.4: Mean and standard error of KJC X at the catch

Jul-07(i), Oct-07(j), Dec-07(k), Mar-08(l), Jun-08(m). The letters above the columns are the testing sessions that the column value was significantly greater than ($p < 0.05$).

Figure 8.4 shows that there was significant change in the position of the athletes' KJC in the X direction comparing the various sessions. The data logged in Dec 2007 was significantly higher than it was in June 2008. Hence the location of KJC was further from the FOB transmitter, or put another way, more medial to the athletes in the earlier testing sessions. This suggests that there may have been less hip abduction, and hence less space to anteriorly rotate the pelvis at the catch in the 2007 tests than there was in the 2008 test.

Figure 8.5 shows that as the rowing season progressed athletes' AJC was displaced increasingly more superiorly and anteriorly at the catch of the stroke. The results showed that these changes were statistically significant considering the June 2008 testing session and the 2007 sessions. Regardless of testing session, the least superior displacement and the least anterior displacement of AJC at the catch came during Step 6. The data logged for AJC Y in October 2007, during Step 4 was found to be not normally distributed, hence two of the pairwise comparisons that were found to be significant and included in Figure 8.5a should be viewed with caution.

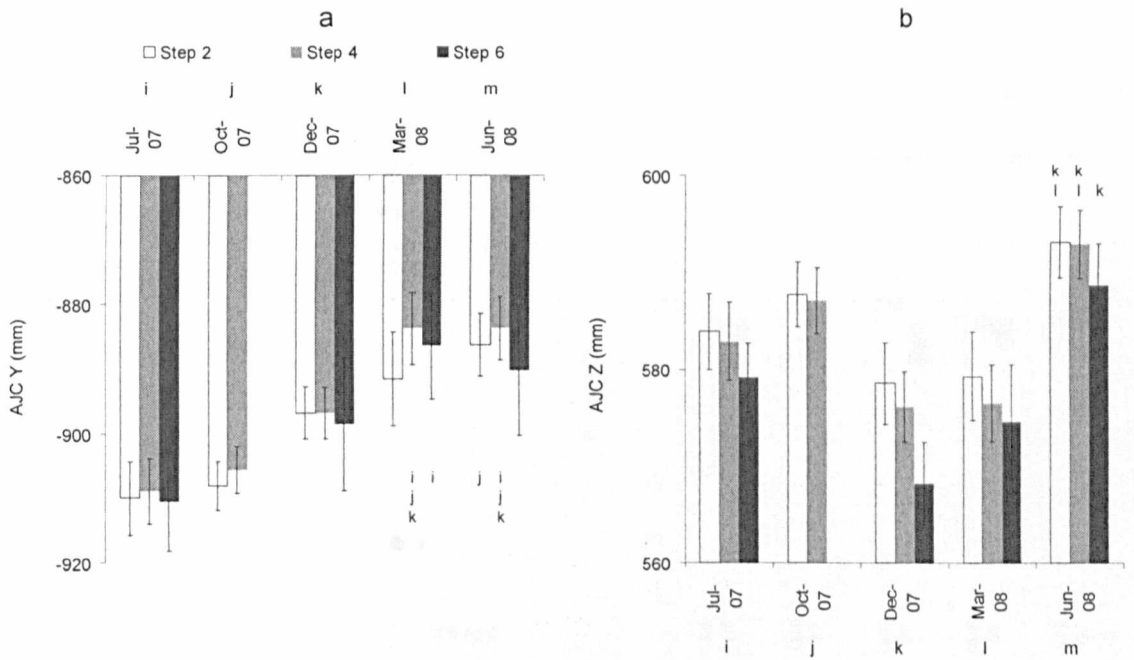


Figure 8.5: Mean and standard error of AJC Y at the catch (a) and AJC Z at the catch (b) Jul-07(i), Oct-07(j), Dec-07(k), Mar-08(l), Jun-08(m). The letters above and below the columns are the testing sessions that the column value was significantly greater than ($p < 0.05$).

8.1.3 Kinematics at peak handle force during the drive phase

As for at the catch (Figure 8.2b), Figure 8.6 shows that as the current study progressed from July 2007 to June 2008 the position of LSJ in the Y direction increased in elevation during the drive phase of the stroke, specifically when peak tensile force was being exerted on the handle (up to 51 mm difference between the first and last testing sessions). Again, because when in a solid upright, non kyphotic pose the position of LSJ would be elevated, this may be an indicator of higher quality postural control in 2008 than in 2007, this is discussed in more detail in Chapter 10.

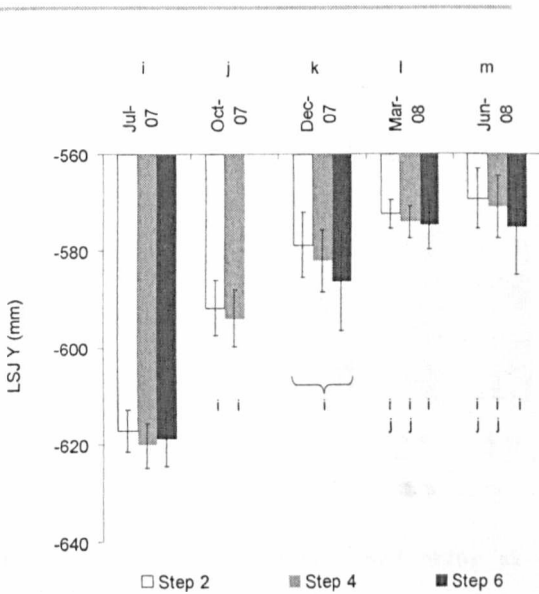


Figure 8.6: Mean and standard error of LSJ Y at peak handle force
Jul-07(i), Oct-07(j), Dec-07(k), Mar-08(l), Jun-08(m). The letters below the columns are the testing sessions that the column value was significantly greater than ($p < 0.05$).

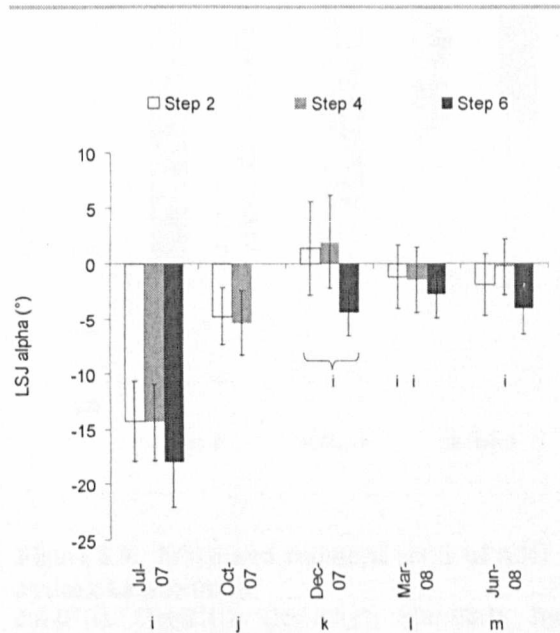


Figure 8.7: Mean and standard error of LSJ alpha at peak handle force
Jul-07(i), Oct-07(j), Dec-07(k), Mar-08(l), Jun-08(m). The letters below the columns are the testing sessions that the column value was significantly greater than ($p < 0.05$).

Again similar to the results noted at the catch, Figure 8.7 shows that in December 2007, March 2008 and June 2008 the magnitude of the intersegmental angle at LSJ was significantly less than it had been in the summer test in 2007. Considering Steps 2, 4 and 6 together, it may be offered that the data logged in March 2008 was of the highest quality. However, Figure 8.7 also shows that Step 4 in June 2008 was the individual Step exhibiting the lowest intersegmental LSJ alpha during the drive phase.

Figure 8.8 shows that during the drive phase, when peak handle force was being exerted, KJC was displaced further from the FOB transmitter in the X direction in December 2007 than in any other testing session. The tests conducted in July 2007 yielded results that were a little higher than in March 2008 and June 2008, and, as with the position of KJC at the catch (Figure 8.4), the month when the athletes' moved their knee laterally the least during the drive was October 2007.

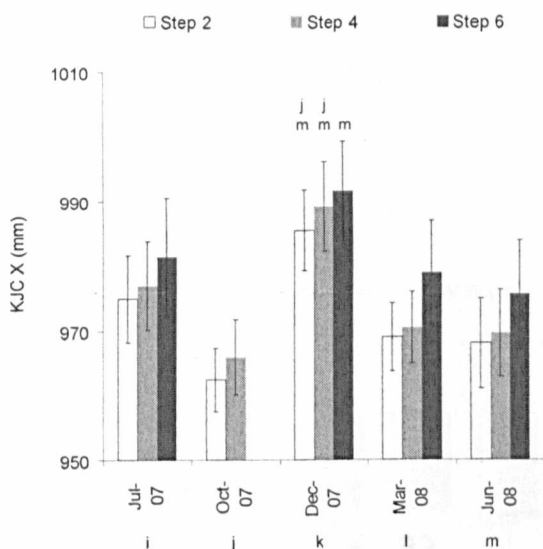


Figure 8.8: Mean and standard error of KJC X at peak handle force

Jul-07(i), Oct-07(j), Dec-07(k), Mar-08(l), Jun-08(m). The letters above the columns are the testing sessions that the column value was significantly greater than ($p < 0.05$).

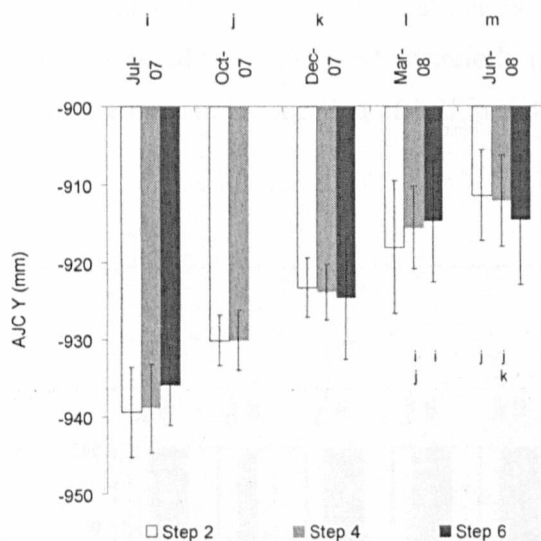


Figure 8.9: Mean and standard error of AJC Y at peak handle force

Jul-07(i), Oct-07(j), Dec-07(k), Mar-08(l), Jun-08(m). The letters below the columns are the testing sessions that the column value was significantly greater than ($p < 0.05$).

In the middle of the drive phase the position of AJC in the Y direction was found to be progressively more elevated as the current study developed. It was found that the data logged during Step 2 in July 2007, March 2008 and June 2008 was not normally distributed, and hence one of the significant pairwise comparisons shown in Figure 8.9 may be inaccurate. In the current study, when peak handle force was being exerted, the coordinates measured for AJC Y ranged from 911 mm to 939 mm below the FOB transmitter.

8.1.4 Kinematics at the finish of the stroke

The results of the tests conducted in the second half of the season revealed that when at the finish of the stroke, the location of LSJ was significantly more elevated, and significantly more posterior than it had been in the first half of the season. The data collected for LSJ Y during Step 6 in March 2008 was found to be not normally distributed, hence one of the pairwise comparisons identified in Figure 8.10a should be viewed with caution, however, the other fourteen significant comparisons are valid, and show that the location of LSJ was up to 40 mm more elevated in June 2008 than it was in July 2007. Figure 8.10 also shows that during all testing sessions the athlete group under consideration displaced their LSJ most posteriorly (Z) during Step 6, and that there was not a great deal of difference in the location of LSJ in the Y direction with changing Step.

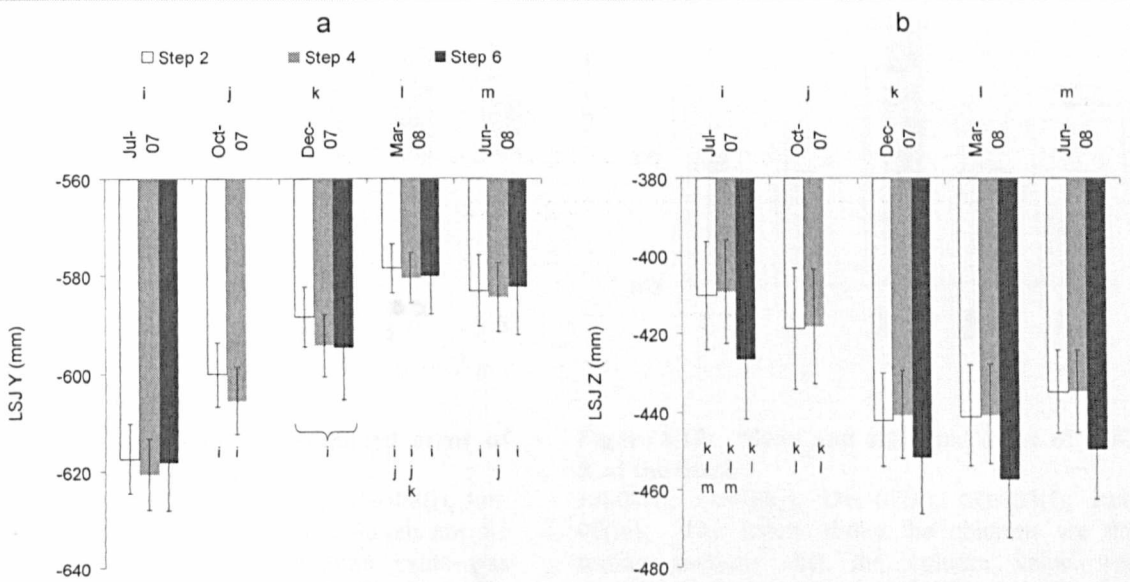


Figure 8.10: Mean and standard error of LSJ Y at the finish (a) and LSJ Z at the finish (b) Jul-07(i), Oct-07(j), Dec-07(k), Mar-08(l), Jun-08(m). The letters below the columns are the testing sessions that the column value was significantly greater than ($p < 0.05$).

At the finish of the stroke the intersegmental angle at LSJ was greater in the summer test 2008 than it was in 2007, though not significantly so. Figure 8.11 shows that the lowest LSJ alpha at the finish was observed in July 2007; after this time the lumbar region of the spine was found to extend beyond the pelvis at the rear of the stroke in all tests, which results are in agreement with the increases in posterior displacement of LSJ shown above (Figure 8.10b). The magnitude of lumbar extension was generally less in Step 6 than it was in lower intensity exercise. Overall, during race pace exertions the lowest intersegmental angles were noted in July 2007 (3° lumbar flexion) and June 2008 (4° lumbar extension).

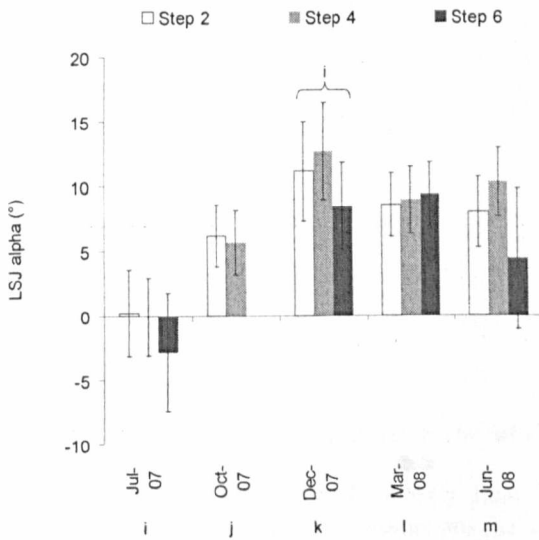


Figure 8.11: Mean and standard error of LSJ alpha at the finish

Jul-07(i), Oct-07(j), Dec-07(k), Mar-08(l), Jun-08(m). The letters above the columns are the testing sessions that the column value was significantly greater than ($p < 0.05$).

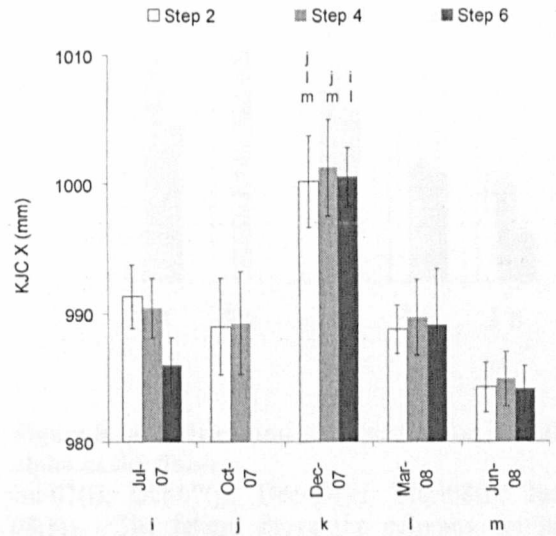


Figure 8.12: Mean and standard error of KJC X at the finish

Jul-07(i), Oct-07(j), Dec-07(k), Mar-08(l), Jun-08(m). The letters above the columns are the testing sessions that the column value was significantly greater than ($p < 0.05$).

At the finish of the stroke some significant differences were noted regarding the location of KJC in the X direction (Figure 8.12) however the global coordinate of this joint centre, at this point in the stroke was always within a range of 17 mm.

In general Figure 8.13 shows that the location of the AJC in the Y direction was more elevated in the 2008 tests than in the earlier testing sessions, and statistically significant comparisons were made between the data logged in July 2007 and March 2008. Every coordinate logged during the current research for AJC Y at the finish was within a range of 18 mm.

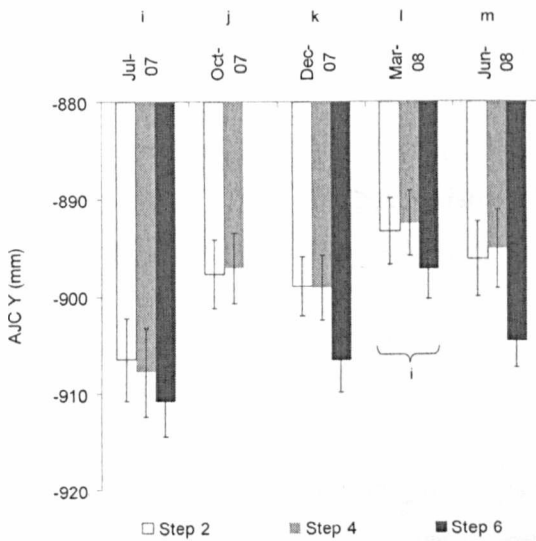


Figure 8.13: Mean and standard error of AJC Y at the finish
 Jul-07(i), Oct-07(j), Dec-07(k), Mar-08(l), Jun-08(m). The letters below the columns are the testing sessions that the column value was significantly greater than ($p < 0.05$).

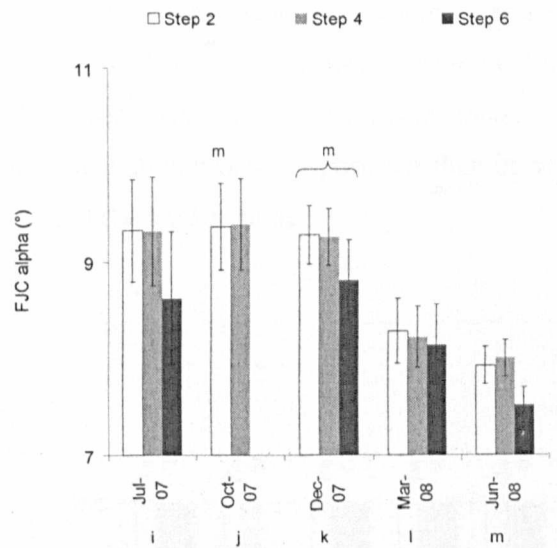


Figure 8.14: Mean and standard error of FJC alpha at the finish
 Jul-07(i), Oct-07(j), Dec-07(k), Mar-08(l), Jun-08(m). The letters above the columns are the testing sessions that the column value was significantly greater than ($p < 0.05$).

Recalling that because of the way in which the direction of POSFOOT was defined by anatomical points AJC and FJC, there was a forced offset on the calculation of all FJC alpha values (Section 4.1.8.1); it is therefore suggested that the magnitude of the angles presented in Figure 8.14 will be subject to some error. However the changes in angle noted across months are reliable, as such we can see that at the finish of the stroke the athletes' heel was separated away from the footstretcher less as the study progressed. Indeed Figure 8.14 shows that for all Steps the values logged in June 2008 were significantly 1° less than those computed in December 2007. Keeping the heels down is an aspect of technique that coaches actively promote in rowing (Thompson, 2005) and so the data shown above may be considered to show better rowing technique in June 2008 than in December 2007 for this parameter. This in turn may be related to the type of training being carried out by rowers at different times in the year and is properly discussed in Chapter 10.

8.1.5 Kinematics at knees up in the recovery phase

Results from all of the tests carried out between October 2007 and June 2008 were found to show greater elevation of LSJ during the recovery phase of the rowing stroke than were recorded in the first test in July 2007 (Figure 8.15a). The largest difference in LSJ Y coordinate between testing sessions was 50 mm, and the results in March 2008 and June 2008 were within 2 mm of each other for each Step measured. It is possible that this elevated location is linked to maintenance of better postural control, and rotation about the hips rather than bending forwards through the lumbar region of the spine. This possibility of better posture may be supported by the results presented in Figure 8.15b; where, as the knees break during the recovery phase the location of LSJ in December 2007, March 2008 and June 2008 was more posterior than in was in July 2007 and October 2007 indicating less flexion of the lumbar spine.

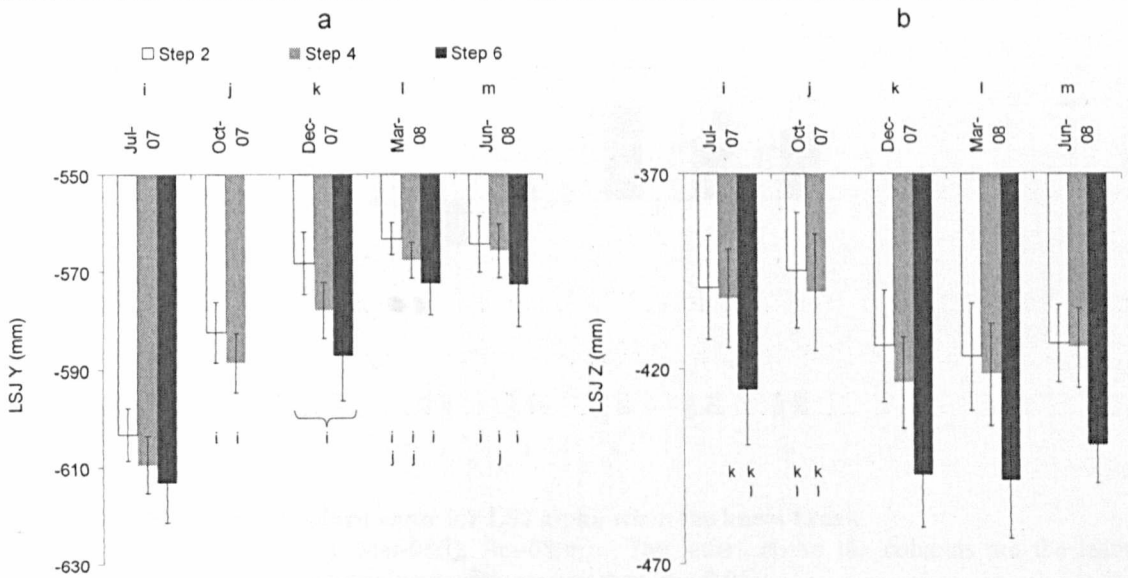


Figure 8.15: Mean and standard error of LSJ Y when knees break (a) and LSJ Z when knees break (b)
 Jul-07(i), Oct-07(j), Dec-07(k), Mar-08(l), Jun-08(m). The letters below the columns are the testing sessions that the column value was significantly greater than ($p < 0.05$).

The suggestion of decreased lumbar flexion during the recovery phase in 2008 that was offered above is supported by Figure 8.16. The figure below shows that whilst there was between 4° and 7° of lumbar flexion as the knees broke in July 2007; this had changed to between 1° and 2° of lumbar extension in October 2007. In the testing session in December 2007 the largest amount of lumbar extension at knees up was noted, and this lordotic posture was gradually reduced in the subsequent months. In June 2008 the athletes still exhibited some degree of lordosis during the recovery phase of the stroke, though it had been reduced by one third from December 2007. Considering all of the Steps in a testing session, and just the magnitude of the intersegmental alpha angle calculated at LSJ, Figure 8.16 shows that the best performances were logged in July 2007 and June 2008.

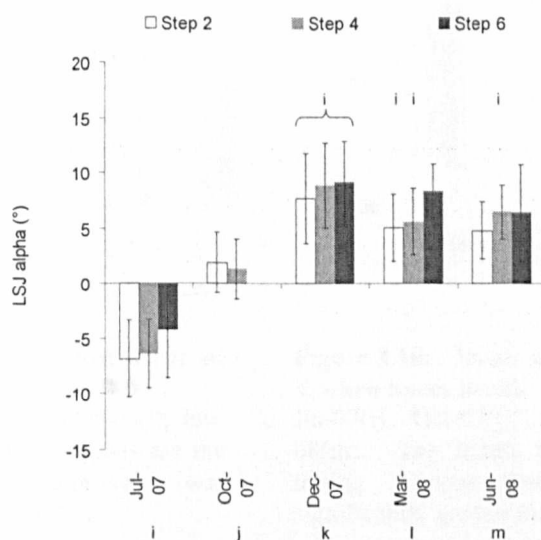


Figure 8.16: Mean and standard error for LSJ alpha when the knees break Jul-07(i), Oct-07(j), Dec-07(k), Mar-08(l), Jun-08(m). The letters above the columns are the testing sessions that the column value was significantly greater than ($p < 0.05$).

In December 2007 the position of the KJC in the X direction was significantly further from the FOB transmitter than it was in either of the tests conducted in 2008. And, discounting the December 2007 session, all of the coordinates logged for the location of KJC X when the knees broke were within 6 mm of each other (Figure 8.17).

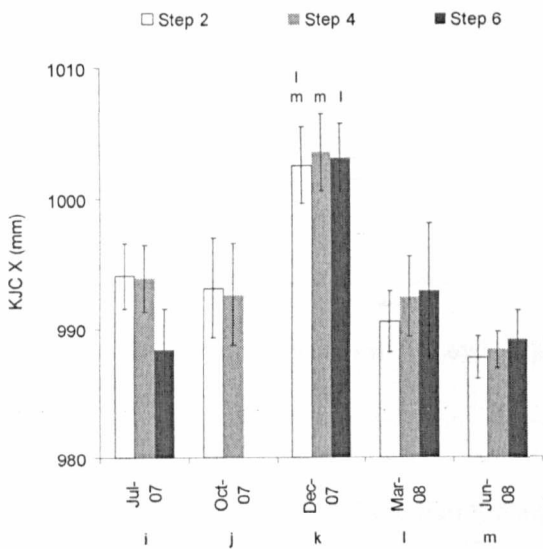


Figure 8.17: Mean and standard error of KJC X when knees break
Jul-07(i), Oct-07(j), Dec-07(k), Mar-08(l), Jun-08(m). The letters above the columns are the testing sessions that the column value was significantly greater than ($p < 0.05$).

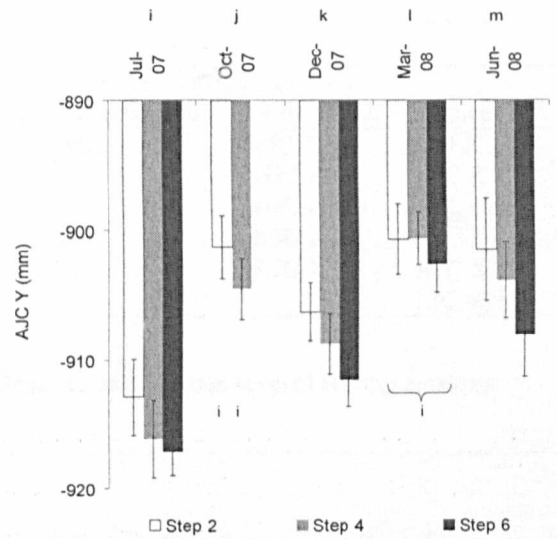


Figure 8.18: Mean and standard error of AJC Y when knees break
Jul-07(i), Oct-07(j), Dec-07(k), Mar-08(l), Jun-08(m). The letters above the columns are the testing sessions that the column value was significantly greater than ($p < 0.05$).

All of the coordinates logged for the position of the AJC in the Y direction, when the knees broke during the recovery phase of the stroke were within 901 and 917 mm below the height of the FOB transmitter. Despite only having a range of 16 mm there were significant differences noted in the position between March 2008 and October 2007 as compared to July 2007. Furthermore, regardless of the testing session being considered, Figure 8.18 shows that as the knees broke in the recovery phase the AJC was more elevated in lower intensity Steps than it was in Step 6.

8.2 Significant results for Step 2

Table 8.2 stated that there were 43 dependent variables that were found to vary significantly over several months of testing, and 23 of these were presented in Section 8.1. The other 20 variables are shown in Table 8.4.

Stroke profile	Three-dimensional kinematics			
	at the catch	at peak handle force	at the finish	at knees up
Max H Force/BM (N/kg×100)	KJC Y	HJC alpha	LSJ X	LSJ X
Power output (W)	KJC Z	KJC Y	HJC Z	HJC Z
	AJC X	KJC Z	HJC alpha	HJC alpha
		AJC X	KJC Z	KJC Z
			AJC X	AJC X
			FJC alpha	

Table 8.4: Dependent variables that showed significant change across several testing sessions during Step 2

The normalised peak handle force that the athletes pulled in Step 2 was significantly greater in June 2008 (1070.8 N/kg×100) than it was both July 2007 and December 2007 (1006.5 and 1014.6 N/kg×100 respectively). In addition to this, stroke power output was greater in March 2008 than in October 2007 and December 2007 (223.3 W vs 215.7 and 216.9 W), and was greater in June 2008 (224.0 W) than it was in December 2007 (216.9 W).

The position of KJC was significantly up to 30 mm more superior at the catch, and was up to 25 mm more superior in the middle of the drive when peak handle force was being exerted as the testing year progressed.¹ Furthermore, KJC was up to 32 mm more posterior in March 2008, December 2007 and October 2007 than it was in July 2007 at the catch, and was 35 mm more posterior as peak handle force was exerted in December 2007 than in July 2007. Also, at the catch and at the instant of peak handle force, the position of AJC was up to 19 mm further from the transmitter in December 2007 than it was in the first, second and final testing sessions. There was significantly less hip flexion as peak handle force was being exerted in July 2007 than there was in December 2007.

At the finish of the stroke and as the knees broke in the recovery phase, the position of LSJ was significantly up to 16 mm further from the FOB transmitter in the X direction in October 2007 than it was in June 2008, and the position of HJC was up to 23 mm more posterior as the testing year progressed. There was significantly more hip flexion at the finish in December 2007 than

¹ Some data for KJC Y at peak handle force was found to be not normally distributed.

there was in July 2007,¹ and there was more hip flexion as the knees began to rise in October 2007 than in July 2007. These changes in hip flexion may well have resulted from the pelvis not being posteriorly rotated as far in October 2007 and December 2007 as it was in July 2007, which in turn is probably strongly linked to the increased levels of lumbar extension at the finish and as the knees broke that were noted in Section 8.1 (Figure 8.11 and Figure 8.16). That is, if we imagine the femur and lumbar spine as being in unchanging orientation in space; decreasing posterior rotation of the pelvis would result in increased lumbar extension and increased hip flexion (Figure 8.19).

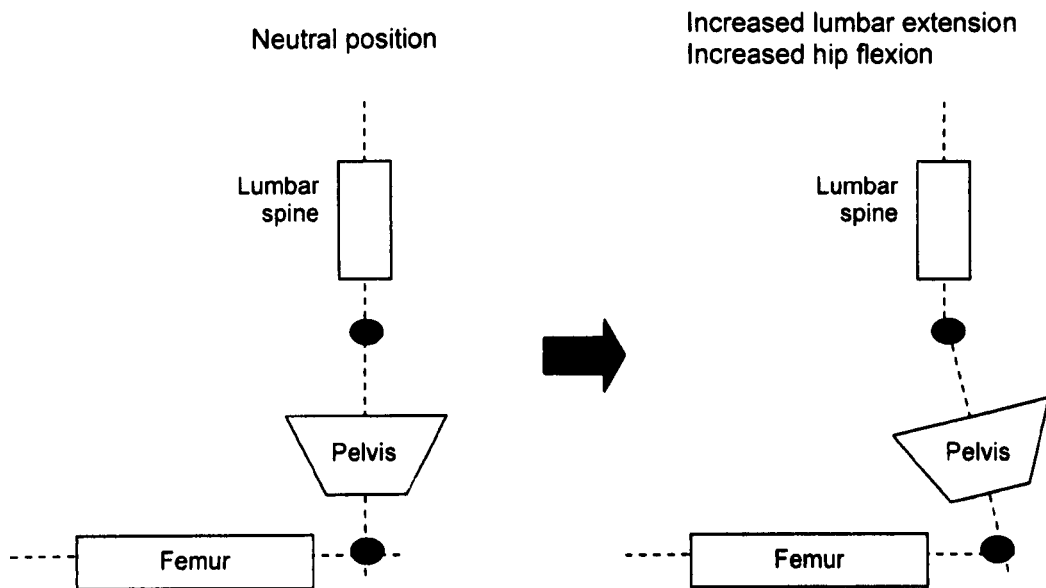


Figure 8.19: Schematic showing the effect of decreasing posterior rotation of the pelvis on intersegmental flexion/extension angles at LSJ and HJC

The data recorded during Step 2 also shows that the location of the KJC was significantly more inferior in December 2007 than it was in July 2007 or October 2007 at the finish, and was significantly more inferior in June 2008, March 2008 and December 2008 than it was in July 2007 as the knees broke in the recovery phase of the stroke. In addition to this the position of the AJC was up to 13 mm more lateral to the ergometer slider in June 2008 than it was in March 2008, December 2007 and July 2007, both at the finish and into the recovery phase, and after rock over when the knees started to rise, the athletes' heels separated from the footstretcher significantly less in June 2008 than they did in December 2007 or October 2007.²

¹ Data for HJC alpha at the finish in July 2007 was found to be not normally distributed.

² Data for FJC alpha at knees break in October 2007 was found to be not normally distributed.

8.3 Significant results for Step 4

Table 8.2 stated that there were 52 dependent variables that varied significantly over several months of testing, and 23 of these were presented in Section 8.1. The other 29 variables are shown in Table 8.5.

Stroke profile	Three-dimensional kinematics			
	at the catch	at peak handle force	at the finish	at knees up
Max handle force (%)	KJC Y	HJC alpha	LSJ X	LSJ X
Knees up (%)	AJC X	HJC gamma	HJC Z	HJC Z
Max H Force/BM (N/kg×100)		KJC Y	HJC alpha	HJC alpha
Power output (W)		AJC X	HJC beta	HJC beta
Slope of handle force		AJC Z	KJC Z	KJC Z
Work done (J)			AJC X	AJC X
			AJC Z	AJC Z
				AJC alpha

Table 8.5: Dependent variables that showed significant change across several testing sessions during Step 4

Peak handle force and the timing of the knees breaking in the recovery were significantly later in the stroke in July 2007 versus October 2007¹ and October 2007 versus March 2008 respectively. The maximum normalised handle force was significantly higher in March 2008 than it was in October 2007 ($\Delta = 35.6 \text{ N/kg}\times 100$), and in June 2008 was significantly greater than July 2007, October 2007 and December 2007 ($\Delta = 81.4, 71.9, \text{ and } 67.0 \text{ N/kg}\times 100$ respectively). The athletes also produced more power per stroke in June 2008 than they did in October 2007 or December 2007 ($\Delta = 12.2, \text{ and } 7.4 \text{ W}$ respectively), they did 31.2 J more work per stroke in June 2008 than in October 2007,² and the rate at which they developed force through the handle in June 2008 was significantly greater than it was in July 2007 (approximately 1906.5N/s versus 1716.7N/s).

Similar to Step 2 (Section 8.2), at the catch the location of KJC was significantly higher in June 2008, March 2008 and December 2007 than it was in July 2007, and was also higher in June 2008 than in October 2007, and furthermore was significantly more superior at the instant of peak handle force in June 2008 than in July 2007. Also at the catch and at peak handle force, the location of AJC was significantly further from the FOB transmitter in the X direction than it was in other testing sessions, and, at peak force only, was significantly more posterior in

¹ Data for Max Handle Force (%) in October 2007, March 2008 and June 2008 was not normally distributed.

² Data for Work (J) in October 2007 was not normally distributed.

March 2008 than it was in July 2007, October 2007 and June 2008.¹ Again similar to Step 2; in the middle of the drive phase, as maximum force was exerted through the ergometer handle, the intersegmental angle at HJC showed significantly less flexion in July 2007 than in December 2007. And at peak handle force, whilst there was less than 1° of internal or external rotation about the hip in March 2008 or June 2008, there was 7° of external rotation in July 2007.

At the finish of the stroke, and as the knees began to rise during the recovery phase the changes noted across months for LSJ X, HJC Z, HJC alpha, KJC Z² and AJC X followed the same trends as were reported for Step 2 (Section 8.2), and additional observations of significant change were shown for HJC beta, AJC Z and AJC alpha. In March 2008 there was no more than 1° of HJC abduction at the finish or as the knees broke, this was respectively 6.9° and 5.5° less than the level noted in July 2007 (7°).³ AJC was significantly more anterior at the finish and at knees up in July 2007, October 2007 and December 2007 than in March 2008, and athletes exhibited significantly more plantar flexion at knees up in October 2007 than in December 2007 or June 2008.

8.4 Significant results for Step 6

Table 8.2 stated that there were 27 dependent variables that varied significantly over several months of testing, and 23 of these were presented in Section 8.1. The other 4 variables are shown in Table 8.6. In March 2008 compared to July 2007; the timing of knees break in the recovery phase was significantly earlier ($\Delta = 2.7\%$ of the stroke), at the catch there was significantly more hip flexion ($\Delta = 17^\circ$), and the magnitude of the intersegmental angle at KJC, as the knees broke was less ($\Delta = 6^\circ$). At peak handle force LSJ X was displaced further from the FOB transmitter in December 2007 than in March 2008 or June 2008.

Stroke profile	Three-dimensional kinematics			
	at the catch	at peak handle force	at the finish	at knees up
Knees up (%)	HJC alpha	LSJ X	-	KJC alpha

Table 8.6: Dependent variables that showed significant change across several testing sessions during Step 4

¹ Data for AJC Z at peak handle force in June 2008 was not normally distributed.

² Data for KJC Z at the finish in December 2007 and March 2008, and at knees up in March 2008 was not normally distributed.

³ Data for HJC beta at knees up in July 2007 was not normally distributed.

8.5 All Steps: significant ANOVA RM, non significant post hoc

Table 8.2 showed that of the 363 variables (121 for each Step) that were originally tested for change with longitudinal training 14, 9 and 19; Step 2, Step 4 and Step 6 respectively, resulted in a p-value of significance for the ANOVA RM output, but that the Bonferroni post hoc failed to identify the specific, significant pairwise comparisons. These 42 variables are listed in Table 8.7. As was done for the investigation into exercise intensity (Chapter 7), in an attempt to identify the specific changes seen for the variables shown in Table 8.7 new ANOVA RM were run and the Sidak post hoc analysis was utilised.

Stroke profile	Three-dimensional kinematics			
	at the catch	at peak handle force	at the finish	at knees up
STEP 2				
COP drift, Recovery (mm)	HJC Y	LSJ X	HJC X	HJC X
COP Z @ Finish	HJC beta	HJC gamma	HJC beta	HJC beta
Work done (J)		AJC Z	AJC Z	AJC Z
STEP 4				
COP Z @ Finish	HJC Y HJC beta KJC Z	LSJ X KJC Z AJC alpha	HJC X HJC X	-
STEP 6				
Finish (%)	LSJ Z	HJC alpha	HJC Z	LSJ gamma
Max H Force/BM (N/kg×100)	HJC X	HJC gamma	KJC Z	HJC Z
Quality LP ratio @ MHF	HJC beta KJC Y AJC X	KJC Y AJC X AJC Z		KJC Z AJC X

Table 8.7: Longitudinal training: Significant variables from ANOVA RM with non-significant Bonferroni post hoc

For each of the general linear models run using ANOVA RM and the Sidak correction, 10 pairwise comparisons were made concerning Step 2 variables, 10 pairwise comparisons were made for each Step 4 variable, and 6 pairwise comparisons were made for each Step 6 variable; thus 344 pairwise comparisons were made in total. Of these, none identified a significant effect that had been missed by the previously conducted Bonferroni investigations. Within the scope of this thesis it has not been possible to identify why the ANOVA RM provided a significant result for the variables listed in Table 8.7.

8.6 Flagged variables

The fourth category into which the results of the ANOVA RM were grouped specified that the assumption of sphericity had been violated, the data was corrected using the GG or HF adjustment and the resulting GG and HF p-values in the ANOVA RM results output disagreed as to whether a significant difference existed. Field (2000) states that when this occurs one may consider the average of the two p-values in conjunction with the significance of the multivariate tests provided in the SPSS output (Pillai's Trace, Wilks' Lambda, Hotellings's Trace, Roy's Largest Root). Table 8.2 showed that in the current study only 1 variable fell into this category: the location of LSJ, in the Z direction, at the catch, during Step 4. The GG and HF p-values for this variable were 0.051 and 0.035 respectively, consequently the average of these is 0.043, and, because the multivariate p statistic for this analysis was equal to 0.036 it was thought that there may be a real difference in the data logged over the testing year. However, neither a Bonferroni nor Sidak adjusted post hoc analysis identified specific pairwise differences for the trajectory of LSJ Z at the catch.

8.7 Summary of results regarding longitudinal training

Twenty three of the dependent variables considered in this chapter varied significantly over the testing year (July 2007 to June 2008) in the data logged for Step 2, Step 4 and Step 6. A further twenty variables were found to change significantly for Step 2, there were an additional twenty nine for Step 4, and an additional four for Step 6. A short summary of these results is accompanied by some comment in this section.

As the year progressed the athletes achieved higher peak forces in all of the Steps considered, with year maximums coming in June 2008 for Step 2 and Step 4, and in December 2007 for Step 6 (2 N higher than in June 2008). Between the autumn to winter tests in 2007 and the spring to summer tests in 2008 the athletes also increased power output in Step 2 and Step 4, and in Step 4 increased the magnitude of work done per stroke, and the rate at which handle force was developed in the drive phase. Considering that the athletes in question focus more on work intensive training in the winter months to improve physiological parameters such as strength and aerobic capacity, and focus more on technical development and physiological maintenance in the spring and summer months, the gains in parameters such as peak pulling force and power output between winter 2007 and summer 2008 are perhaps even more noteworthy than they first appear. In all Steps the length of the rowing stroke reduced between July 2007 and June 2008, with the summer 2008 data showing a 2% decline. And in addition to this some changes in the timing of key stroke events; peak handle force, finish, and knees break, were noted in Step 4 and Step 6. These small but significant changes did not appear to follow any particular pattern.

The trajectory of LSJ was found to vary in the X and Y direction at all four key points in the stroke cycle, and at the finish and when the knees broke only, in the Z direction. The measurements logged for the vertical location of LSJ showed that each testing session saw further elevation of the joint centre which could possibly indicate that the athletes were holding a stronger, more upright posture through the trunk. This suggestion is supported by the data for LSJ alpha, which showed that the intersegmental angle reduced significantly at the catch and as peak handle force was being exerted, as the testing year progressed. At the finish, and during stroke recovery there was increased extension of the lumbar spine as the year progressed, and the Z coordinate showed that LSJ was more posterior in later testing sessions. The data presented in this chapter shows that at the catch and during the drive phase rowers flexed their lumbar spine more when exercising at higher intensity, and the intersegmental angle was generally larger at the finish and when the knees broke too; this is in agreement with the results presented in Chapter 7. In addition to agreement with the study into the effect of exercise intensity, the current results show that longitudinal coaching, training, and assessment can be an effective way to improve postural control of the lower back and pelvis complex in rowing, particularly during the drive phase.

The HJC did not show the same consistency of change across all Steps as LSJ, with the only significant difference noted in Step 6 being an increased level of flexion at the catch. This increased flexion may be linked to the results for LSJ; decreased LSJ alpha at the catch suggests more anterior rotation of the pelvis, and increased anterior rotation of the pelvis would likely result in gains in measured hip flexion. During lower intensity Steps the current study also noted more hip flexion during the drive, at the finish, and as the knees broke in the recovery, and changes in the Z coordinate of the HJC. As the level of hip flexion increased at the finish and as the knees broke, HJC Z became more posterior, and the timing of these changes also links to the increased levels of lumbar extension noted above. All of these changes at HJC and LSJ may be explained in part by increases in anterior rotation of the pelvis at the catch, during the drive, at the finish, and when the knees break.

At the finish and as the knees broke, there was also changes in the level of abduction about HJC as the year progressed, which is linked to the changes seen in the X coordinate for KJC; where the athletes' right knee was more lateral in the summer 2008 than it was in summer 2007. The location of KJC X was also more lateral at the catch and during the drive in later tests, and while this did not lead to significantly increased hip abduction, it may have produced some, which in turn would have provided more space for the athletes to increase the anterior rotation of their pelvis, thus decreasing lumbar flexion at the catch and during the drive (above). There were also some changes noted in the trajectory of KJC in the Y and Z directions, however data

was occasionally not distributed parametrically which could have affected the outcome of the statistical tests.

There were some small, but significant changes noted in the trajectory of the AJC in the X and Z directions for some of the Steps considered, the most interesting of which was the location of AJC being more posterior in spring 2008 than it was in earlier tests at the finish and during the recovery of the stroke. This links with the finding that, as the year progressed the location of AJC became more elevated; because the foot was strapped to the ergometer at the level of the metatarsal heads, and the length of POSFOOT could not change within any individual athlete, when the position of AJC moved vertically upwards, rotating about FJC, and away from the footstretcher towards the finish of the stroke, it automatically moved to a more posterior location too. This does seem somewhat discordant with the reported reduction in FJC alpha (the heels coming away from the footstretcher), however the change in FJC alpha was only 1°, and its effect on AJC location could have been cancelled out by increased plantar flexion about AJC.

This section has demonstrated how some of the dependent variables of stroke profile and 3D kinematics are linked to one another. The next chapter considers how many of the dependent variables that have been introduced thus far may be statistically related to each other, and subsequently, if any can be used as surrogates for others, offering insight into the development of athletic performance, and injury prevention and management.

Chapter 9

Correlation and Regression Analyses

The data collected during all athlete testing sessions was used during the investigations presented in this Chapter. That is, the stroke profile and kinematic observations collected during all 1,115 Steps were included in each stage of the analysis process. The aims of this chapter considered the fourth and fifth hypotheses listed in Section 5.5; that high levels of performance could be predicted by aspects of athletes' technique and rowing kinematics, and that some aspects of elite rowers' technique, performance and rowing kinematics could be exploited to reduce the risk of injury and pain.

The dataset used in all of the calculations consisted of 98 variables (Table 9.1). Of these, 17 were stroke profile variables that had previously been found to change significantly with exercise intensity, longitudinal training, or both. In addition to this, 4 were stroke profile variables that had been identified by UK Sport and GB Rowing as being of interest, thus feedback on the nature of these variables was requested. There were also 68 variables describing 3D kinematics; these included joint centre trajectories and alpha angles at each of the four key points in the stroke that have been discussed thus far (the catch, the occurrence of maximum handle force, the finish, and Knee Up). The reason for excluding the beta and gamma angles is found by analysing results from Chapter 7 and Chapter 8. The previous chapters presented a total of 215 significant ANOVA RM tests (Table 7.1 and Table 8.2), of these only 2 were for beta angles, and only 8 were for gamma angles; compared to stroke profile (48 tests), X trajectory (36 tests), Y trajectory (41 tests), Z trajectory (42 tests), alpha angles (38 tests). Furthermore, in the analyses into the effects of exercise intensity and longitudinal training, there were a total of 2,244 pairwise comparisons carried out post hoc for beta and gamma kinematics. Only 12 of these were found to be significant, that is, for beta and gamma in Chapters 7 and 8; 0.53% of the pairwise comparisons conducted showed significant changes. Due to the relatively low importance of the beta and gamma angles analysed previously (demonstrated by the results shown in Chapter 7 and Chapter 8), and because it was thought that implementing training interventions based on changes in beta and gamma would be difficult (for example designing a training programme to change the level of external rotation that athletes exhibit at their AJC at the catch), those variables were excluded from the dataset used in the current chapter. The current dataset included the gender and bodyweight of the athletes; gender was included as a binary dummy variable (0 for male athletes, 1 for female). An additional 7 variables that were calculated for each Step were either used as measures of rowing performance, or linked with injury. In total, 11 of the 98 variables were considered to be measures of rowing performance or linked to injury; it was these 11 that were the dependent

variables considered during regression analyses and a full description of them is offered in the next section.

Non 3D kinematic variables	Kinematic data*
COP drift – MHF (mm)	LSJ X
COP drift – Finish (mm)	LSJ Y
COP Z @ Catch	LSJ Z
COP Z @ Finish	LSJ alpha
	HJC X
Max handle force (%)	HJC Y
Finish (%)	HJC Z
Knee Up (%)	HJC alpha
	KJC X
Max handle force (N)	KJC Y
Max H Force/BM (N/kg*100)	KJC Z
Slope of handle force	KJC alpha
Max seat force (N)	AJC X
Min seat force (N)	AJC Y
	AJC Z
Suspension 1 (BW(s))	AJC alpha
Suspension 2 (BW(s))	FJC alpha
Power output (W)	
Stroke length (mm)	Δ LSJ alpha – catch – MHF
Stroke rate (/min)	Max[(inst m LSJ alpha) \times inst HF] – Catch – Finish
Work done (J)	Min[(inst m LSJ alpha) \times inst HF] – Catch – Finish
	HJC beta when KJC alpha = 20°
Quality LP ratio @ Catch	
Quality LP ratio @ MHF	
Quality LP ratio @ Finish	
Sex	
Bodyweight (N)	
\sum inst seat force \times inst COP – MHF	
\sum inst seat force \times inst COP – Finish	
Min seat force – BW (BWs)	

Table 9.1: Variables included in the current dataset

All of the variables that were included in the analyses presented in this chapter are shown. * The kinematic data that is not highlighted was logged four times: the value at the catch, at the point in the stroke when maximum force was being exerted on the handle, at the finish, and at the point in the stroke recovery when the knees started to rise. The highlighted variables are those that are used for the first time in the thesis; a full description of these variables is given in Section 9.1.

9.1 Dependent variables

The dependent variables considered during regression analyses are presented in Table 9.2. Of these 11 variables, 4 have been introduced in previous chapters and 7 have not. 7 of the 11 were defined as performance predicting variables, and 4 were considered to be related to injury.

Performance variables	Injury variables
Finish (%)	Δ LSJ alpha – catch – MHF*
Slope of handle force	Max[(inst m LSJ alpha) \times inst HF] – Catch – Finish*
Stroke length (mm)	Min[(inst m LSJ alpha) \times inst HF] – Catch – Finish*
Power output (W)	HJC beta when KJC alpha = 20°*
\sum inst seat force \times inst COP – MHF*	
\sum inst seat force \times inst COP – Finish*	
Min seat force – BW (BW _s)*	

Table 9.2: The dependent variables considered during regression analyses

The performance variables consider measurements taken from the handle and seat instrumentation, and describe the quality of athletes' rowing in performance terms. The injury variables consider information relevant to two of the most prevalent anatomical joints that rowers injure. Full description of the variables is given in Sections 9.1.1 and 9.1.2. Variables marked with * have not been introduced thus far in the thesis.

9.1.1 Performance variables

To address the fourth hypothesis listed in Section 5.5; that deviation in elite rowers' technique would result in changes in performance predicting variables, the 7 performance variables shown in Table 9.2 were considered to be measures of the rowing performance of the athletes. Finish (%) was the timing of the finish of the stroke, slope of handle force was the magnitude of the peak force divided by the timing of peak handle force, power output was measured in Watts and stroke length was measured in mm. Delays in the timing of the finish during the stroke (a wider handle force profile), greater power output and longer stroke length were all considered to reflect improvement in rowing performance. There is some debate as to what is the best practice considering the rate of handle force production and rowing performance, hence this study only sought to describe which stroke profile and kinematic variables were linked to the slope of handle force production in the drive.

\sum inst seat force \times inst COP – MHF and \sum inst seat force \times inst COP – Finish were calculated using the seat instrumentation. The scores were the sum of the instantaneous seat force multiplied by the absolute value of the instantaneous medial/lateral COP coordinate, between the catch and the occurrence of maximum handle force, and the catch and the finish respectively. It was thought that, in a rowing boat, deviations of athlete's COP in the medial/lateral direction could be deleterious to boat speed, as large enough displacements could induce the boat to roll, affecting the magnitude of drag forces between the shell and the water (Soper and Hume, 2004a). Furthermore, it was thought that COP deviations would be particularly harmful to performance if the athlete was also applying large contact forces through their seat. The recovery phase was not considered because the athletes tested in this study exhibited far less medial/lateral displacement of their COP during the recovery than the drive (Figure 6.5, Section 6.3.1). Lower values were considered to reflect higher performance.

Min seat force – BW was also calculated using the seat instrumentation. The measure considered the difference in the magnitude of individual athlete’s BW and the maximum absolute value of the BM adjusted seat force exerted on the seat during a stroke. In the example shown in Figure 9.1 the athlete’s BW was 780.88 N and the maximum absolute value of BM adjusted seat force was 1095.39 N. Hence the score for *Min seat force – BW* was 0.4; the maximum absolute seat force was equal to 1.4 times the athlete’s BW. This measure was included as it was thought that very large forces exerted downwards by rowers accelerating the body onto the seat would induce boats to sit lower in the water, thus increasing drag and being deleterious to boat speed. Lower values were considered to reflect higher performance.

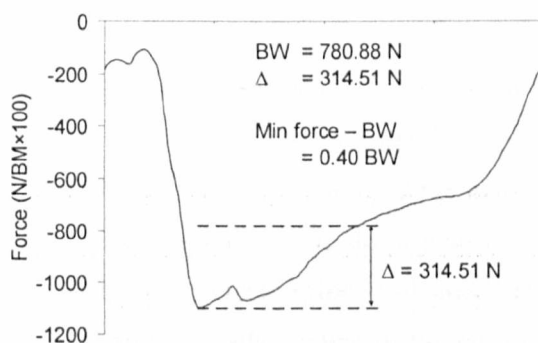


Figure 9.1: Calculation of a performance indicating dependent variable

The solid black line is the seat force series recorded during one complete rowing stroke. The X axis is 0-100% of a rowing stroke. The top dashed line represents the magnitude of the athlete’s bodyweight, and the bottom dashed line represents the magnitude of the minimum seat force recorded. The difference between these two values is noted as Δ , and the calculation of absolute *Min seat force – BW* (Table 9.2) is shown.

9.1.2 Injury variables

To address the fifth hypothesis listed in Section 5.5; that some aspects of elite rowers’ technique and performance would be related to an increased risk of injury, the four injury variables shown in Table 9.2 were considered to be linked with injury. As stated in Chapter 1; Hickey et al.’s (1997) study of ten years of medical records for 172 elite rowers found that in females the most common sites of injury were the chest (22.6%), lumbar spine (15.2%), and forearm/wrist (14.7%), whilst in males they were the lumbar spine (25%), forearm/wrist (15.5%), and knee (12.9%). In the current work, information on the kinematics of the lumbar spine and knee were known, thus the focus was at these joints.

9.1.2.1 Injury variables – Relevant to the lumbar spine

Of interest regarding possible injury mechanisms for the lumbar spine was the way in which LSJ alpha changed whilst under load. The measurement $\Delta LSJ\ alpha - catch - MHF$ was the

difference in the flexion/extension angle about LSJ from the catch of the stroke to the point in the stroke when maximum handle force was being exerted. If the calculated variable was less than zero then it showed that the athlete's lumbar spine became more flexed during the early part of the stroke, and if the value was greater than zero then it showed that the athlete's lumbar spine became more extended. Concurrently if the variable was equal to zero then the spinal posture of the athlete did not change during the phase of the stroke being considered. It was thought that, as in general lifting movements, exhibiting no change in the flexion/extension angle about LSJ under loading would be the gold standard technique. However it was not known whether a tendency to extend about LSJ or flex about LSJ would be more or less influential on injury potential; this study only sought to identify variables associated with LSJ delta.

Max and Min[(inst m LSJ alpha) × inst HF] – Catch – Finish (Figure 9.2) considered the rate of change of the flexion/extension angle about LSJ and the force exerted through the handle. Using the data collected during athlete testing sessions and the associated LSJ alpha series, the rate of change of LSJ alpha was calculated for the drive phase. Negatively sloped rates of change represented motion flexing the lumbar spine, and positively sloped rates of change represented extending the lumbar spine. Each element of the rates of change series were then multiplied by the associated instantaneous handle force to give a value of rate of change of intersegment angle normalised by the force being transmitted through the body. It has been suggested that low back pain and injury in rowers is due to the repetitive nature of their sport, the spinal mechanics that constitute this action, and the lumbar compressive load experienced (often greater than 5kN) (Hase et al., 2004; Morris et al., 2000; Munro and Yanai, 2000). Thus reducing the magnitude of the product of the rate of change of LSJ alpha and handle force would be beneficial in reducing injury risk to the lumbar spine; reducing the positive and negative peaks shown in Figure 9.2c thus exhibiting a more stable, static spinal posture during high loading. Figure 9.2 shows an example of a particular athlete's LSJ alpha series, the rate of change of that series, and the rate of change multiplied by the handle force. For descriptive purposes, the timing of Max and Min[(inst m LSJ alpha) × inst HF] – Catch – Finish were also calculated relative to the timing of maximum handle force; the timing values were the timing of maximum handle force minus the timing of Max and Min[(inst m LSJ alpha) × inst HF] – Catch – Finish.

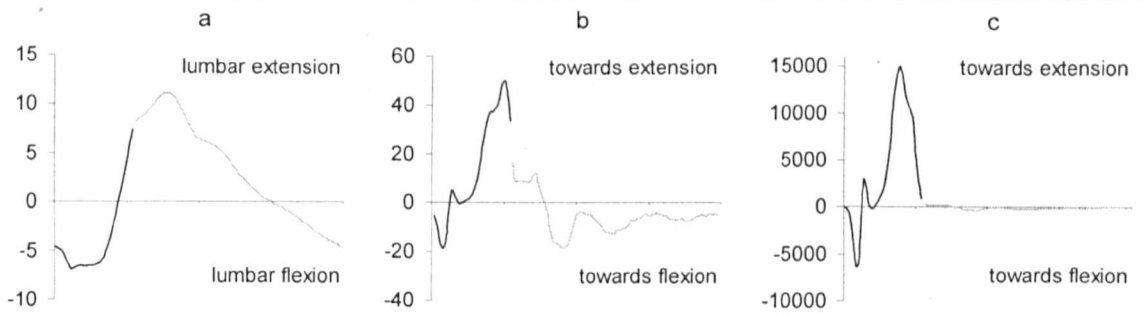


Figure 9.2: Calculation of variables linked to LSJ injury

The change in LSJ alpha (a), the rate of change of LSJ alpha (b), and the product of the rate of change of LSJ alpha and the handle force (c) are shown for one entire stroke. The X axis is 0-100% of a rowing stroke. The Y axis is degrees (a), degrees/s (b), and degrees/s \times handle force (c). The black line shows the data for the catch to the finish of the stroke, and the grey line shows the data for the remainder of the stroke. Only the data calculated for the drive phase was considered when logging maximums and minimums for use as dependent variables; the rest of the data is included for completeness and to illustrate that the values in part c of the figure are close to zero after the finish of the stroke.

9.1.2.2 Injury variable – Relevant to the knee

Two common mechanisms by which injuries occur at the knee are through an increase in valgus moment (Shin et al., 2009), and through an increase in the Q angle (Mizuno et al., 2001). As no information was available regarding valgus motion (KJC beta, Section 4.3) athlete data was assessed with reference to knee injury by exploiting the Q angle. The morphology of the patellofemoral joint and its articular surfaces do not automatically provide great stability, hence normal function relies upon static, active and passive stability factors (Amis et al., 2004). The Q angle is measured as the difference in direction between the line of action of the patellar tendon and the force exerted by the quadriceps muscle, and, the presence of the Q angle causes a lateral force component to act on the patella (Amis et al., 2004). Indeed the geometry of the knee bones has in some respects evolved to resist this force; the lateral facet of the patella is larger than the medial. It is also known, that when in deeper knee flexion, patellofemoral joint forces are higher in the posterior direction, and towards knee extension joint forces are greater in the lateral direction, thus joint stability is greater in the flexed knee (Amis et al., 2004). Amis et al. (2004) state that the patella is least stable in 20° of KJC flexion. Mizuno et al. (2001) cited the role of the Q angle in changes to patellofemoral kinematics, and concluded that an increase in the Q angle could lead to lateral patellar dislocation or increased lateral patellofemoral contact pressures, particularly at low levels of knee flexion. It was therefore thought that if athletes were to exhibit increased levels of HJC abduction whilst the KJC was in 20° of flexion their Q angle would be reduced, thus reducing their risk of injury via patellar dislocation. *HJC beta when KJC alpha = 20°* was used to measure this in the current study.

9.2 Introduction to statistical methods

The main statistical technique used in this investigation was regression modelling of dependent variables with multiple explanatory variables (MREG). Regression analysis calculates the coefficients of the equation, involving one or more independent (explanatory) variables, which best predict the value of the dependent variable.

9.2.1 Assumptions underlying multiple regression

In order to conduct parametric regression analysis: the dependent and independent variables should be quantitative; for each value of an independent variable, the distribution of the dependent variable must be normal; and the variance of the distribution of dependent variables should be consistent for all values of the independent variable. However, it should be noted that it is possible to satisfy these last two conditions in virtually any dataset by manipulating the selection of what constitutes a *value* or *limit range* within independent variables.

Regression analysis may be linear or non-linear; linear analysis assumes that the relationship between the dependent variable and any individual explanatory variable can be described by a linear function, and non-linear regression requires the user to define some function that describes the non-linear relationship between the dependent variable and each independent variable. Descriptive non-linear functions can often be found by using the curve estimation procedures that are available in some software packages. It should be noted that some seemingly non-linear relationships, such as polynomials are considered to be linear in regression analysis:

If - $Y = A + BX^2$ = Polynomial

And - $W = X^2$

Then - $Y = A + BW$ = Linear

9.2.2 Evaluating the appropriateness of regression models

Care should be taken to assess a dataset to see if the above assumptions can be met prior to regression modelling. However, because of the difficulties associated with defining a *limit range* within the independent variables, the most powerful evaluation of the quality of a regression model comes from post test assessment of the R^2 and *adjusted R^2* values, the model residuals, and the predicted/fitted values. R^2 is a measure of the goodness of fit of a regression model, however if several models must be compared to determine an optimum prediction, then, if the separate models have different numbers of explanatory variables the adjusted R^2 value must be used. R^2 values reflect the amount of the variation in the dependent variable that is

explained by its relationship with the explanatory variables. A histogram constructed from the unstandardised or standardised model residuals¹ can be used to verify the assumption of normality, a scatter plot of the standardised residuals against the standardised fitted values² can be used to verify the assumption of constant variance, and, in linear MREG, scatter plots of the standardised residuals against each explanatory variable can be used to assess linearity. Constant variance may be assumed if there is no funnel effect visible in the appropriate plotted data, and linearity may be assumed if there are no trends apparent in the appropriate plotted data (Petrie and Watson, 1999).

One of the outputs from regression analysis in SPSS is an analysis of variance (ANOVA). After assessing the appropriateness of a model, a significant F-test within the ANOVA shows that at least one of the explanatory variables is associated with the dependent variable. The model output concerning the regression equation coefficients can then be assessed to see which of the explanatory variable's coefficients are significantly different from zero, and hence have a true effect on the model; in SPSS this is done automatically by conducting a t-test for each coefficient.

It is also common for some of the explanatory variables used in MREG to be related to each other. This can be determined by conducting a correlation analysis of all of the variables in a dataset; extremely highly correlated explanatory variables often result in collinearity in the multiple regression analysis and can make the model difficult to interpret. However, by screening the dataset prior to running any MREG models, and by using the automatic explanatory variable selection procedures available in most statistical software packages this problem can be alleviated (Section 9.2.3).

9.2.3 Designing a multiple regression model

In general the number of observations in a dataset should not be less than ten times the number of explanatory variables included in any one regression model. SPSS includes several explanatory variable selection methods; when selected these techniques offer an automatic selection of the *best* explanatory variables for any one dependent variable. The relevant methods in SPSS are Enter, Stepwise, Backward Elimination, and Forward Selection. The Enter method selects all of the variables defined by the user and constructs a regression equation with all. The Stepwise technique iteratively includes and removes independent variables that

¹ Unstandardised residuals – The difference between the observed value and the value predicted by a regression model. Standardised residual – The residual divided by an estimate of its standard deviation. Also known as a Pearson residual.

² Standardised fitted values – For each observation (row of data) in a dataset, the difference between the fitted value (predicted by the regression model) and the mean of all of the predicted values is found. Then the result is divided by the standard deviation of the predicted values.

have an improving effect on the model F-test, the method terminates when no more variables are eligible for inclusion or removal. Backward Elimination initially includes all of the explanatory variables defined by the user; it then removes the variable that has the smallest partial correlation with the dependent variable (providing it meets some exclusion criteria) and continues until the method finds its optimal equation. Forward Selection is essentially the reverse of Backward Elimination. SPSS can conduct MREG using any one, or a combination of the various variable selection methods. Despite these variable selection methods, some effort should be exerted to include fewer rather than more potential explanatory variables in regression models.

9.3 Current method for data analysis

In order to address the aims of this chapter, the current approach was carried out in three distinct stages; these are described in Sections 9.3.1, 9.3.2 and 9.3.3

9.3.1 Data reduction

Because associations in the dataset may have come from 1 or more of 97 possible directions for any one dependent variable (recall that the dataset was 98 columns/variables by 1,115 rows/observations), and in line with the good practice described in Section 9.2.3; it was decided that reducing the dimensions of the data matrix would be desirable before conducting any MREG analysis. This was done through correlation analyses.

It was thought that the calculation of correlation matrices would highlight those potential independent variables that were significantly related to the dependent variables of performance and injury. Furthermore, Pearson correlation coefficients would provide information on whether or not the dependent and independent variables were linearly related to each other, and thus would aid in the design of MREG models (linear or non-linear). Pearson's and Spearman's rho correlation matrices were calculated using Matlab. In order to reduce the dimensionality of the dataset (relative to each dependent variable), a new set of potential explanatory variables could then be constructed for each dependent variable by observing which of the other variables it had a significant Pearson and Spearman correlation with.

9.3.2 Curve estimation

After considering the results of correlation analyses it was necessary to determine functions that defined the relationship between the potential independent variables and the dependent variables of interest. This process was conducted in SPSS, and considered eight different types of function to describe the relationship between pertinent pairs of variables. The eight groups of

functions were: linear, logarithmic, inverse, quadratic, cubic, compound, sigmoid, and exponential. It was hoped that it would be possible to use linear MREG, and assess the linearity of the explanatory variables and model residuals as previously described.

9.3.3 Multiple regression analysis

After using correlation analysis and curve estimation procedures to design MREG models for each of the dependent variables identified in Table 9.2, regression analyses were carried out. The processes described in Section 9.3.1 were done to reduce the dimensionality of the dataset associated with each dependent variable; however it was still not sure that the optimal regression equation would incorporate all of the potential explanatory variables that were defined. Thus MREG was performed using the *Stepwise* automatic variable selection procedure. This process generally produces several regression equations of varying quality, each incorporating a different selection of the possible independent variables defined by the user. Once this choice of equations was available the optimal equation was chosen. This was done by assessing the R^2 and adjusted R^2 values, by ensuring a significant F-test in the ANOVA output, and by ensuring that each regression coefficient included in the equation was significantly different from zero.

When the optimal equation had been discovered MREG analysis was conducted again using the appropriate independent variables and the *Enter* variable selection method (Section 9.2.3). The standardised fitted values and the standardised residuals of the model were saved for subsequent use in assessing the appropriateness of the model. The quality of the analysis was assessed by observing the distribution of the model residuals (normality assumption), the relationship between the fitted values and the residuals (assumption of constant variance), and, where appropriate, the relationship between each of the explanatory variables and the residuals (linearity assumption).

Provided that a regression equation explaining much of the variance in the dependent variable, and meeting the assumptions associated with validating the test could be defined using the current method; the regression coefficients were then used to describe how the dependent variables might be affected by the explanatory variables used within each model. The unstandardised coefficients describe the change in the value of the dependent variable with a one unit increase in the explanatory variable, providing all other parameters remain constant. Due to the potential for differences in range and variance between individual independent variables; observing the magnitude of unstandardised coefficients is not appropriate for comparing the relative effect of separate explanatory variables on the model. The standardised coefficients may be used to this end.

9.4 Results

Initial results from correlation analyses and curve estimation procedures were inconclusive as to the best approach to use regarding the functions that would describe the relationship between dependent and explanatory variables. For simplicity, and because no non-linear functions could be found that were more appropriate than linear functions, a decision was made to construct all MREG models linearly and afterwards, to validate the method using the appropriate techniques described in Section 9.22. The descriptive statistics for the dependent variables, and selected others are shown in Table 9.3.

Variable	Abbreviation	Mean	Standard deviation	Maximum	Minimum
PERFORMANCE VARIABLES					
Finish (%)	-	30.55	3.81	44.00	24.00
Slope of handle force	-	49.36	9.64	77.97	26.66
Stroke length (mm)	-	1518.35	81.53	1761.80	1272.27
Power output (W)	-	254.26	64.70	542.06	153.05
\sum inst seat force \times inst COP – MHF	Seat 1	38.40	28.25	165.45	1.87
\sum inst seat force \times inst COP – Finish	Seat 2	115.81	62.09	381.37	20.43
Min seat force – BW (BW _s)	Seat BW	0.67	0.20	1.59	0.31
INJURY VARIABLES					
Δ LSJ alpha – catch – MHF (°)	LSJ delta	1.52	3.36	21.32	-10.63
Max[(inst m LSJ alpha) \times inst HF] – Catch – Finish	Max LSJ HF	17871.49	8457.03	70682.31	754.30
Min[(inst m LSJ alpha) \times inst HF] – Catch – Finish	Min LSJ HF	-3692.32	3760.20	0.00	-31593.97
HJC beta when KJC alpha = 20°	HJC Q	94.22	6.20	112.72	75.63
Timing of MHF minus Max LSJ HF	Max LSJ HF %	-4.51	6.47	12.00	-18.00
Timing of MHF minus Min LSJ HF	Min LSJ HF %	9.42	5.08	22.00	-19.00
KJC alpha actual at HJC Q, minus 20°	KJC actual	-0.04	1.78	4.85	-4.84

Table 9.3: Descriptive statistics of selected variables

Descriptive statistics of all of the previously defined dependent variables are shown as well as timing data of two of the dependent variables relative to the point in the stroke when maximum handle force was exerted. Initially it was stated that when HJC Q was calculated the knee was in 20° of flexion; because exactly 20° of KJC flexion was not always measured, the difference between the true KJC alpha angle when calculating HJC Q and 20° is shown.

Table 9.3 shows that the finish occurred between 24% and 44% of the way through the stroke, the rate of handle force production was between 26 and 78 N/stroke %, Power output ranged from 153 to 542 W, and stroke length was between 1272 and 1762 mm. These reasonably large ranges are a result of including all Steps, both sexes, and all body sizes. An accurate account of these four variables for each Step, and between boat classes was presented in Chapter 6.

It is also clear that there were large ranges in the data recorded for the variables Seat 1 and Seat 2 (Table 9.3); this was expected as large variations between different athletes were easily observed from the real time feedback during testing. It was thought that these large differences between athletes might be attributed to the level of suspension achieved by athletes, with some suspending almost completely away from their seat, leaving only very light, and medially or laterally displaced seat contact force, whereas others suspended less, and thus more of their bodyweight was supported through contact with the seat. The scores for Seat BW are possibly related to this. Seat BW shows that on average the maximum downwards force exerted onto the seat during rowing was equal to 1.67 (± 0.20) times the athletes' BW. However Table 9.3 also shows that this value was as low as 1.31 times BW and as high as 2.59 times BW.

In 36% of the Steps completed athletes were found to become more flexed about LSJ between the catch and the point in the stroke when they exerted maximum handle force, thus, in 64% of the Steps the opposite was true and athletes extended about LSJ. Results regarding LSJ delta show that on average the athletes moved by 1.52° ($\pm 3.36^\circ$), to a more extended posture about LSJ (Table 9.3). There were large ranges in the calculation of this variable.

The orders of magnitude of the values calculated for Max LSJ HF and Min LSJ HF, were far greater than any of the other variables used in the current study. Moreover the ranges of this data were vast (Table 9.3). This shows that on some occasions the rate of change of LSJ alpha during the drive phase was very high, and sometimes, there may have been virtually no change at all; indeed the maximum value calculated for Min LSJ HF (0.00) shows that there were instances when individuals showed no increases in flexion about LSJ during the entire drive phase (additional analysis revealed that this occurred 6% of the time). On the other hand, the minimum score for Max LSJ HF reveals that there were no Steps conducted in the current study where there was not some period of active lumbar extension during the propulsive phase of the stroke. It was thought that those athletes who exhibited very large rates of LSJ alpha change whilst they loaded their bodies may be at a greater risk of injuring the lumbar region of the spine. Table 9.3 also shows that on average Max LSJ HF (tending to extend the lumbar spine) occurred 4.51% ($\pm 6.47\%$) later in the stroke than the point when maximum handle force was being exerted, and Min LSJ HF (tending to flex the lumbar spine) occurred 9.42% ($\pm 5.08\%$) before maximum handle force. This, along with the example shown in Figure 9.2, and the results shown in Figure 6.19 (Page 125) shows that athletes generally picked up the catch of the stroke in some base posture, then flexed slightly about LSJ and then extended about LSJ.

The results shown in Table 9.3, for HJC Q show that on average athletes exhibited 4.22° ($\pm 6.20^\circ$) of hip abduction when their knee was in 20° of flexion. This is a good result considering the positive effect that HJC abduction can have on the Q angle (Section 9.1.2.2).

Table 9.3 also shows that, when in 20° of knee flexion, there were instances of athletes abducting about their HJC by up to 22.72°, though there were also occurrences of up to 14.37° of adduction. It is thought that excessive hip adduction whilst the knee is in 20° of flexion and the lower limb is under load can be a mechanism for knee injury through accentuating the Q angle. The measurement of HJC Q assumed that HJC beta was measured when KJC alpha was equal to 20°; in fact a measurement of exactly 20° was only taken during 1 of the 1,115 Steps; 36% of the time the KJC alpha angle closest to 20° was between 19° and 21°, 72% of the time it was between 18° and 22°, 92% of the time it was between 17° and 23°, 99% of the time it was between 16° and 24°, and 100% of the time it was between 15.1° and 24.9° (Table 9.3).

9.4.1 Concerning rowing performance

In this section the results of MREG analysis conducted upon the seven performance dependent variables are presented (Table 9.2, Page 191). For each variable the results of reducing the number of potential explanatory variables through correlation analyses precede details of the MREG analysis.

9.4.1.1 Timing of the finish

Through correlation analyses 59 of the original 97 potential explanatory variables were found to be significantly related to Finish timing ($p < 0.05$). Stroke rate was, as expected, found to be highly correlated with Finish timing (Pearson correlation coefficient = 0.94, Spearman = 0.90) and thus, in order not to overshadow the effect of other explanatory variables on Finish timing, was not included in MREG analysis. The variables that were included in the initial MREG procedure included stroke profile variables; the quality of the lumbopelvic ratio at the catch, at maximum handle force, and at the finish; and 3D kinematics concerning X,Y,Z joint trajectories, and alpha joint angles.

The *Stepwise* MREG analysis produced 46 possible equations whose adjusted R^2 values ranged from .697 to .975. The F-tests associated with all of these models were significant ($p < 0.01$) The model that was chosen for use in describing the explanatory variables related to Finish timing included 32 explanatory variables, all of which had significant regression coefficients (as determined by a t-test, $p < 0.05$). Of the independent variables; 11 were stroke profile variables and the gender of the athletes, 6 considered kinematics at the catch of the stroke, 6 were for kinematics at maximum handle force, 3 were kinematics at the finish, and 6 were kinematics observed when the knees broke. These variables were input using the *Enter* automatic variable selection method into a new MREG analysis and the model residuals and predicted dependent variables were calculated. The residuals of the analysis were plotted in a histogram to assess the normality of their distribution (Figure 9.3), and a scatter plot of the residuals against the 1,115

values predicted by the model was produced to assess the assumption of constant variance (Figure 9.3). In addition to this, scatter plots of the residuals against each of the 32 explanatory variables included in the model were produced to assess the assumption of linearity (Figure 9.4). The output of the model is shown in Table 9.4; the coefficients describe the direction and magnitude of the relationship between each explanatory variable and Finish timing, the standard error of the unstandardised coefficients is also included, along with the t-statistic, and significance of the p-value for the t-test for each explanatory variable.

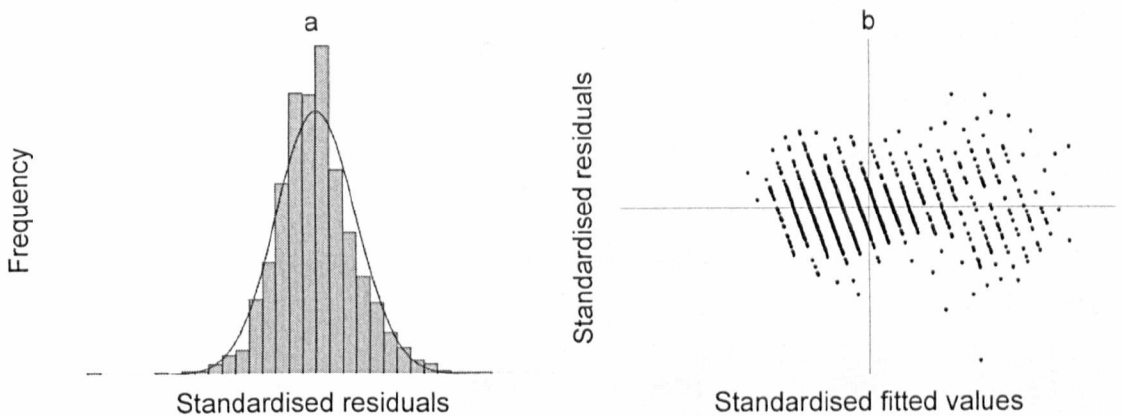


Figure 9.3: Assessment of the assumptions of normality and constant variance with respect to Finish timing

The frequency of the standardised residuals is plotted beneath a normal distribution curve (a); any departures from normal distribution may be deleterious to the validity of the MREG model. The standardised residuals are also plotted against the standardised fitted values (b); any funnelling effect of data along the X axis indicates that the assumption of constant variance may have been violated.

Figure 9.3 shows that the assumptions of normality and constant variance were adhered to in the current model. There is no funnelling effect present in the scatter plot concerning constant variance, thus the assumption of constant variance is met. Furthermore, Figure 9.4 does not show any trends between the model's explanatory variables and the standardised residuals; thus it may be assumed that the assumption of linearity was also satisfied in this case.

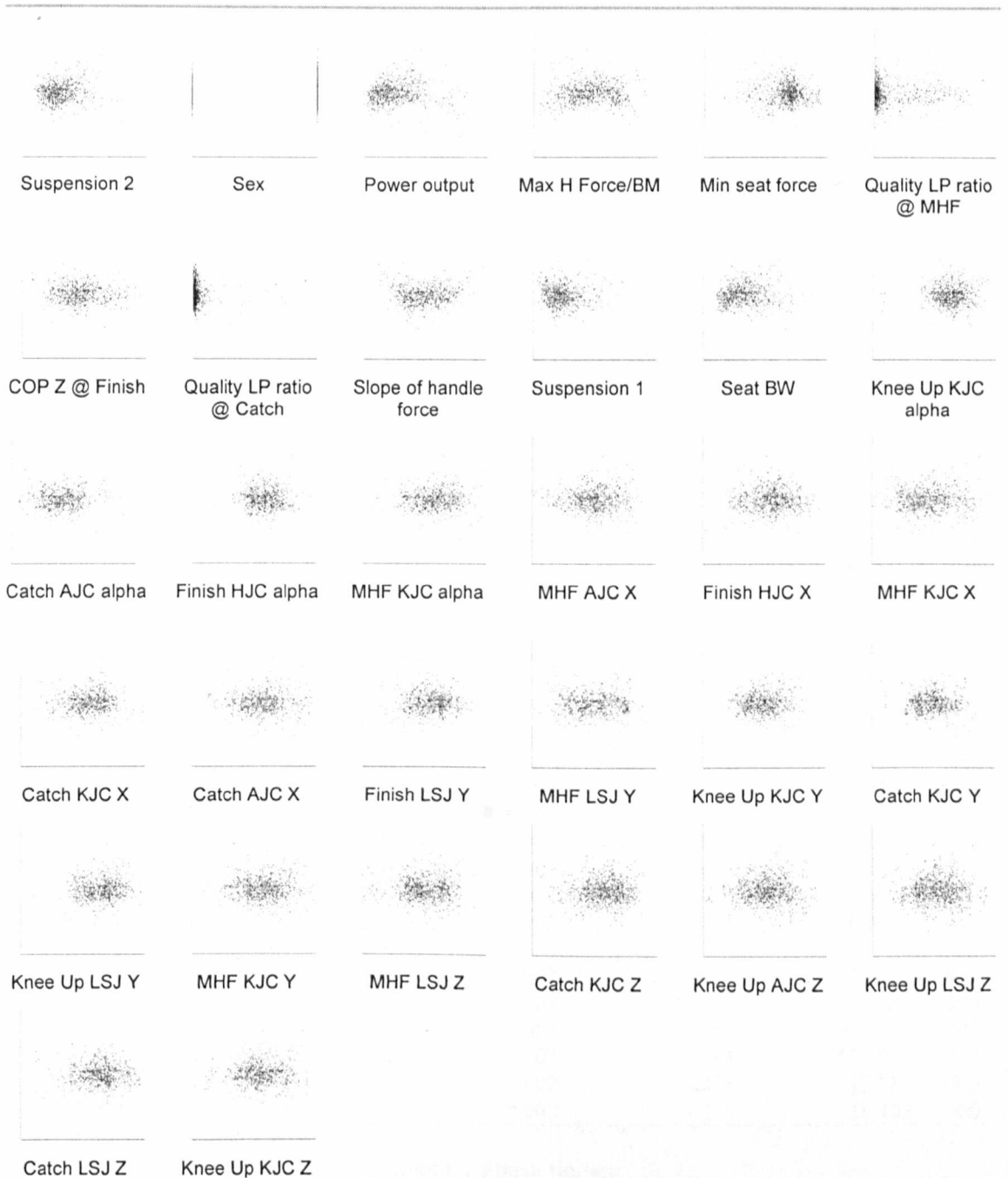


Figure 9.4: Assessment of the assumption of linearity with respect to Finish timing

Each of the plots shows the relationship between a single explanatory variable and the MREG model standardised residuals. The X axes are labelled according to the appropriate independent variable. The Y axis is always the residuals. If no trend is apparent then the assumption of linearity is met.

Variable	Regression coefficients			t-test	
	Unstandardised	Standard error	Standardised	t	p
CONSTANT	-16.748	2.840		-5.896	.000
Suspension 2 (BW(s))	.516	.013	.575	41.006	.000
Sex	.199	.088	.024	2.250	.025
Power output (W)	.021	.001	.361	21.646	.000
Max H Force/BM (N/kg×100)	.007	.001	.264	13.889	.000
Min seat force (N)	-.005	.000	-.160	-13.977	.000
Quality LP ratio @ MHF	-.010	.003	-.020	-3.169	.002
COP Z @ Finish	-.011	.002	-.043	-5.867	.000
Quality LP ratio @ Catch	-.019	.005	-.025	-3.861	.000
Slope of handle force	-.238	.006	-.603	-38.852	.000
Suspension 1 (BW(s))	-.345	.035	-.112	-9.730	.000
Seat BW	-5.151	.207	-.276	-24.876	.000
Knee Up KJC alpha	.080	.009	.119	9.179	.000
Catch AJC alpha	.023	.002	.098	9.713	.000
Finish HJC alpha	.010	.002	.032	4.665	.000
MHF KJC alpha	-.057	.009	-.116	-6.068	.000
MHF AJC X	.015	.003	.050	4.408	.000
Finish HJC X	.005	.001	.024	3.920	.000
MHF KJC X	.004	.002	.021	2.590	.010
Catch KJC X	-.004	.001	-.029	-3.185	.001
Catch AJC X	-.008	.003	-.032	-2.518	.012
Finish LSJ Y	.017	.003	.111	5.980	.000
MHF LSJ Y	.006	.002	.035	2.373	.018
Knee Up KJC Y	-.010	.003	-.050	-3.686	.000
Catch KJC Y	-.010	.002	-.082	-4.325	.000
Knee Up LSJ Y	-.014	.003	-.090	-5.096	.000
MHF KJC Y	-.015	.003	-.123	-6.007	.000
MHF LSJ Z	.032	.002	.442	18.875	.000
Catch KJC Z	.020	.002	.225	12.548	.000
Knee Up AJC Z	.020	.003	.106	7.756	.000
Knee Up LSJ Z	-.008	.002	-.094	-5.392	.000
Catch LSJ Z	-.021	.002	-.255	-12.782	.000
Knee Up KJC Z	-.037	.002	-.318	-16.103	.000

Table 9.4: The MREG calculated equation for Finish timing

The coefficients describe the direction and magnitude of the relationship between each explanatory variable and the dependent variable, the standard error of the unstandardised coefficients is also included, along with the t-statistic, and significance of the p-value for the t-test for each explanatory variable. The order of the variables is: equation constant, followed by stroke profile explanatory variables (sorted by the magnitude and direction of their unstandardised regression coefficient), rotational kinematics, X trajectory kinematics, Y trajectory kinematics, and finally Z trajectory kinematics. Kinematics are either measured at the catch of the stroke, at the point in the stroke when maximum handle force was being exerted (MHF), at the finish of the stroke, or at the point in the recovery when the knees started to rise (Knee Up).

The R^2 and adjusted R^2 values for this model were .976 and .975 respectively. This means that over 97% of the variability in the timing of the finish can be accounted for by its relationship with the explanatory variables included in the regression model. In order to concentrate on the

results regarding 3D kinematics, the stroke profile variables shown in Table 9.4 will be discussed in Section 9.4.1.9.

Superiorly displacing LSJ during the drive and at the finish was associated with increasing drive duration. This is a possible indicator of improved lumbar posture. It was also found to be beneficial to performance to reduce anterior displacement of LSJ at the catch and not displace it too quickly during the drive; at the catch this could be linked with not curling forwards through the lumbar region of the spine. Wider force profiles were also linked to decreased HJC flexion at the finish and decreased KJC flexion as maximum handle force was being exerted during the drive. In addition to this, improved performance was linked with a more lateral KJC position at the catch followed by a more medial mid-drive; this may be linked to increased HJC abduction at the catch, moving quickly towards adduction as the drive progressed. More inferior KJC coordinates throughout the stroke, more anterior KJC position at the catch, and increased plantar flexion at the catch were also found to be associated with improving performance by increasing drive duration.

9.4.1.2 Rate of force production

Initial analysis found that 66 of the original 97 potential explanatory variables were significantly related to the Slope of handle force ($p < 0.05$). The *Stepwise* MREG analysis suggested 39 possible equations whose adjusted R^2 values ranged from .399 to .937. The F-tests associated with all of these models were significant ($p < 0.01$). The optimal model included 26 significant explanatory variables ($p < 0.05$); 10 of these were stroke profile, 5 considered kinematics at the catch of the stroke, 3 were kinematics at the occurrence of maximum handle force, 5 were kinematics at the finish, and 3 were kinematics recorded during the recovery, when the knees broke. These variables were input using the *Enter* automatic variable selection method into a new MREG analysis and the model residuals and predicted dependent variables were calculated. The assumptions of normality, constant variance, and linearity were assessed in the same way as described previously (Figure 9.5 and Figure 9.6). The output of the model is shown in Table 9.5.

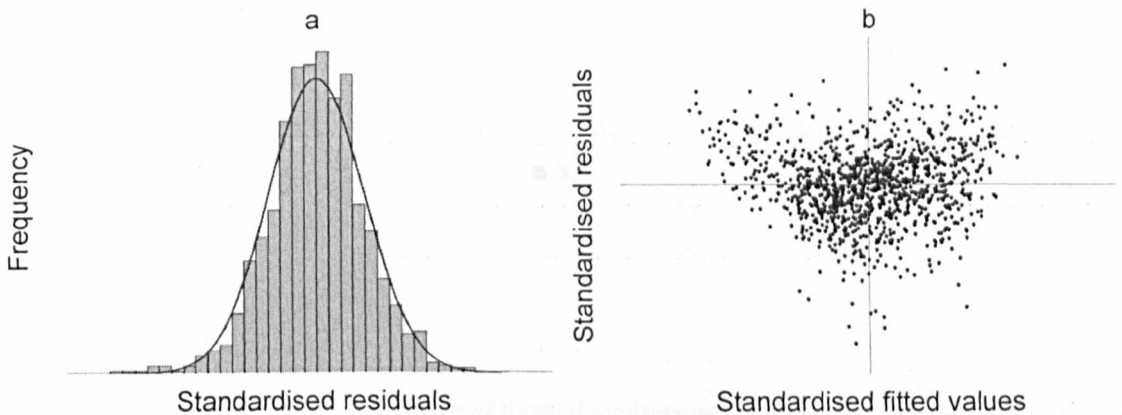


Figure 9.5: Assessment of the assumptions of normality and constant variance with respect to Slope of handle force

The frequency of the standardised residuals is plotted beneath a normal distribution curve (a); any departures from normal distribution may be deleterious to the validity of the MREG model. The standardised residuals are also plotted against the standardised fitted values (b); any funnelling effect of data along the X axis indicates that the assumption of constant variance may have been violated.

Figure 9.5 shows that the assumptions of normality and constant variance were adhered to in the current model. There is no funnelling effect present in the scatter plot concerning constant variance, thus the assumption of constant variance is met. Figure 9.6 does not show any trends between the model's explanatory variables and the standardised residuals; thus the assumption of linearity was satisfied in this case.

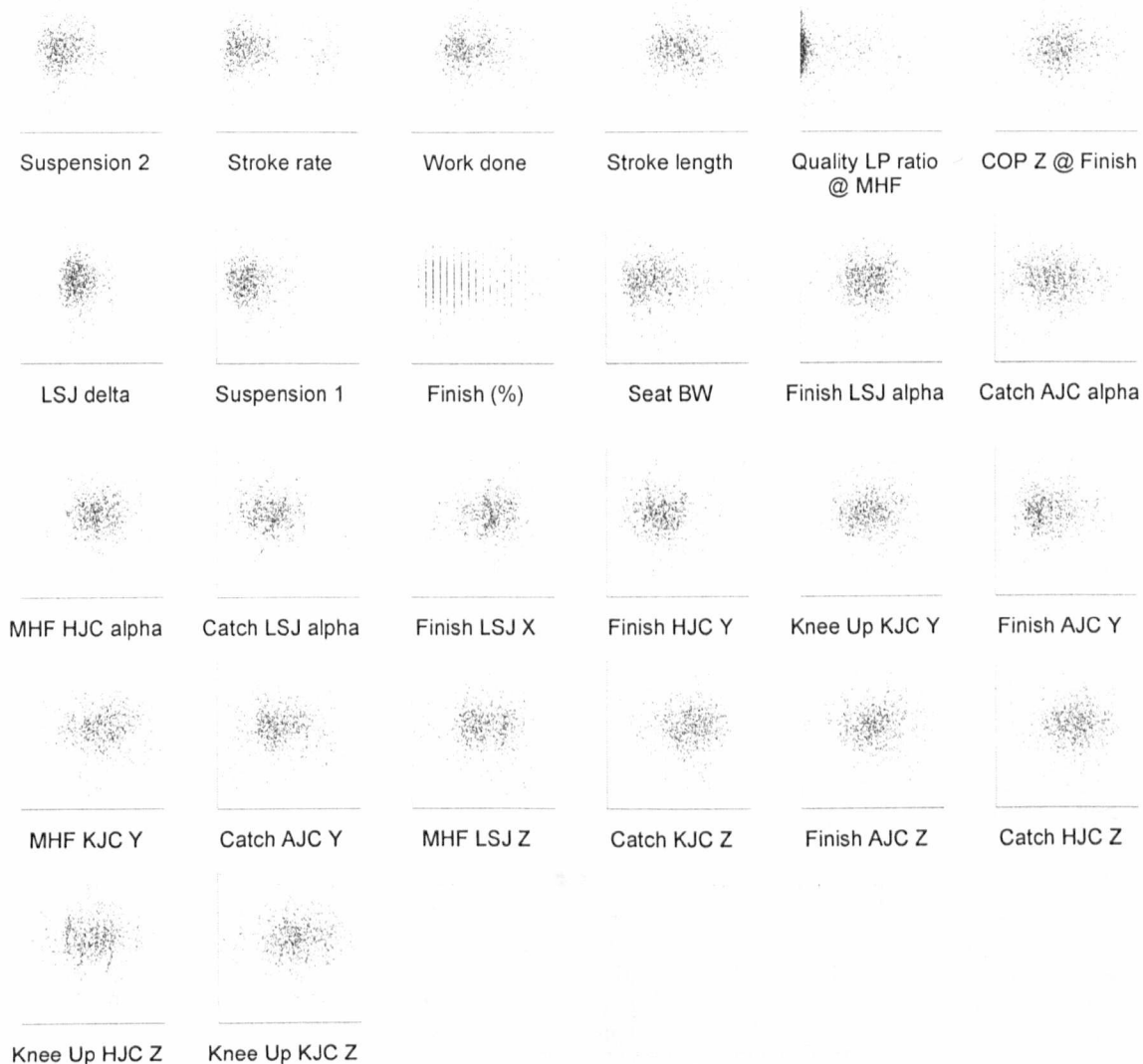


Figure 9.6: Assessment of the assumption of linearity with respect to Slope of handle force
 Each of the plots shows the relationship between a single explanatory variable and the MREG model standardised residuals. The X axes are labelled according to the appropriate independent variable. The Y axis is always the residuals. If no trend is apparent then the assumption of linearity is met.

Variable	Regression coefficients			t-test	
	Unstandardised	Standard error	Standardised	t	p
CONSTANT	-31.854	8.639		-3.687	.000
Suspension 2 (BW(s))	1.435	.052	.631	27.402	.000
Stroke rate (/min)	.713	.078	.307	9.099	.000
Work done (J)	.068	.002	.717	38.423	.000
Stroke length (mm)	-.029	.002	-.249	-14.847	.000
Quality LP ratio @ MHF	-.039	.011	-.032	-3.366	.001
COP Z @ Finish	-.043	.007	-.067	-6.109	.000
LSJ delta (°)	-.177	.032	-.062	-5.533	.000
Suspension 1 (BW(s))	-1.846	.113	-.237	-16.287	.000
Finish (%)	-2.965	.095	-1.171	-31.048	.000
Seat BW	-8.711	.600	-.185	-14.519	.000
Finish LSJ alpha	.117	.019	.126	6.077	.000
Catch AJC alpha	.115	.009	.190	12.810	.000
MHF HJC alpha	-.109	.012	-.164	-9.136	.000
Catch LSJ alpha	-.259	.022	-.285	-11.967	.000
Finish LSJ X	.030	.006	.053	5.177	.000
Finish HJC Y	.042	.005	.101	7.647	.000
Knee Up KJC Y	.034	.007	.067	5.044	.000
Finish AJC Y	-.023	.006	-.049	-3.923	.000
MHF KJC Y	-.046	.008	-.146	-5.466	.000
Catch AJC Y	-.077	.008	-.205	-9.837	.000
MHF LSJ Z	.077	.004	.422	18.333	.000
Catch KJC Z	.055	.006	.242	9.402	.000
Finish AJC Z	.027	.008	.057	3.556	.000
Catch HJC Z	-.043	.006	-.218	-7.531	.000
Knee Up HJC Z	-.053	.005	-.243	-9.984	.000
Knee Up KJC Z	-.068	.008	-.227	-8.099	.000

Table 9.5: The MREG calculated equation for Slope of handle force

The coefficients describe the direction and magnitude of the relationship between each explanatory variable and the dependent variable, the standard error of the unstandardised coefficients is also included, along with the t-statistic, and significance of the p-value for the t-test for each explanatory variable. The order of the variables is: equation constant, followed by stroke profile explanatory variables (sorted by the magnitude and direction of their unstandardised regression coefficient), rotational kinematics, X trajectory kinematics, Y trajectory kinematics, and finally Z trajectory kinematics. Kinematics are either measured at the catch of the stroke, at the point in the stroke when maximum handle force was being exerted (MHF), at the finish of the stroke, or at the point in the recovery when the knees started to rise (Knee Up).

The R^2 and adjusted R^2 values for this model were .936 and .934 respectively. This means that over 93% of the variability in the Slope of handle force during the first half of the drive phase can be accounted for by its relationship with the explanatory variables included in the regression model. In order to concentrate on the results regarding 3D kinematics, the stroke profile variables shown in the above table will be discussed in Section 9.4.1.9.

The results show that whilst only 1 kinematic variable in the X direction was found to be associated with increasing the slope of handle force production, there were 5 in the Y direction

and 6 in the Z direction. As might be expected, it appears that the way in which athletes move in the vertical and anterior/posterior directions is far more influential upon the rate of handle force production than is the way in which they move in the medial/lateral direction. Increases in the rate of force production through the handle occurred as the lumbar spine became more flexed at the catch of the stroke, was also associated with increased extension about LSJ at the finish, and with a more anterior position of LSJ in the middle of the drive phase. It was also noted that the rate of handle force production increased as the HJC was more flexed in the middle of the drive, was more superior at the finish, and more inferior at the catch of the stroke; recall that one method of increasing HJC flexion is to anteriorly rotate the pelvis. Increases in slope of handle force were linked with more anterior displacement of the KJC at the catch, and more posterior and superior displacement as the knees broke in the recovery. Slope also increased with greater plantar flexion at the catch, a more inferior AJC coordinate at the catch and the finish, and a more anterior coordinate at the finish; the results regarding the AJC at the finish are in line with coaching philosophy to “keep the heels down”.

9.4.1.3 Stroke length

66 of the explanatory variables were significantly related to Stroke length ($p < 0.05$). Because Work done was directly influenced by the motion of the ergometer handle it was decided that Work should not be included as a potential explanatory variable. The *Stepwise* MREG analysis suggested 54 possible equations whose adjusted R^2 values ranged from .297 to .842. The F-tests associated with all of these models were significant ($p < 0.01$). The optimal model included 36 significant explanatory variables ($p < 0.05$); 8 of these were stroke profile, 9 considered kinematics at the catch of the stroke, 5 were kinematics at the occurrence of maximum handle force, 8 were kinematics at the finish, and 6 were kinematics recorded during the recovery, when the knees broke. These variables were input using the *Enter* automatic variable selection method into a new MREG analysis and the model residuals and predicted dependent variables were calculated. The assumptions of normality, constant variance, and linearity were assessed in the same way as described previously (Figure 9.7 and Figure 9.8). The output of the model is shown in Table 9.6.

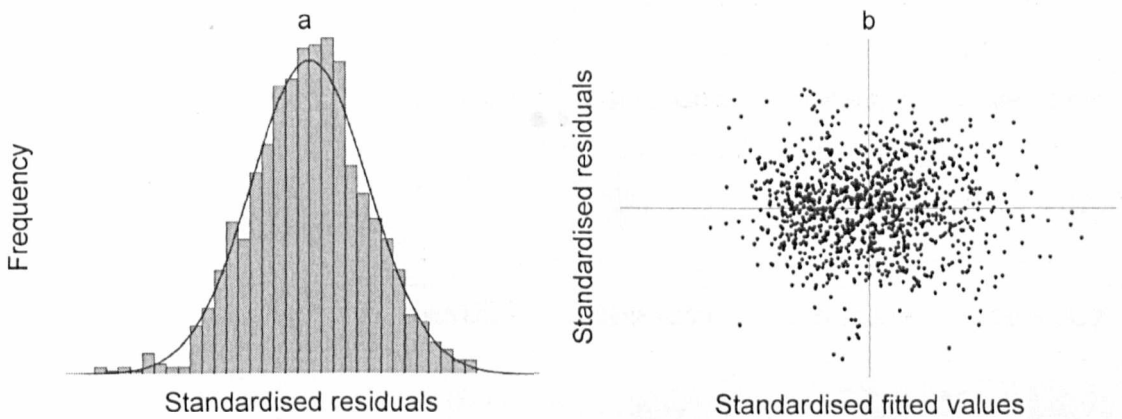


Figure 9.7: Assessment of the assumptions of normality and constant variance with respect to Stroke length

The frequency of the standardised residuals is plotted beneath a normal distribution curve (a); any departures from normal distribution may be deleterious to the validity of the MREG model. The standardised residuals are also plotted against the standardised fitted values (b); any funnelling effect of data along the X axis indicates that the assumption of constant variance may have been violated.

Figure 9.7 shows that the assumptions of normality and constant variance were adhered to in the current model. There is no funnelling effect present in the scatter plot concerning constant variance, thus the assumption of constant variance is met. Figure 9.8 does not show any trends between the model's explanatory variables and the standardised residuals; thus the assumption of linearity was satisfied in this case.

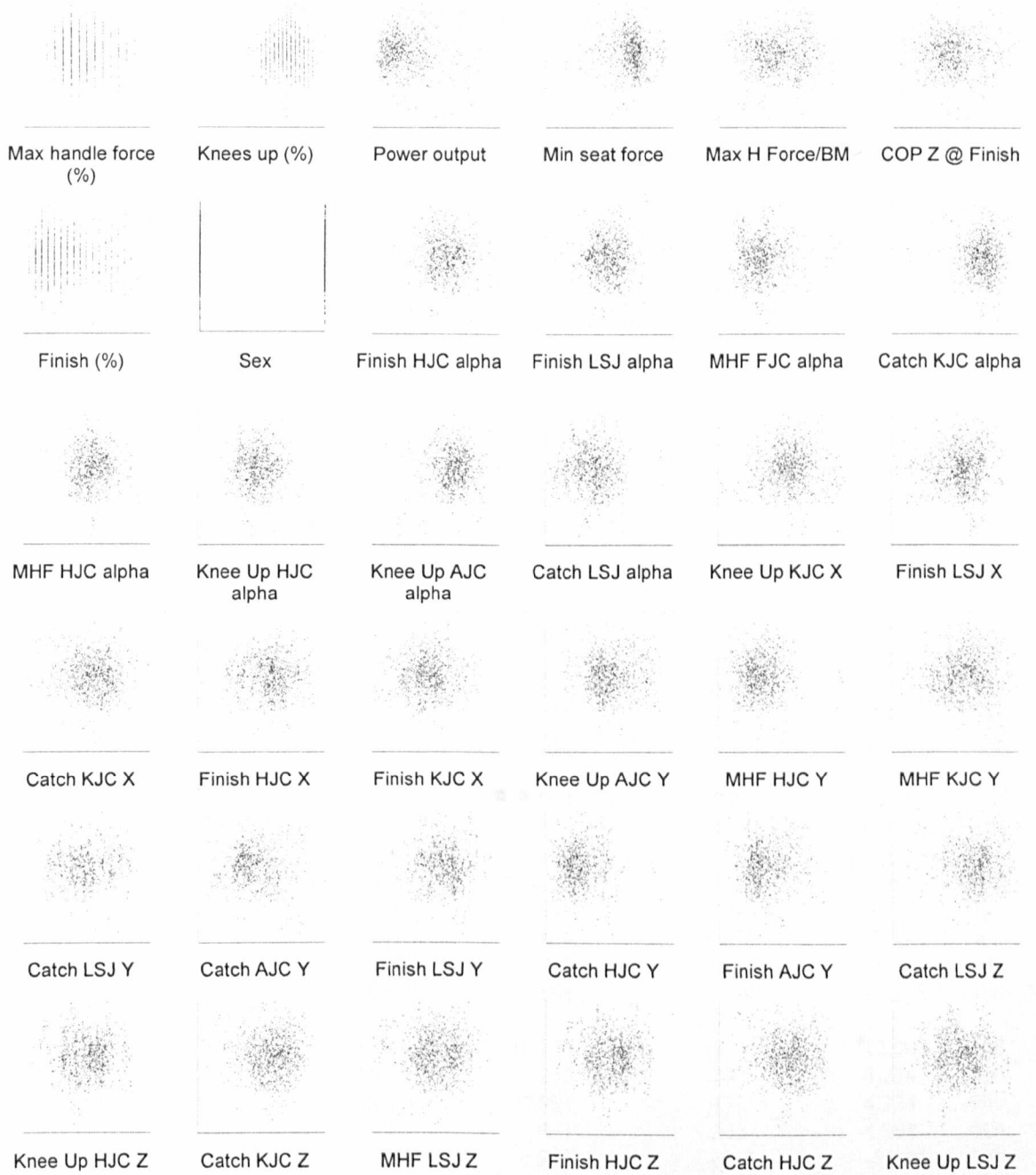


Figure 9.8: Assessment of the assumption of linearity with respect to Stroke length

Each of the plots shows the relationship between a single explanatory variable and the MREG model standardised residuals. The X axes are labelled according to the appropriate independent variable. The Y axis is always the residuals. If no trend is apparent then the assumption of linearity is met.

Variable	Regression coefficients			t-test	
	Unstandardised	Standard error	Standardised	t	p
(Constant)	1989.665	164.203		12.117	.000
Max handle force (%)	12.786	1.555	.400	8.222	.000
Knees up (%)	1.828	.529	.075	3.456	.001
Power output (W)	.519	.058	.412	8.951	.000
Min seat force (N)	.143	.018	.195	8.046	.000
Max H Force/BM (N/kg×100)	-.176	.015	-.301	-11.412	.000
COP Z @ Finish	-.536	.101	-.098	-5.328	.000
Finish (%)	-9.452	1.059	-.441	-8.923	.000
Sex	-28.213	4.572	-.158	-6.171	.000
Finish HJC alpha	4.518	.256	.694	17.647	.000
Finish LSJ alpha	3.237	.234	.412	13.844	.000
MHF FJC alpha	3.218	.585	.107	5.499	.000
Catch KJC alpha	1.065	.340	.088	3.128	.002
MHF HJC alpha	-1.691	.228	-.301	-7.409	.000
Knee Up HJC alpha	-2.843	.285	-.504	-9.978	.000
Knee Up AJC alpha	-3.222	.320	-.285	-10.065	.000
Catch LSJ alpha	-4.262	.286	-.554	-14.913	.000
Knee Up KJC X	1.414	.304	.161	4.651	.000
Finish LSJ X	.440	.101	.091	4.357	.000
Catch KJC X	.278	.045	.099	6.148	.000
Finish HJC X	-.293	.090	-.064	-3.246	.001
Finish KJC X	-2.381	.286	-.295	-8.317	.000
Knee Up AJC Y	4.108	.249	.868	16.491	.000
MHF HJC Y	1.527	.251	.414	6.075	.000
MHF KJC Y	.383	.086	.143	4.430	.000
Catch LSJ Y	-.409	.153	-.122	-2.679	.008
Catch AJC Y	-.626	.075	-.197	-8.377	.000
Finish LSJ Y	-1.199	.134	-.372	-8.953	.000
Catch HJC Y	-1.308	.278	-.361	-4.712	.000
Finish AJC Y	-1.558	.169	-.399	-9.214	.000
Catch LSJ Z	1.663	.139	.935	12.003	.000
Knee Up HJC Z	1.078	.255	.582	4.224	.000
Catch KJC Z	.341	.081	.177	4.224	.000
MHF LSJ Z	.311	.071	.203	4.388	.000
Finish HJC Z	-1.208	.205	-.642	-5.887	.000
Catch HJC Z	-1.375	.132	-.833	-10.383	.000
Knee Up LSJ Z	-1.515	.170	-.808	-8.894	.000

Table 9.6: The MREG calculated equation for Stroke length

The coefficients describe the direction and magnitude of the relationship between each explanatory variable and the dependent variable, the standard error of the unstandardised coefficients is also included, along with the t-statistic, and significance of the p-value for the t-test for each explanatory variable. The order of the variables is: equation constant, followed by stroke profile explanatory variables (sorted by the magnitude and direction of their unstandardised regression coefficient), rotational kinematics, X trajectory kinematics, Y trajectory kinematics, and finally Z trajectory kinematics. Kinematics are either measured at the catch of the stroke, at the point in the stroke when maximum handle force was being exerted (MHF), at the finish of the stroke, or at the point in the recovery when the knees started to rise (Knee Up).

The R^2 and adjusted R^2 values for this model were .847 and .842 respectively. This means that over 84% of the variability in Stroke length can be accounted for by its relationship with the

explanatory variables included in the regression model. In order to concentrate on the results regarding 3D kinematics, the stroke profile variables shown in the above table will be discussed in Section 9.4.1.9.

The results obtained concerning stroke length identified more kinematic variables than did MREG analysis for any of the other performance related dependent variables (Table 9.2, Page 191). Performance was improved by increasing lumbar flexion at the catch, lumbar extension at the finish, inferiorly displacing LSJ at the catch and finish, more anterior LSJ coordinates at the catch and in the middle of the drive, and more posterior LSJ coordinates in the second half of the stroke. Stroke length also improved with increased HJC flexion in the middle of the drive and during the recovery, decreased HJC flexion at the finish, a more inferior HJC coordinate at the catch, and a more superior in the first portion of the drive phase; this increase in vertical height in the early drive was probably induced by athletes suspending away from their seat, and was beneficial to stroke length. Increasing posterior displacement of HJC at the finish did increase stroke length, though perhaps more surprisingly a more anterior HJC coordinate at the catch did not. This may indicate that in order to achieve greater stroke length at the front of the stroke it is better to rotate about the pelvis and trunk about the hips rather than bring the hips forward and rotate the trunk anteriorly through the lumbar region. Improvements in stroke length also came with increased KJC flexion at the catch, a more lateral KJC at the catch, a more medial KJC at the finish of the stroke, increased superior displacement of KJC in the middle of the drive, and a more anterior position at the catch of the stroke. Stroke length was improved by decreasing plantar flexion during the recovery phase as the knees broke, and was associated with more inferior trajectories of AJC at the catch and the finish. In addition to this, in the middle of the drive it was found that stroke length could be increased by increased separation of the athletes' heels from the footstretcher.

9.4.1.4 Power output

75 potential explanatory variables were significantly related to Power output ($p < 0.05$). Power was directly influenced by Stroke rate, Work done, and the timing of maximum handle force, the finish, and knees up; none of these were included as independent variables in MREG models. The *Stepwise* analysis suggested 44 possible equations whose adjusted R^2 values ranged from .404 to .926. The F-tests associated with these models were significant ($p < 0.01$). The optimal model included 25 significant explanatory variables ($p < 0.05$); 11 were stroke profile, 5 considered kinematics at the catch of the stroke, 4 were kinematics at the occurrence of maximum handle force, 3 were kinematics at the finish, and 2 were kinematics recorded during the recovery, when the knees broke. These variables were input using the *Enter* automatic variable selection method into a new MREG analysis and the model residuals and predicted dependent variables were calculated. The assumptions of normality, constant variance, and linearity were assessed in the same way as described previously (Figure 9.9 and Figure 9.10). The output of the model is shown in Table 9.7.

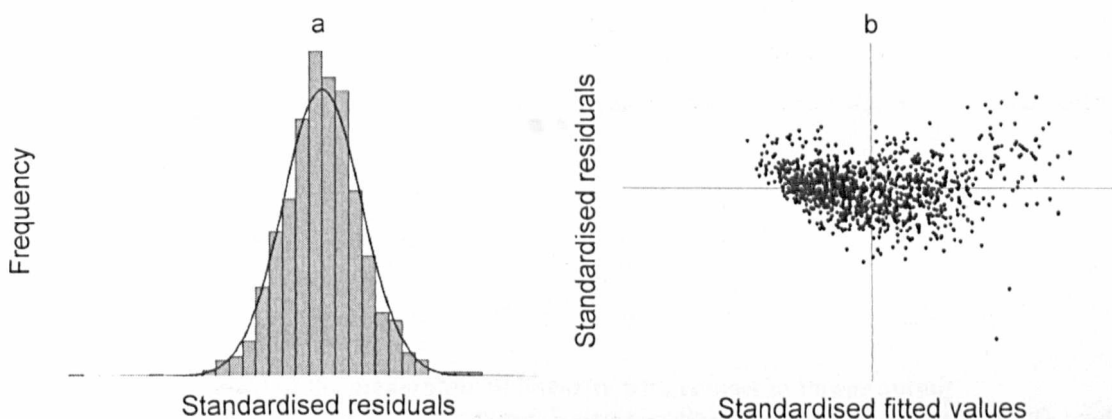


Figure 9.9: Assessment of the assumptions of normality and constant variance with respect to Power output

The frequency of the standardised residuals is plotted beneath a normal distribution curve (a); any departures from normal distribution may be deleterious to the validity of the MREG model. The standardised residuals are also plotted against the standardised fitted values (b); any funnelling effect of data along the X axis indicates that the assumption of constant variance may have been violated.

Figure 9.9 shows that the assumptions of normality and constant variance were adhered to in the current model. There is no funnelling effect present in the scatter plot concerning constant variance, thus the assumption of constant variance is met. Figure 9.10 does not show any trends between the model's explanatory variables and the standardised residuals; thus the assumption of linearity was satisfied in this case.

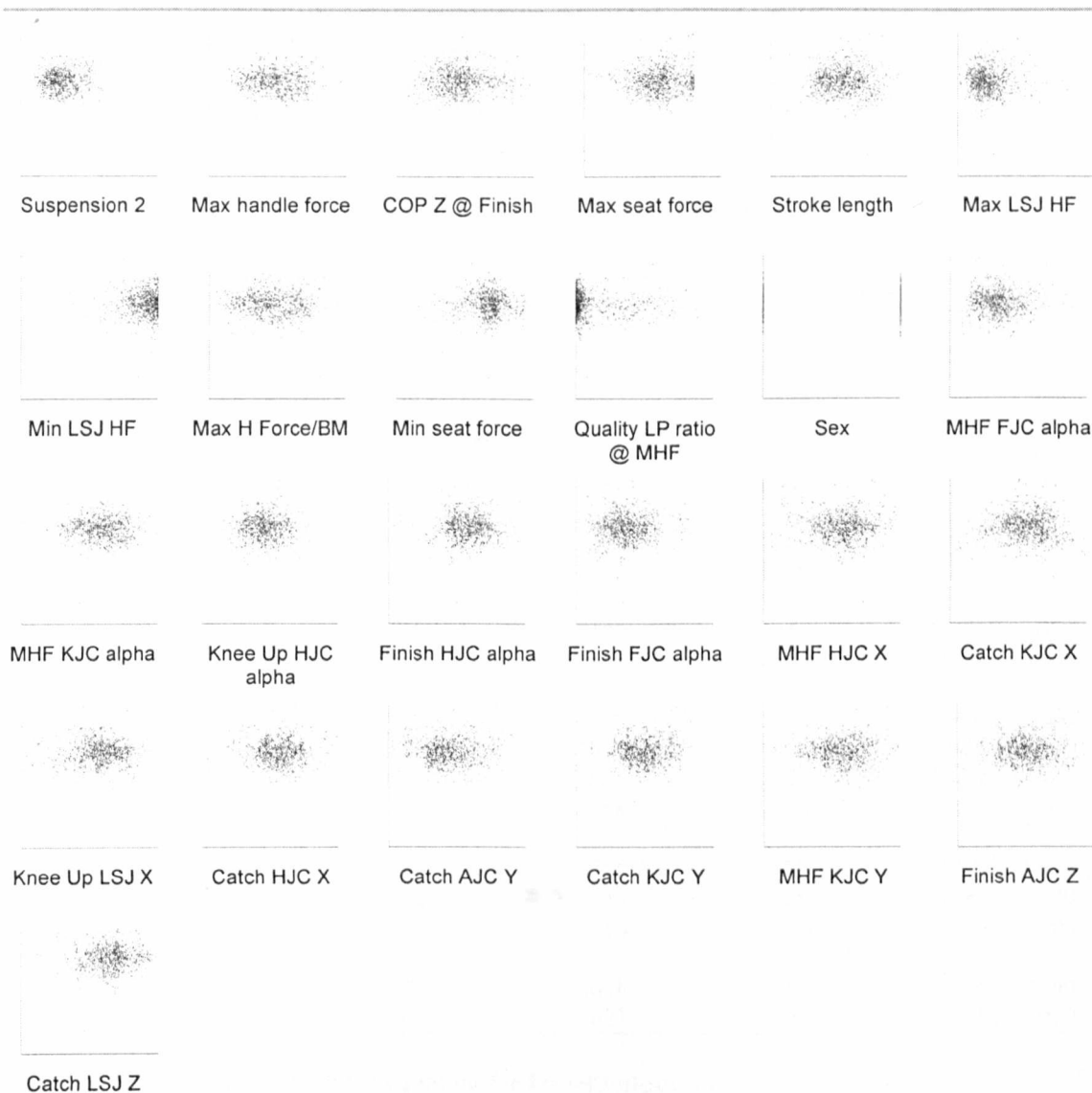


Figure 9.10: Assessment of the assumption of linearity with respect to Power output
 Each of the plots shows the relationship between a single explanatory variable and the MREG model standardised residuals. The X axes are labelled according to the appropriate independent variable. The Y axis is always the residuals. If no trend is apparent then the assumption of linearity is met.

Variable	Regression coefficients			t-test	
	Unstandardised	Standard error	Standardised	t	p
CONSTANT	-273.426	81.500		-3.355	.001
Suspension 2 (BW(s))	6.609	.235	.433	28.122	.000
Max handle force (N)	.368	.021	.545	17.154	.000
COP Z @ Finish	.353	.055	.081	6.450	.000
Max seat force (N)	.341	.025	.185	13.614	.000
Stroke length (mm)	.086	.012	.108	6.922	.000
Max LSJ HF	.000	.000	.059	5.640	.000
Min LSJ HF	.000	.000	-.026	-2.582	.010
Max H Force/BM (N/kg×100)	-.057	.015	-.122	-3.737	.000
Min seat force (N)	-.161	.009	-.277	-17.889	.000
Quality LP ratio @ MHF	-.351	.092	-.044	-3.822	.000
Sex	-5.867	2.437	-.041	-2.407	.016
MHF FJC alpha	1.150	.293	.048	3.923	.000
MHF KJC alpha	.614	.136	.074	4.527	.000
Knee Up HJC alpha	.607	.084	.136	7.208	.000
Finish HJC alpha	-.548	.100	-.106	-5.466	.000
Finish FJC alpha	-5.796	.545	-.139	-10.626	.000
MHF HJC X	.922	.130	.219	7.074	.000
Catch KJC X	.155	.025	.070	6.270	.000
Knee Up LSJ X	-.500	.063	-.104	-7.932	.000
Catch HJC X	-.644	.118	-.164	-5.457	.000
Catch AJC Y	.361	.045	.144	7.957	.000
Catch KJC Y	.172	.048	.085	3.569	.000
MHF KJC Y	-.452	.058	-.213	-7.729	.000
Finish AJC Z	.472	.036	.147	13.153	.000
Catch LSJ Z	-.265	.023	-.188	-11.361	.000

Table 9.7: The MREG calculated equation for Power output

The coefficients describe the direction and magnitude of the relationship between each explanatory variable and the dependent variable, the standard error of the unstandardised coefficients is also included, along with the t-statistic, and significance of the p-value for the t-test for each explanatory variable. The order of the variables is: equation constant, followed by stroke profile explanatory variables (sorted by the magnitude and direction of their unstandardised regression coefficient), rotational kinematics, X trajectory kinematics, Y trajectory kinematics, and finally Z trajectory kinematics. Kinematics are either measured at the catch of the stroke, at the point in the stroke when maximum handle force was being exerted (MHF), at the finish of the stroke, or at the point in the recovery when the knees started to rise (Knee Up).

The R^2 and adjusted R^2 values for this model were .914 and .912 respectively. This means that over 91% of the variability in Power output can be accounted for by its relationship with the explanatory variables included in the regression model. In order to concentrate on the results regarding 3D kinematics, the stroke profile variables shown in the above table will be discussed in Section 9.4.1.9.

Recall that in Chapter 1 it was stated that the majority of the force and power an athlete develops during their stroke should be generated by the legs, not the back and arms. The results in this section show that only 2 kinematic variables describing LSJ were associated with

improving power output: a decreased anterior coordinate at the catch, and displacement to the athletes' right during the recovery phase. This medial/lateral result is hard to explain. On the other hand, 12 kinematic variables associated with the level of power output by athletes described the motion of the main source of power generation: the legs. Increased performance was associated with decreased HJC flexion during the drive phase, increased HJC flexion at the finish, lateral displacement of HJC at the catch, and medial displacement in the middle of the drive. At the KJC, performance improved as the KJC became more flexed and inferior in the middle of the drive phase and as it was more medial and superior at the catch. A more superior AJC trajectory (heels raised from the footstretcher in the middle of the drive), and keeping the heels down in contact with the footstretcher at the finish were also linked with increasing stroke power.

9.4.1.5 Seat force and COP 1 (Seat 1)

Recall that this variable was a measure of the sum of the product of instantaneous seat force and instantaneous COP coordinate in the medial/lateral direction, between the catch and the occurrence of maximum handle force. 68 potential explanatory variables were significantly related to Seat 1 ($p < 0.05$). The *Stepwise* MREG analysis suggested 34 possible equations whose adjusted R^2 values ranged from .732 to .950. The F-tests associated with all of these models were significant ($p < 0.01$). The optimal model included 22 significant explanatory variables ($p < 0.05$); 12 were stroke profile, 3 considered kinematics at the catch of the stroke, 1 was for kinematics at the occurrence of maximum handle force, 4 were kinematics at the finish, and 2 were kinematics recorded during the recovery, when the knees broke. These variables were input using the *Enter* automatic variable selection method into a new MREG analysis and the model residuals and predicted dependent variables were calculated. The assumptions of normality, constant variance, and linearity were assessed (Figure 9.11 and Figure 9.12). The output of the model is shown in Table 9.8.

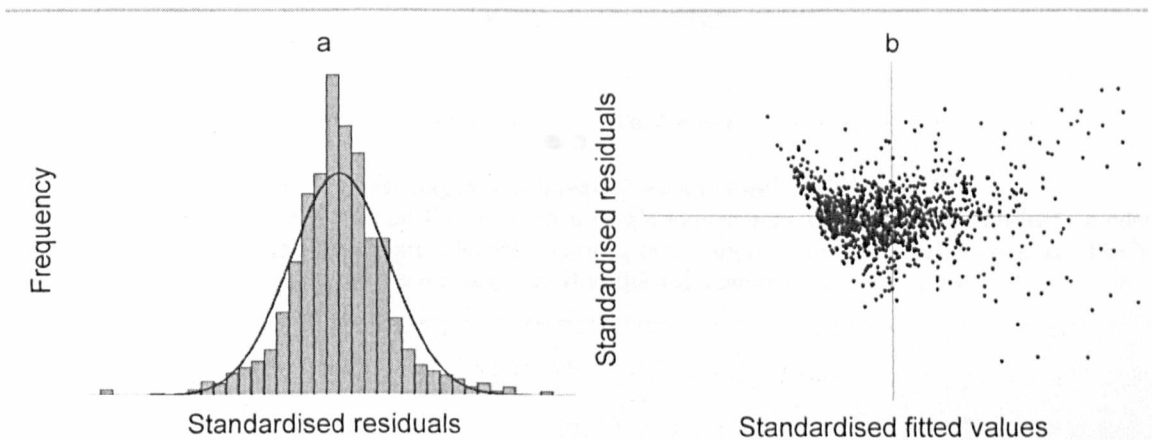


Figure 9.11: Assessment of the assumptions of normality and constant variance with respect to Seat 1

The frequency of the standardised residuals is plotted beneath a normal distribution curve (a); any departures from normal distribution may be deleterious to the validity of the MREG model. The standardised residuals are also plotted against the standardised fitted values (b); any funnelling effect of data along the X axis indicates that the assumption of constant variance may have been violated.

Figure 9.11 shows that the assumptions of normality and constant variance were adhered to in the current model. There is no funnelling effect present in the scatter plot concerning constant variance, thus the assumption of constant variance is met. Figure 9.12 does not show any trends between the model's explanatory variables and the standardised residuals; thus the assumption of linearity was satisfied in this case.

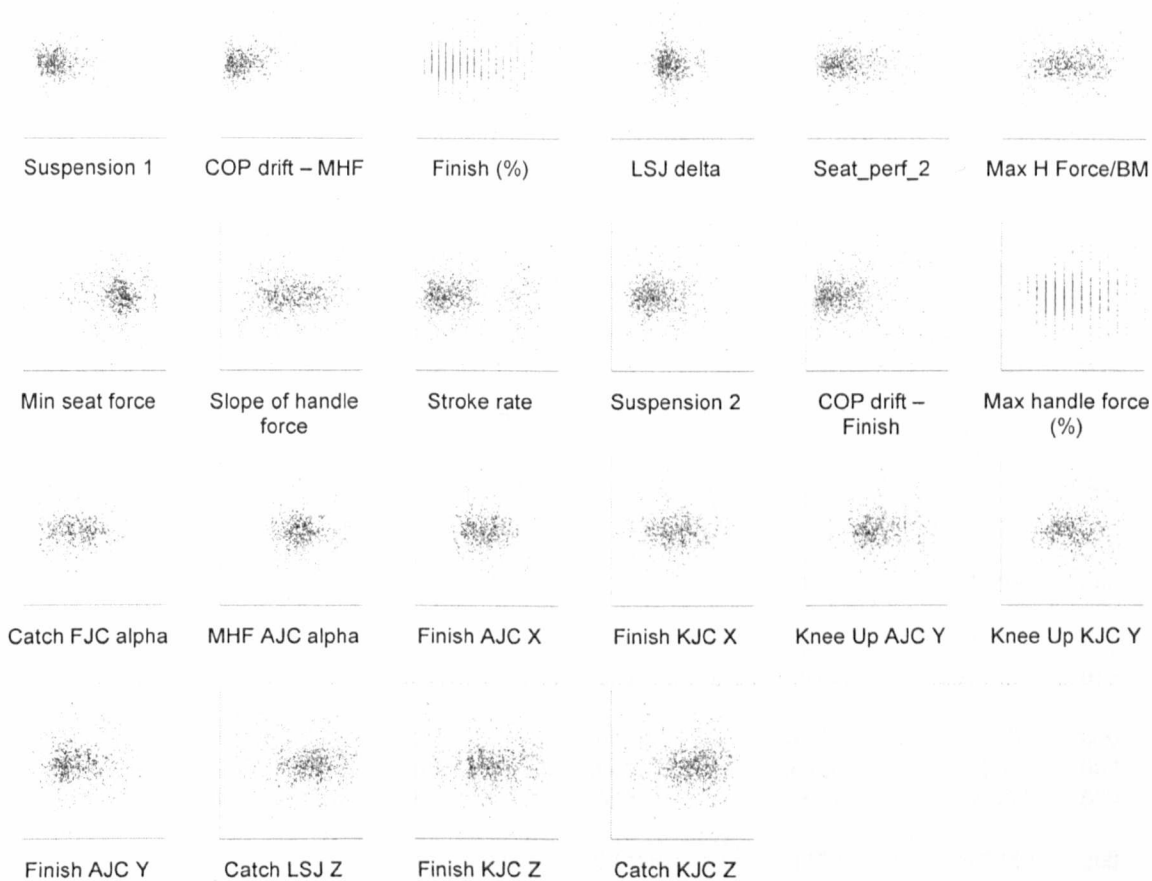


Figure 9.12: Assessment of the assumption of linearity with respect to Seat 1

Each of the plots shows the relationship between a single explanatory variable and the MREG model standardised residuals. The X axes are labelled according to the appropriate independent variable. The Y axis is always the residuals. If no trend is apparent then the assumption of linearity is met.

Variable	Regression coefficients			t-test	
	Unstandardised	Standard error	Standardised	t	p
CONSTANT	157.566	32.285		4.880	.000
Suspension 1 (BW(s))	9.340	.399	.409	23.418	.000
COP drift – MHF (mm)	3.308	.098	2.223	33.647	.000
Finish (%)	2.385	.300	.321	7.950	.000
LSJ delta (°)	.338	.064	.040	5.268	.000
Seat_perf_2	.303	.013	.666	22.919	.000
Max H Force/BM (N/kg×100)	.021	.004	.103	4.876	.000
Min seat force (N)	-.013	.003	-.052	-4.296	.000
Slope of handle force	-.256	.088	-.087	-2.916	.004
Stroke rate (/min)	-.494	.189	-.073	-2.620	.009
Suspension 2 (BW(s))	-1.551	.177	-.233	-8.762	.000
COP drift – Finish (mm)	-2.310	.109	-1.785	-21.226	.000
Max handle force (%)	-4.615	.394	-.417	-11.699	.000
Catch FJC alpha	.139	.054	.023	2.571	.010
MHF AJC alpha	-.086	.023	-.038	-3.796	.000
Finish AJC X	-.053	.016	-.026	-3.330	.001
Finish KJC X	-.053	.021	-.019	-2.476	.013
Knee Up AJC Y	.190	.032	.116	6.009	.000
Knee Up KJC Y	.062	.015	.042	4.203	.000
Finish AJC Y	-.221	.029	-.163	-7.655	.000
Catch LSJ Z	.072	.011	.117	6.725	.000
Finish KJC Z	-.049	.010	-.055	-5.106	.000
Catch KJC Z	-.096	.012	-.145	-8.266	.000

Table 9.8: The MREG calculated equation for Seat 1

The coefficients describe the direction and magnitude of the relationship between each explanatory variable and the dependent variable, the standard error of the unstandardised coefficients is also included, along with the t-statistic, and significance of the p-value for the t-test for each explanatory variable. The order of the variables is: equation constant, followed by stroke profile explanatory variables (sorted by the magnitude and direction of their unstandardised regression coefficient), rotational kinematics, X trajectory kinematics, Y trajectory kinematics, and finally Z trajectory kinematics. Kinematics are either measured at the catch of the stroke, at the point in the stroke when maximum handle force was being exerted (MHF), at the finish of the stroke, or at the point in the recovery when the knees started to rise (Knee Up).

The R^2 and adjusted R^2 values for this model were .951 and .950 respectively. This means that 95% of the variability in Seat 1 can be accounted for by its relationship with the explanatory variables included in the regression model. In order to concentrate on the results regarding 3D kinematics, the stroke profile variables shown in the above table will be discussed in Section 9.4.1.9.

As LSJ is displaced more superiorly at the catch the value of Seat 1 increases, that is, performance decreases. No links between performance measured via Seat 1 and the kinematics of the HJC were observed. It was noted that as the KJC was displaced more laterally and anteriorly at the finish, performance increased, as it did when the KJC was more anterior at the

catch and more inferior during the recovery. Performance also increased with greater plantar flexion during the drive phase, more medial and superior AJC locations at the finish, and more inferior when the knees broke during the recovery. Improvements in the value of Seat 1 were also associated with the heels separated less from the footstretcher at the catch of the stroke. This model is associating variables that occur at different points in the stroke that may be explained by considering that kinematics identified for the finish and when the knees broke were influential in that they allowed the athlete to set up the position in which they would arrive at the catch, and commence the next stroke.

9.4.1.6 Seat force and COP 2 (Seat 2)

Recall that this variable was a measure of the sum of the product of instantaneous seat force and instantaneous COP coordinate in the medial/lateral direction, between the catch and the finish. 58 potential explanatory variables were significantly related to Seat 2 ($p < 0.05$). The *Stepwise* MREG analysis suggested 34 possible equations whose adjusted R^2 values ranged from .581 to .969. The F-tests associated with these models were significant ($p < 0.01$). The optimal model included 26 significant explanatory variables ($p < 0.05$); 13 of these were stroke profile, none considered kinematics at the catch, 3 were kinematics at the occurrence of maximum handle force, 6 were kinematics at the finish, and 4 were kinematics recorded during the recovery, when the knees broke. These variables were input using the *Enter* automatic variable selection method into a new MREG analysis and the model residuals and predicted dependent variables were calculated. The assumptions of normality, constant variance, and linearity were assessed in the same way as described previously (Figure 9.13 and Figure 9.14). The output of the model is shown in Table 9.9.

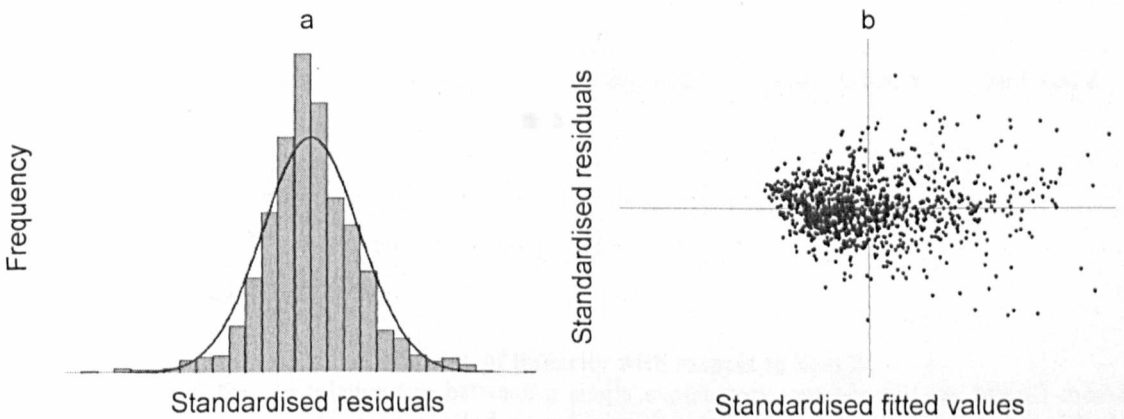


Figure 9.13: Assessment of the assumptions of normality and constant variance with respect to Seat 2

The frequency of the standardised residuals is plotted beneath a normal distribution curve (a); any departures from normal distribution may be deleterious to the validity of the MREG model. The standardised residuals are also plotted against the standardised fitted values (b); any funnelling effect of data along the X axis indicates that the assumption of constant variance may have been violated.

Figure 9.13 shows that the assumptions of normality and constant variance were adhered to in the current model. There is no funnelling effect present in the scatter plot concerning constant variance, thus the assumption of constant variance is met. Figure 9.14 does not show any trends between the model's explanatory variables and the standardised residuals; thus the assumption of linearity was satisfied in this case.

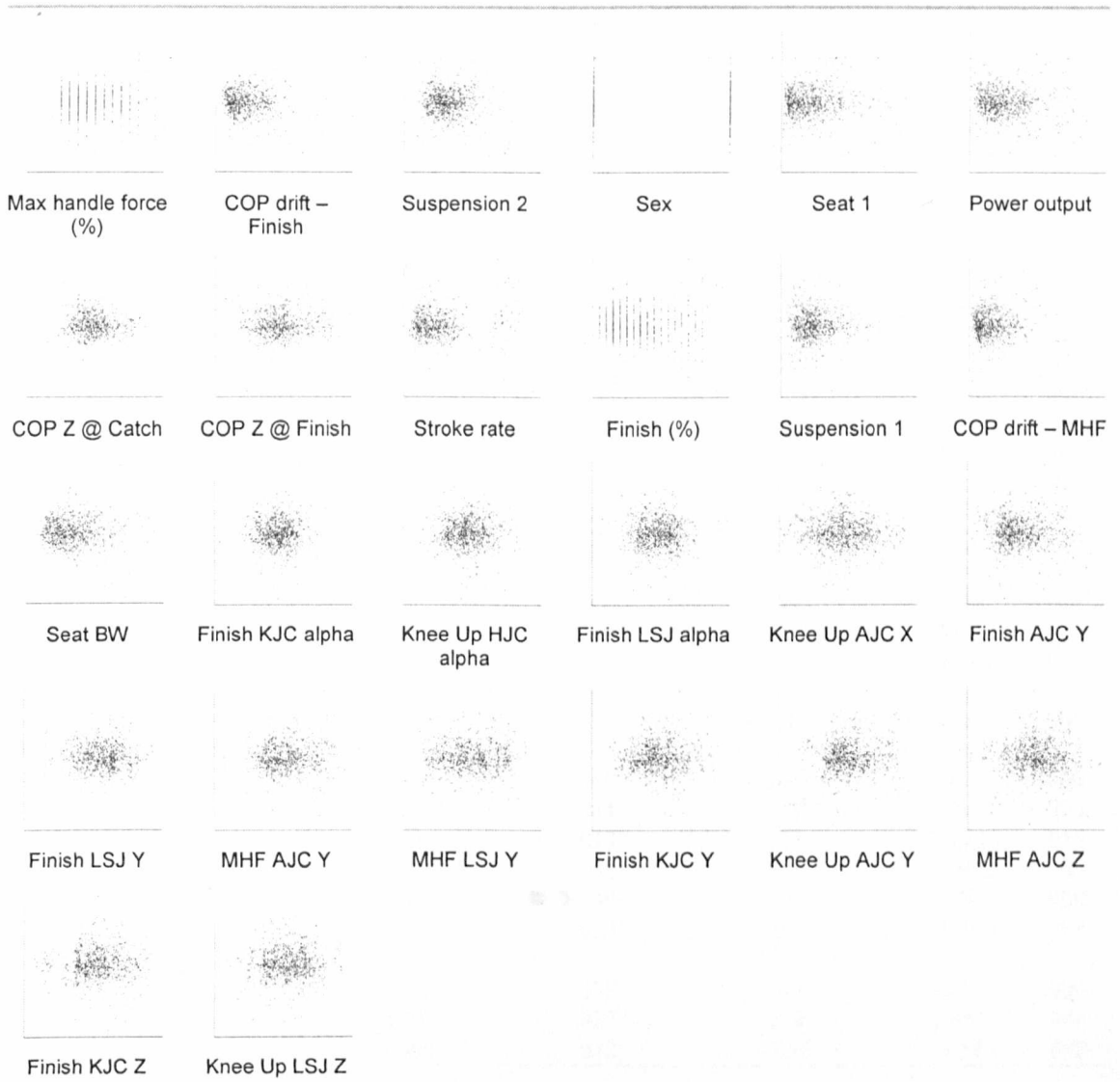


Figure 9.14: Assessment of the assumption of linearity with respect to Seat 2

Each of the plots shows the relationship between a single explanatory variable and the MREG model standardised residuals. The X axes are labelled according to the appropriate independent variable. The Y axis is always the residuals. If no trend is apparent then the assumption of linearity is met.

Variable	Regression coefficients			t-test	
	Unstandardised	Standard error	Standardised	t	p
CONSTANT	-326.657	56.249		-5.807	.000
Max handle force (%)	9.084	.408	.373	22.262	.000
COP drift – Finish (mm)	7.712	.062	2.713	124.478	.000
Suspension 2 (BW(s))	5.240	.321	.358	16.303	.000
Sex	4.691	1.460	.034	3.214	.001
Seat 1	.934	.043	.425	21.807	.000
Power output (W)	.069	.018	.072	3.771	.000
COP Z @ Catch	-.123	.022	-.037	-5.525	.000
COP Z @ Finish	-.128	.033	-.031	-3.944	.000
Stroke rate (/min)	-1.784	.349	-.119	-5.110	.000
Finish (%)	-5.660	.502	-.347	-11.268	.000
Suspension 1 (BW(s))	-6.331	.752	-.126	-8.416	.000
COP drift – MHF (mm)	-7.911	.088	-2.419	-90.191	.000
Seat BW	-27.947	2.837	-.092	-9.852	.000
Finish KJC alpha	.345	.126	.034	2.743	.006
Knee Up HJC alpha	-.106	.040	-.025	-2.638	.008
Finish LSJ alpha	-.213	.048	-.036	-4.409	.000
Knee Up AJC X	.175	.030	.037	5.756	.000
Finish AJC Y	.246	.050	.083	4.918	.000
Finish LSJ Y	.193	.041	.078	4.742	.000
MHF AJC Y	.071	.029	.025	2.422	.016
MHF LSJ Y	-.096	.033	-.037	-2.902	.004
Finish KJC Y	-.194	.040	-.062	-4.907	.000
Knee Up AJC Y	-.216	.057	-.060	-3.790	.000
MHF AJC Z	.164	.035	.047	4.671	.000
Finish KJC Z	.054	.027	.028	1.994	.046
Knee Up LSJ Z	-.080	.023	-.056	-3.534	.000

Table 9.9: The MREG calculated equation for Seat 2

The coefficients describe the direction and magnitude of the relationship between each explanatory variable and the dependent variable, the standard error of the unstandardised coefficients is also included, along with the t-statistic, and significance of the p-value for the t-test for each explanatory variable. The order of the variables is: equation constant, followed by stroke profile explanatory variables (sorted by the magnitude and direction of their unstandardised regression coefficient), rotational kinematics, X trajectory kinematics, Y trajectory kinematics, and finally Z trajectory kinematics. Kinematics are either measured at the catch of the stroke, at the point in the stroke when maximum handle force was being exerted (MHF), at the finish of the stroke, or at the point in the recovery when the knees started to rise (Knee Up).

The R^2 and adjusted R^2 values for this model were .969 and .969 respectively. This means that almost 97% of the variability in Seat 2 can be accounted for by its relationship with the explanatory variables included in the regression model. In order to concentrate on the results regarding 3D kinematics, the stroke profile variables shown in the above table will be discussed in Section 9.4.1.9.

Of the 13 kinematic variables identified as being related to performance variable Seat 2, 6 considered the vertical displacement of joint centres. This shows that, as one would expect,

when considering rowing performance in terms of COP displacement and seat forces, the way in which athletes accelerate their bodies vertically upwards and downwards is important. Performance improved with increasing lumbar extension at the finish, anterior displacement of LSJ during the recovery, additional inferior displacement of LSJ at the finish and, as one might expect a more superior LSJ trajectory during the drive phase. Performance was also improved by exhibiting less HJC flexion during the recovery phase. At the finish of the stroke additional KJC extension and posterior displacement was beneficial to performance. It was also noted that the way in which the AJC was displaced in the medial/lateral direction, the anterior/posterior direction, and more importantly the vertical direction could improve performance measured by Seat 2.

9.4.1.7 Minimum seat force and bodyweight (Seat BW)

Recall that this variable was a measure of the difference between the minimum seat force (normalised using body mass) and the athletes' bodyweight. 75 potential explanatory variables were significantly related to Seat 2 ($p < 0.05$). Min seat force and BW were not included as explanatory variables because the calculation of *Seat BW* was directly influenced by them. *Stepwise* MREG analysis suggested 72 possible equations whose adjusted R^2 values ranged from .339 to .848. The F-tests associated with these models were significant ($p < 0.01$). The optimal model included 39 significant explanatory variables ($p < 0.05$); 13 were stroke profile, 3 considered kinematics at the catch, 6 were kinematics at maximum handle force, 6 were kinematics at the finish, and 11 were kinematics recorded when the knees broke. These variables were input using *Enter* automatic variable selection into a new MREG analysis and the model residuals and predicted dependent variables were calculated. The assumptions of normality, constant variance, and linearity were assessed (Figure 9.15 and Figure 9.16). The output of the model is shown in Table 9.10.

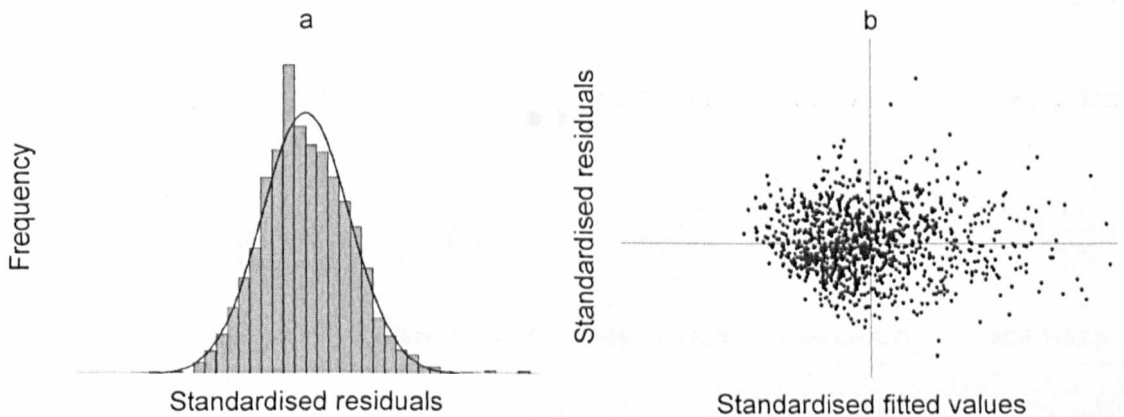


Figure 9.15: Assessment of the assumptions of normality and constant variance with respect to Seat BW

The frequency of the standardised residuals is plotted beneath a normal distribution curve (a); any departures from normal distribution may be deleterious to the validity of the MREG model. The standardised residuals are also plotted against the standardised fitted values (b); any funnelling effect of data along the X axis indicates that the assumption of constant variance may have been violated.

Figure 9.15 shows that the assumptions of normality and constant variance were adhered to in the current model. There is no funnelling effect present in the scatter plot concerning constant variance, thus the assumption of constant variance is met. Figure 9.16 does not show any trends between the model's explanatory variables and the standardised residuals; thus the assumption of linearity was satisfied in this case.

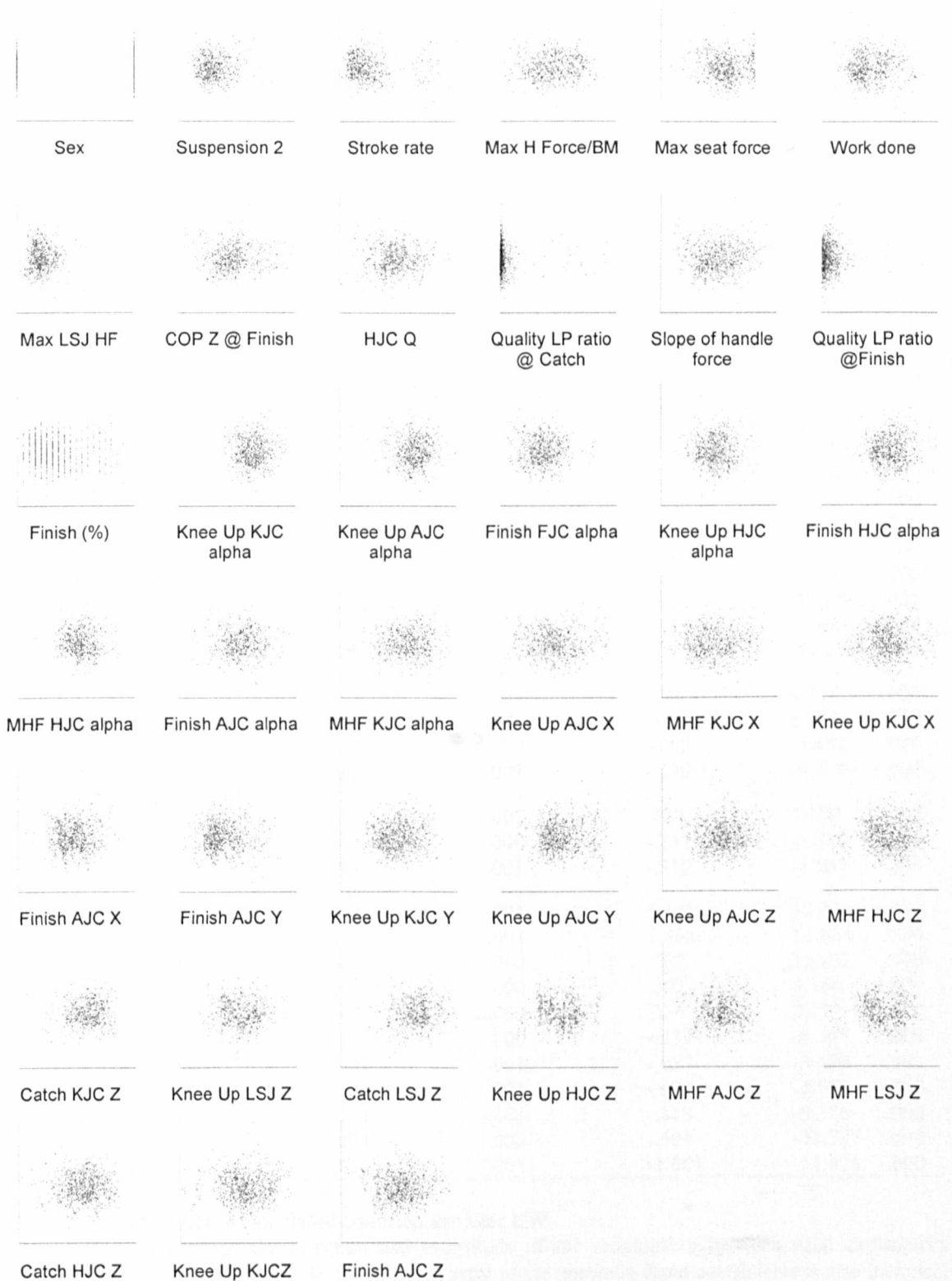


Figure 9.16: Assessment of the assumption of linearity with respect to Seat BW

Each of the plots shows the relationship between a single explanatory variable and the MREG model standardised residuals. The X axes are labelled according to the appropriate independent variable. The Y axis is always the residuals. If no trend is apparent then the assumption of linearity is met.

Variable	Regression coefficients			t-test	
	Unstandardised	Standard error	Standardised	t	p
CONSTANT	1.277	.594		2.150	.032
Sex	.112	.011	.251	10.118	.000
Suspension 2 (BW(s))	.049	.002	1.018	27.221	.000
Stroke rate (/min)	.035	.003	.719	13.369	.000
Max H Force/BM (N/kg×100)	.001	.000	.557	14.991	.000
Max seat force (N)	.001	.000	.146	7.113	.000
Work done (J)	.001	.000	.419	11.053	.000
Max LSJ HF	.000	.000	.037	2.317	.021
COP Z @ Finish	-.001	.000	-.044	-2.595	.010
HJC Q	-.002	.000	-.056	-3.923	.000
Quality LP ratio @ Catch	-.002	.001	-.038	-2.325	.020
Slope of handle force	-.019	.001	-.897	-17.497	.000
Quality LP ratio @Finish	-.041	.011	-.051	-3.797	.000
Finish (%)	-.089	.004	-1.661	-23.417	.000
Knee Up KJC alpha	.024	.002	.672	13.400	.000
Knee Up AJC alpha	.016	.002	.550	7.058	.000
Finish FJC alpha	.012	.003	.089	3.637	.000
Knee Up HJC alpha	.005	.001	.352	8.584	.000
Finish HJC alpha	.004	.001	.257	6.525	.000
MHF HJC alpha	-.009	.001	-.608	-11.860	.000
Finish AJC alpha	-.013	.002	-.579	-6.160	.000
MHF KJC alpha	-.021	.002	-.784	-12.830	.000
Knee Up AJC X	.003	.001	.191	4.110	.000
MHF KJC X	.001	.000	.113	6.915	.000
Knee Up KJC X	-.002	.000	-.068	-4.482	.000
Finish AJC X	-.003	.001	-.230	-4.778	.000
Finish AJC Y	.004	.001	.420	3.100	.002
Knee Up KJC Y	-.003	.000	-.238	-6.330	.000
Knee Up AJC Y	-.004	.001	-.310	-2.667	.008
Knee Up AJC Z	.011	.001	1.126	12.313	.000
MHF HJC Z	.007	.001	1.868	11.664	.000
Catch KJC Z	.002	.000	.507	11.855	.000
Knee Up LSJ Z	.002	.000	.342	4.364	.000
Catch LSJ Z	.001	.000	.336	3.777	.000
Knee Up HJC Z	-.002	.000	-.537	-6.167	.000
MHF AJC Z	-.002	.001	-.157	-3.479	.001
MHF LSJ Z	-.002	.001	-.639	-4.521	.000
Catch HJC Z	-.003	.000	-.813	-9.526	.000
Knee Up KJCZ	-.004	.000	-.604	-11.707	.000
Finish AJC Z	-.010	.001	-1.001	-11.625	.000

Table 9.10: The MREG calculated equation for Seat BW

The coefficients describe the direction and magnitude of the relationship between each explanatory variable and the dependent variable, the standard error of the unstandardised coefficients is also included, along with the t-statistic, and significance of the p-value for the t-test for each explanatory variable. The order of the variables is: equation constant, followed by stroke profile explanatory variables (sorted by the magnitude and direction of their unstandardised regression coefficient), rotational kinematics, X trajectory kinematics, Y trajectory kinematics, and finally Z trajectory kinematics. Kinematics are either measured at the catch of the stroke, at the point in the stroke when maximum handle force was being exerted (MHF), at the finish of the stroke, or at the point in the recovery when the knees started to rise (Knee Up).

The R^2 and adjusted R^2 values for this model were .853 and .848 respectively. This means that approximately 85% of the variability in Seat 2 can be accounted for by its relationship with the explanatory variables included in the regression model. In order to concentrate on the results regarding 3D kinematics, the stroke profile variables shown in the above table will be discussed in Section 9.4.1.9.

After stroke length, this performance variable was linked with more kinematic parameters than any other. This suggests that modifying the way athletes move may surely be used to improve their performance. Performance increased as athletes displaced LSJ more posteriorly at the catch, and as the knees broke during the recovery, though more anteriorly in the middle of the drive. It was also desirable to exhibit more anterior displacement of the hips at the catch, and at knees up, though was better to posteriorly displace HJC mid-drive. Increased HJC flexion at the finish, and decreased HJC flexion during the drive was also beneficial to performance as measured by Seat BW. Additional KJC flexion during the drive, and keeping the knees down for longer during the recovery was useful in increasing performance, as was displacing the KJC more posteriorly at the catch, more laterally during the drive, and more medially, superiorly and anteriorly during the recovery. For the AJC, increased plantar flexion at the finish, and some dorsi flexion during the recovery was beneficial, as was adopting a more anterior trajectory during the drive, a more medial, inferior and anterior trajectory at the finish, and a more lateral, superior and posterior trajectory during the recovery. The association of FJC alpha and Seat BW again showed the benefit to performance of keeping the heels down at the finish of the stroke.

9.4.1.8 Summary regarding 3D kinematics and performance

Of the 68 potential explanatory variables that described 3D kinematics (Table 9.1), 58 were included in at least one of the optimal MREG equations described thus far. Furthermore, of these 58 variables, 9 were found, that if modified, had an improving effect on at least 3 separate performance predicting variables. That is, 9 variables were identified that were associated with multiples measures of athletic performance (Table 9.11).








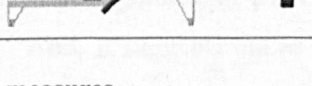
Explanatory kinematic variable	Linked with performance predicting variables	Favourable motion for performance gains
Catch LSJ Z	Finish timing Power output Seat 1 Seat BW	
MHF LSJ Z	Finish timing Slope of handle force Stroke length Seat BW	
Finish LSJ alpha	Slope of handle force Stroke length Seat 2	Increased lumbar extension
Knee Up LSJ Z	Finish timing Stroke length Seat BW	
Catch KJC Z	Finish timing Slope of handle force Stroke length Seat 2	
MHF KJC Y	Finish timing Slope of handle force Power output	
Finish AJC Y	Slope of handle force Stroke length Seat 2 Seat BW	
Finish AJC Z	Slope of handle force Power output Seat BW	
Knee Up AJC Y	Stroke length Seat 2 Seat BW	

Table 9.11: Kinematic variables linked with multiple performance measures

When an athlete's LSJ was located less anteriorly at the catch and more anteriorly whilst maximum handle force was being exerted, his performance improved, as measured by four separate variables. In addition to this, when athletes extended the lumbar spine at the finish of the stroke, or when they exhibited additional posterior displacement of LSJ in the recovery of the stroke when the knees broke, performance improved according to three separate measures. All of these relationships recommend against athletes adopting any kyphotic poses at any point in the stroke. It was also found that additional anterior displacement of the KJC at the catch,

could improve the scores of four performance variables, and that additional inferior displacement of the KJC in the middle of the drive could improve the scores of three performance parameters. At the finish of the stroke, as the AJC was positioned more inferiorly and anteriorly athletes performance improved in terms of up to five measured performance indicators; this is in line with the coaching principle to keep the heels in contact with the footstretcher at the finish of the stroke. It was also found that when an athlete's AJC was more superior as the knees broke in the recovery phase, three performance variables improved.

Recall that in Section 9.1.1 it was stated that there is some debate as to what is the best practice considering the rate of handle force production and rowing performance; the results presented here suggest that a faster rate of handle force production is favourable for performance measures alone. This would need to be investigated in terms of injury measures to make any definitive statements. In addition to the variables described above, there were three others, that although associated with power output and at least two other performance predicting variables, disagreed on the effect that changing them would have on performance as measured by power output or any of the other variables. For example, it was found that if the level of HJC flexion at the finish was decreased, the duration of the drive would be longer, and the stroke length would be longer, however there was also a small decrease in power output. This suggests that depending on the particular performance variable that is most important to an athlete, different interventions regarding modifications to the way in which movement is executed are appropriate.

9.4.1.9 Relationships between dependent variables, and other stroke profile variables linked with improving performance

During the drive female athletes exhibited wider handle force profiles than male athletes (Table 9.4). However they also performed shorter and less powerful strokes than their male counterparts (Table 9.6 and Table 9.7). Female athletes also scored higher for the variables Seat 2 and Seat BW (Table 9.9 and Table 9.10); this means that the magnitude of peak force exerted on the seat by females was greater than that for males. And, it suggests males either suspended more completely from the seat during the drive phase, or displaced their COP less medial/laterally. Figure 6.5 (Section 6.3.1) showed that LWM actually displaced their COP more medial/laterally than the majority of females, therefore it is likely that the current association reflects increased suspension by males.

Increases in stroke rate were associated with an increased rate of force production, and decreases in the product of medial/lateral COP trajectory and seat forces during the drive (Table 9.5, Table 9.8, and Table 9.9). However, increased stroke rate was also linked with greater peaks in the downward forces exerted on the seat (Table 9.10). This, in combination

with the result shown in Figure 6.5 (Section 6.3.1); that medial/lateral COP trajectory increases with intensity; may suggest that contact with the seat during the first half of the drive decreases as stroke rate increases, but also that athletes' bodyweight is then returned to the seat with higher acceleration causing increasing magnitudes of seat force peaks around the finish of the stroke. Some of these relationships were also observed for the seat variables relative to the timing of maximum handle force, the finish, and knees up (Table 9.4, Table 9.8, Table 9.9, and Table 9.10).

Peak handle force, normalised by body mass was associated with improved performance by increasing the duration of the drive, and improving power output (Table 9.4 and Table 9.7). Performance deteriorated in terms of stroke length as peak handle forces increased (Table 9.6). Increases in peak handle force were also related to poorer performance as measured by the variables Seat 1, Seat 2, and Seat BW (Table 9.8, Table 9.9, and Table 9.10). As the slope of handle force increased, performance measured by Seat 1 was improved (Table 9.8); this was possibly linked with increased suspension during the drive. Indeed MRERG analysis also showed that as the rate of handle force production increased, so did the magnitude of suspension during the first half of the drive phase (Table 9.5). The rate of force production was negatively related to increases in stroke length (Table 9.5). Power output increased with delays in the timing of the finish, and was linked with increased stroke length (Table 9.4, Table 9.6, Table 9.7). However the product of medial/lateral COP trajectory and seat forces during the drive phase (Seat 2) also increased with greater power output (Table 9.9).

Performance measured by the width of the force profile (Finish timing) was positively affected by greater suspension during the first half of the drive, though negatively affected by greater suspension during the second half of the drive (Table 9.4). As stated previously, the rate of handle force production improved with greater suspension during the first half of the drive, however the opposite was true considering the magnitude of suspension during the entire drive phase (Table 9.5). Measurement of performance via variables Seat 1 and Seat 2 improved and deteriorated respectively as the magnitude of suspension during the first half of the drive increased; again, the opposite was true considering suspension during the whole drive phase (Table 9.8 and Table 9.9). In keeping with this; power output improved as the magnitude of suspension during the whole drive decreased (Table 9.7), and also improved with an increase in the maximum seat force recorded, that is the minimum downwards force, or the greatest level of instantaneous suspension (Table 9.7). These results suggest that it is beneficial to performance to suspend as far as possible during the initial portion of the drive phase, but that it is desirable to suspend less during the second half of the drive. This could be explained by the athletes ability to remain balanced whilst suspended as they generate the highest propulsive forces, and their body's centre of mass is forward of the seat; on the other hand they may find better balance

and thus performance in the second half of the drive by increasing their base of support on the seat as propulsive, stabilising forces become less and the body centre of mass moves posteriorly.

As stated above; during the first half of the drive phase; lower magnitudes of the least downward force exerted on the seat were associated with increased power output (Table 9.7). Concurrently, as the magnitude of the greatest downwards force on the seat became more, performance was improved; by a wider force profile and increased power output, however, there was also a negative effect on stroke length (Table 9.4, Table 9.6, and Table 9.7). It is not thought that this is necessarily a causal relationship, but rather that the MREG models merely reflected what athletes did in the current study. Unlike the relationship noted above; that increasing reliance on a seat base of support during the late drive is beneficial to performance, it is not thought that very large, sharp downward peaks in seat force would be beneficial to increasing the bow-wards velocity of a rowing boat.

Considering the trajectory of COP in the anterior/posterior direction; there was some evidence to suggest a reduction in power output associated with a more posterior COP coordinate at the finish (Table 9.7). However, MREG analysis also showed that a more posterior coordinate at the finish was associated with a wider force profile, an increase in the rate of handle force production, a longer rowing stroke, and improvements in performance as measured by variables Seat 2 and Seat BW (Table 9.4, Table 9.5, Table 9.6, Table 9.9, and Table 9.10).

Other results showed that improvements in the rate of handle force production were linked with increases in the work done during the stroke (Table 9.5). And, as would be expected, improvements in performance variable Seat 1 were strongly influenced by the magnitude of suspension achieved during the early drive phase, and the level of COP medial/lateral displacement (Table 9.8); the standardised coefficients shown in Table 9.8 show that control of the displacement of COP was more influential on Seat 1 than suspension was.

The statistical tests conducted in this chapter also show that improving performance by exhibiting a wider handle force profile, producing handle force more quickly during the drive, and increasing power output are all associated with increased alignment of the PELVIS and BACK at the catch and during the drive phase as peak handle forces are exerted (Table 9.4, Table 9.5, and Table 9.7). Furthermore, power output was found to be linked to the rate of change of LSJ alpha during the drive phase (Table 9.7). Due to the very large range in values recorded for Max LSJ HF and Min LSJ HF, the unstandardised coefficients shown in Table 9.7, at three decimal places, do not appear to be relevant to the model. However the standardised

coefficients show that increased power was linked to higher Max LSJ HF scores and lower Min LSJ HF scores, this relationship is discussed more fully in Sections 9.4.2.2 and 9.5.

9.4.2 Concerning injury

In this section the results of MREG analysis conducted upon the four injury related dependent variables are presented (Table 9.2, Page 191). For each variable the results of reducing the number of potential explanatory variables through correlation analyses precede details of the MREG analysis.

9.4.2.1 Change in flexion/extension about LSJ during the drive phase

54 of the original 97 potential explanatory variables were significantly related to LSJ delta ($p < 0.05$). Because LSJ delta was directly influenced by LSJ alpha at the catch and at the point in the stroke when maximum handle force was being exerted, these two variables were not included as potential explanatory variables. The *Stepwise* MREG analysis suggested 41 possible equations whose adjusted R^2 values ranged from .362 to .745. The F-tests associated with all of these models were significant ($p < 0.01$). The optimal model included 26 significant explanatory variables ($p < 0.05$); 9 of these were stroke profile, 4 considered kinematics at the catch of the stroke, 8 were kinematics at the occurrence of maximum handle force, 2 were kinematics at the finish, and 3 were kinematics recorded during the recovery, when the knees broke. These variables were input using the *Enter* automatic variable selection method into a new MREG analysis and the model residuals and predicted dependent variables were calculated. The assumptions of normality, constant variance, and linearity were assessed in the same way as described previously (Figure 9.17 and Figure 9.18). The output of the model is shown in Table 9.12.

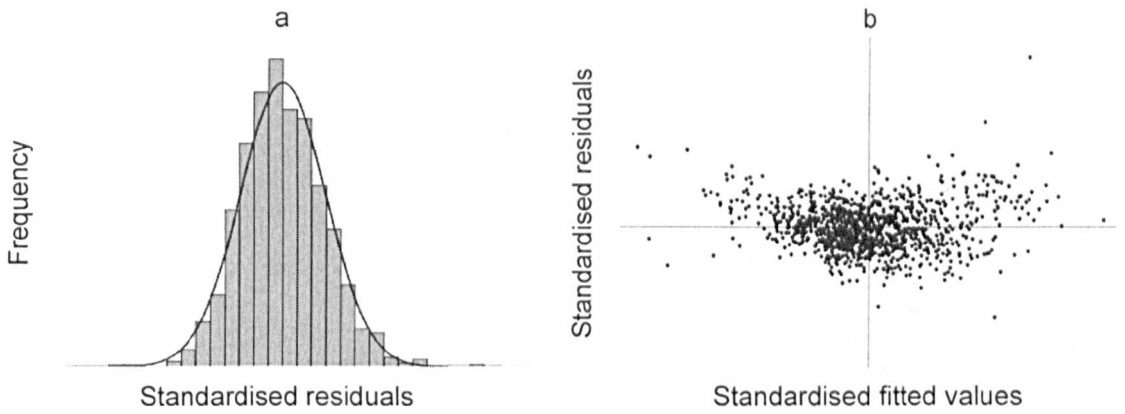


Figure 9.17: Assessment of the assumptions of normality and constant variance with respect to LSJ delta

The frequency of the standardised residuals is plotted beneath a normal distribution curve (a); any departures from normal distribution may be deleterious to the validity of the MREG model. The standardised residuals are also plotted against the standardised fitted values (b); any funnelling effect of data along the X axis indicates that the assumption of constant variance may have been violated.

Figure 9.17 shows that the assumptions of normality and constant variance were adhered to in the current model. There is no funnelling effect present in the scatter plot concerning constant variance, thus the assumption of constant variance is met. Figure 9.18 does not show any trends between the model's explanatory variables and the standardised residuals; thus the assumption of linearity was satisfied in this case.

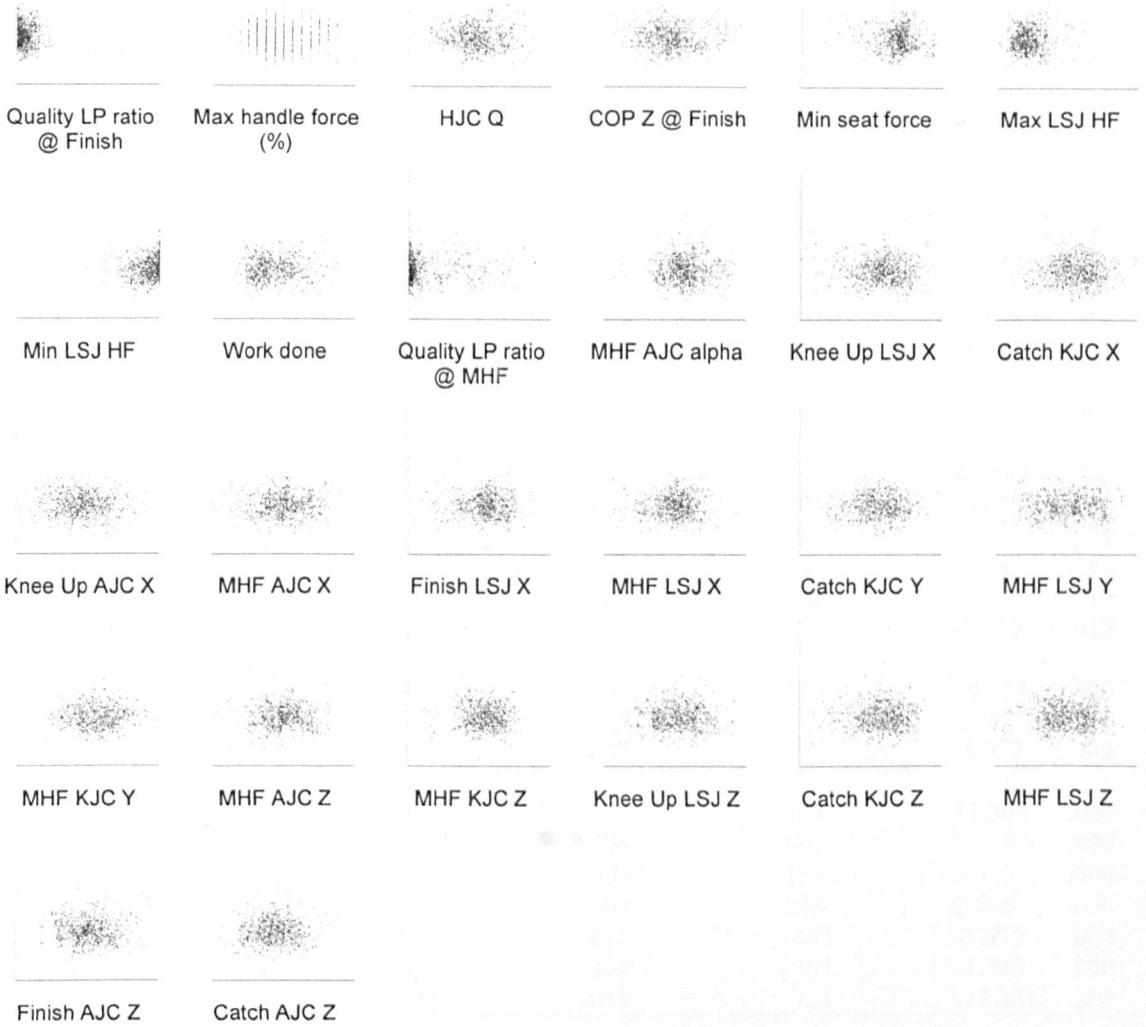


Figure 9.18: Assessment of the assumption of linearity with respect to LSJ delta

Each of the plots shows the relationship between a single explanatory variable and the MREG model standardised residuals. The X axes are labelled according to the appropriate independent variable. The Y axis is always the residuals. If no trend is apparent then the assumption of linearity is met.

Variable	Regression coefficients			t-test	
	Unstandardised	Standard error	Standardised	t	p
CONSTANT	62.887	9.418		6.678	.000
Quality LP ratio @ Finish	1.440	.220	.109	6.536	.000
Max handle force (%)	.251	.035	.190	7.187	.000
HJC Q	.058	.010	.107	5.892	.000
COP Z @ Finish	.018	.005	.080	3.752	.000
Min seat force (N)	.002	.001	.050	2.033	.042
Max LSJ HF	.000	.000	.408	22.376	.000
Min LSJ HF	.000	.000	.392	22.489	.000
Work done (J)	-.007	.001	-.208	-7.625	.000
Quality LP ratio @ MHF	-.066	.008	-.157	-8.523	.000
MHF AJC alpha	.086	.008	.317	11.197	.000
Knee Up LSJ X	.061	.014	.246	4.389	.000
Catch KJC X	-.010	.002	-.083	-4.624	.000
Knee Up AJC X	-.019	.006	-.077	-3.031	.002
MHF AJC X	-.023	.007	-.085	-3.242	.001
Finish LSJ X	-.024	.009	-.120	-2.581	.010
MHF LSJ X	-.026	.010	-.092	-2.527	.012
Catch KJC Y	.080	.006	.770	14.034	.000
MHF LSJ Y	.010	.003	.069	2.923	.004
MHF KJC Y	-.049	.006	-.443	-8.620	.000
MHF AJC Z	.160	.013	.845	12.308	.000
MHF KJC Z	.054	.006	.691	9.778	.000
Knee Up LSJ Z	.012	.003	.154	3.722	.000
Catch KJC Z	.004	.002	.048	2.096	.036
MHF LSJ Z	-.022	.004	-.355	-5.670	.000
Finish AJC Z	-.050	.007	-.303	-7.390	.000
Catch AJC Z	-.155	.012	-.754	-13.305	.000

Table 9.12: The MREG calculated equation for LSJ delta

The coefficients describe the direction and magnitude of the relationship between each explanatory variable and the dependent variable, the standard error of the unstandardised coefficients is also included, along with the t-statistic, and significance of the p-value for the t-test for each explanatory variable. The order of the variables is: equation constant, followed by stroke profile explanatory variables (sorted by the magnitude and direction of their unstandardised regression coefficient), rotational kinematics, X trajectory kinematics, Y trajectory kinematics, and finally Z trajectory kinematics. Kinematics are either measured at the catch of the stroke, at the point in the stroke when maximum handle force was being exerted (MHF), at the finish of the stroke, or at the point in the recovery when the knees started to rise (Knee Up).

The R^2 and adjusted R^2 values for this model were .745 and .739 respectively. This means that approximately 74% of the variability in LSJ delta can be accounted for by its relationship with the explanatory variables included in the regression model. As stated in Section 9.1.2.1, it was thought that exhibiting no change in the flexion/extension angle about LSJ under loading would be the gold standard technique. However it was not known whether a tendency to extend about LSJ or flex about LSJ would exert more influence on injury potential.

Table 9.3 showed that on average, in the initial part of the drive phase, the athletes extended about LSJ by 1.52° ($\pm 3.36^{\circ}$). MREG analysis found that between the catch and the occurrence of maximum handle force LSJ alpha was found to move towards increased extension as the timing of maximum handle force became later in the stroke. Athletes who extended their lumbar spine during this part of the drive phase exhibited lower peaks of downwards force on the seat, did less work during the stroke, and had a more anterior COP coordinate at the finish. Extending about LSJ during the early drive was also associated with increased HJC abduction later in the drive phase and higher quality of lumbopelvic postural control in the middle of the drive; this is most likely due to most athletes' posture at the catch being slightly flexed (Figure 6.19, Page 125), thus extending the lumbar spine during the initial portion of the drive would result in better posture by the time maximum handle force was being exerted. Evidently however, those who extended their lumbar spine in the early drive continued to do so for the remainder of the drive; resulting in hyper extension and a lower quality lumbopelvic ratio at the finish. As would be expected, LSJ delta was also associated with measures of the rate of change of LSJ alpha (Max LSJ HF and Min LSJ HF).

Table 9.12 shows that changes in LSJ delta were associated with changes in four kinematic variables at the catch, and eight at maximum handle force; this may show that variation in LSJ delta is not necessarily reliant upon whatever base posture is adopted at the catch of the stroke, especially as none of the catch variables identified were associated with LSJ. Extension about LSJ during the first half of the drive was linked with additional rightwards displacement of LSJ at maximum handle force and the finish, additional leftwards displacement of LSJ when the knees broke, more superior and posterior displacement of LSJ in the middle of the drive, and a more anterior LSJ coordinate as the knees broke. No links between LSJ delta and HJC alpha, X,Y,Z kinematics were noted. Extending about LSJ was linked to increased lateral, superior, and anterior displacement of the knee at the catch, and more inferior and anterior displacement as maximum handle force was exerted. The only rotational kinematic found to be linked with changes in LSJ delta stated that increased extension about LSJ was associated with increased plantar flexion in the middle of the drive. In addition to this, changes in LSJ delta were linked with greater posterior displacement of the AJC at the catch, greater lateral and anterior displacement of AJC at maximum handle force, posterior displacement of AJC at the finish, and increased lateral displacement of AJC as the knees broke.

9.4.2.2 Rate of change of LSJ alpha under loading – LSJ extension

56 of the original 97 potential explanatory variables were significantly related to Max LSJ HF ($p < 0.05$). The *Stepwise* MREG analysis suggested 19 possible equations whose adjusted R^2 values ranged from .193 to .682. The F-tests associated with all of these models were significant ($p < 0.01$). The optimal model included 19 significant explanatory variables

($p < 0.05$); 9 of these were stroke profile, 5 of which considered kinematics at the catch of the stroke, 1 considered kinematics at the occurrence of maximum handle force, 3 were kinematics at the finish, and 1 considered kinematics recorded during the recovery, when the knees broke. These variables were input using the *Enter* automatic variable selection method into a new MREG analysis and the model residuals and predicted dependent variables were calculated. The assumptions of normality, constant variance, and linearity were assessed in the same way as described previously (Figure 9.19 and Figure 9.20). The output of the model is shown in Table 9.13.

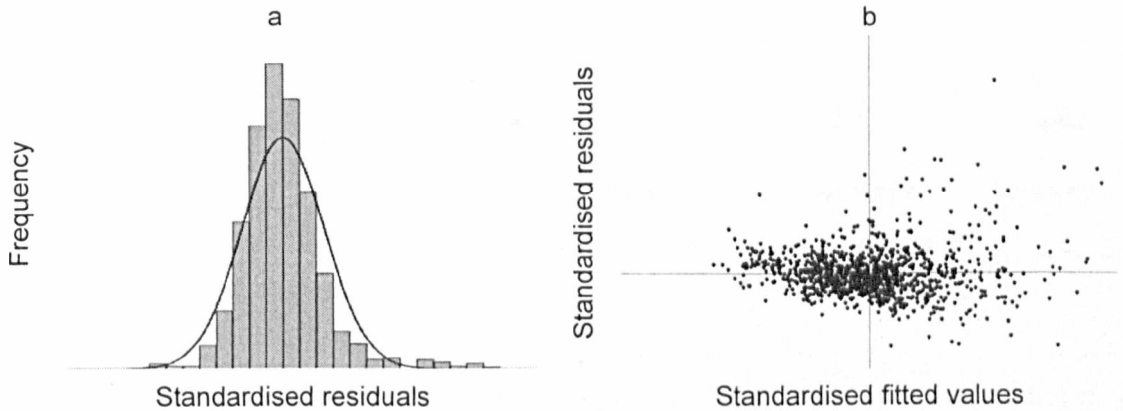


Figure 9.19: Assessment of the assumptions of normality and constant variance with respect to Max LSJ HF

The frequency of the standardised residuals is plotted beneath a normal distribution curve (a); any departures from normal distribution may be deleterious to the validity of the MREG model. The standardised residuals are also plotted against the standardised fitted values (b); any funnelling effect of data along the X axis indicates that the assumption of constant variance may have been violated.

Figure 9.19 shows that the assumptions of normality and constant variance were adhered to in the current model. There is no funnelling effect present in the scatter plot concerning constant variance, thus the assumption of constant variance is met. Figure 9.20 does not show any trends between the model's explanatory variables and the standardised residuals; thus the assumption of linearity was satisfied in this case.

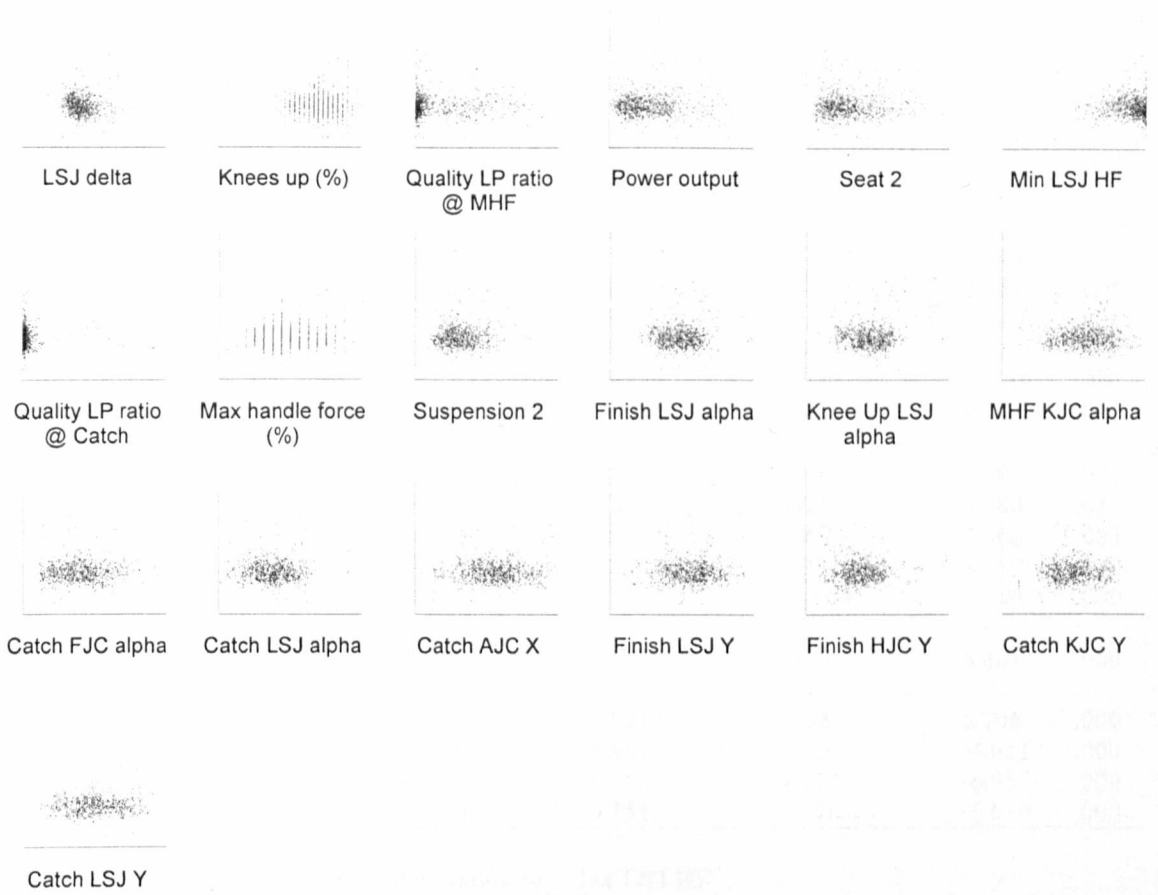


Figure 9.20: Assessment of the assumption of linearity with respect to Max LSJ HF
 Each of the plots shows the relationship between a single explanatory variable and the MREG model standardised residuals. The X axes are labelled according to the appropriate independent variable. The Y axis is always the residuals. If no trend is apparent then the assumption of linearity is met.

Variable	Regression coefficients			t-test	
	Unstandardised	Standard error	Standardised	t	p
CONSTANT	-124817.172	11847.078		-10.536	.000
LSJ delta (°)	842.696	70.993	.335	11.870	.000
Knees up (%)	228.356	54.463	.090	4.193	.000
Quality LP ratio @ MHF	165.423	23.322	.157	7.093	.000
Power output (W)	59.438	3.847	.455	15.449	.000
Seat 2	7.313	2.630	.054	2.781	.006
Min LSJ HF	-.373	.050	-.166	-7.436	.000
Quality LP ratio @ Catch	-129.930	36.880	-.078	-3.523	.000
Max handle force (%)	-264.531	95.876	-.080	-2.759	.006
Suspension 2 (BW(s))	-440.018	53.097	-.221	-8.287	.000
Finish LSJ alpha	755.146	44.502	.926	16.969	.000
Knee Up LSJ alpha	95.815	40.251	.120	2.380	.017
MHF KJC alpha	74.417	25.087	.069	2.966	.003
Catch FJC alpha	-150.759	34.122	-.082	-4.418	.000
Catch LSJ alpha	-801.761	35.161	-1.004	-22.803	.000
Catch AJC X	71.010	10.442	.127	6.801	.000
Finish LSJ Y	69.682	12.213	.208	5.706	.000
Finish HJC Y	-36.391	8.984	-.100	-4.051	.000
Catch KJC Y	-46.991	6.756	-.179	-6.955	.000
Catch LSJ Y	-61.040	9.151	-.176	-6.670	.000

Table 9.13: The MREG calculated equation for Max LSJ HF

The coefficients describe the direction and magnitude of the relationship between each explanatory variable and the dependent variable, the standard error of the unstandardised coefficients is also included, along with the t-statistic, and significance of the p-value for the t-test for each explanatory variable. The order of the variables is: equation constant, followed by stroke profile explanatory variables (sorted by the magnitude and direction of their unstandardised regression coefficient), rotational kinematics, X trajectory kinematics, Y trajectory kinematics, and finally Z trajectory kinematics. Kinematics are either measured at the catch of the stroke, at the point in the stroke when maximum handle force was being exerted (MHF), at the finish of the stroke, or at the point in the recovery when the knees started to rise (Knee Up).

The R^2 and adjusted R^2 values for this model were .687 and .682 respectively. This means that over 68% of the variability in Max LSJ HF can be accounted for by its relationship with the explanatory variables included in the regression model. As stated in Section 9.1.2.1; it was thought that reducing the magnitude of the product of the rate of change of LSJ alpha and handle force would be beneficial in reducing injury risk to the lumbar spine.

As LSJ delta increased, reflecting greater total extension of the lumbar spine between the catch and maximum handle force, so did the peak of Max LSJ HF. Increases in Max LSJ HF, and thus a greater risk of injury, were also associated with poorer quality of lumbopelvic ratio in the middle of the drive, greater values of performance variable Seat 2, increased power output, and delays in the timing of the knees breaking in the recovery. The associations between Max LSJ HF and these stroke profile variables are likely linked to increases in exercise intensity, and thus show that the risk of injury to athletes is greater whilst exercising at greater

intensity. An increased risk of injury was also associated with a decrease in the timing of maximum handle force; this shows that very high rates of force development in the initial portion of the drive are a potential mechanism by which athletes' lumbar spines could be injured. Peak Max LSJ HF is linked with peak Min LSJ HF, this suggests that athletes who extend their lumbar spine rapidly whilst under load, may also exhibit some rapid changes in flexion (probably earlier in the drive, Section 9.4); this in turn suggests that general postural control is important in reducing the risk of injury. Furthermore, as the magnitude of suspension became less across the entire drive the risk of injury increased; this may be related to the balance issues discussed previously (Section 9.4.1.9).

The result shown in Table 9.13 regarding the quality of lumbopelvic ratio at the catch states that as alignment of PELVIS and BACK becomes closer at the catch, their risk of injury increases. However this is in contrast to the result shown for LSJ alpha at the catch; this states that as an athlete's lumbar spine becomes more flexed about LSJ at the catch, so their risk of injury to the lumbar spine significantly increases. The standardised coefficient for LSJ alpha at the catch is almost thirteen times stronger than that for the quality of the lumbopelvic ratio at the catch, indicating that it is far more influential on the model. It is therefore thought that poorer posture, specifically a more flexed spinal pose at the catch puts athletes at risk of lumbar injury.

As well as improving posture at the catch, the model shows that not hyper extending LSJ at the finish or during the rock over as the knees break is associated with a decreased risk of lumbar injury. The standardised coefficients show that, considering the flexion/extension angle about LSJ, the most effective way to reduce injury to the lumbar spine during rowing exercise is to reduce the level of lumbar flexion exhibited at the catch of the stroke, closely followed by reducing the magnitude of hyper extension at the finish. Other kinematic variables linked to decreasing the risk of injury, as measured by Max LSJ HF were more superior displacement of HJC at the finish, decreased KJC flexion in the middle of the drive, more superior displacement of the KJC at the catch, increased lateral displacement of AJC at the catch, and greater separation of the heels from the footstretcher at the catch of the stroke.

9.4.2.3 Rate of change of LSJ alpha under loading – LSJ flexion

57 of the original 97 potential explanatory variables were significantly related to Min LSJ HF ($p < 0.05$). The *Stepwise* MREG analysis suggested 11 possible equations; none of these models achieved an R^2 or adjusted R^2 value of greater than .467 and .463 respectively. Because less than half of the variability of Min LSJ HF could be explained by the best model offered by MREG analysis this variable was not considered any further.

9.4.2.4 Level of HJC abduction/adduction when in 20° of KJC flexion

53 of the original 97 potential explanatory variables were significantly related to HJC Q ($p < 0.05$). The *Stepwise* MREG analysis suggested 23 possible equations; none of these models achieved an R^2 or adjusted R^2 value of greater than .374 and .365 respectively. Because so little of the variability of HJC Q could be explained by the best model offered by MREG analysis this variable was not considered any further.

9.4.2.5 Summary regarding kinematics and injury

It was not possible to define a regression equation that satisfactorily explained the variance observed in two of the injury related variables. However through the MREG analyses conducted into variables LSJ delta, and Max LSJ HF, it was observed that increased HJC Q abduction and Min LSJ HF were related to LSJ delta, and that Min LSJ HF was associated with Max LSJ HF.

Extending about LSJ during the initial portion of the drive phase was linked with increased alignment of PELVIS and BACK in the middle of the drive, and athletes who extended their lumbar spine in the early drive phase adopted increasingly lordotic lumbar posture at the finish. This additional hyper extension was found to present an increased risk of injury as measured by Max LSJ HF. Changes in spinal posture, towards lumbar extension in the drive phase were also associated with increased lateral, superior and anterior displacement of the knee at the catch, and more inferior displacement of the knee in the middle of the drive. If the hip flexor muscles were tight, bringing the knees down in this way during the drive could have caused the pelvis to anteriorly rotate, thus increasing the observed extension of the lumbar spine about LSJ. Increased risk of injury to the lumbar spine was found to be associated with increased flexion of the lumbar spine at the catch of the stroke and poor postural control in the middle of the drive phase. In addition to this, athletes who produced high peaks of Max LSJ HF, also produced large peaks of Min LSJ HF. This could be explained by a technical error in rowing known as *bum shoving* (Bull and McGregor, 2000). Bum shoving describes motion away from the catch in rowing when the legs and pelvis are pushed bow-wards leaving the higher spine and upper limbs behind; this often results in rapidly increased lumbar flexion (peaks in Min LSJ HF). This motion is followed by the trunk quickly swinging posteriorly to “catch up” (peaks in Max LSJ HF). Bum shoving has previously been shown to significantly influence the kinematics of the femur, pelvis and lumbar spine in ergometer rowing (Bull and McGregor, 2000).

9.5 Summary

Using a database of 1,115 rowing tests completed by elite athletes, this chapter sought to define the relationship between athletes' technique, and their performance and risk of injury. Correlation analysis and multiple regression analysis was successfully completed with respect to seven rowing performance predicting variables, and two variables that were thought to be related to injury prevention in the region of the lumbar spine. Nine key 3D kinematic parameters were identified that it is believed can influence the performance of elite rowers. The relationships between performance variables and other stroke profile variables, such as how an athlete suspends from their seat during the drive phase, were also described. In addition to this, key kinematic and stroke profile variables were identified that it is believed may be used to reduce the risk of injury to rowers' lumbar spines.

The regression equations used to model the dependent performance and injury variables met all of the assumptions required of data included in such analysis, and were found to represent the variability of the dependent variables well; adjusted R^2 values ranged from .842 to .975 for performance, and .682 to .739 for injury related dependent variables. Some of the scatter plots showing the model residuals against individual explanatory variables indicated, not trends, but outliers and possibly skewed data. Because all of the assumptions associated with MREG analysis were adhered to it is not thought that this data invalidates any of the results presented in this chapter, however it may have been interesting to define Cook's distance, and the centred leverage associated with the models; these tests would have fully described the effect that any outliers had upon the slope of regression lines.

On average there were 28 explanatory variables in any one optimal MREG model, of which 11 related to stroke profile variables, and 4 related to 3D kinematics at any particular stroke event (for example, the catch). Generally, the way in which joint centres were displaced in the sagittal plane, and flexed or extended was more relevant than their trajectories in the medial/lateral direction (Table 9.14). The joint centre most commonly linked with dependent variables was the KJC (44 associations), this was followed by LSJ and AJC (both 39 associations), then by HJC, and finally FJC (27 and 6 associations respectively).

Dependent variable	Number of explanatory variables in the model																
	r ²	adjusted r ²	All	Stroke profile											AJC	FIC	
				Catch	MHF	Finish	Knee Up	alpha	X	Y	Z	LSJ	HJC	KJC			
Finish (%)	.976	.975	32	11	6	6	3	6	4	5	6	6	6	2	9	4	0
Slope of handle force (N%)	.936	.934	26	10	5	3	5	3	4	1	5	6	4	4	4	4	0
Stroke length (mm)	.847	.842	36	8	9	5	8	6	8	5	8	7	8	9	6	4	1
Power output (W)	.914	.912	25	11	5	4	3	2	5	4	3	2	2	4	4	2	2
Seat 1	.951	.950	22	12	3	1	4	2	2	2	3	3	1	0	4	4	1
Seat 2	.969	.969	26	13	0	3	6	4	3	1	6	3	4	1	3	5	0
Seat BW	.853	.848	39	13	3	6	6	11	8	4	3	11	3	6	7	9	1
LSJ delta (°)	.745	.739	26	9	4	8	2	3	1	6	3	7	6	0	5	6	0
Max LSJ HF	.687	.682	19	9	5	1	3	1	5	1	4	0	5	1	2	1	1

Table 9.14: Summary of the quality of fit of MREG models, and the number of associated explanatory variables

Nine 3D kinematic variables were identified that were strongly associated with improving multiple measures of rowing performance (9.4.1.8). It was shown that adopting kyphotic poses in the lower back was deleterious to performance, and that keeping the heels in close contact with the footstretcher at the finish of the stroke was beneficial to five different performance measures. It was found that various performance gains were associated with improving the quality of the lumbopelvic ratios observed at the catch and in the middle of the drive.

Some differences in the stroke profile and performance of athletes was noted between the sexes. The results also illustrated that generating force more quickly in the early portion of the drive was desirable, and provided evidence linking stroke rate, and the timing of key stroke events with performance. Five separate measures of rowing performance indicated that it was desirable to suspend as fully as possible away from the ergometer seat during the first half of the drive phase, but that bodyweight should then be returned to the seat before the finish; it was thought that these associations might be linked with athletes ability to balance themselves during the stroke, and despite this, it is not thought that very large, sharp downward peaks in seat force exerted as bodyweight is accelerated into the seat would be beneficial to increasing the velocity of a rowing boat. At the finish, posteriorly displacing the COP on the seat was associated with improvements in five performance variables. Other results suggested that, depending on the particular performance variable, for example power output or stroke length, which is of most importance to an athlete or coach, there may be different mechanisms by which to acquire performance gains.

As well as being linked to improvements in performance, alignment of PELVIS and BACK – postural control – was noted to reduce the risk of injury to athletes’ lumbar spines.

Furthermore, reducing forward flexion of the lumbar spine about the lumbosacral junction at the catch of the stroke, and avoiding hyper extension at the finish were both shown to be beneficial in avoiding possible injury mechanisms. It is possible that one way in which to avoid over flexing the lumbar spine at the catch may be to raise the heels from the footstretcher; increasing the sagittal angle between the anterior and posterior parts of the foot and thus raising the heels from the footstretcher was shown to reduce the risk of injury to the lower back. Just as it was linked with improving performance, it was found that returning the bodyweight to the seat after maximum handle force had been achieved, but before the finish aided in avoiding motion that was thought to be associated with spinal injury. Other results linking power output, and the timing of key stroke events to undesirable movement patterns suggested that athletes were at a higher risk of experiencing an injury during high intensity exercise (Table 9.7 and Table 9.13).

The final part of this thesis discusses the work presented thus far. Chapter 10 comments on selected results obtained from the descriptive and statistical analyses of athlete data, before Chapter 11 goes on to discuss the thesis in its entirety.

PART 3

Discussion and conclusions

Chapter 10

Discussion of PART 2

The aim of this chapter is to summarise and discuss with respect to performance and injury the results of the studies presented in Chapters 6 to 9.

10.1 Rowing technique and performance

Previous work has shown how biomechanical analysis can be used in monitoring and improving the quality and repeatability of rowing performance (Baudouin and Hawkins, 2002; Baudouin and Hawkins, 2004; Hartmann et al., 1993; Hofmijster et al., 2008; Macfarlane et al., 1997; Schabert et al., 1999). Although the above studies have shown that factors such as fluid drag, equipment design, peak force and power output have a significant influence on the velocity of rowing shells, undoubtedly the most important performance factor in rowing is the rower; previous studies on the rower have not focused on the three-dimensional kinematics of the athlete. Often they have considered only the sagittal trajectories and rotations of body segments, presented results that were weakened by error, or limited their analysis to qualitative description (Caldwell et al., 2003; Colloud et al., 2006a; Hase et al., 2004; Hawkins, 2000; Holt et al., 2003; McGregor et al., 2004a; McGregor et al., 2005; O'Sullivan et al., 2003; Page and Hawkins, 2003; Pudlo et al., 2005). This study is the most comprehensive analysis of the technique, kinematics, and performance of elite rowers to date.

10.1.1 Descriptive

Chapter 6 used descriptive statistics, and column and scatter graphs to illustrate the technique of elite athletes' ergometer rowing. In general the stroke profile and motion characteristics of elite rowers were comparable across all of the boat classes considered. There were some differences noted in the timing of key stroke events and measured kinematics as the intensity of effort was increased, particularly when comparing race pace efforts to lower intensity exertions. Data considered the motion and output (stroke profile) of heavyweight female scullers, heavyweight female sweep rowers, lightweight men, and lightweight women. Considering all of the anatomical joint centres relevant to this study, on average the most variable kinematic measures were for the HJC; up to ± 55.6 mm in the anterior/posterior direction, and up to $\pm 20.4^\circ$ in flexion/extension, and the least were for the AJC and FJC; up to ± 7 mm in the medial/lateral direction, and up to $\pm 1.9^\circ$ in flexion/extension. This variability was a reflection of differences in the size, the shape, and the technique of individual athletes. When considering the largest variability of each of the kinematic parameters and each of the athlete classes it was found that

53% of the extremes in variability were logged during Step 6; the Step that mimics race conditions most effectively. This shows that the largest intra and inter athlete differences in motion characteristics occurred during maximal intensity exercise and concurrently, at the highest stroke ratings measured. This may show that athletes' technique is less reliable and repeatable under race conditions than at lower training intensities.

Previous work has stated that the majority of the rowing action can be described in the sagittal plane, and that the majority of joint rotations occur about flexion/extension axes (Bull and McGregor, 2000; Halliday et al., 2004). However, few studies provide explicit accounts of intersegmental angles in two or three dimensions; this issue was addressed in Chapter 6. The current study supports the claim that the majority of the displacement of joint centres occurs in the sagittal plane and emphasises the importance of flexion/extension movements in rowing. Two studies from the literature that did present intersegmental angles found that, at the catch, the angle between the shank and thigh was $53.0^{\circ} (\pm 3.7^{\circ})$ and $52.5^{\circ} (\pm 2.0^{\circ})$ (Hume et al., unreferenced, and Elliot et al., 2002; as cited by Soper and Hume, 2004). These studies considered the ergometer performance of junior national and world championship level rowers; their results when converted to this study's convention were $127.0^{\circ} (\pm 3.7^{\circ})$ and $127.5^{\circ} (\pm 2.0^{\circ})$; this compares to the average knee flexion in this study of $132.5^{\circ} (\pm 6.7^{\circ})$. The small differences between the current and the previous research may be explained by world junior rowers generally demonstrating less flexion near the catch than elite individuals (Soper and Hume, 2004a). The larger standard deviation noted in the current study may be explained by the wider variety of athletes tested. Normative data for trajectory and rotation ranges of motion of LSJ, HJC, KJC, AJC, and FJC measured in this study are shown in Table 10.1 and Table 10.2.

			HW W SCULL	HW W SWEEP	LWM	LWW		All athletes		% of total			
			range	(±SD)	range	(±SD)	range	(±SD)	range	(±SD)	motion		
LSJ	X	Step 2	11.7	(4.0)	12.2	(4.1)	23.6	(7.5)	25.1	(8.3)	26.4	(6.4)	3.9
		Step 4	12.3	(4.0)	12.4	(4.1)	26.0	(8.4)	28.9	(9.8)	29.0	(7.2)	
		Step 6	12.4	(3.4)	13.4	(3.6)	28.8	(9.0)	33.3	(11.4)	33.7	(7.9)	
	Y	Step 2	34.5	(11.4)	41.6	(13.0)	40.6	(12.3)	29.4	(9.4)	66.2	(16.8)	8.6
		Step 4	33.6	(10.8)	38.1	(12.2)	37.5	(11.5)	32.0	(9.9)	66.1	(16.5)	
		Step 6	29.4	(8.7)	28.6	(8.8)	26.5	(8.9)	31.4	(8.9)	64.2	(15.4)	
	Z	Step 2	661.7	(242.3)	661.8	(241.8)	677.5	(247.3)	614.8	(224.4)	697.1	(239.5)	87.6
		Step 4	662.6	(244.6)	659.3	(243.0)	674.2	(248.1)	607.6	(222.7)	687.7	(240.0)	
		Step 6	611.3	(228.8)	602.8	(225.7)	615.2	(230.0)	547.1	(204.3)	624.8	(222.6)	
HJC	X	Step 2	16.6	(5.3)	17.0	(5.3)	26.0	(8.1)	24.0	(7.7)	32.9	(7.9)	4.9
		Step 4	16.3	(5.3)	17.0	(5.3)	28.7	(9.2)	27.8	(9.2)	34.4	(8.3)	
		Step 6	14.4	(4.5)	15.7	(4.6)	32.0	(9.7)	34.1	(10.9)	42.8	(9.2)	
	Y	Step 2	79.4	(28.4)	86.2	(30.7)	86.9	(31.2)	69.2	(24.4)	101.7	(29.5)	13.0
		Step 4	77.8	(27.9)	85.6	(30.7)	86.1	(30.8)	67.7	(23.5)	99.4	(29.0)	
		Step 6	69.0	(24.8)	76.0	(27.7)	82.6	(29.8)	59.3	(21.0)	92.5	(26.9)	
	Z	Step 2	595.7	(220.0)	589.5	(218.0)	633.8	(232.2)	560.8	(205.3)	642.7	(219.6)	82.1
		Step 4	598.8	(222.2)	586.6	(218.1)	630.3	(232.6)	554.9	(203.9)	634.0	(219.7)	
		Step 6	550.4	(206.9)	533.7	(201.4)	573.9	(215.1)	505.2	(189.4)	578.9	(203.7)	
KJC	X	Step 2	50.5	(17.5)	60.0	(21.3)	46.0	(16.0)	37.2	(12.1)	60.0	(17.2)	5.4
		Step 4	48.2	(16.5)	56.5	(20.2)	39.6	(13.8)	30.1	(9.6)	56.5	(15.6)	
		Step 6	35.5	(10.7)	32.0	(10.9)	26.8	(8.8)	21.3	(5.0)	37.6	(9.5)	
	Y	Step 2	313.3	(124.9)	297.4	(120.6)	310.2	(124.0)	279.6	(113.1)	323.8	(120.7)	34.7
		Step 4	312.8	(124.0)	296.3	(119.2)	308.7	(123.4)	286.0	(114.5)	327.3	(120.3)	
		Step 6	316.7	(121.6)	294.7	(114.0)	315.1	(121.7)	302.5	(115.2)	332.9	(118.2)	
	Z	Step 2	557.9	(204.2)	561.4	(206.6)	571.5	(208.0)	521.4	(190.4)	584.5	(202.1)	59.9
		Step 4	560.9	(205.6)	560.8	(206.6)	571.7	(208.8)	515.3	(189.1)	584.3	(202.2)	
		Step 6	516.8	(190.4)	514.1	(189.7)	519.3	(191.5)	465.2	(172.7)	531.3	(185.8)	
AJC	X	Step 2	15.5	(4.9)	20.8	(7.6)	14.2	(3.8)	15.2	(4.6)	20.8	(5.6)	11.9
		Step 4	14.2	(4.4)	21.1	(7.3)	14.3	(3.7)	14.5	(4.1)	21.1	(5.3)	
		Step 6	10.8	(2.9)	19.2	(5.5)	15.5	(4.2)	12.1	(3.2)	20.2	(4.5)	
	Y	Step 2	40.0	(13.4)	38.3	(13.9)	47.1	(14.9)	42.5	(14.3)	67.1	(16.7)	40.3
		Step 4	42.5	(13.6)	37.9	(13.7)	52.1	(15.6)	46.9	(15.5)	72.7	(17.8)	
		Step 6	45.1	(13.4)	33.6	(11.7)	52.7	(15.2)	42.5	(14.4)	71.7	(18.2)	
	Z	Step 2	61.6	(24.4)	68.5	(27.2)	57.3	(22.4)	60.3	(24.6)	82.2	(25.6)	47.8
		Step 4	58.9	(23.1)	66.5	(26.1)	56.0	(21.6)	59.3	(23.7)	82.1	(24.7)	
		Step 6	60.7	(23.0)	66.2	(25.1)	58.9	(22.0)	65.1	(24.4)	86.3	(25.0)	

Table 10.1: Average range of motion and standard deviation (SD) of joint centres' trajectory during elite ergometer rowing

Values are in mm. X is medial/lateral, Y is superior/inferior, and Z is anterior/posterior. Normative data for the range of motion of the lumbosacral junction, the hip joint centre, the knee joint centre and the ankle joint centre is shown for heavyweight female scullers and rowers, and lightweight males and females. The two columns on the right are the average data for all athletes, and the percentage of the total range of motion accounted for by the X,Y,Z directions.

			HWW SCULL	HWW SWEEP	LWM		LWW		All athletes	% of total	
			range	(±SD)	range	(±SD)	range	(±SD)	range	(±SD)	motion
LSJ	alpha	Step 2	19.0	(5.8)	18.3	(5.8)	17.5	(5.7)	24.0	(7.9)	69.1
		Step 4	19.6	(6.1)	18.1	(5.7)	19.1	(6.3)	22.5	(7.6)	
		Step 6	22.2	(7.2)	18.9	(6.2)	21.9	(7.6)	23.9	(8.0)	
	beta	Step 2	2.1	(0.7)	1.6	(0.5)	2.5	(0.8)	1.3	(0.3)	11.8
		Step 4	2.0	(0.6)	2.0	(0.7)	2.4	(0.7)	2.1	(0.5)	
		Step 6	2.1	(0.7)	2.1	(0.6)	2.5	(0.7)	3.5	(1.1)	
	gamma	Step 2	1.2	(0.3)	1.3	(0.4)	2.4	(0.6)	5.4	(1.6)	19.1
		Step 4	1.6	(0.4)	1.4	(0.4)	2.8	(0.8)	4.8	(1.4)	
		Step 6	1.2	(0.4)	1.8	(0.5)	3.8	(1.0)	3.1	(0.9)	
HJC	alpha	Step 2	106.5	(39.5)	100.1	(38.1)	105.2	(39.2)	102.9	(38.7)	79.5
		Step 4	106.0	(39.3)	100.9	(38.2)	105.7	(39.2)	104.1	(38.8)	
		Step 6	101.5	(37.0)	93.9	(35.3)	105.2	(38.0)	100.6	(36.5)	
	beta	Step 2	10.9	(4.3)	8.7	(3.2)	10.8	(4.1)	13.4	(4.7)	9.0
		Step 4	10.7	(4.3)	9.0	(3.3)	11.3	(4.2)	12.0	(4.1)	
		Step 6	10.6	(4.1)	9.8	(3.7)	10.4	(4.1)	11.9	(4.2)	
	gamma	Step 2	14.4	(4.4)	10.4	(3.4)	11.9	(3.5)	11.9	(3.5)	11.5
		Step 4	14.8	(4.5)	10.4	(3.4)	10.6	(3.2)	12.1	(3.5)	
		Step 6	16.4	(5.0)	10.5	(3.4)	11.1	(3.1)	11.5	(3.1)	
KJC	alpha	Step 2	138.7	(51.8)	138.3	(52.0)	140.2	(52.2)	136.6	(51.1)	-
		Step 4	138.7	(51.7)	137.6	(51.6)	139.5	(51.8)	136.8	(51.1)	
		Step 6	131.3	(48.4)	127.9	(47.4)	131.2	(48.4)	128.5	(47.4)	
AJC	alpha	Step 2	92.1	(36.1)	88.5	(36.2)	91.1	(35.4)	100.4	(39.9)	75.9
		Step 4	91.3	(35.3)	88.1	(35.5)	89.0	(33.9)	101.0	(39.3)	
		Step 6	82.6	(30.7)	82.1	(31.8)	79.3	(28.7)	85.3	(31.8)	
	beta	Step 2	11.7	(4.5)	14.0	(5.7)	13.7	(5.1)	15.4	(6.0)	12.9
		Step 4	11.0	(4.2)	13.9	(5.7)	13.5	(4.9)	13.6	(5.3)	
		Step 6	10.3	(3.8)	13.2	(5.2)	11.1	(3.9)	11.1	(3.8)	
	gamma	Step 2	6.4	(2.0)	6.7	(2.2)	6.4	(2.0)	13.4	(4.4)	11.2
		Step 4	6.4	(2.1)	7.0	(2.2)	6.2	(1.8)	14.3	(4.6)	
		Step 6	6.3	(2.0)	6.2	(1.8)	6.6	(1.7)	14.9	(4.5)	
FJC	alpha	Step 2	7.3	(2.3)	10.4	(3.3)	9.1	(2.7)	9.4	(2.8)	-
		Step 4	7.6	(2.4)	10.3	(3.4)	9.7	(3.0)	10.5	(3.2)	
		Step 6	8.1	(2.8)	9.8	(3.3)	9.3	(3.1)	11.1	(3.9)	

Table 10.2: Average range of motion and standard deviation (SD) of joint centres' rotation during elite ergometer rowing

Values are in degrees. alpha is flexion/extension, beta is lateral flexion, abduction/adduction, or eversion/inversion, and gamma is twist, or internal/external rotation. Normative data for the range of motion of the lumbosacral junction, the hip joint centre, the knee joint centre, the ankle joint centre, and the foot joint centre is shown for heavyweight female scullers and rowers, and lightweight males and females. The two columns on the right are the average data for all athletes, and the percentage of the total range of motion accounted for by the alpha, beta, gamma directions.

Halliday et al. (2004) observed that most of the motion of university level rowers could be described by flexion/extension of body segments with some levels of abduction/adduction and internal/external rotation. They did not publish the magnitude of these movements. The current study is in agreement with these qualitative observations and has shown that depending on the joint centre, between 47.8% and 87.6% of the trajectory of elite athletes' lower limb and lumbar joint centres occurs in the anterior/posterior direction, and between 88.1% and 96.1% occurs in the sagittal plane (Table 10.1). Table 10.2 shows that 69.1%, 79.5% and 75.9% of the rotation of LSJ, HJC and AJC respectively was about their individual flexion/extension axis; it is unclear

if similar magnitudes apply to the KJC and FJC; only the flexion/extension of KJC and FJC was measured in this study though one might expect most of the rotations to be flexion/extension as these joints can be more closely approximated by a hinge than joints such as HJC.

Chapter 6 reported that the magnitudes of flexion/extension angles about LSJ for all athlete groups were reasonably comparable to each other, and that the trends of motion were similar between groups across the duration of the rowing stroke. The lumbopelvic ratio varied far more between athlete groups. This seeming unevenness in measurements of rotation of the pelvis and lumbar spine was explained by the global orientation of the body segments (Section 6.3.4.1). Kinematic measurements showed that at the catch of the stroke, female athletes, particularly heavyweight females, anteriorly rotated their pelvis far more than the male athletes who were tested (on average, 148%, 102% and 51% more, HWW-SWEEP, HWW-SCULL and LWW vs LWM). This suggests that male athletes may rely more heavily than females do on anterior lumbar and thoracic rotation and reaching forwards through the shoulders to achieve stroke length at the catch; this was not measured in the current study. Increased anterior thoracic displacement and rotation has previously been shown to increase the loads and stresses experienced by the lower thoracic and lumbar regions of the spine, particularly at L5S1 (LSJ) and L3L4 (Harrison et al., 2005). At the catch and with increasing intensity, all boat classes displaced their AJC more superiorly and posteriorly, exhibited less anterior displacement of LSJ, HJC, KJC and COP, and achieved less dorsi flexion, knee flexion, and hip flexion. This would have resulted in a need for increased spinal flexion to maintain stroke length. This is particularly undesirable during high intensity efforts, as peak forces and power being generated and transmitted by the rower are higher (McGregor et al., 2004a; McGregor et al., 2005; Smith and Spinks, 1995) and thus the risk of injury is increased when compared to lower, training intensities (Section 10.2).

The higher quality LP ratios (greater alignment of PELVIS and BACK) and increased pelvic flexion noted above may be related to differences that were observed in the way separate athlete groups suspended away from the ergometer seat in the initial part of the drive phase; heavyweight women achieved their maximum suspension at the catch whilst lightweights, particularly lightweight men, continued to increase suspension for at least the first 10% of the stroke; this feature was not statistically assessed but may have increased with intensity, Figure 6.4. It is plausible that increasing anterior rotation of the pelvis and achieving greater sagittal alignment of the pelvis and lumbar spine facilitated a stronger position at the catch that was more easily levered into suspension. Alternatively, the differences in suspension could have been the result of lightweights initialising the stroke by developing bow-wards force and motion with their trunk and arms rather than their legs; this would have delayed the maximum suspension they achieved. These suppositions may be partly supported by observing the

displacement of the HJC in the superior direction during the drive of Step 6. Figure 6.12 shows a slower rate of ascent of lightweights' HJC during the Step 6 drive than for heavyweights. Other differences in the way that heavyweights and lightweights moved concerned the anterior coordinate of the HJC at the catch. Lightweights generally displaced this joint more anteriorly; it was thought that this was due to differences in athletes' anthropometrics and, lightweight men flexing the knee more at the catch. The LWM displaced their HJC anteriorly even more than LWW; this may link with the previously observed reduced anterior pelvic tilt LWM achieved compared to other athletes. It is interesting to consider whether LWM anteriorly displace their HJC and flex their knees as far as they do in order to increase stroke length, and, because they can not anteriorly rotate their pelvis due to muscle tightness. Or could it be, that LWM achieve very little pelvic flexion as a direct result of anteriorly displacing their HJC and flexing their knees. Additional knee flexion and HJC displacement in the anterior direction would be likely to advance the magnitude of interaction between the quadriceps and trunk, thus reducing the space available for the pelvis to anteriorly rotate (the opposite of the effect shown in Figure 8.19). All of this may be linked to the flexibility and relative length of the soleus muscle, which Soper et al. (2004) showed to limit the leg positions achievable at the catch, and is very probably associated with the flexibility of the hamstrings. Other results highlighted differences in the way LWW rotated their HJC and AJC about the coronal axis compared to the other athlete groups. These differences are hard to explain, however it may be that because fewer LWW than any other athlete group were tested, the data was slightly skewed in favour of a particular LWW athlete's technique.

All of the athletes displaced LSJ less superiorly in the rockover when exercising at higher intensity. This suggests that they did not get "*up and over*" as effectively, and implies a poorer rockover with less rotation about the hips when leaving the finish position and beginning the stroke recovery. One possible mechanism for this is that, when exercising at higher intensities there was less extension of the KJC at the finish of the stroke, and the knees broke earlier and faster in the recovery – occasionally at the same time as the heels lost contact with the footstretcher in the early part of the recovery. If the knees were not fully extended then the legs would not have been braced against the initialisation of sternward motion after the finish, thus the seat would have started to translate in the direction of the ergometer flywheel and it would have been much harder for the athletes to rockover about their hips. All of this was observed in the current study. Comparison of heavyweight female scullers and heavyweight female rowers suggests that higher quality postural control of the lower spine and pelvis was displayed by scullers at the finish, and by rowers at the catch. It is also offered that heavyweight female scullers and rowers exhibit higher quality postural control of the lower spine and pelvis than either their lightweight male or lightweight female contemporaries. For the purposes of intervening on and coaching spinal motion and postural control it is of interest that the data

complied by this study shows strong relationships between LSJ flexion/extension at different points in the stroke. This may allow the coaching of catch and drive postures by instructing an athlete to maintain desirable motion characteristics during less physically stressful parts of the stroke; *setting themselves up* for the catch. Correlation coefficients for LSJ alpha at different points in the stroke are shown in Table 10.3.

LSJ α	Catch		MHF		Finish		Knee Up	
	r_1	r_2	r_1	r_2	r_1	r_2	r_1	r_2
Catch	1.00	1.00	0.95	0.95	0.84	0.85	0.84	0.83
MHF	0.95	0.95	1.00	1.00	0.89	0.90	0.87	0.85
Finish	0.84	0.85	0.89	0.90	1.00	1.00	0.90	0.89
Knee Up	0.84	0.83	0.87	0.85	0.90	0.89	1.00	1.00

Table 10.3: Correlation coefficients for LSJ alpha at different points in the rowing stroke

Correlation coefficients are shown comparing LSJ alpha at the catch, at the occurrence of maximum handle force, at the finish, and at the point in the stroke when the knees broke in the recovery. r_1 are Pearson's correlation coefficients, and r_2 are Spearman's rho.

10.1.2 Exercise intensity

The effect of exercise intensity was analysed in Chapter 7 and variables that changed significantly as athletes exercised at various intensities were found. Several variables were found to vary with increases in Step for each of the boat classes considered, and 10 variables changed for all boat classes. The timing of peak handle force and the finish occurred later in the stroke as intensity was increased. These findings are in line with those reported by McGregor et al. (2005) and Martin and Bernfield (1980), and possibly contradict those of Secher (1993). More specifically, the current study found an average delay in the timing of the finish of 37.5% from Step 1 to Step 6, this is similar to the 40% increase reported by Soper and Hume (2004a) based on original work by McBride (1998 – unobtainable article) regarding rowing performed at 20.0 to 35.7 strokes per minute.

The current study noted increases in peak handle force, and decreases in the rate of handle force production expressed in stroke percentages. The increases in the magnitude of peaks are in agreement with previous work (McGregor et al., 2004a; McGregor et al., 2005), and the decreases in the rate of force production are misleading. The dips in the rate of handle force production from low to high intensity exercise, as calculated when normalised by stroke percentage occurred because total stroke time decreased dramatically. This is shown by the significant increases in stroke rate (Figure 7.4, Section 7.2.1). The dips in rate of handle force production shown in Figure 7.2 (Section 7.2.1) do show that there were significant differences between Steps. The average stroke rate can be used to approximate the actual rate at which handle force was developed, and this shows that all athletes increased the rate at which they

generated force as intensity increased, again this agrees with McGregor et al. (2005). Power output significantly and consistently increased as Step increased. There were occasional increases in stroke length and work done for the HWW-SCULL and HWW-SWEEP as intensity increased between Steps 1 and 5. This is in opposition to McGregor et al. (2005), who reported consistency in stroke length for similar intensity increments, and noted a decline in stroke length during maximal intensity pieces. The current study observed minimum test stroke lengths during Step 6, however they were not found to be significantly shorter than Steps 1-5. A greater number of pairwise Step comparisons were found to be significant considering the rate of handle force production, and the minimum force exerted on the seat by HWW-SWEEP and LWM, than HWW-SCULL. This may indicate that compared to other athletes, HWW-SCULL have an increased ability to maintain a good technique as the intensity of ergometer exercise becomes more demanding. Recall that Section 6.3.3 showed that the kinematics of HWW-SCULL changed less going into Step 6 than for other athlete groups. Another difference noted for HWW-SCULL concerned the maximum recorded forces on the seat (that is the minimum downwards force). These results suggested that HWW-SCULL may not choose, or have, to utilise suspension as much as other athletes do until they are exercising at a moderate intensity. It was found that the magnitude of all athletes' suspension away from the seat during the entire drive phase of the stroke became less as Step increased. This is something of a surprise as one might expect suspension to be more easily achieved when accelerating more quickly and generating more force away from the catch. However, it may be that it is this increased acceleration, and thus inevitable deceleration and return of bodyweight to the seat towards the finish that caused the decrease in total drive suspension. That is increased suspension during the initial part of the drive may have been cancelled out by large seat forces when the body was returned to the seat in the second portion of the drive.

As was suggested from descriptive results (Section 10.1.1), all athletes displaced their HJC significantly less anteriorly (sternwards), and flexed their knee significantly less at the catch in Step 6 than they did during lower intensity efforts. In addition to this, the graphs in Chapter 6 and results in Chapter 7 showed that during Step 6 athletes extended the KJC less at the finish than in lower intensity Steps; it was the only Step where an extended knee was not observed in many of the rowers. This last result agrees with findings by McGregor et al. (2005). Considering that stroke length in Step 6 was not found to be significantly shorter than any other Steps (above) and there was less KJC flexion at the catch, and less KJC extension at the finish, it is likely that at higher intensities the athletes in this study used increased lumbar and thoracic flexion in order to maintain stroke length. This has previously been shown to increase the risk of injury to the lower back and is discussed in Section 10.2.

10.1.3 Longitudinal training

Chapter 8 determined several variables which consistently changed over the course of one year (July 2007 to June 2008), often regardless of exercise intensity. Test retest protocols evaluating rowers on ergometers have been shown to be repeatable (Schabert et al., 1999), and the use of the Concept II ergometer has been shown to be more repeatable than other systems such as the RowPerfect (Soper and Hume, 2004b). The repeatability of the current test was also improved because it was one with which the athletes were very familiar. As the test year progressed athletes achieved higher peak forces in all of the Steps considered, with year maxima coming in June 2008 for Step 2 and Step 4, and in December 2007 for Step 6 (2 N higher than in June 2008). Between the autumn to winter tests in 2007 and the spring to summer tests in 2008 the athletes also increased power output in Step 2 and Step 4, and in Step 4 increased the magnitude of work done per stroke, and the rate at which handle force was developed in the drive phase. Considering that the athletes in question focus more on work intensive training in the winter months; to improve physiological parameters such as strength and aerobic capacity, and focus more on technical development and physiological maintenance in the spring and summer months, the gains in parameters such as peak pulling force and power output between winter 2007 and summer 2008 are perhaps even more noteworthy than they first appear. This is possibly linked to increased motivation during preparation for the Beijing Olympic Games. In all Steps the length of the rowing stroke reduced between July 2007 and June 2008, with the summer 2008 data showing a 2% decline, and in addition to this some changes in the timing of key stroke events; peak handle force, finish, and knees break, were noted in Step 4 and Step 6. These small but significant changes did not appear to follow any particular pattern. Smith and Loschner (2002) reproduced Korner and Schwanitz's (1987 – unobtainable article) model of key variables that determine the race time of rowers and their shells. Korner and Schwanitz (1987 - unobtainable article) showed that factors such as the distance covered during the separate stroke phases, as well as instantaneous velocities, power output, work done, and the propulsive forces generated were intimately connected to performance. Considering this, and the results of the current study, it is clear that, with the exception of small decreases in stroke length, the athletes tested in this study showed improvements in performance as the test year progressed.

Only one study was found in the literature that reported the kinematics of athletes over long periods of time (McGregor et al., 2007); the study assessed elite oarswomen twice, and found that improvements in performance variables were coincident with improvements in spinal kinematics and posture two years after an original assessment. The current study observed changes in both the trajectory and rotations about LSJ and HJC at different points in the rowing stroke between July 2007 and June 2008. These changes reflected increased control of spinal posture throughout the duration of the rowing stroke, with increased anterior pelvic rotation at

the catch, and consistently better alignment of the pelvis and lumbar spine; it is suggested that these improvements occurred in response to feedback, and other training and coaching interventions over several months. In addition to this, visual assessments of some data were in agreement with previous findings regarding exercise intensity. The coordinates of joint centres suggested, and the flexion/extension angles showed, significant decreases in the intersegmental LSJ angle at all points in the stroke. Coincidentally there were significant increases in the lateral displacement of KJC and in HJC abduction as the year progressed. This is relevant because with increased lateral displacement of KJC at the catch, the inevitable lateral motion of the femur, would possibly allow the pelvis to more freely anteriorly rotate; resulting in the improvements in LSJ alpha (above). As identified as being desirable by coaches, the athletes also lifted their heels less from the footstretcher at the finish in the pre-Olympic test than they had done six to eight months previously.

10.1.4 Athletic performance

One of the key aims of this work was to identify aspects of rowers' stroke profile and kinematics that could predict high levels of performance. Many previous studies have commented on this problem (Baudouin and Hawkins, 2002; Baudouin and Hawkins, 2004; Hartmann et al., 1993; Hofmijster et al., 2008; Macfarlane et al., 1997; McGregor et al., 2008; Schabort et al., 1999; Secher, 1993; Shephard, 1998; Smith and Loschner, 2002; Soper and Hume, 2004b; Soper and Hume, 2004a). All agree that the most important performance measure of rowing is race time; this has been shown to be influenced by boat speed, the distance travelled during individual strokes, the timing of entire strokes and stroke phases, the mass of the boat and athlete, the sex and anthropometrics of the athlete, propulsive forces generated, power output and work done by the athlete, stroke smoothness, and resistive air and water drag forces. Some authors have also described the effect of the sequencing of body segments on rowing performance (Smith and Loschner, 2002; Soper and Hume, 2004a). However, none have provided explicit kinematic information on what does or does not influence rowing performance. Soper and Hume (2004a) stated that *"There are no clear guidelines available to coaches, selectors or rowers on the ideal biomechanical rowing stroke"*. The current study attempted to address this issue.

Seven different measures were defined as performance variables; all had either previously been identified as being influential on performance (by authors such as those cited above), or were derived from performance theories, or were in line with coaching philosophy: the timing of the finish of the stroke, the rate of handle force production, stroke length, and power output were all used; these are standard measures of performance in rowing, for example; a 2.0% change in average power output may effect a 0.7% change in boat speed; depending on the quality of the athlete, and hence their boat speed this would be equal to a few seconds over a 2000 m race

(Hopkins et al., 2001). In addition to this, three variables that described the interaction of the rower and the ergometer seat were assessed. In order to minimise the effects of drag forces on the speed of rowers and their boats, whole system velocity should be kept as constant as possible through limiting accelerations and decelerations. Furthermore, it has been reported that a boat which is balanced about each of its axes, and rowers who optimise the vertical component of seat force will experience less deleterious hydrodynamic drag (Smith and Loschner, 2002; Soper and Hume, 2004a); although no one has clearly reported what this vertical seat force optimisation entails. Stroke smoothness may also be used to assess rowing performance and categorise athletes' technique (Secher, 1993; Shephard, 1998). The variables *Seat 1* and *Seat 2* were used in the current study; they were the sum of the instantaneous seat force multiplied by the absolute value of the instantaneous medial/lateral COP coordinate, between the catch and the occurrence of maximum handle force, and the catch and the finish respectively. *Seat BW* was the difference in the magnitude of individual athlete's BW and the maximum absolute value of the BM adjusted seat force exerted on the seat during a stroke; Smith and Loschner (2002) proposed that large "humps" in force profiles were inversely related to stroke smoothness. It was thought that lower values of the three seat variables would be indicative of better rowing performance, however these would have to be incorporated in a model of boat dynamics to validate this assumption.

The gender of rowers was found to impact upon five performance variables. Females spent a larger proportion of the stroke in the drive phase. Males performed longer and more powerful strokes, and, probably through increased early drive suspension rather than minimising medial/lateral COP displacement, performed better as measured by *Seat 2* and *Seat BW*. Some similar associations have previously been noted by Hartmann et al. (1993) and McGregor et al. (2008). The results also suggested that increasing the rate of handle force production in the drive phase was beneficial to performance (on the water this should be considered along with exerting peak handle force when the blades are perpendicular to the boat), and provided evidence linking increased stroke rate and delays in key stroke events with greater performance. Five separate measures of rowing performance indicated that it is desirable to suspend as fully as possible away from the ergometer seat during the first half of the drive phase, but that bodyweight should then be returned to the seat before the finish; it was thought that these associations might be linked with athletes' ability to balance themselves during the stroke. This may invalidate the use of *Seat 2* as a performance measure. Mester et al. (1982) previously suggested that trained rowers have heightened vestibular regulation during rowing and that balance was an issue relevant to technique. At the finish, posteriorly displacing COP on the seat was associated with improvements in five performance variables, and it may be that greater suspension during the early portion of the drive is accompanied by anterior displacement of COP in this phase of the stroke; this was nearly always the pattern exhibited by the rowers in

this study (Chapter 6). Other results presented in Chapter 9 suggested that, depending on the particular performance variable which is of most importance to an athlete or coach, there may be different mechanisms by which to develop technique.

Just as the majority of the rowing action was described in the sagittal plane, or using flexion/extension joint angles (Section 10.1.1); the way in which joint centres were displaced in the sagittal plane, and flexed or extended was more relevant than their trajectories in the medial/lateral direction for performance enhancement. The motion of the joint centre most commonly linked with performance was the KJC, this was followed by LSJ and AJC, then by HJC, and finally FJC. It was found that various performance gains were associated with improving the quality of the lumbopelvic ratios observed at the catch and in the middle of the drive. When an athlete's LSJ was located less anteriorly at the catch and more anteriorly whilst maximum handle force was being exerted, their performance improved, as measured by four separate variables. In addition to this, when athletes increased lumbar extension at the finish of the stroke, or when they exhibited additional posterior displacement of LSJ in the recovery of the stroke when the knees broke, performance improved according to three separate measures. All of these relationships recommend against athletes adopting any quasi kyphotic postures at any point in the stroke. It was also found that additional anterior displacement of the KJC at the catch, probably linked to increased compression of the lower limb, improved the scores of four performance variables, and that additional inferior displacement of the KJC in the middle of the drive improved the scores of three performance parameters. At the finish of the stroke, as the AJC was positioned more inferiorly and anteriorly athletes' performance improved in terms of up to five measured performance indicators; this is in line with the coaching principle to keep the heels in contact with the footstretcher at the finish of the stroke. It was also found that when athletes' AJC were displaced superiorly as the knees broke in the recovery phase, three performance variables improved. In addition to these universal recommendations, as with stroke profile variables, depending on the particular performance variable that is most important to an athlete, different modifications to the way in which movement is executed are appropriate for performance enhancement.

Soper and Hume (2004a) recently provided a review of some of the questions that biomechanical analysis can answer in rowing. They also posed some other questions. Relevant to these, the current work has provided results showing, amongst other things, that an increased rate of force production is desirable for performance, that coaches and selectors may use force application profiles along side other parameters to predict rowing performance, and that changes in athletes' kinematics does influence their performance. It is also suggested that because of the sometimes very small changes in technique and kinematics that influence performance, elite

individuals and their support staff require very accurate feedback in order to effect change on what is already a highly proficient skill set.

10.2 Spinal injury and low back pain

Hickey et al. (1997) demonstrated the high rate of lumbar injury in rowers. Bahr and Holme (2003) stated that lower back pain (LBP) is common in rowing populations, with up to 63% reporting incidences of the condition; indeed Bono (2004) concluded the sport of rowing is associated with a higher incidence of lumbar pain and injury than the general population. It has been suggested that the high incidence of pain and injury is due to the repetitive nature of the rowing action, the spinal mechanics that constitute this action, and the lumbar compressive load experienced which is often in excess of 4.5 times to 6 times ($> 5\text{kN}$) the athlete's bodyweight, (Hase et al., 2004; Morris et al., 2000; Munro and Yanai, 2000). The current study used measurements of the change, and rate of change of the flexion/extension angle at the junction of the fifth lumbar and first sacral vertebral bodies (LSJ alpha), and measurements of external loading (force exerted through the ergometer handle) to represent athletes' risk of lumbar injury. Statistics were employed to identify other kinematic parameters and stroke profile variables that were related to the injury risk. This section discusses the findings of this analysis.

The current study found that an increased risk of injury to the lower back through rapidly extending the lumbar spine during the drive phase was associated with increased forward flexion of the lumbar spine at the catch of the rowing stroke. This finding is in agreement with literature published on the mechanisms of spinal injury (discussed below); when lumbar flexion is exhibited, the human body's natural lumbar lordosis is flattened and the load experienced by the discs increases (Gray's Anatomy, 2008). Spinal anatomy dictates that the zygoapophyseal joints protect the intervertebral discs from the effects of excessive shear and torsion, whilst the intervertebral ligaments prevent excessive bending. The zygoapophyseal joints are synovial and hence are vulnerable to degeneration as a result of load. Furthermore, if the protective structures mentioned above are damaged, not only can this in itself cause injury and pain, but the risk of damage to the intervertebral discs increases; this has previously been demonstrated in relation to intradiscal pressure (Adams et al., 1993) and with respect to disc prolapse (Panjabi et al., 1982). Lumbar discs are vulnerable to prolapse, sciatica, pain, and further injury. They are large avascular structures, and therefore do not have a high capacity for healing after injury.

In rowing, it is not unreasonable to assume that injuries may occur due to the interaction of the transmission of high magnitudes of load exceeding the tolerance of individual tissues, and unfavourable movement. During weight lifting lumbar compressive force has been measured up to 1.9 kN when lifting a 10 kg weight, and up to 5.5 kN when a healthy young man lifts a

weight of 29 kg (Nachemson, 1981; Potvin et al., 1991). It is fair to assume that because muscular activity is the key contributor to increases in compressive spinal loads, rowers propelling their bodies through the drive phase will experience compressive forces that are comparable or greater than these, indeed Munro and Yanai (2000) calculated possible compressive forces of 5344 N during rowing activity. It has been shown that in flexion when the spine is transmitting load, and it is in compressive load of over 500 N, tension generated in the ligaments can compress the intervertebral discs, inducing increases of hydrostatic intradiscal pressure in excess of 100% (Adams and Dolan, 1995). Whilst during lifting, propulsive motion has been shown to increase peak compressive loads on the spine by up to 100% (Dolan et al., 1994). The drive phase of the rowing stroke may be likened to a high pull in weightlifting, and during competitive lifting Cholewicki et al. (1991) report relevant compressive loads of up to 18 kN. Forward flexion of the lumbar spine causes the inferior facets to be bent forwards and downwards (Green et al., 1994) and, bending of superior lumbar vertebrae's neural arch about the pedicles, which may in turn increase shear forces that must be resisted by the zygoapophyseal joints (Adams and Dolan, 1995). If this motion is combined with compressive load, as is surely the case in the drive in rowing, anterior wedge fractures can result (Hutton and Adams, 1982).

It is also thought that the bending moment that acts upon osteoligamentous structures in flexion is associated with damage observed in intervertebral discs and spinal ligaments. It has been shown that these moments increase in heavy lifting and also when the quadriceps become fatigued compelling the back to bear more of the lift (Dolan et al., 1994; Trafimow et al., 1993). It is interesting to note that rowers' tendency to train early in the morning may be dangerous to the lower back due to diurnal variations in spinal mechanics, which in turn lead to changes in the structural properties of the whole spine. Specifically; increased intradiscal pressure present in the early morning is associated with increasing the bending moment; possibly increasing the risk of injury to discs and ligaments (Adams and Dolan, 1995). Reid and McNair (2000) suggested that 60 seconds of unloaded flexion and extension movement of gradually increasing amplitude should be carried out in a sitting position before rowing to reduce this effect.

In flexion the first signs of ligament damage have been noted to occur between 5° and 20°, depending on the lumbar level (Adams and Dolan, 1995). In the current study the average level of maximum flexion about LSJ was 11.8° ($\pm 10.6^\circ$). Furthermore, a combination of even moderate compressive loading and lumbar flexion has been shown to induce gradual disc prolapse (Panjabi et al., 1982), and has been linked with low back pain in rowers (O'Sullivan et al., 2003). Interestingly, and with relevance to injury risk in rowers who have never before had problems of lumbar injury or pain, Adams and Hutton (1982; 1985) showed that intervertebral

discs that were most easily prolapsed in the laboratory came from individuals of less than fifty years of age, and exhibited no signs of degeneration.

So far this section has concentrated on the ways in which the osteoligamentous lumbar structures may be injured through lumbar flexion in the drive of the rowing stroke. This kind of kyphotic posture specifically directs load bearing away from muscle groups such as erector spinae, and hence presumably reduces energy expenditure, and can be beneficial in preventing muscular injury (Gracovetsky et al., 1990). Straker (2003) suggested that during lifting, a less kyphotic posture should be assumed because *“one would prefer muscle tissue injury rather than a ligament injury due to the muscles’ ability to heal”*.

As stated above, athletes in the current study who exhibited rapid extension of LSJ, during the drive and thus under loading, adopted increased lumbar flexion at the catch. It was also found that rapidly extending the lumbar spine was associated with rapidly flexing the spine for short periods at the beginning of the drive phase (on average, peak rate of extension multiplied by instantaneous handle force occurred 13.9% ($\pm 7.1\%$) later in the stroke than peak rate of flexion multiplied by instantaneous handle force). This rapid flexion flowed by rapid extension was thought to be associated with a technical error known as a “bum shove”. Brown and Abani (1985) suggested that bum shoving may occur as a result of the hip extensor muscles being weaker than the knee extensors. More importantly with reference to the current study’s findings, is that some of the athletes’ rapidly flexed their spine in the early portion of the drive; this is because rapid flexion about LSJ increases the risk of injury to the intervertebral discs and ligaments (Adams and Dolan, 1995). The rapid changes observed in LSJ alpha during the drive may also cause the spinal structures to be “jerked”, which, according to MacKinnon and Li (1998) is associated with an increased risk of damage. This finding supports the injury relevance of the variables chosen to represent injury risk in the current study.

In Chapter 9 it was shown that increasing the sagittal angle between the anterior and posterior parts of the foot (separated along the line of the metatarsal heads), and thus raising the heels from the footstretcher at the catch was related to reducing the risk of injury to the lower spine. It is probable that the reason for this is that by raising the heels at the catch the magnitude of lumbar flexion is reduced. In order to maintain a long rowing stroke athletes must displace the ergometer handle or, in the boat, the blade anteriorly at the catch and pull it close to their torso at the finish. Because the front of the foot is constrained in rowing, raising the heels from the footstretcher when approaching the catch increases knee flexion and hip flexion; this serves to anteriorly displace the seat, pelvis, and hips, and thus for no additional lumbar flexion the athlete gains stroke length. This demonstrates how changing the motion of proximal body segments can influence the posture of regions higher up the kinematic chain. Chapter 7 showed

that at higher intensity athletes anteriorly displaced their HJC less and flexed their KJC less at the catch; this suggests that lumbar flexion would necessarily be increased if stroke length was to be maintained. When exercising at high intensity, the current study observed small but statistically insignificant increases in LSJ flexion, and small but statistically insignificant decreases in stroke length (Chapter 6 and Chapter 7). A cautionary note here is that hyper flexion of the knee at the catch may be deleterious to the health of the knee joint. In rowing this aspect of technique is often coached by encouraging athletes to exhibit “vertical shins” at the catch; in the current study athletes’ KJC was measured to be 81 mm (± 41 mm) anterior to their AJC at the catch. By using the X,Y,Z catch coordinates of the KJC and AJC as measured in the current study, the average length of athletes’ tibias was calculated to be 425 mm (± 22 mm); this was 55 mm longer than the average tibial length reported in a cadaver study by Lopez-Casero et al. (1995), and almost identical to that measured from an elite rowing population by Dimakopoulou et al. (2007); 419 mm (± 19 mm). In the current study, by displacing the KJC 81 mm anterior to the AJC at the catch athletes affected an additional 11° of rotation that was probably distributed between increased flexion of the AJC, KJC and HJC.

Athletes who extended about LSJ during the drive of the stroke also exhibited lumbar extension at the finish. This type of movement (constant forwards and backwards bending) causes large stress reversals in the pars interarticularis, and may explain why spondylolysis is so regularly observed in athletes who, like rowers, frequently flex and extend their lumbar spine (Hardcastle et al., 1992). In the current study average flexion of the lumbar spine at the catch was 10.4° ($\pm 10.6^\circ$), and extension at the finish was 3.5° ($\pm 10.4^\circ$); range of flexion being greater than extension is in agreement with the literature (Gray's Anatomy, 2008; Pearcy et al., 1984). Adams and Dolan (1995) reported that “*fluid flow within and from the disc reduces its resistance to bending and shear*”, furthermore, the compressive strength of vertebral bodies has been shown to weaken by 50% if subjected to 5,000 loading cycles (Brinckmann et al., 1988; Hansson et al., 1987). Chapter 1 stated that elite athletes perform approximately 4,000 rowing strokes every day of their training lives, as well as weight training, cycling, running and circuit training; there is little doubt that the cumulative effect of this may be deleterious to the acute and chronic health of the spine.

As with lumbar flexion, the association noted in the current study linking increased lumbar extension at the finish of the stroke and injury is of concern. This type of movement may indicate less involvement of the knee extensors and an increased reliance on the hip and back extensors (Holt et al., 2003; Sparto et al., 1997). When the natural lumbar lordosis of the lumbar spine is accentuated by extension about LSJ additional compressive stress is exerted onto the posterior elements of the spine, and often leads to LBP (Adams and Dolan, 1995). This deterioration in posture has been linked to weakened abdominal muscles, tight hamstrings, and

unequal antagonistic muscular activity acting on the spine (Adams and Dolan, 1995; Gray's Anatomy, 2008). Although one function of the muscles is to move the spinal column, muscular activity is also involved in providing the stability needed to maintain posture and provide a platform for limb function, furthermore, providing the coactivation of muscle groups is appropriately balanced, greater activation of the muscles often provides added stability. Because spinal stability decreases when under less loading (Cholewicki and McGill, 1996), it is possible that in rowing, as force generation dissipates when nearing the finish of the stroke, activation of the trunk muscles will be less. If this is the case then athletes' lumbar spines would not only be at risk from damage caused by hyper extension about LSJ, but also, in the absence of appropriate motor control, from general instability. Increased lumbar extension and instability has previously been linked with increased compressive stress on the posterior portion of the annulus fibrosus, damage to the zygoapophyseal joints, bending of the inferior articular processes about the pars interarticularis, and thus deformation of the posterior margin of the joint capsule (Cholewicki and McGill, 1996; Green et al., 1994). Furthermore, Cholewicki and McGill (1996) state that even if large muscle groups exhibit significant activation there is a risk of lumbar buckling if the small internal muscles do not.

The erector spinae, internal oblique, and transversus abdominis are anatomically and functionally connected by the thoracolumbar fascia. This fascia plays an important role in resisting forward bending of the trunk, and probably has an important function in transferring load between the trunk and lower limbs; this is vital in rowing. All of this information confirms the important role of the osteoligamentous and the muscular tissues of the lumbar spine in controlling stability and motion, and providing protection to vulnerable structures in flexion and extension during rowing. It was stated earlier that transmission of high magnitudes of load exceeding the tolerance of individual tissues was relevant to spinal injury, and the above information relating to increased spinal instability with decreased muscular activation at the finish is in line with a hypothetical model of injury risk proposed by Cholewicki and McGill (1996). The model suggested that spinal injury may be caused by the disruption of tissue by high loading, or by instability facilitating local joint movement and subsequent damage to soft tissue (Figure 10.1). As Caldwell et al. (2003) cited an awareness of increased lumbar flexion and muscular fatigue as being important for injury prevention in rowing, so Chapter 9 of this thesis reported that the athletes tested had a greater risk of injury to their lower back if they exhibited increased levels of LSJ flexion at the catch, increased LSJ extension at the finish, and lower quality postural control throughout the drive phase. It is offered, that in rowing an athlete may experience lumbar injury due a combination of lumbar flexion, lumbar extension, rapid changes in the flexion/extension angle about LSJ, tissue failure whilst exerting peak forces, and because of instability and poor postural control. Of these, at least lumbar flexion at the catch may be ameliorated by certain motion behaviour of the lower limbs. The results presented may

suggest that a straight back posture would equalise the compressive stresses across the vertebral disc, and may be the “ideal” technique for rowers to adopt when they are performing.

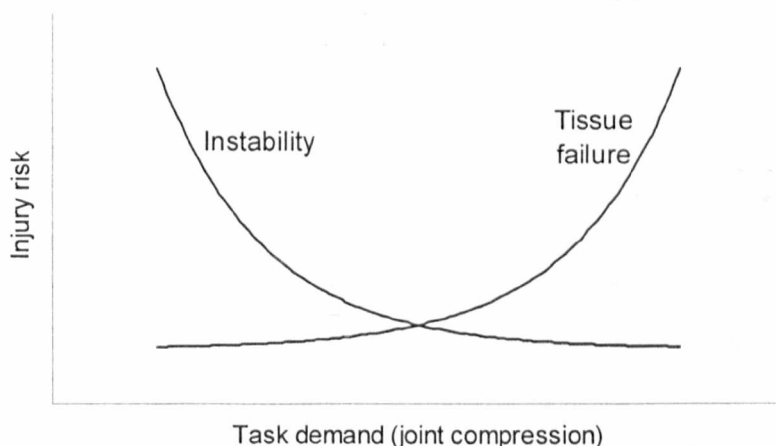


Figure 10.1: Hypothetical model of lumbar injury risk to the spine
Proposed by Cholewicki and McGill (1996)

In the current study greater risk of injury was also associated with greater values of performance variable Seat 2, increased power output, and delays in the timing of the knees breaking in the recovery. These relationships are linked to increases in exercise intensity (Chapter 6 and Chapter 7), and thus show that the risk of injury to athletes’ lumbar spine is increased whilst exercising at greater intensity. Interestingly the kinematics of LSJ, HJC, KJC, and AJC, and the displacement of COP measured in the current study all suggested athletes may use increased lumbar and thoracic rotation at higher intensities (Section 10.1). This assertion is somewhat supported by the work of Taimela et al. (1999) who showed that fatigued lumbar muscles impaired proprioception, and more specifically the ability of subjects to sense the orientation of their trunk when in flexion; thus as athletes become more fatigued as they exercise at higher intensity they may not be aware of adopting increased lumbar flexion. An increased risk of injury was also associated with a decrease in the timing of maximum handle force; this shows that very high rates of force development in the initial portion of the drive are a potential mechanism by which athletes’ lumbar spines could be injured.

It is beyond the scope of this study to comment on whether any of the athletes tested suffered any of the structural damage cited above. Furthermore, because lumbar injury and pain is often the product of long term mechanical and physiological interactions, the longitudinal aspects of rowers’ spinal health remains obscure. Information taken from the literature was presented to demonstrate the possible consequences of lumbar flexion and extension whilst the spine is being loaded. Further study into technical parameters indicative of spinal health in rowers is merited.

Along with reviewing the thesis in its entirety, the next and final chapter discusses the approaches that were used to obtain the results discussed in this chapter. Recommendations for improvements to the current system, and areas for future research are also offered.

Chapter 11

General Discussion, Summary and Future Work

The main aim of this thesis was to describe and analyse performance parameters of elite rowers in terms of three-dimensional mechanics of movement on an ergometer. This chapter summarises all of the work that was carried out, discusses some key issues regarding the methodologies that were developed and the whole thesis work in the context of the prior literature. A summary of the key results is presented, and some suggestions for future work are offered.

This study has quantified the level to which the environment in which motion tracking is conducted is detrimental to the performance of the electromagnetic system used in this thesis. The layout of a human performance laboratory was optimised to minimise this error for the extended range Flock of Birds electromagnetic motion tracking system. The Flock of Birds system was found to be a suitable technology for measuring the trajectory of moving body segments, and thus the kinematics of rowers during ergonomic training. This was in agreement with previous studies that considered the motion of the lower limbs and lumbar spine (Bergman, 2005; Bull et al., 1998; Bull and McGregor, 2000; Gatton and Peacy, 1999; Koerhuis et al., 2003; Mannion and Troke, 1999; McGregor et al., 2004a; McGregor et al., 2005). In addition to this a calibration procedure was carried out on a bespoke arrangement of force transducers housed under the seat of a rowing ergometer in the same human performance laboratory. After calibration the system was able to very accurately report the magnitude and position of forces applied to the apparatus (post calibration maximum and mean system errors were 2.95% and 0.51% of the applied load, and 3.43 mm and 1.10 mm for force magnitude and COP respectively).

The description of a kinematic model developed specifically for this study was presented, and a relevant and repeatable experimental testing protocol was designed. This protocol was used in conjunction with a bespoke instrumented ergometer to measure the rowing performance and technique of elite athletes on 1,115 occasions over a period of 26 months. The trajectories of anatomical locations were not tracked relative to a single “parent” body segment or from some other fixed laboratory axis system and therefore it was critical that placement of the transmitter in the laboratory be made consistent if comparisons were to be made between testing sessions. Furthermore, because the medial lateral axis of the ankle joint centre was defined as being coincident with the medial lateral axis of the FOB source inconsistencies in the orientation of transmitter placement could be detrimental to the calculation of ankle angles. This issue had no impact upon the calculation of intersegmental angles at other joints. A pilot study revealed that

placement of the transmitter in the current study was highly repeatable, and potential measurement error due to misplacement of the transmitter was not an issue when quantifying differences of more than 1.5 mm to 9.9 mm, or 0.1° to 1.0° depending on the direction being considered. This is an area where the current method may be improved in the future.

The location of the junction of the fifth lumbar and first sacral vertebral bodies within a local pelvis axis system was determined by an experiment described in Chapter 4. The technique determined the location of the lumbosacral junction within a local pelvis coordinate frame in sixteen CT stacks. This permitted derivation of a regression equation for locating the joint centre in the athletes who participated in testing; a vital input for the current kinematic model. Similar techniques have previously been used to determine the location of the hip joint centre (Andriacchi et al., 1980; Bell et al., 1989; Bell et al., 1990; Seidel et al., 1995; Tylkowski et al., 1982). Results of the experiment showed that on average the current technique was able to provide the location of the lumbosacral junction to within 8.4 mm (± 3.3 mm) of its true coordinate within the pelvis. A subsequent leave one out analysis (Section 4.1.6.2) increased this average error to 8.9 mm (± 3.6 mm), with a maximum error of 18.8 mm. This is a greater error than would be desirable, though is less than that reported for hip joint centre location using the techniques from the literature, and by utilising approaches combining favourable aspects of those separate techniques. Errors reported from the studies cited above ranged from 11 to 27 mm in two dimensions, and 26 to 33 mm in three dimensions. The current technique was deemed to be valid for use in determining athletes' kinematics. In the future, refinement of the current method would be desirable as it is not yet as accurate as other methods that have been used to determine the centre of rotation of joints. Specifically, the functional method for hip joint centre location has been shown to be a more accurate technique (Camomilla et al., 2006; Cappozzo et al., 1995; Cereatti et al., 2004; De Momi et al., 2009; Piazza et al., 2001; Piazza et al., 2004). However, because of the complex interaction of individual vertebral bodies, and their small individual ranges of motion, the functional method is not practical for determining the location of the lumbosacral junction.

The way in which the posterior foot segment was defined in the current study was another source of error. As it was not possible to monitor the motion of the calcaneus there was an offset in the calculated flexion/extension angles of body segments about the ankle joint centre and about the junction of the posterior and anterior foot segments. Despite the magnitude of these angles being incorrect, it was possible to determine important recommendations for body kinematics by observing the change in the angles during the rowing stroke. It was also not possible to calculate the angles of knee varus/valgus or internal/external rotation using the current hardware and software systems. Such rotations may be linked to rowing performance,

and measurement of varus/valgus would possibly give insight into injury mechanisms at the knee.

A data analysis method was presented and, in part, constructed in this thesis. The method allowed the calculation of relevant information, the reduction of datasets, and the extraction of key information relating to athletes' rowing technique and performance. Much thought was given to choosing the most appropriate statistical techniques to employ throughout this thesis, however reliance on Microsoft Excel, Matlab, and SPSS had some shortcomings. Calculation of descriptive statistics and some correlation analyses aside, all statistical modelling was conducted using SPSS. In SPSS there is a limited choice of non-parametric tests which perform analysis of variance with repeated measures, and there are no tests in the "base" package for non-parametric regression modelling. Furthermore, the choice of post hoc procedures is limited within repeated measures designs. This lack of choice may have been a limiting factor when determining the results presented in Chapter 7, Chapter 8, and Chapter 9. In the future it might be possible to improve the data analysis method, either through the use of more powerful statistics packages such as Stata (StataCorp LP, Texas, USA), or by producing custom programs that would perform the required operations. This could provide a wider choice of non-parametric tests, and permit use of post hoc procedures such as Tukey's HSD and WSD, Gabriel's, Hochberg's GT2, Games-Howell, or Ryan, Einot, Gabriel & Welsch Q (REGWQ). Such post hoc procedures reduce the probability of making type I or type II statistical errors, are robust to deviations from homogeneity of variance, and allow groups of uneven sizes to be compared; this would have allowed more athletes' data to be included in Chapter 8. In the current study most of the athlete data was parametrically distributed, and the distribution of regression model residuals, and their relationship to fitted and independent variables validated the assumptions required by Chapter 9. However, limited data was not appropriately distributed in Chapter 7 and Chapter 8. As such a wider range of statistical algorithms may have provided additional insights.

Data analysis was carried out to address five hypotheses:

1. That a full description of the stroke profile and three-dimensional kinematics of elite rowers could be produced (Chapter 6).
2. That some aspects of elite rowers' technique and performance would be affected by the intensity of their exertions (Chapter 7).
3. That some aspects of elite rowers' technique and performance would change with longitudinal training (Chapter 8).
4. That high levels of performance could be predicted by aspects of athletes' technique and rowing kinematics (Chapter 9).

5. That some aspects of elite rowers' technique, performance and rowing kinematics could be exploited to reduce the risk of injury and pain (Chapter 9).

A detailed description of elite athletes' rowing technique and kinematics that is unmatched in the literature was produced. The effects of exercise intensity and longitudinal training were assessed with reference to this technique. Aspects of technique and motion characteristics were identified and shown to be predictors of high levels of rowing performance, and acute and chronic lumbar injury and pain. A finding of this work was that the correlation between kinematics recorded at key points in the stroke, for example the catch, were strongly and significantly correlated with the stroke maximum and minimum measurements. This information may be useful in the design of future measurement systems for rowing biomechanics, and, depending on the requirements and constraints of any particular system, negate the need to measure variables at specific stroke events. In general the technique and kinematics of different athlete groups was similar, though some differences were noted regarding movement patterns and technical parameters such as how the athletes suspended away from their seat during the propulsive part of the stroke. These were fully described and may have been a result of training status, skill level, muscular strength and flexibility, or body size and bulk. Increasing exercise intensity influenced some of the measured parameters, with a general decline in the "quality" and repeatability of athletes' motion at higher intensity. Longitudinal feedback, training, and coaching interventions were effective in influencing the technique of elite individuals. Adopting a kyphotic posture in the region of the lower back at any point in the rowing stroke was found to be detrimental to rowing performance, and may be linked to an increased risk of lumbar injury. Regarding injury risk, this is also true of extension of the lumbar spine (lordotic poses); however it was found that athletes who moved towards lumbar extension at the finish of the stroke exhibited better performance than those who did not. In addition to this, differences in the kinematic characteristics of the lower limbs may positively influence a rowers' performance, and provide some protection against spinal injury; particularly keeping the heels down at the finish of the stroke, and raising them at the catch. Anecdotal evidence has shown that this system and the feedback provided by it have influenced coaching behaviour and terminology within Great Britain's elite rowing squad.

It is suggested that in the future it would be valuable to develop the current structure of measurement and analysis in a few ways. Firstly, attempts should be made to track the motion of more of the body; specifically the thoracic spine and both legs (the current study only tracked the right leg, Section 4.1). This would increase our knowledge of how athletes might gain performance advantages, and could provide insight into injury mechanisms over the entire vertebral column, whilst also describing the bilateral symmetry of the lower limbs. A more detailed investigation of the influence of technique and kinematics during the recovery phase of the rowing stroke is also merited, as it is in this part of the stroke when maximal boat velocity occurs on the water. Along with increased kinematic assessment, instrumentation of the ergometer footstretcher would permit inverse dynamics to be carried out, thus allowing the calculation of intersegmental forces and moments, and expanding the useful information available to sport scientists, coaches, other support staff, and athletes. This increased dataset would allow continual development of the training regimes, coaching, and rehabilitation strategies available to rowers. Conducting testing sessions where the athletes competed in races may increase the understanding of factors that influence performance, and the integration of real athlete data collected using systems like the current one, with computer simulations of rowing on the water might also be used to further this understanding. It would also be interesting to compare athletes' technique and motion between the first few strokes from a standing start, and when they were "up to pace"; this might allow developments to be made regarding starting strategies in race situations – "getting out of the blocks". Monitoring biomechanical and physiological parameters (such as respiration, oxygen uptake, or blood lactate accumulation) in parallel would improve the field's knowledge base on the mechanical efficiency of rowing, and describe kinematic patterns that maintain mechanical output whilst reducing physiological cost – this could be linked to the smoothness of the rowing stroke. Furthermore, examination of the medical history of athletes would add insight into injury mechanisms. All of this data may then be used not only in training elite individuals, but also for talent identification amongst younger rowers, or those further down the competitive ladder.

It is widely accepted that the specificity of sports training and assessment is a key component of best practice. Thus any progress of the current system that permitted measurement of athletes' technique and kinematics on the water is highly recommended. This might involve the development of wireless telemetry systems, subject specific instrumentation, and technology allowing the athlete to observe themselves and their output in real time as they rowed and tried out new things on the water; this could be achieved with video goggles or lightweight feedback displays mounted on the canvas of the boat. Chapter 2 described the interdisciplinary approach that is commonplace in today's elite sporting environment. It is this type of approach that best serves the needs and goals of athletes and this should always be given due consideration when designing a structure of training, support and assessment. In addition to specificity is

individualisation; this study has found some universal recommendations that rowers should consider when refining their skill set, however it is also thought that furthering the individualisation of feedback would be a desirable advancement. Individualisation is commonplace in sport science, and the development of such biomechanical interventions may include detailed athlete specific anthropometrics in kinematic modelling, medical and anatomical pathology history, athlete specific instrumentation, incorporation of measures of physical strength and fitness, and more detailed analysis of different styles of rowing. The method that was developed for the current study is transferable to other groups of athletes and other sports too. With just a few modifications, the current method could be used to observe the technique, performance, and injury mechanisms of adaptive rowers (physically disabled), or could be used to monitor kayakers, cyclists, cross country skiers, runners, lifters, wheelchair athletes involved with many track and field sports, or could be applied to clinical and occupational situations. Whilst this study has refreshed and significantly enhanced the knowledge base of rowing technique, further work remains to be done.

References

- Adams, M. A., Dolan, P., (1995). Recent advances in lumbar spinal mechanics and their clinical significance. *Clinical Biomechanics* 10, 3-19.
- Adams, M. A., Hutton, W. C., (1985). Gradual Disc Prolapse. *Spine* 10, 524-531.
- Adams, M. A., Hutton, W. C., (1982). Prolapsed Intervertebral Disc: A Hyperflexion Injury. *Spine* 7, 184-191.
- Adams, M. A., McNally, D. S., Wagstaff, J., Goodship, A. E., (1993). Abnormal stress concentrations in lumbar intervertebral discs following damage to the vertebral bodies: a cause of disc failure? *European Spine Journal* 1, 214-221.
- Amis, A. A., Bull, A. M. J., Farahmand, F., Senavongse, W., Shih, Y. F., (2004). Patellofemoral joint biomechanics. In: Biedert, R. M. (Ed.), *Patellofemoral disorders: Diagnosis and treatment*. John Wiley & Sons, Ltd, pp. 37-53.
- Andriacchi, T. P., Andersson, G. B. J., Fermier, R. W., Stern, D., Galante, J. O., (1980). A study of lower-limb mechanics during stair-climbing. *Journal of Bone and Joint Surgery* 62, 749.
- Ascension Technology Corporation, (2002). *Flock of Birds Installation and Operation Guide*. Burlington, VT, USA.
- Bahr, R., Holme, I., (2003). Risk factors for sports injuries – a methodological approach. *British Journal Of Sports Medicine* 37, 384-392.
- Baker, R., (1997). The "Poker" Test: A Spot Check to confirm the accuracy of Kinetic Gait Data. *Gait & posture* 5, 177.
- Baudouin, A., Hawkins, D., (2002). A biomechanical review of factors affecting rowing performance. *British Journal of Sports Medicine* 36, 396-402.
- Baudouin, A., Hawkins, D., (2004). Investigation of biomechanical factors affecting rowing performance. *Journal of Biomechanics* 37, 969-976.
- Bell, A. L., Brand, R. A., Pederson, D. R., (1989). Prediction of hip joint centre location from external landmarks. *Human Movement Science* 8, 3.
- Bell, A. L., Pederson, D. R., Brand, R. A., (1990). A comparison of the accuracy of several hip center location prediction methods. *Journal of Biomechanics* 23, 617-621.
- Bergman, G. J. D., (2005). Variation in the cervical range of motion over time measured by the "Flock of Birds" electromagnetic tracking system. *Spine* 30, 650-654.
- Bernstein, I. A., Webber, O., Woledge, R., (2002). An ergonomic comparison of rowing machine designs: possible implications for safety. *British Journal of Sports Medicine* 36, 108-112.
- Bobbert, M. F., Schamhardt, H. C., (1990). Accuracy of determining the point of force application with piezoelectric force plates. *Journal of Biomechanics* 23, 705-710.
- Bono, C. M., (2004). Low-Back Pain in Athletes. *Journal of Bone and Joint Surgery* 86, 382-396.

- Bottlang, M., Marsh, J. L., Brown, T. D., (1998). Factors influencing accuracy of screw displacement axis detection with a DC-based electromagnetic tracking system. *Journal of Biomechanical Engineering* 120, 431-435.
- Brinckmann, P., Biggemann, M., Hilweg, D., (1988). Fatigue fracture of human lumbar vertebrae. *Clinical Biomechanics* 3.
- Brown, E. W., Abani, K., (1985). Kinematics and kinetics of the dead lift in adolescent power lifters. *Medicine and Science in Sports and Exercise* 17, 554-563.
- Browne, J., O'Hare, N., (2000). A quality control procedure for force platforms. *Physiological Measurement* 21, 515.
- Bull, A. M. J., Berkshire, F. H., Amis, A. A., (1998). Accuracy of an electromagnetic measurement device and application to the measurement and description of knee joint motion. *Proceedings of the Institution of Mechanical Engineers, Part H: Journal of Engineering in Medicine* 212, 347-355.
- Bull, A. M. J., Earnshaw, P. H., Smith, A., Katchburian, M. V., Hassan, A. N. A., Amis, A. A., (2002). Intraoperative measurement of knee kinematics in reconstruction of the anterior cruciate ligament. *The Journal of Bone and Joint Surgery* 84, 1075-1081.
- Bull, A. M. J., McGregor, A. H., (2000). Measuring spinal motion in rowers the use of an electromagnetic device. *Clinical Biomechanics* 15, 772-776.
- Caldwell, J. S., McNair, P., Williams, M., (2003). The effects of repetitive motion on lumbar flexion and erector spinae muscle activity in rowers. *Clinical Biomechanics* 18, 704-711.
- Camomilla, V., Cereatti, A., Vannozzi, G., Cappozzo, A., (2006). An optimized protocol for hip joint centre determination using the functional method. *Journal of Biomechanics* 39, 1096-1106.
- Caplan, N., Gardner, T. N., (2005). The influence of stretcher height on the mechanical effectiveness of rowing. *Journal of Applied Biomechanics* 21, 286-296.
- Cappello, A., Lenzi, D., Chiari, L., (2004). Periodical in-situ re-calibration of force platforms: A new method for the robust estimation of the calibration matrix. *Medical & Biological Engineering & Computing* 42, 350-355.
- Cappozzo, A., Cantani, F., Della Croce, U., Leardini, A., (1995). Position and orientation in space of bones during movement: anatomical frame definition and determination. *Clinical Biomechanics* 10, 171.
- Cereatti, A., Camomilla, V., Cappozzo, A., (2004). Estimation of the centre of rotation: a methodological contribution. *Journal of Biomechanics* 37, 413-416.
- Chee, S. T. H., Loh, J. M. H., McGregor, A. H., Bull, A. M. J., (2009). Unpublished PhD thesis.
- Cholewicki, J., McGill, S. M., (1996). Mechanical stability of the in vivo lumbar spine: implications for injury and chronic low back pain. *Clinical Biomechanics* 11, 1-15.
- Cholewicki, J., McGill, S. M., Norman, R. W., (1991). Lumbar spine loads during the lifting of extremely heavy weights. *Medicine and Science in Sports and Exercise* 23, 1179-1186.
- Colloud, F., Bahuaud, P., Cheze, L., (2006a). Symmetry in rowing air-braked ergometers. *Journal of Biomechanics* 39, S458.

- Colloud, F., Bahuaud, P., Doriot, N., Champely, S., Cheze, L., (2006b). Fixed versus free-floating stretcher mechanism in rowing ergometers: mechanical aspects. *Journal of Sports Sciences* 24, 479-493.
- Dandachli, W., Nakhla, A., Iranpour, F., Kannan, V., Cobb, J. P., (2009). Can the Acetabular Position be Derived from a Pelvic Frame of Reference? *Clinical Orthopaedics and Related Research* 476, 886-893.
- Day, J. S., Dumas, G. A., Murdoch, D. J., (1998). Evaluation of a long-range transmitter for use with a magnetic tracking device in motion analysis. *Journal of Biomechanics* 31, 957-961.
- Day, J. S., Murdoch, D. J., Dumas, G. A., (2000). Calibration of position and angular data from a magnetic tracking device. *Journal of Biomechanics* 33, 1039-1045.
- De Groot, J. H., (1997). The variability of shoulder motions recorded by means of palpation. *Clinical Biomechanics* 12, 461-472.
- De Momi, E., Lopomo, N., Cerveri, P., Zaffagnini, S., Safran, M. R., Ferrigno, G., (2009). In-vitro experimental assessment of a new robust algorithm for hip joint centre estimation. *Journal of Biomechanics* 42, 989-995.
- Della Croce, U., Leardini, A., Chiari, L., Cappozzo, A., (2005). Human movement analysis using stereophotogrammetry. Part 4: assessment of anatomical landmark misplacement and its effects on joint kinematics. *Gait and Posture* 21, 226-237.
- Dimakopoulou, E., Blazeovich, A. J., Kaloupsis, S., Diafas, V., Bachev, V., (2007). Prediction of stroking characteristics of elite rowers from anthropometric variables. *Serbian Journal of Sports Sciences* 1, 89-96.
- Dolan, P., Earley, M., Adams, M. A., (1994). Bending and compressive stresses acting on the lumbar spine during lifting activities. *Journal of Biomechanics* 27, 1237-1248.
- Fairburn, P. S., Palmer, R., Whybrow, J., Fielden, S., Jones, S., (2000). A prototype system for testing force platform dynamic performance. *Gait & posture* 12, 25.
- Field, A., (2000). *Discovering Statistics using SPSS for Windows*. SAGE Publications Ltd.
- Fleming, H., Hall, M. G., Dolan, M. J., Paul, J. P., (1997). Quality framework for force plate testing. *Proceedings of the Institution of Mechanical Engineers, Part H: Journal of Engineering in Medicine* 211, 213-219.
- Gatton, M. L., Peacy, M. J., (1999). Kinematics and movement sequencing during flexion of the lumbar spine. *Clinical Biomechanics* 14, 376-383.
- Gill, H. S., O'Connor, J. J., (1997). A new testing rig for force platform calibration and accuracy tests. *Gait & posture* 5, 228-232.
- Gracovetsky, S., Kary, M., Levy, S., Said, R. B., Pitchen, I., Helie, J., (1990). Analysis of Spinal and Muscular Activity During Flexion/Extension and Free Lifts. *Spine* 15, 1333-1339.
- Gray's Anatomy, (2008). *Gray's Anatomy: The anatomical basis of clinical practice*. Churchill Livingstone Elsevier.
- Green, T. P., Allvey, J. C., Adams, M. A., (1994). Spondylolysis: bending of the inferior articular processes of lumbar vertebrae during simulated spinal movements. *Spine* 19, 2683-2691.

- Good, E. S., Sontay, W. J., (1983). A joint coordinate system for the clinical description of three-dimensional motions: application to the knee. *Journal of Biomechanical Engineering* 105, 136-144.
- Hall, M. G., Fleming, H. E., Dolan, M. J., Millbank, S. F. D., Paul, J. P., (1996). Static in situ calibration of force plates. *Journal of Biomechanics* 29, 659-665.
- Halliday, S. E., Zavatsky, A. B., Hase, K., (2004). Can functional electric stimulation-assisted rowing reproduce a race-winning rowing stroke? . *Archives of Physical Medicine and Rehabilitation* 85, 1265-1272.
- Hansson, T. H., Keller, T., Spengler, D., (1987). Mechanical behaviour of the human lumbar spine. II. Fatigue strength during dynamic compressive loading. *Journal of Orthopaedic Research* 5, 479-487.
- Hardcastle, P., Annear, P., Foster, D. H., (1992). Spinal abnormalities in young fast bowlers. *Journal of Bone and Joint Surgery* 74, 421-425.
- Harrison, D. E., Colloca, C. J., Harrison, D. D., Janik, T. J., Haas, J. W., Keller, T. S., (2005). Anterior thoracic posture increases thoracolumbar disc loading. *European Spine Journal* 14, 234-242.
- Hartmann, U., Mader, A., Wasser, K., Klauer, I., (1993). Peak force, velocity, and power during five and ten maximal rowing ergometer strokes by world class female and male rowers. *International Journal of Sports Medicine* 14, S42-S45.
- Hase, K., Kaya, M., Zavatsky, A. B., Halliday, S. E., (2004). Musculoskeletal loads in ergometer rowing. *Journal of Applied Biomechanics* 20.
- Hawkins, D., (2000). A new instrumentation system for training rowers. *Journal of Biomechanics* 33, 241-245.
- Hickey, G., Fricker, P. A., McDonald, W. A., (1997). Injuries to elite rowers over a 10-yr period. *Medicine and Science in Sports and Exercise* 29, 1567-1572.
- Hofmijster, M. J., Van Soest, A. J., De Koning, J. J., (2008). Rowing skill affects power loss on a modified rowing ergometer. *Medicine and Science in Sports and Exercise* 40, 1101-1110.
- Holt, P. J. E., Bull, A. M. J., Cashman, P. M. M., McGregor, A. H., (2003). Kinematics of spinal motion during prolonged rowing. *International Journal of Sports Medicine* 24, 597-602.
- Hopkins, W., Schabort, E. J., Hawley, J. A., (2001). Reliability of power output in physical performance tests. *Sports Medicine* 31, 211-234.
- Hutton, W. C., Adams, M. A., (1982). Can the lumbar spine be crushed in heavy lifting? *Spine* 7, 586-590.
- Jaberzadeh, S., Scutter, S., Zoghi, M., (2005). Accuracy of an electromagnetic tracking device for measuring hip joint kinematics during gait: effects of metallic total hip replacement prosthesis, source-sensor distance and sensor orientation. *Australasian Physical and Engineering Sciences in Medicine* 28, 184-189.
- Kent, M., (1998). *Oxford Dictionary of Sports Science and Medicine*. Oxford University Press, Oxford.
- Kindratenko, V., (2001). A comparison of the accuracy of an electromagnetic and a hybrid ultrasound-inertia position tracking system. *Presence* 10, 657-663.

- Kirkup, L., (1994). *Experimental methods. An introduction to the analysis and presentation of data.* John Wiley & Sons, Brisbane, New York, Chichester, Toronto, Singapore.
- Kleshnev, V., (2005). *Biomechanical methods and protocols in rowing.*
- Koerhuis, C. L., Winters, J. C., Van Der Helm, F. C. T., Hof, A. L., (2003). Neck mobility measurement by means of the Flock of Birds electromagnetic tracking system. *Clinical Biomechanics* 18, 14-18.
- Lamb, D. H., (1989). A kinematic comparison of ergometer and on-water rowing. *The American Journal of Sports Medicine* 17, 367-373.
- LaScalza, S., Arico, J., Hughes, R., (2003). Effect of metal and sampling rate on accuracy of flock of birds electromagnetic tracking system. *Journal of Biomechanics* 36, 141-144.
- Lopez-Casero, R., De Pedro, J. A., Rodriguez, E., Masquelet, A. C., (1995). Distal vascular pedicle-hemisoleus to tibial length ratio as a main predictive index in preoperative flap planning. *Surgical and Radiologic Anatomy* 17, 113-119.
- Macfarlane, D. J., Edmond, I. M., Walmsley, A., (1997). Instrumentation of an ergometer to monitor the reliability of rowing performance. *Journal of Sports Sciences* 15, 167-173.
- MacKinnon, S., Li, J. C., (1998). Temporal relationships of load and lumbar spine kinematics during lifting. *International Journal of Industrial Ergonomics* 22, 359-366.
- Mannion, A., Troke, M., (1999). A comparison of two motion analysis devices used in the measurement of lumbar spinal mobility. *Clinical Biomechanics* 14, 612-619.
- Martin, T. P., Bernfield, J. S., (1980). Effect of stroke rate on velocity of a rowing shell. *Medicine and Science in Sports and Exercise* 12, 250-256.
- McArdle, W. D., Katch, F. I., Katch, V. L., (2001). *Exercise physiology. Energy, Nutrition, and human performance.* Lippincott Williams & Wilkins.
- McGill, S. M., (1997). Methodological considerations for using inductive sensors (3SPACE ISOTRAK) to monitor 3-D orthopaedic joint motion. *Clinical Biomechanics* 12, 190-194.
- McGregor, A. H., Anderton, L., Gedroyc, W., (2002). The assessment of intersegmental motion and pelvic tilt in elite oarsmen. *Medicine and Science in Sports and Exercise* 34, 1143-1149.
- McGregor, A. H., Bull, A. M. J., Byng-Maddick, R., (2004a). A comparison of rowing technique at different stroke rates: A description of sequencing, force production and kinematics. *International Journal of Sports Medicine* 25, 465-470.
- McGregor, A. H., Hill, A., Grewar, J., (2004b). Trunk strength patterns in elite rowers. *Isokinetics and Exercise Science* 12, 253-261.
- McGregor, A. H., Patankar, Z. S., Bull, A. M. J., (2007). Longitudinal changes in the spinal kinematics of oarswomen during step testing. *Journal of Sports Science and Medicine* 6, 29-35.
- McGregor, A. H., Patankar, Z. S., Bull, A. M. J., (2008). Do men and women row differently? A spinal kinematic and force perspective. *Proceedings of the Institution of Mechanical Engineers, Part P: Journal of Sports Engineering and Technology* 222, 77-83.
- McGregor, A. H., Patankar, Z. S., Bull, A. M. J., (2005). Spinal kinematics in elite oarswomen during a routine physiological step test. *Medicine and Science in Sports and Exercise* 37, 1014-1020.

- Meskers, C. G. M., Fraterman, H., Van Der Helm, F. C. T., Vermeulen, H. M., Rozing, P. M., (1999). Calibration of the Flock of Birds electromagnetic tracking device and its application in shoulder motion studies. *Journal of Biomechanics* 32, 629-633.
- Mester, J., Grabow, V., De Marees, H., (1982). Physiologic and anthropometric aspects of vestibular regulation in rowing. *International Journal of Sports Medicine* 3, 174-176.
- Milne, A. D., Chess, D. G., Johnson, J. A., King, G. J. W., (1996). Accuracy of an electromagnetic tracking device a study of the optimal operating range and metal interference. *Journal of Biomechanics* 29, 791-793.
- Mizuno, Y., Kumagai, M., Mattessich, S. M., Elias, J. J., Ramrattan, N., Cosgarea, A. J., Chao, E. Y. S., (2001). Q-angle influences tibiofemoral and patellofemoral kinematics. *Journal of Orthopaedic Research* 19, 834-840.
- Moriguchi, C. S., Carnaz, L., Silva, L. C. C. B., Salasar, L. E. B., Carregaro, R. L., Sato, T. de O., Coury, H. J. C. G., (2009). Reliability of intra- and inter-rater palpation discrepancy and estimation of its effects on joint angle measurements. *Manual Therapy* 14, 299-305.
- Morris, F. L., Smith, R. M., Payne, W. R., Galloway, M. A., Wark, J. D., (2000). Compressive and shear force generated in the lumbar spine of female rowers. *International Journal of Sports Medicine* 21, 518-523.
- Morris, T., Summers, J., (1995). *Sport psychology; theory, applications and issues*. John Wiley & Sons Australia, Queensland.
- Morton, N. A., Maletsky, L. P., Pal, S., Laz, P. J., (2007). Effect of variability in anatomical landmark location on knee kinematic description. *Journal of Orthopaedic Research* 25, 1221-1230.
- Munro, C., Yanai, T., (2000). Forces on the lower back during rowing performance in a single scull. *Proceedings of the 18th International Symposium of Biomechanics in Sports* 186-189.
- Nachemson, A. L., (1981). Disc pressure measurements. *Spine* 6, 93-97.
- Nixon, M. A., McCallum, B. C., Fright, W. R., Price, N. B., (1998). The effects of metals and interfering fields and on electromagnetic trackers. *Presence* 7, 204-218.
- Nolte, V., (2005). *Rowing faster*. Human Kinetics.
- O'Sullivan, F., O'Sullivan, J., Bull, A. M. J., McGregor, A. H., (2003). Modelling multivariate biomechanical measurements of the spine during a rowing exercise. *Clinical Biomechanics* 18, 488-493.
- Page, R. N., Hawkins, D. A., (2003). A real-time biomechanical feedback system for training rowers. *Sports Engineering* 6, 67.
- Panjabi, M. M., Goel, V. K., Takata, K. O. I. C., (1982). Physiologic Strains in the Lumbar Spinal Ligaments: An In Vitro Biomechanical Study. *Spine* 7, 192-203.
- Pearcy, M., Portek, I., Shepherd, J., (1984). Three-dimensional x-ray analysis of normal movement in the lumbar spine. *Spine* 9, 294-297.
- Perie, D., Tate, A. J., Cheng, P. L., Dumas, G. A., (2002). Evaluation and calibration of an electromagnetic tracking device for biomechanical analysis of lifting tasks. *Journal of Biomechanics* 35, 293-297.

- Petrie, A., Watson, P., (1999). *Statistics for veterinary and animal science*. Blackwell Science Ltd., Oxford, UK.
- Piazza, S. J., Erdemir, A., Okita, N., Cavanagh, P. R., (2004). Assessment of the functional method of hip joint center location subject to reduced range of hip motion. *Journal of Biomechanics* 37, 349-356.
- Piazza, S. J., Okita, N., Cavanagh, P. R., (2001). Accuracy of the functional method of hip joint center location: effects of limited motion and varied implementation. *Journal of Biomechanics* 34, 967-973.
- Potvin, J. R., McGill, S. M., Norman, R. W., (1991). Trunk muscle and lumbar ligament contributions to dynamic lifts with varying degrees of trunk flexion. *Spine* 16, 1099-1108.
- Pudlo, P., Pinti, A., Lepoutre, F. X., (2005). Experimental laboratory apparatus to analyze kinematics and 3D kinetics in rowing. *Sports Engineering* 8, 39-46.
- Rabuffetti, M., Ferrarin, M., Mazzoleni, P., Benvenuti, F., Pedotti, A., (2003). Optimised procedure for the calibration of the force platform location. *Gait & posture* 17, 75.
- Reid, D. A., McNair, P. J., (2000). Factors contributing to low back pain in rowers. *British Journal of Sports Medicine* 34, 321-322.
- Schabort, E. J., Hawley, J. A., Hopkins, W. G., Blum, H., (1999). High reliability of performance of well-trained rowers on a rowing ergometer. *Journal of Sports Sciences* 17, 627-632.
- Schmiedmayer, H., Kastner, J., (2000). Enhancements in the Accuracy of the Center of Pressure (COP) Determined With Piezoelectric Force Plates Are Dependent on the Load Distribution. *Journal of Biomechanical Engineering* 122, 523.
- Secher, N. H., (1993). Physiological and biomechanical aspects of rowing; implications for training. *Sports Medicine* 15, 24-42.
- Seidel, G. K., Marchinada, D. M., Dijkers, M., Soutas-Little, R. W., (1995). Hip joint center location from palpable bony landmarks: a cadaver study. *Journal of Biomechanics* 28, 995.
- Shephard, R. J., (1998). Science and medicine of rowing: A review. *Journal of Sports Sciences* 16, 603-620.
- Shiang, T. Y., Tsai, C. B., (1998). The kinetic characteristics of rowing movement. In: Haake, S. J. (Ed.), *The engineering in sport*. Blackwell Science, pp. 219-224.
- Shin, C. S., Chaudhari, A. M., Andriacchi, T. P., (2009). The effect of isolated valgus moments on ACL strain during single-leg landing: A simulation study. *Journal of Biomechanics* 42, 280-285.
- Shin, H., (1999). *Experimental designs for orientation models*. PhD Queen's University.
- Slobounov, S. M., Simon, R. F., Bush, J. A., Kraemer, W. J., Sebastianelli, W., Slobounova, E., (1999). An alternate method of range of motion measurement. *Journal of Strength and Conditioning Research* 13, 389-393.
- Smith, R. M., Loschner, C., (2002). Biomechanics feedback for rowing. *Journal of Sports Sciences* 20, 783-791.
- Smith, R. M., Spinks, W. L., (1995). Discriminant analysis of biomechanical differences between novice, good and elite rowers. *Journal of Sports Sciences* 13, 377-385.

- Soper, C., Hume, P. A., (2004a). Towards an Ideal Rowing Technique for Performance: The Contributions from Biomechanics. *Sports Medicine* 34, 825.
- Soper, C., Hume, P. A., (2004b). Reliability of power output during rowing changes with ergometer type and race distance. *Sports biomechanics* 3, 237-248.
- Soper, C., Reid, D., Hume, P. A., (2004). Reliable passive ankle range of motion measures correlate to ankle motion achieved during ergometer rowing. *Physical Therapy in Sport* 5, 75.
- Sparto, P. J., Parnianpour, M., Reinsel, T. E., Simon, S., (1997). The Effect of Fatigue on Multijoint Kinematics and Load Sharing During a Repetitive Lifting Test. *Spine* 22, 2647-2654.
- Straker, L., (2003). Evidence to support using squat, semi-squat and stoop techniques to lift low-lying objects. *International Journal of Industrial Ergonomics* 31, 149-160.
- Taimela, S., Kankaanpaa, M., Luoto, S., (1999). The Effect of Lumbar Fatigue on the Ability to Sense a Change in Lumbar Position: A Controlled Study. *Spine* 24, 1322-1327.
- Thompson, P., (2005). Sculling. Training, technique and performance. The Crowood Press Ltd, Marlborough.
- Torres-Moreno, R., Tanaka, C., Penney, K. L., (2000). Joint excursion, handle velocity, and applied force: a biomechanical analysis of ergometric rowing. *International Journal of Sports Medicine* 21, 41-44.
- Trafimow, J. H., Schipplein, O. D., Novak, G. J., (1993). The effects of quadriceps fatigue on the technique of lifting. *Spine* 18, 364-367.
- Tylkowski, C. M., Simon, S. R., Mansour, J. M., (1982). Internal rotation gait in spastic cerebral palsy in the hip.
- Weinberg, R. S., Gould, D., (1999). Foundations of sport and exercise psychology. *Human Kinetics*.
- Winter, D. A., (2005). Biomechanics and Motor Control of Human Movement. John Wiley & Sons, Inc..

Appendix 1

The 969 arrangements of electromagnetic sensors used during the laboratory optimisation study

Refer to Figure 3.3 (Page 38), Figure 3.4 (Page 38), and Figure 3.5 (Page 39).

Setup	Position of FOB receiver				Distance (m)			Ergometer in situ?
	i	ii	iii	iv	Board - Slider	FOB source - floor	FOB source - slider	
1	A	E	P	T	0.1	1.0	0.95	Yes
2	A	E	P	S	0.1	1.0	0.95	Yes
3	A	E	P	R	0.1	1.0	0.95	Yes
4	A	E	P	Q	0.1	1.0	0.95	Yes
5	A	E	P	O	0.1	1.0	0.95	Yes
6	A	E	P	N	0.1	1.0	0.95	Yes
7	A	E	P	M	0.1	1.0	0.95	Yes
8	A	E	P	L	0.1	1.0	0.95	Yes
9	A	E	P	K	0.1	1.0	0.95	Yes
10	A	E	P	J	0.1	1.0	0.95	Yes
11	A	E	P	I	0.1	1.0	0.95	Yes
12	A	E	P	H	0.1	1.0	0.95	Yes
13	A	E	P	G	0.1	1.0	0.95	Yes
14	A	E	P	F	0.1	1.0	0.95	Yes
15	A	E	P	D	0.1	1.0	0.95	Yes
16	A	E	P	C	0.1	1.0	0.95	Yes
17	A	E	P	B	0.1	1.0	0.95	Yes
18-34	As above				0.3	1.0	0.95	Yes
35-51	As above				0.5	1.0	0.95	Yes
56-68	As above				0.1	0.7	0.95	Yes
69-85	As above				0.3	0.7	0.95	Yes
86-102	As above				0.5	0.7	0.95	Yes
103-119	As above				0.1	0.4	0.95	Yes
120-136	As above				0.3	0.4	0.95	Yes
137-153	As above				0.5	0.4	0.95	Yes
154-170	As above				0.1	1.0	1.25	Yes
171-187	As above				0.3	1.0	1.25	Yes
188-204	As above				0.5	1.0	1.25	Yes
205-221	As above				0.1	0.7	1.25	Yes
222-238	As above				0.3	0.7	1.25	Yes
239-255	As above				0.5	0.7	1.25	Yes
256-272	As above				0.1	0.4	1.25	Yes
273-289	As above				0.3	0.4	1.25	Yes
290-306	As above				0.5	0.4	1.25	Yes
307-323	As above				0.1	1.0	1.55	Yes
324-340	As above				0.3	1.0	1.55	Yes
341-357	As above				0.5	1.0	1.55	Yes
358-374	As above				0.1	0.7	1.55	Yes
375-391	As above				0.3	0.7	1.55	Yes
392-408	As above				0.5	0.7	1.55	Yes
409-425	As above				0.1	0.4	1.55	Yes
426-442	As above				0.3	0.4	1.55	Yes
443-459	As above				0.5	0.4	1.55	Yes
919-935	As above				0.1	1.3	0.95	Yes
936-952	As above				0.3	1.3	0.95	Yes
953-969	As above				0.5	1.3	0.95	Yes
460-918	AS FOR ARRANGEMENTS 1 - 459							No

Appendix 2

Matlab code used to validate the identification of individual rowing strokes

The code produces scatter plots that are visually assessed for errors in stroke identification.

```
clear all
clc

%Reads all available .xls files in the directory
AllFiles = dir('*.xls');

%Sets up a loop to repeat operations for each average stroke,
%and loads the k'th file in the directory list.
for k = 1:length(AllFiles)
%for k = 1:1

filename = AllFiles(k).name;
data = load (filename);
data1 = data(:,1);
data2 = data(:,2);
data3 = 100*ones(length(data),1);

if length(filename)>20
tit1 = filename(1:length(filename)-20);
tit2 = filename(length(filename)-18:length(filename)-16);
tit3 = filename(length(filename)-14:length(filename)-13);
tit4 = filename(length(filename)-11);
tit5 = filename(length(filename)-9:length(filename)-8);
else
tit1 = filename(1:length(filename)-16);
tit2 = filename(length(filename)-14:length(filename)-12);
tit3 = filename(length(filename)-10:length(filename)-9);
tit4 = filename(length(filename)-7);
tit5 = filename(length(filename)-5:length(filename)-4);
end

tit = ([tit1,' ',tit2,' ',tit3,' ',tit4,' ',tit5]);

% Create figure
figure1 = figure('PaperSize',[20.98 29.68]);

axes('Parent',figure1);
hold('all');

scatter(data1,data2,data3,'Marker','.', 'DisplayName','data1, data2,
data3');
title(tit)

saveas(figure1,['Valid - ',tit,'.jpg']);

close all
end
```

Appendix 3

Matlab code used to calculate average rowing strokes for each Step test conducted

Also performs some assessment to validate identification of individual rowing strokes.

```
[Average_Stroke] = EXTRACT_MEAN_STROKE ();

function [Average_Stroke] = EXTRACT_MEAN_STROKE ()

clear all

%Reads all available .xls files in the directory
AllFiles = dir('*.xls');

%Sets up a loop to repeat operations for each average stroke,
%and loads the k'th file in the directory list.
for k = 1:length(AllFiles)
%for k = 1:1

filename = AllFiles(k).name;
data = load (filename);

strokecount = find(data(:,1)>99);
strokecount = length(strokecount);

%%%%%%%%%%%%%%%%%%%%%%%%%%%%%%%%%%%%%%%%%%%%%%%%%%%%%%%%%%%%%%%%%%%%%%%%
%CREATES A CELL ARRAY WITH EACH CELL CONTAINING ONE STROKE
for n = 1:strokecount
    strokes(n) = {data((n-1)*101+1:n*101,1:50)};
end

%CREATES AN AVERAGE STROKE - TRIMS FIRST AND LAST 5 STROKES
strokesSum = zeros(101,50);

for n = 6:strokecount-5
    strokesSum = strokesSum + strokes{n};
end

strokesMean = strokesSum ./ (strokecount-10);

%%%%%%%%%%%%%%%%%%%%%%%%%%%%%%%%%%%%%%%%%%%%%%%%%%%%%%%%%%%%%%%%%%%%%%%%
%USES THE 1st to the 40th PERCENTAGE POINT OF HANDLE FORCE TO
%VALIDATE THAT A TRUE STROKE IS BEING READ
for n = 1:strokecount
    strokeValid(n,1) = max(data((n-1)*101+1:(n-1)*101+40,2));
end

strokeValidMin = min(strokeValid);

%USES THE 41st to the 99th PERCENTAGE POINT OF HANDLE FORCE TO
%VALIDATE THAT A TRUE STROKE IS BEING READ
```

```

for n = 1:strokecount
    strokeValidb(n,1) = max(data((n-1)*101+41:(n-1)*101+99,2));
end

strokeValidMinb = min(strokeValidb);

if strokeValidMin>100 && strokeValidMinb<100
    Are_all_strokes_valid = [filename,' - YES']
else
    Are_all_strokes_valid = [filename,' - NO']
end

%%%%%%%%%%%%%%%%%%%%%%%%%%%%%%%%%%%%%%%%%%%%%%%%%%%%%%%%%%%%%%%%%%%%%%%%
%Corrects the previously calculated average stroke for COP and seat
%force values. This is based on the calibration experiment that was
%carried out in order to optimise the accuracy of seat transducers.

FL = strokesMean(:,3);
FLF = FL*1.0029;
FLAP = FL*5.5642;
FLML = FL*-4.8777;
FR = strokesMean(:,4);
FRF = FR*0.9953;
FRAP = FR*5.4667;
FRML = FR*4.4559;
RL = strokesMean(:,5);
RLF = RL*1.0028;
RLAP = RL*-5.3181;
RLML = RL*-4.2383;
RR = strokesMean(:,6);
RRF = RR*1.0017;
RRAP = RR*-5.6231;
RRML = RR*4.3053;

Force = FLF+FRF+RLF+RRF;

APmoment = FLAP+FRAP+RLAP+RRAP;
MLmoment = FLML+FRML+RLML+RRML;

    for i = 1:101
        APpos(i,1) = APmoment(i,1)/Force(i,1);
    end

    for i = 1:101
        MLpos(i,1) = MLmoment(i,1)/Force(i,1);
    end

%Loads the ML(x1) and AP(z1) COP data

x1 = MLpos;
z1 = APpos;
aa = strokesMean(:,1:6);
ab = [MLpos APpos Force];
ac = strokesMean(:,10:50);
Average_Stroke = [aa ab ac];

for n = 1:101
    if Average_Stroke(n,9)>-5;
        Average_Stroke(n,7) = 0;
    else
        Average_Stroke(n,7) = Average_Stroke(n,7);
    end
end
end

```


Appendix 4

Matlab code used to calculate average Step strokes for groups of athletes

```
clear all
clc

answer1 = input('Are there Step 1 files being considered? (Y or N):',
's');
answer2 = input('Are there Step 2 files being considered? (Y or N):',
's');
answer3 = input('Are there Step 3 files being considered? (Y or N):',
's');
answer4 = input('Are there Step 4 files being considered? (Y or N):',
's');
answer5 = input('Are there Step 5 files being considered? (Y or N):',
's');
answer6 = input('Are there Step 6 files being considered? (Y or N):',
's');

name = input('Enter the desired output file name (e.g. HWW-
SCULL_JUN_08) (minimum 8 characters):', 's');

if answer1 == 'Y'
    ans1 = 1;
elseif answer1 == 'y'
    ans1 = 1;
else
    ans1 = 0;
end

if answer2 == 'Y'
    ans2 = 1;
elseif answer2 == 'y'
    ans2 = 1;
else
    ans2 = 0;
end

if answer3 == 'Y'
    ans3 = 1;
elseif answer3 == 'y'
    ans3 = 1;
else
    ans3 = 0;
end

if answer4 == 'Y'
    ans4 = 1;
elseif answer4 == 'y'
    ans4 = 1;
else
    ans4 = 0;
end

if answer5 == 'Y'
    ans5 = 1;
elseif answer5 == 'y'
```

```

        ans5 = 1;
else
    ans5 = 0;
end

if answer6 == 'Y'
    ans6 = 1;
elseif answer6 == 'y'
    ans6 = 1;
else
    ans6 = 0;
end

if ans1 == 1
[Group_Average_Stroke_Step_1] = EXTRACT_GROUP_MEAN_STROKE_step1
(name);
end

if ans2 == 1
[Group_Average_Stroke_Step_2] = EXTRACT_GROUP_MEAN_STROKE_step2
(name);
end

if ans3 == 1
[Group_Average_Stroke_Step_3] = EXTRACT_GROUP_MEAN_STROKE_step3
(name);
end

if ans4 == 1
[Group_Average_Stroke_Step_4] = EXTRACT_GROUP_MEAN_STROKE_step4
(name);
end

if ans5 == 1
[Group_Average_Stroke_Step_5] = EXTRACT_GROUP_MEAN_STROKE_step5
(name);
end

if ans6 == 1
[Group_Average_Stroke_Step_6] = EXTRACT_GROUP_MEAN_STROKE_step6
(name);
end

```


Appendix 5

Matlab code used to extract variables of interest from Step stroke matrices

```
clear all

%Reads all available AVE.xls files in the directory
AllFiles = dir('*AVE.xls');

%Sets up a loop to repeat operations for each average stroke, and
loads the
%i'th file in the directory list.
%for i = 1:length(AllFiles)
for i = 1:1

filename = AllFiles(i).name;
data = load (filename);
title_size = size(filename);
titvalue = title_size(1,2);

%uses the filename to extract titles for the Output columns and output
file
tit1 = filename(1:titvalue-20);
tit2 = filename(titvalue-18:titvalue-16);
tit3 = filename(titvalue-14:titvalue-13);
tit4 = filename(titvalue-11);
tit5 = filename(titvalue-9:titvalue-8);

testdate = ([tit2,'-',tit3]);

tit = ([tit1,' ',tit2,' ',tit3,' ',tit4,' ',tit5]);

%%%%%%%%%%%%%%%%%%%%%%%%%%%%%%%%%%%%%%%%%%%%%%%%%%%%%%%%%%%%%%%%%%%%%%%%
%%%%%%%%%%%%%%%%%%%%%%%%%%%%%%%%%%%%%%%%%%%%%%%%%%%%%%%%%%%%%%%%%%%%%%%%
%Calls functions to perform operations to extract useful data

[BM,BW,length,rate,work,power,max_h_force,max_h_force_BM,row_max_h_for
ce,row_finish,duration_recovery,slope_h_force,...
min_s_force,max_s_force,s_f_at_MHF,quality_of_suspension_initial_drive
,quality_of_suspension_entire_drive,row_knees_up] = ...
    EXTRACT_NON_3D_OUTPUT (data);

[DriveCoordinates,leftmotion1,leftmotion2,leftmotion3...
leftmotion4,leftmotion5,rightmotion1,rightmotion2,rightmotion3,...
rightmotion4,rightmotion5,mediolat_total1,mediolat_total2,...
mediolat_total3,mediolat_total4,mediolat_total5] = ...
    EXTRACT_COP_OUTPUT (data,row_max_h_force,row_finish);

[LP_catch,LP_maxhforce,LP_finish,...
Quality_LP_catch,Quality_LP_maxhforce,Quality_LP_finish] = ...
    EXTRACT_LP_RATIOS (data,row_max_h_force,row_finish);

[15s1_hjc_x,hjc_kjc_x,kjc_ajc_x,ajc_fjc_x,...
15s1_hjc_y,hjc_kjc_y,kjc_ajc_y,ajc_fjc_y,...
15s1_hjc_z,hjc_kjc_z,kjc_ajc_z,ajc_fjc_z,...
maximums,minimums,at_the_catch,at_MHF,at_the_finish,at_knees_up,...
aphandle,aphandle_kneeZ] = ...
    EXTRACT_3D_KINE (data,row_max_h_force,row_finish,row_knees_up);
```

%%
%%

%Generates a matrix of outputs for all average strokes

Output(1,1:43) = {'Athlete' 'Test Date' 'Month' 'Year' 'Step' ...
'BM' 'BW' 'Max H Force %' 'Finish %' 'Knees Up %' 'Recovery
Duration' ...
'Max H Force' 'Max H Force/BM' 'Slope H Force' ...
'Min S Force' 'Max S Force' 'S Force @ MHF' ...
'Length' 'Rate' 'Work' 'Power' ...
'Suspension 1' 'Suspension 2' ...
'Drift - MHF' 'Drift - Finish' 'Drift - MHF - Finish' 'Drift -
Recovery' 'Drift - All' ...
'Catch X' 'MHF X' 'Finish X' 'Qual Catch X' 'Qual MHF X' 'Qual
Finish X' 'Catch Z' 'MHF Z' 'Finish Z' ...
'LP @ Catch' 'LP @MHF' 'LP @ Finish' ...
'Qual LP @ C' 'Qual LP @ MHF' 'Qual LP @ F'};

Output(i+1,1) = {tit1};%#ok<AGROW>
Output(i+1,2) = {testdate};%#ok<AGROW>
Output(i+1,3) = {tit2};%#ok<AGROW>
Output(i+1,4) = {tit3};%#ok<AGROW>
Output(i+1,5) = {tit4};%#ok<AGROW>
Output(i+1,6) = {BM};%#ok<AGROW>
Output(i+1,7) = {BW};%#ok<AGROW>
Output(i+1,8) = {row_max_h_force-1};%#ok<AGROW>
Output(i+1,9) = {row_finish-1};%#ok<AGROW>
Output(i+1,10) = {row_knees_up-1};%#ok<AGROW>
Output(i+1,11) = {duration_recovery};%#ok<AGROW>
Output(i+1,12) = {max_h_force};%#ok<AGROW>
Output(i+1,13) = {max_h_force_BM};%#ok<AGROW>
Output(i+1,14) = {slope_h_force};%#ok<AGROW>
Output(i+1,15) = {min_s_force};%#ok<AGROW>
Output(i+1,16) = {max_s_force};%#ok<AGROW>
Output(i+1,17) = {s_f_at_MHF};%#ok<AGROW>
Output(i+1,18) = (Lopez-Casero et al., 1995);%#ok<AGROW>
Output(i+1,19) = {rate};%#ok<AGROW>
Output(i+1,20) = (Fleming et al., 1997);%#ok<AGROW>
Output(i+1,21) = {power};%#ok<AGROW>
Output(i+1,22) = {quality_of_suspension_initial_drive};%#ok<AGROW>
Output(i+1,23) = {quality_of_suspension_entire_drive};%#ok<AGROW>
Output(i+1,24) = {mediolat_total1};%#ok<AGROW>
Output(i+1,25) = {mediolat_total3};%#ok<AGROW>
Output(i+1,26) = {mediolat_total2};%#ok<AGROW>
Output(i+1,27) = {mediolat_total4};%#ok<AGROW>
Output(i+1,28) = {mediolat_total5};%#ok<AGROW>
Output(i+1,29) = {DriveCoordinates(1,1)};%#ok<AGROW>
Output(i+1,30) = {DriveCoordinates(2,1)};%#ok<AGROW>
Output(i+1,31) = {DriveCoordinates(3,1)};%#ok<AGROW>
Output(i+1,32) = {abs(DriveCoordinates(1,1))};%#ok<AGROW>
Output(i+1,33) = {abs(DriveCoordinates(2,1))};%#ok<AGROW>
Output(i+1,34) = {abs(DriveCoordinates(3,1))};%#ok<AGROW>
Output(i+1,35) = {DriveCoordinates(1,2)};%#ok<AGROW>
Output(i+1,36) = {DriveCoordinates(2,2)};%#ok<AGROW>
Output(i+1,37) = {DriveCoordinates(3,2)};%#ok<AGROW>
Output(i+1,38) = {LP_catch};%#ok<AGROW>
Output(i+1,39) = {LP_maxhforce};%#ok<AGROW>
Output(i+1,40) = {LP_finish};%#ok<AGROW>
Output(i+1,41) = {Quality_LP_catch};%#ok<AGROW>
Output(i+1,42) = {Quality_LP_maxhforce};%#ok<AGROW>
Output(i+1,43) = {Quality_LP_finish};%#ok<AGROW>

Output2(i+1,1:169) = [maximums(:,13:40) minimums(:,13:40)
at_the_catch(:,13:40) at_MHF(:,13:40) at_the_finish(:,13:40)
at_knees_up(:,13:40) ahandle_kneeZ];

```

Output_for_coaches(1,1:13) = {'Athlete' 'Test Date' 'Step' 'Length'
'Power' 'Force' ...
'End Drive %' 'LP@Catch' 'LP@MHF' 'LP@Finish' 'Q of S 1' 'ML drift
drive' ...
'ML drift recovery'};

```

```

Output_for_coaches(i+1,1) = {tit1};%#ok<AGROW>
Output_for_coaches(i+1,2) = {testdate};%#ok<AGROW>
Output_for_coaches(i+1,3) = {tit4};%#ok<AGROW>
Output_for_coaches(i+1,4) = (Lopez-Casero et al., 1995);%#ok<AGROW>
Output_for_coaches(i+1,5) = {power};%#ok<AGROW>
Output_for_coaches(i+1,6) = {max_h_force};%#ok<AGROW>
Output_for_coaches(i+1,7) = {row_finish-1};%#ok<AGROW>
Output_for_coaches(i+1,8) = {LP_catch};%#ok<AGROW>
Output_for_coaches(i+1,9) = {LP_maxhforce};%#ok<AGROW>
Output_for_coaches(i+1,10) = {LP_finish};%#ok<AGROW>
Output_for_coaches(i+1,11) =
{quality_of_suspension_initial_drive};%#ok<AGROW>
Output_for_coaches(i+1,12) = {mediolat_total3};%#ok<AGROW>
Output_for_coaches(i+1,13) = {mediolat_total4};%#ok<AGROW>

```

```

%%%%%%%%%%%%%%%%%%%%%%%%%%%%%%%%%%%%%%%%%%%%%%%%%%%%%%%%%%%%%%%%%%%%%%%%
%OTHER VARIABLES

```

```

seat_perf1 =
sum(abs(data(1:row_max_h_force,7)).*abs(data(1:row_max_h_force,9)./BM)
);

```

```

seat_perf2 =
sum(abs(data(1:row_finish,7)).*abs(data(1:row_finish,9)./BM));

```

```

seat_perf3 = ((min_s_force*-100/BM)-BW)/BW;

```

```

delta_lsj_alpha = data(row_max_h_force,28)-data(1,28);

```

```

%%%%%%%%%%%%%%%%%%%%%%%%%%%%%%%%%%%%%%%%%%%%%%%%%%%%%%%%%%%%%%%%%%%%%%%%

```

```

kjckjc = abs(data(1:row_finish,34)-20);
kjckjc_is_20 = find(kjckjc==min(kjckjc));
diff_actual_kjc_alpha_and_kjc_alpha_20 = data(kjckjc_is_20(1,1),34)-
20;
hjc_beta_at_kjc_alpha_20 = data(kjckjc_is_20(1,1),32);

```

```

%%%%%%%%%%%%%%%%%%%%%%%%%%%%%%%%%%%%%%%%%%%%%%%%%%%%%%%%%%%%%%%%%%%%%%%%

```

```

rate_of_change(1,1) = 0;
for n = 1:99
rate_of_lsj_alpha_change(n+1,1) = (data(n+2,28)-
data(n,28))/(60/data(1,48)*(2/101));

```

```

rate_of_lsj_with_force(n,1) =
rate_of_lsj_alpha_change(n,1)*data(n,2);
end
lsj_and_force_1a = max(rate_of_lsj_with_force(1:row_finish,1));

```

```

lsj_and_force_1b = min(rate_of_lsj_with_force(1:row_finish,1));

```

```

peak_f_minus_lsj_force_1a_timing = row_max_h_force-
find(rate_of_lsj_with_force==lsj_and_force_1a);

```

```

peak_f_minus_lsj_force_1b_timing = max(row_max_h_force-
find(rate_of_lsj_with_force==lsj_and_force_1b));

```

```

%%%%%%%%%%%%%%%%%%%%%%%%%%%%%%%%%%%%%%%%%%%%%%%%%%%%%%%%%%%%%%%%%%%%%%%%

```

```

Output(1,44:53) = {'Seat Perf MHF' 'Seat Perf Finish' 'Seat Perf BW
over' ...
  'LSJ alpha delta' 'HJC beta at KJC alpha 20' ...
  'max lsj force' 'min lsj force' ...
  'max lsj force %' 'min lsj force %' ...
  'KJC 20 - KJC actual at 20'};

Output(i+1,44) = {seat_perf1};%#ok<AGROW>
Output(i+1,45) = {seat_perf2};%#ok<AGROW>
Output(i+1,46) = {seat_perf3};%#ok<AGROW>
Output(i+1,47) = {delta_lsj_alpha};%#ok<AGROW>
Output(i+1,48) = {hjc_beta_at_kjc_alpha_20};%#ok<AGROW>
Output(i+1,49) = {lsj_and_force_1a};%#ok<AGROW>
Output(i+1,50) = {lsj_and_force_1b};%#ok<AGROW>
Output(i+1,51) = {peak_f_minus_lsj_force_1a_timing};%#ok<AGROW>
Output(i+1,52) = {peak_f_minus_lsj_force_1b_timing};%#ok<AGROW>
Output(i+1,53) = {diff_actual_kjc_alpha_and_kjc_alpha_20};%#ok<AGROW>

```

end

```

function
[BM,BW,length,rate,work,power,max_h_force,max_h_force_BM,row_max_h_force,
row_finish,duration_recovery,slope_h_force,...
min_s_force,max_s_force,s_f_at_MHF,quality_of_suspension_initial_drive
,quality_of_suspension_entire_drive,row_knees_up] =
EXTRACT_NON_3D_OUTPUT (data)

BM = data(1,12);
BW = BM*9.81;

length = data(1,49);

rate = data(1,48);

work = data(101,46);

power = data(1,47);

maximum_h_force = max(data(:,2));
max_h_force = maximum_h_force(1,1);
max_h_force_BM = max_h_force/BM*100;

row_maximum_h_force = find((data(:,2))==max_h_force);
row_max_h_force = row_maximum_h_force(1,1);

rowfinish = find((data(:,2))<50);
rowfinishb = find(rowfinish>20);
rowfinishc = min(rowfinishb);
row_finish = rowfinish(rowfinishc,1);

duration_recovery = 100-row_finish;

rowknees = data(2:101,20)-data(1:100,20);
row_kneesup = find(rowknees((row_finish+10):80,:)>2.5);
row_knees_up = row_kneesup(1,1)+row_finish+10;

slope_h_force = max_h_force/row_max_h_force;

minimum_s_force = min(data(:,9));
min_s_force = minimum_s_force(1,1);

maximum_s_force = max(data(:,9));
max_s_force = maximum_s_force(1,1);
s_f_at_MHF = data(row_max_h_force,9);

%Calculates a measure of the quality of suspension acheived throught
%the initial portion of the drive, and the entire drive phase
sforce = data(:,9);
sforce = sforce.*-1;
sforce = sforce./BM;
sforce = sforce.*100;

possforceforsuspension = sforce(1:row_finish,:);
possforceforsuspensionbyBW = possforceforsuspension./BW;

quality_of_suspension_initial_drive =
sum(possforceforsuspensionbyBW(1:row_max_h_force,:));
quality_of_suspension_entire_drive= sum(possforceforsuspensionbyBW);

```

```

function [DriveCoordinates, leftmotion1, leftmotion2, leftmotion3...
    leftmotion4, leftmotion5, rightmotion1, rightmotion2, rightmotion3, ...
    rightmotion4, rightmotion5, mediolat_total1, mediolat_total2, ...
    mediolat_total3, mediolat_total4, mediolat_total5] =
EXTRACT_COP_OUTPUT (data, row_max_h_force, row_finish)

x = data(:,7);
z = data(:,8);

%For Drive CoOrdinates

ala = x(1,1);
bla = z(1,1);
alb = x(row_max_h_force,1);
blb = z(row_max_h_force,1);
alc = x(row_finish,1);
blc = z(row_finish,1);

a1 = [ala;alb;alc];
a1 = a1*10;
b1 = [bla;blb;blc];
b1 = b1*10;

DriveCoordinates = [a1 b1];

for n = 1:101
    if x(n,1)<0
        leftseatttotal(n,1) = x(n,1);
    else
        leftseatttotal(n,1) = 0;
    end
    if x(n,1)>0
        rightseatttotal(n,1) = x(n,1);
    else
        rightseatttotal(n,1) = 0;
    end
end

leftmotion1 = sum(leftseatttotal(1:row_max_h_force));
leftmotion2 = sum(leftseatttotal(row_max_h_force+1:row_finish));
leftmotion3 = sum(leftseatttotal(1:row_finish));
leftmotion4 = sum(leftseatttotal(row_finish+1:101));
leftmotion5 = sum(leftseatttotal);

rightmotion1 = sum(rightseatttotal(1:row_max_h_force));
rightmotion2 = sum(rightseatttotal(row_max_h_force+1:row_finish));
rightmotion3 = sum(rightseatttotal(1:row_finish));
rightmotion4 = sum(rightseatttotal(row_finish+1:101));
rightmotion5 = sum(rightseatttotal);

mediolat_total1 = abs(leftmotion1)+abs(rightmotion1);
mediolat_total2 = abs(leftmotion2)+abs(rightmotion2);
mediolat_total3 = abs(leftmotion3)+abs(rightmotion3);
mediolat_total4 = abs(leftmotion4)+abs(rightmotion4);
mediolat_total5 = abs(leftmotion5)+abs(rightmotion5);

```

```

function [LP_catch,LP_maxhforce,LP_finish,...
    Quality_LP_catch,Quality_LP_maxhforce,Quality_LP_finish] =
EXTRACT_LP_RATIOS (data,row_max_h_force,row_finish)

%Calculate lumbopelvic ratios
for n = 1:101
    if data(n,11) < 0 && n == 1
        LPratio(n,1) = abs(data(n,10))+abs(data(n,11));
    elseif data(n,11) < 0 && data(n,10) > 0 && n == row_max_h_force
        LPratio(n,1) = abs(data(n,10))+abs(data(n,11));
    elseif data(n,11) > 0 && data(n,11) < 0.99 && abs(data(n,11)) <
abs(data(n,10))
        LPratio(n,1) = abs(data(n,10))-abs(data(n,11));
    elseif data(n,10) > 0 && n > row_finish
        LPratio(n,1) = 99;
    else LPratio(n,1) = data(n,10)/data(n,11); %#ok<AGROW>
    end
end

LP_catch = LPratio(1,1);
LP_maxhforce = LPratio(row_max_h_force,1);
LP_finish = LPratio(row_finish,1);

Quality_LP_catch = abs(1-LP_catch);
Quality_LP_maxhforce = abs(1-LP_maxhforce);
Quality_LP_finish = abs(1-LP_finish);

```

```

function [l5s1_hjc_x,hjc_kjc_x,kjc_ajc_x,ajc_fjc_x,...
        l5s1_hjc_y,hjc_kjc_y,kjc_ajc_y,ajc_fjc_y,...
        l5s1_hjc_z,hjc_kjc_z,kjc_ajc_z,ajc_fjc_z,...
        maximums,minimums,at_the_catch,at_MHF,at_the_finish,at_knees_up,...
        ahandle,ahandle_kneeZ] = EXTRACT_3D_KINE
(data,row_max_h_force,row_finish,row_knees_up)

%POSITIONAL STUFF

%12 COLUMNS FOR X,Y,Z coordinate
%OF L5S1 - HJC, HJC - KJC, KJC - AJC and AJC - FJC

% x direction

l5s1_hjc_x = data(:,13)-data(:,16);
hjc_kjc_x = data(:,16)-data(:,19);
kjc_ajc_x = data(:,19)-data(:,22);
ajc_fjc_x = data(:,22)-data(:,25);

% y direction

l5s1_hjc_y = data(:,14)-data(:,17);
hjc_kjc_y = data(:,17)-data(:,20);
kjc_ajc_y = data(:,20)-data(:,23);
ajc_fjc_y = data(:,23)-data(:,26);

% z direction

l5s1_hjc_z = data(:,15)-data(:,18);
hjc_kjc_z = data(:,18)-data(:,21);
kjc_ajc_z = data(:,21)-data(:,24);
ajc_fjc_z = data(:,24)-data(:,27);

% coordinates and angles, max, min, during the stroke

maximums = max(data(:,:));
minimums = min(data(:,:));

at_the_catch = data(1,:);
at_MHF = data(row_max_h_force,:);
at_the_finish = data(row_finish,:);
at_knees_up = data(row_knees_up,:);

% obtains the position of the handle relative to the FOB

ahandle = data(:,44);
ahandle(:,2) = data(1,27)+550;
ahandle(:,3) = -1620-(data(1,44));
ahandle(:,4) = ahandle(:,2)+ahandle(:,3);
ahandle(:,5) = data(:,44)-data(1,44);
ahandle(:,6) = ahandle(:,4)-ahandle(:,5);

% obtains the Z pos of the handle minus the
% Z pos of the KJC at knees up in recovery

ahandle_kneeZ = ahandle(row_knees_up,6)-data(row_knees_up,21);

```